A COMPARISON OF FETO-PLACENTAL VASCULARITY IN NORMAL AND GROWTH RESTRICTED PREGNANCIES

A thesis submitted to the University of Manchester for the degree of Ph.D. in the Faculty of Biology, Medicine and Health

2016

TOLUWALOPE OLUWAFUNMILAYO JUNAID (M.B.Ch.B., MRes)

School of Medical Sciences

Contents

List of figures

List of tables

Abbreviations

Ang   Angiopoietin

BMI   Body mass index

CC3   Cleaved caspase 3

CLARITY   Clear Lipid-exchanged Acrylamide-hybridized Rigid

Imaging/Immunostaining/In situ hybridization-compatible Tissue hYdrogel

DMEM   Dulbecco's modified Eagle's medium

DMSO   Dimethyl sulfoxide

EBM-2   Endothelial basal medium-2

EGM-2   Endothelial growth medium-2

EGM-MV   Endothelial growth medium-microvascular

eNOS   Endothelial nitric oxide synthase

FCS   Fetal calf serum

FGF   Fibroblast growth factor

FGR   Fetal growth restriction

FZD   Frizzled

HPAEC   Human placental artery endothelial cell

HPVEC   Human placental vein endothelial cell

HUVEC   Human umbilical vessel endothelial cell

IBR   Individualised birth ratio

KOH	Potassium hydroxide
LRP	Low density lipoprotein receptor
MAPK	Mitogen-activated protein kinase
Micro-CT	Micro-computed tomography
NO	Nitric oxide
PA	Placental surface area
PBS	Phosphate buffered saline
PDGF	Platelet derived growth factor
PFA	Paraformaldehyde
PlGF	Placental growth factor
PMMA	Polymethylmethacrylate
PW	Placental weight
SDS	Sodium dodecyl sulfate
THBS	Thrombospondin
TLS	Tube-like structure
TSP	Thrombospondin
VEGF	Vascular endothelial growth factor
VEGFR	Vascular endothelial growth factor receptor
WNT	Wingless-related integration site

Abstract

A Comparison of Feto-placental Vascularity in Normal and Growth Restricted Pregnancies

Toluwalope Oluwafunmilayo JUNAID

The University of Manchester

PhD Medicine

August 2016

In human pregnancy, the feto-placental vessels are crucial for efficient materno-fetal transfer; hence they play a pivotal role in the pathogenesis of fetal growth restriction (FGR). We, as well as other research groups, have observed abnormalities in the FGR feto-placental vasculature, which, though inconclusive, were suggestive of a state of panhypovascularity. The goal of the work presented in this thesis was to investigate this. We hypothesised that the placenta may be panhypovascular in FGR due to failed angiogenesis; and enhancing angiogenesis in the placenta may improve fetal growth.

Custom-designed techniques including advanced imaging, computer-aided analyses and tube-forming experiments were employed to compare feto-placental vessels and endothelial cells in placentas from normal and FGR-complicated pregnancies while aiming to answer two main research questions: (i) is the FGR placenta panhypovascular? (ii) can angiogenesis be induced or enhanced to improve placental vascularity?

Findings include: (i) shorter arterial [$p = 0.03$ and 0.009 when data adjusted for placental surface area (PA) and weight (PW) respectively] and longer venous path [$p = 0.05$ and 0.03, adjusted for PA and PW respectively] in FGR placentas though no difference in the total number of arterial or venous branches, diameter, and tortuosity of the vessels compared to normal; (ii) altered angiogenic behaviour/response of FGR placental endothelial cells following *in vitro* pharmacological manipulation of WNT signalling; (iii) human placental endothelial cells are capable of regaining their angiogenic potential following withdrawal of WNT inhibition.

These findings discount the hypothesis of panhypovascularity in FGR placentas, but identify additional, previously unreported, feto-placental vascular abnormalities associated with FGR. Also, the findings provide evidence that impairment of WNT signalling may play a role in defective angiogenesis and consequent dysvascularity in the FGR placenta. The evidence suggests the WNT pathway should be explored as a potential new target for therapeutic interventions to correct placental dysvascularity in FGR.

Declaration

No portion of the work referred to in this thesis has been submitted in support of an application for another degree or qualification of this or any other university or other institute of learning.

Copyright statement

i. The author of this thesis (including any appendices and/or schedules to this thesis) owns certain copyright or related rights in it (the "Copyright") and s/he has given The University of Manchester certain rights to use such Copyright, including for administrative purposes.

ii. Copies of this thesis, either in full or in extracts and whether in hard or electronic copy, may be made **only** in accordance with the Copyright, Designs and Patents Act 1988 (as amended) and regulations issued under it or, where appropriate, in accordance with licensing agreements which the University has from time to time. This page must form part of any such copies made.

iii. The ownership of certain Copyright, patents, designs, trademarks and other intellectual property (the "Intellectual Property") and any reproductions of copyright works in the thesis, for example graphs and tables ("Reproductions"), which may be described in this thesis, may not be owned by the author and may be owned by third parties. Such Intellectual Property and Reproductions cannot and must not be made available for use without the prior written permission of the owner(s) of the relevant Intellectual Property and/or Reproductions.

iv. Further information on the conditions under which disclosure, publication and commercialisation of this thesis, the Copyright and any Intellectual Property and/or Reproductions described in it may take place is available in the University IP Policy (see http://documents.manchester.ac.uk/display.aspx?DocID=24420), in any relevant Thesis restriction declarations deposited in the University Library, The University Library's regulations (see http://www.manchester.ac.uk/library/aboutus/regulations) and in The University's policy on Presentation of Theses.

About the author

TOJ developed profound interest in obstetrics during her undergraduate study in Medicine at Olabisi Onabanjo University, Nigeria. She graduated with the M.B.Ch.B degree in 2008. As a clinician, she had discarded many placentas without realising how much of a research tool the placenta is. However, this changed when she undertook the one-year long Master of Research (MRes) in Maternal and Fetal Health at The University of Manchester, UK. She graduated from the Masters programme in 2011, with distinction. Subsequently, in 2012, she was awarded the University of Manchester's President's Doctoral Scholarship Award which provided full funding for this PhD research project. During the combined five years of academic training at Masters and PhD levels under the supervision of Prof John Aplin and Dr Edward Johnstone, she has acquired laboratory research skills, as well as invaluable transferrable skills such as effective oral and written communication of scientific data, grantsmanship, teaching and mentoring. Now, with heightened interest in obstetric research and high risk pregnancies, she is moving on to undertake a National Institute of Health (NIH) funded post-doctoral fellowship in obstetric fetal pharmacology at The University of Pittsburgh, Pennsylvania, USA and hopes to someday be an independent and productive physician scientist.

Contributions from collaborators

The work presented in chapter 2 has been submitted for publication and is currently at peer review stage. The work is an extension of two preceding studies which are part of TOJ's PhD project, are available in published literature (Junaid *et al.*, 2014) and are referred to in various sections of this thesis. Authors on the current manuscript include, in this order, Dr Toluwalope O Junaid, Dr Robert S Bradley, Prof Rohan M Lewis, Prof John D Aplin and Dr Edward D Johnstone. The study was conceptualized and planned by TOJ, RML, JDA and EDJ. All vessel casts were prepared by TOJ. MicroCT imaging and Avizo analyses were performed by TOJ, with training and guidance provided by RSB. All analyses on the Analyze software were performed by TOJ in the laboratory of Dr. Rainer Hinz of the Wolfson Molecular Imaging Centre, Manchester. The manuscript was written by TOJ and all authors contributed to editing and revising it.

The work presented in chapter 3 was performed by TOJ at The New York State Institute for Basic Research, Staten Island, New York, USA and was funded by The Royal Society International Exchange Award 2014/R2. All collaborators on the project, in no particular order, include:

Manchester Team	New York Team
Dr. Toluwalope Junaid	Dr. Wojciech. Kaczmarski
Dr. Edward Johnstone	Ms. Valerie Schwenk
Prof. John Aplin	Dr. George Merz
	Dr. Carolyn Salafia

The work presented in chapter 4 was performed by TOJ.

Publications

Publications from TOJ's PhD research project include:

<u>**Research articles**</u>

- **Junaid, T. O.**, Brownbill, P., Chalmers, N., Johnstone, E. D. & Aplin, J. D. Fetoplacental vascular alterations associated with fetal growth restriction. Placenta. 2014 Oct; 35(10): 808-15. doi: 10.1016/j.placenta.2014.07.013. Epub 2014 Aug 6.

- **Junaid, T. O.**, Bradley, R. S., Lewis, R. M., Aplin, J. D. & Johnstone, E. D. Whole organ vascular casting and microCT examination of the human placental vascular tree reveals novel alterations associated with pregnancy disease.

  Manuscript submitted in July 2016.Currently at review stage.

<u>**Published abstracts**</u>

- **Toluwalope O. Junaid**, Edward Johnstone, John D. Aplin. Resolving Human Placental Vascularity by Advanced Imaging Technique. Reproductive Sciences 2014 March; Vol 21, No. 3 (supplement): 287A (F-151). doi: 10.1177/1933719114528275.

- John D. Aplin, **Toluwalope Junaid**, Paul Brownbill, Edward D. Johnstone. 2014. Microvascular regression contributes to placental vascular impoverishment in fetal growth restriction. Placenta. 2014 June; 35(9): A42. doi: 10.1016/j.placenta.2014.07.013.

- **Toluwalope Junaid**, Robert Bradley, John Aplin, Edward Johnstone. A Novel Technique for Ex Vivo Examination of Human Placental Vessels. Reproductive Sciences 2015 March; Vol. 22, No. 1 (supplement): 189A (T-257). doi: 10.1177/1933719115579631.

Conference presentations and prizes

Poster presentations

- Institute of Human Development Postgraduate Research Showcase, Manchester UK – June 2013.

- Research & Innovation Conference, Central Manchester University Hospitals/National Institute for Health Research, UK – December 2013.
    Best poster presentation award.

- Northern Vascular Biology Conference, Sheffield UK – December 2013.

- Society for Reproductive Investigation (SRI) 61st annual scientific meeting, Florence Italy – March 2014.
    Best new investigator poster award.

- Institute of Human Development Postgraduate Research Showcase, Manchester UK – June 2014

- University of Manchester Postgraduate Summer Research Showcase, UK – July 2014

- International Federation of Placenta Associations (IFPA) Annual Meeting, Paris France – September 2014.

- Society for Reproductive Investigation (SRI) 62nd annual scientific meeting, San Francisco USA – March 2015.

Oral presentation

- Institute of Human Development Postgraduate Research Showcase, Manchester UK – June 2015.

Acknowledgements

My profound appreciation goes:

First and foremost, to the ever-faithful Giver of every good and perfect gift for making yet another dream of mine a reality.

To The University of Manchester President's Doctoral Scholarship award body for finding me deserving of this highly prestigious award. I am indeed grateful for the full financial support.

To Prof John Aplin and Dr Edward Johnstone for supervising and mentoring me for five years (a year of Masters and four years of PhD supervision). Your guidance has heightened my interest in obstetric research and helped shape an academic career I am devotedly pursuing.

To Dr Paul Brownbill and Dr Rebecca Jones for their invaluable inputs.

To the very kind mothers who donated their placentas post-delivery for my research, and the midwives at St Mary's Hospital who helped with collection of the placentas.

To everyone at Maternal and Fetal Health Research Centre for accommodating me during my time in the department.

To my adorable parents and siblings, friends, and mentors for their unflinching support.

Finally, last but surely not least, to my Rex, thank you for your unfailing love, sacrifices, patience and understanding through it all.

Dedication

This thesis is dedicated to every educator who has imparted knowledge in me and mentored me to greater heights; especially to Prof A.B Ejiwunmi whose academic career inspired mine.

1   Chapter 1: Introduction

1.1 Overview

Most pregnancies are uneventful, but sometimes complications occur such as fetal growth restriction (FGR). FGR is difficult to detect prenatally, although it may be suspected based on a combination of biochemical parameters and uterine Doppler findings (Falo, 2009). Depending on the underlying cause, it may recur in subsequent pregnancies (Ananth *et al.*, 2009; Berghella, 2007) and is associated with adverse prenatal, perinatal and postnatal sequelae.

The placenta, which in pregnancy mediates the complex interplay between the fetus and its mother, is central in the pathogenesis of many pregnancy complications, including FGR (Benirschke *et al.*, 2006b). One of the many possible problems that can arise is failure to efficiently transfer essential nutrients to the fetus. Nutrients and oxygen are conveyed from the mother to the fetus in blood flowing through placental blood vessels. Abnormalities in the structure of these blood vessels may be associated with increased vascular resistance (Mitra *et al.*, 2000), which may lead to hypoperfusion, deficient nutrient supply to the fetus, and then growth restriction (Reynolds *et al.*, 2006; Jackson *et al.*, 1995).

Following our observations of previously unidentified alterations in the feto-placental arterial vasculature of placentas from FGR complicated pregnancies (Junaid *et al.*, 2014), the overall broad objective of the work presented in this thesis was to further investigate feto-placental vascularity in FGR. Here in the first chapter is a literature review aimed to evaluate what we already know. Two studies aimed to ascertain the extent of altered vascularity in the FGR placenta are presented in the second and third chapters. A final study aimed to investigate one of the possible molecular mechanisms that may be defective during placental angiogenesis in FGR is presented in the fourth chapter.

1.2 The human placenta

1.2.1 Origin of the human placenta

In human pregnancy, implantation occurs at around 6-7th day post conception (dpc)(Benirschke and Kaufmann, 2000). The implanting blastocyst (figure 1.1) is made up of two cell groups – an outer (trophectoderm) and an inner cell mass (embryoblast) – surrounding a fluid cavity (blastocele). Placental trophoblast develops from the trophectoderm while the embryoblast forms the embryo and the extraembryonic mesoderm, amnion and umbilical cord, which connects the embryo to the placenta.
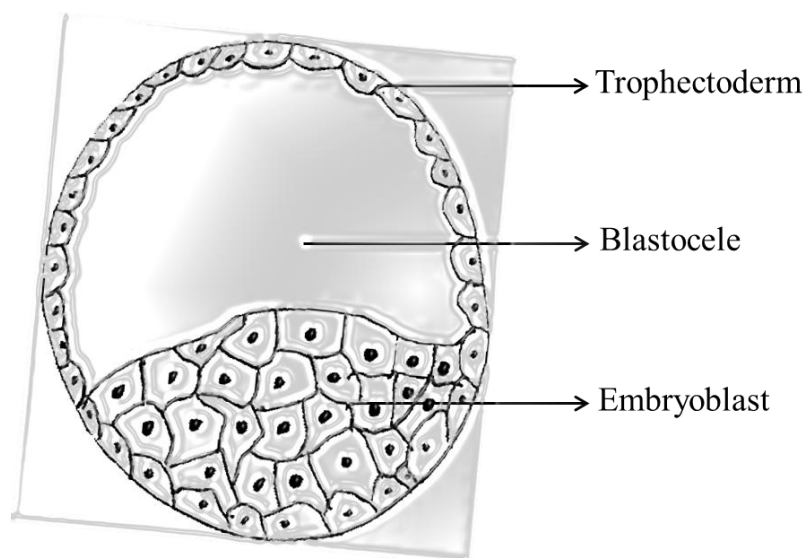
Figure 1.1: The human blastocyst.

Schematic diagram showing the cellular and non-cellular components of the human blastocyst at the time of implantation.

1.2.2 Anatomy of the human placenta

1.2.2.1 Development of the feto-placental vasculature

The human placenta is made up of two anatomically separate though physiologically continuous vascular systems – the utero-placental and the feto-placental systems. In the feto-placental system, arteries convey deoxygenated blood and waste products from the fetus to the villi while veins convey oxygenated blood from the villi to the fetus. Within the villi are fetal capillaries where exchange occurs. The utero-placental system is made up of vessels arranged to maximise the exchange of substances between the maternal blood within the intervillous space and fetal blood vessels in the villous placenta (Benirschke *et al.*, 2006c).

1.2.2.1.1 Placental villi development and vascularisation

By 13th dpc, primitive (primary) villi form from proliferation of trabeculae into the intervillous space (Benirschke and Kaufmann, 2000). At this stage, the villi are only composed of two trophoblast cell layers - a cytotrophoblast core enveloped by a layer of syncytiotrophoblast. Within few days, extra-embryonic mesenchyme from the chorionic plate invades the cytotrophoblast cell layer, transforming the villi into secondary villi. Further invasion of cytotrophoblasts by mesenchymal cells initiates the process of vascularisation within the villi. Consequently, blood vessels are seen within the villi. The villi at this stage, and all subsequent generations of villi, are referred to as tertiary.

The placenta becomes vascularised by formation of capillaries within the villi (Benirschke and Kaufmann, 2000). Mesenchyme-derived macrophages expressing angiogenic growth factors initiate vasculogenesis so that by the 21st dpc (~14th day post implantation), placental blood vessels begin to form in the tertiary villous

mesenchyme/mesenchymal villi (Arroyo and Winn, 2008; Aplin and Jones, 2008; Kaufmann *et al.*, 2004; Demir *et al.*, 2006; Demir *et al.*, 2007; Aplin *et al.*, 2015). They arise via a series of differentiation events from pluripotent mesodermal stem cells to progenitor haemangiogenic stem cells, haemangioblasts, angioblasts and finally endothelial cells (Cogle and Scott, 2004; Arroyo and Winn, 2008; Hanahan, 1997; Demir *et al.*, 2006). Once formed, endothelial cells proliferate, migrate and interact with one another, aligning into tubes which subsequently become enveloped by supporting structures (pericytes, smooth muscle, basement membrane) to form stable vessels (Beck and D'Amore, 1997; Charnock-Jones *et al.*, 2004; Arroyo and Winn, 2008; Demir *et al.*, 2006; Diaz-Flores *et al.*, 1991). This process continues until 32dpc when the vessels connect to the fetal circulation via the connecting stalk which later becomes the umbilical cord. Mesenchymal villi are slender, comprising of abundant Langhans cells, early vessels and under-developed stroma. Subsequently, they differentiate either into immature or mature intermediate villi (Benirschke *et al.*, 2006a).

By 32dpc, erythrocytes are detected and the process of vascularisation switches mainly to sprouting and non-sprouting angiogenesis within the placental villi, though some vasculogenesis is still occurring until late first trimester (Aplin *et al.*, 2015). Endothelial cells from pre-existing vessels migrate, and sprout to form new ones, filling up the expanding immature intermediate villi. This multi-stage process, sprouting/branching angiogenesis, lasts until 24 weeks gestation (Arroyo and Winn, 2008). Each immature intermediate villous comprises of ample stroma, abundant macrophages and a dense capillary network (Kingdom *et al.*, 2000; Castellucci *et al.*, 1990). Distal immature intermediate villi revert into their parent (mesenchymal villi) to sustain their generation, while proximal ones progressively metamorphose into stem villi. Within the fibrous stroma of the stem villi, centrally located capillaries differentiate into arterioles and venules while peripheral ones regress (Castellucci et al.,

1990, Kingdom et al., 2000). At this stage, between 32dpc and 24 weeks gestation, the placental circulation remains inactive and the developing embryo receives nutrients via the vitelline circulation from the yolk sac (Baron, 2003). The yolk sac is an extraembryonic membrane attached to the ventral surface of the embryo and is visible on ultrasound at as early as the 5th week of gestation (Berdahl *et al.*, 2010).

By 24 weeks, reversion of distal immature intermediate villi to mesenchymal villi stops and mesenchymal villi switch to production of mature intermediate villi while residual immature intermediate villi are incessantly converted into stem villi (Kingdom *et al.*, 2000). Histologically, mature intermediate villi possess straight elongated capillaries. These capillaries grow longer than the mature intermediate villi and subsequently form loops which further develop into highly vascularised grape-like gas-exchanging structures – the terminal villi (Kaufmann *et al.*, 1985; Kingdom *et al.*, 2000). Within the terminal villi, vessels continue to grow by another multi-stage process called non-sprouting/non-branching angiogenesis. The steps involved in non-branching angiogenesis are summarised in Auguste et al's review article on vascularisation (Auguste *et al.*, 2005). In the third trimester, terminal villi formation by non-branching angiogenesis increases, causing a massive increase in the surface area available for materno-fetal exchange to about $13m^2$ at term, with up to 25% of the entire feto-placental blood volume being within the terminal villous capillaries (Luckhardt *et al.*, 1996). This process of vessel development, as well as maturation of intermediate villi and development of new terminal villi, continues during the third trimester till term (Benirschke *et al.*, 2006a).

1.2.2.1.2 Establishment of the complete feto-placental vasculature: development of the umbilical vessels and the chorionic network of vessels

The umbilical cord derives from the connecting stalk which connects the early placenta to the embryo. Normally the mature umbilical cord houses three blood vessels – two arteries and one vein, enveloped throughout its entire length in loose connective tissue called Wharton's jelly (Standring, 2008). All three umbilical vessels are derivatives of the allantois - a site of angiogenesis that arises from the yolk sac in the 3rd week post conception, and contained in the connecting stalk (Standring, 2008). Initially, four vessels – two allantoic arteries originating from the internal iliac arteries accompanied by two allantoic veins draining into the hepatic veins – develop in the allantois (Standring, 2008). When the umbilical cord forms, the allantoic vessels become umbilical vessels. By the 7th week post conception, the right umbilical vein disappears while the left umbilical vein and both umbilical arteries persist (Wolman *et al.*, 2002; Standring, 2008). From the point of insertion of the umbilical cord on the placenta between 28 – 40th dpc, the umbilical vessels radiate and branch across the surface of the chorionic plate [now called chorionic plate vessels or specifically, chorionic plate arteries and chorionic plate veins] and into the placental core until they reach the bases of the stem villi (Benirschke and Kaufmann, 1990). Here, in the 5th week post conception, the fetal vessels meet and fuse with the locally formed villous vessels establishing the complete feto-placental vasculature (Burton, 2006; Benirschke and Kaufmann, 1990).

The two umbilical arteries are usually connected within the umbilical cord, at or near [within about 3 - 5cm above] its insertion point on the placenta, by the Hyrtl's anastomosis (Ullberg *et al.*, 2001; Raio *et al.*, 2001). Branches of each of the three umbilical vessels form a distinct tree-like network of vessels. Because of the Hyrtl's anastomosis, the two arterial trees are connected and may collectively be seen as the

"arterial tree" (though they are separable). Typically, arteries cross over veins on the chorionic plate (Wang and Zhao, 2010b), but there are no anastomoses between the chorionic networks (except in pathological situations such as twin-twin transfusion syndrome). The chorionic plate veins are all tributaries of a single umbilical vein (the persistent left umbilical vein). The direction of blood flow in these veins is towards the umbilical vein at the cord insertion point. Placental veins have no valves (Weber, 1982) and the placenta is an uninnervated organ (Reilly and Russell, 1977).

1.2.2.2   Structure of the human placenta

The structure, as well as the histological features of the human placenta varies with gestational age.

1.2.2.2.1   Gross anatomy

Early in pregnancy, the placenta is circumferentially around the embryo (figure 1.2) (Baergen, 2011b) and often does not survive undamaged following termination. It is often delivered admixed with other products of conception (decidual and embryonic or fetal tissues) and is usually identified as fine, delicate, white fragments (the immature chorionic villi) attached to shiny and translucent fetal membranes (Baergen, 2011b).

Figure 1.2: The human placenta in early pregnancy.

An intact gestational sac from early termination shows the placenta circumferentially around the embryo. Image adapted from Baergen 2011 (Baergen, 2011b).

By the third trimester, however, the components of the gestational sac are distinct and easily separable. On gross inspection, the normal human placenta at term is a round to oval disk-like organ and has a maternal unit juxtaposed with a fetal unit (Sadler, 2012). The maternal unit comprises the intervillous space and the decidua basalis while the fetal aspect comprises the umbilical cord, the chorionic plate with its prominent blood vessels (figure 1.3) and the villi. When viewed from the maternal side, the placenta has about 15 – 20 lobules (also called cotyledons) separated by visible grooves divided [formed] by septa - invaginations of the decidua (figure 1.3A). At the end of the first trimester, the placenta measures ~5cm wide, ~1cm thick and ~32g heavy while at term, the mature human placenta measures ~22cm in diameter, ~2.5cm thick and weighs 450 – 600g (Benirschke *et al.*, 2006c).
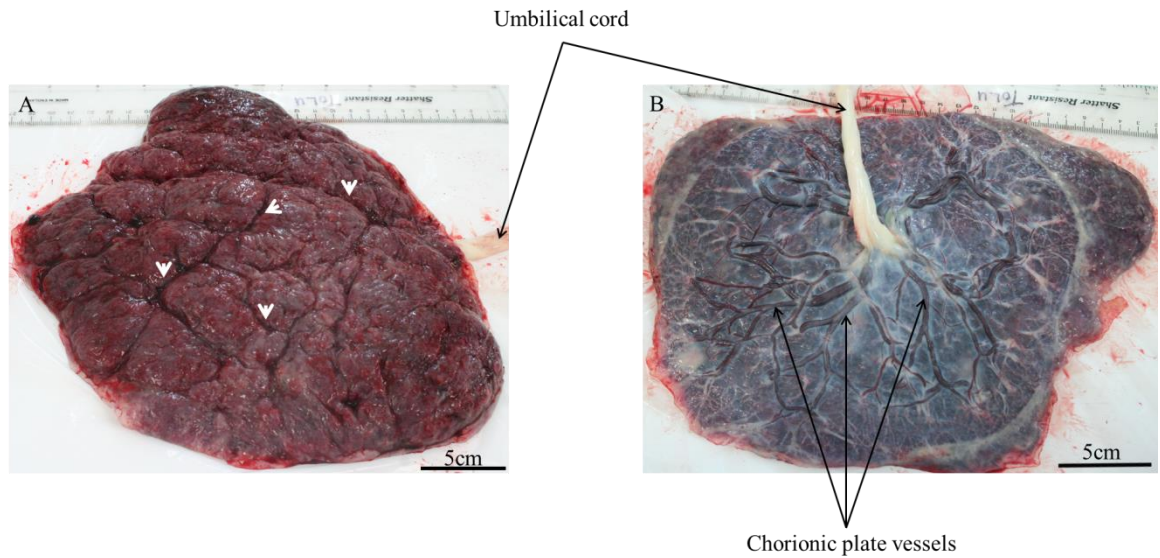
Figure 1.3: The maternal and fetal surfaces of the human placenta at term.

Visible grooves (white arrowheads in A) separate the surface into several lobules/cotyledons. The fetal surface (B) consists of the chorionic plate, on which the numerous branches of the umbilical arteries and vein (the chorionic plate vessels) run.

1.2.2.2.2 Microscopic anatomy

1.2.2.2.2.1 Histological features of the early placenta

The villi are the main structure of the placenta. By mid-first trimester, two distinct cell layers are seen - an outer layer of syncytium made up of multinucleated syncytiotrophoblasts and an inner layer of highly proliferative cytotrophoblasts (Baergen, 2011c). Together these form a thick trophoblast layer around a loose stroma which is mainly filled with connective tissue and fetal macrophages [also called Hofbauer cells] (figure 1.4A) (Lakshmi-Devi, 2013). The syncytium makes close contact with the intervillous space where maternal blood vessels are. Fetal blood vessels are absent within the villus at this age.

By the 12th week, blood vessels are visible within the stroma and, by the end of the first trimester, they would have fully grown into the central parts of the villus supported by connective tissue (figure 1.4B).
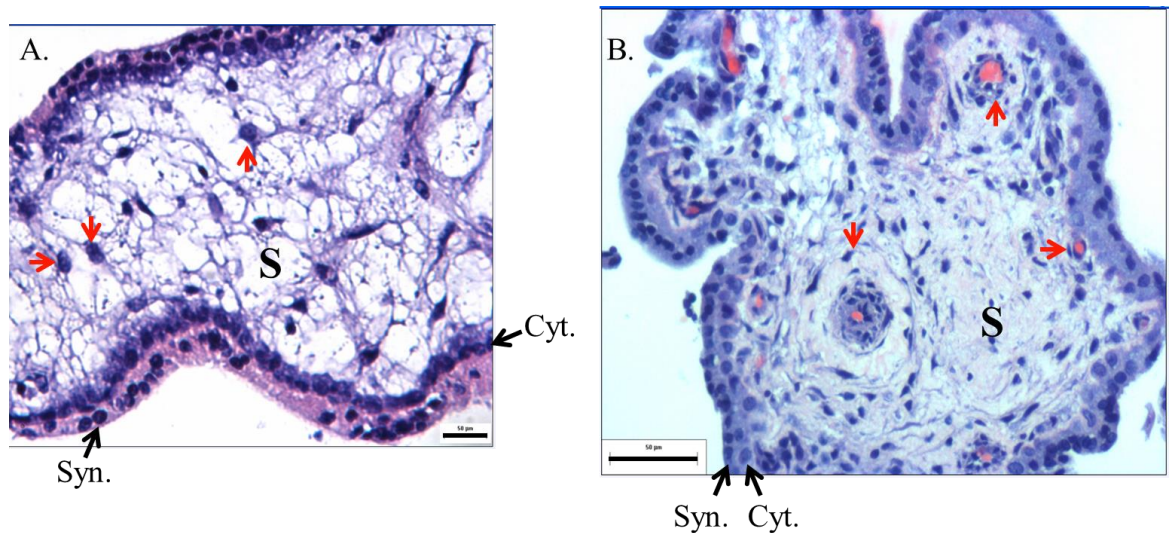
Figure 1.4: Histological features of the early placenta.

Hematoxylin and eosin-stained sections of placental tissue at 6 weeks (A) and 13 weeks (B) of gestation. Syn, syncytiotrophoblast; Cyt, cytotrophoblast; S, stroma, red arrows point to Hofbauer cells in A and blood vessels in B. Note the absence of blood vessels at 6 weeks and their presence by the 13th week. Scale is 50μm.

1.2.2.2.2.2 Histological features of the mature placenta

Ideally, placental specimens for microscopic examination are usually orientated vertically spanning the entire thickness of the tissue (Baergen, 2011c). From top to bottom, the histological features of the mature placenta are described below.

1.2.2.2.2.2.1 The chorionic plate

The chorionic plate is covered by a translucent thin sheath of amnion (figure 1.5A) which goes further to enclose the fetus (Baergen, 2011c). Underneath and closely appressed to the amnion is the more cellular chorion (figure 1.5A). Together, the amnion and chorion are referred to as the fetal membranes. On the plate are the chorionic plate vessels (arteries and veins) and underneath the plate are the villi (figure 1.5A).
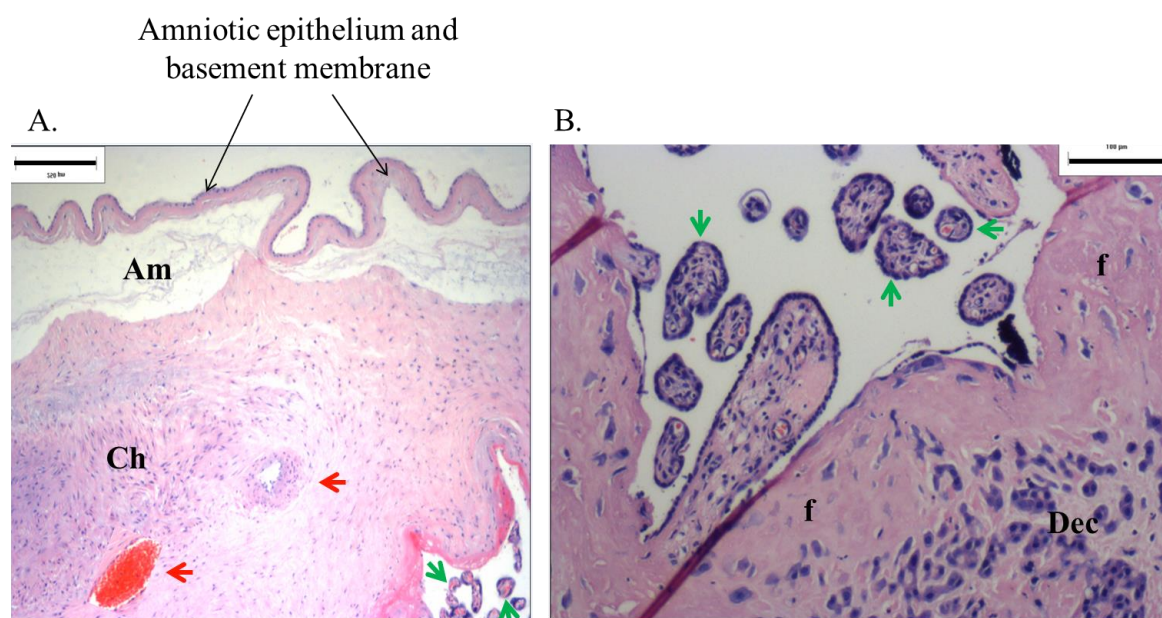
Figure 1.5: The chorionic plate and basal plate in mature placenta.

Hematoxylin and eosin-stained sections of the chorionic plate (A) and basal plate (B) of a placenta delivered at term. Am, amnion; Ch, chorion; Dec, decidua; f, fibrin; red arrows point to chorionic plate vessels (bottom arrow, vein; upper arrow, artery); green arrows point to villus structures. In A, the amnion and the chorion layers of the chorionic plate are shown, as well as few of the villi underneath the plate. In B, from top to bottom, the villi from the overlying villus tissue is seen followed by a layer of fibrin deposits lining the basal plate which comprises mainly of decidua cells. Scale is 250µm in A and 100µm in B.

1.2.2.2.2.2 The chorionic villi

The villous tissue (consisting of a tree of different types of villi) of the mature placenta is bound superiorly by the chorionic plate and inferiorly by the basal plate. Histologically, each villus is characterised by a trophoblast covering (outer syncytiotrophoblast and inner cytotrophoblast), and a stroma containing majorly blood vessels (Baergen, 2011c). As gestational age advances, the cytotrophoblast and syncytiotrophoblast layers become thinner, reducing the diffusional distance between the maternal and fetal circulations.

The largest villi are the stem villi. They are located internally, next to the inner surface of the chorionic plate and range between 150 μm to several thousand microns in luminal diameter (Benirschke *et al.*, 2006d; Baergen, 2011a). Typically, each stem villus contains a dense fibrous stroma surrounding stem vessels (Kaufmann *et al.*, 1988). The larger stem villi usually contain a pair of centrally located stem vessels (an artery accompanied by a vein) (Kaufmann *et al.*, 1988). Stem vessels vary in size and structure. Those in the larger villi measure about a third of the villus calibre and have distinct 3 – 5 layers of smooth muscle wall. The small stem villi contain varying numbers of arterioles and venules with 1 – 2 muscular layers (Kaufmann *et al.*, 1988).

Next, the stem villi branch into slender intermediate villi measuring 60 – 100μm in diameter (Benirschke *et al.*, 2006d). Unlike the stem villi, these contain a very loose stroma and slender small calibre arterioles and venules (the post-capillary venules) with poorly defined or absent muscular walls (figure 1.6) (Kaufmann *et al.*, 1988). Arteriole and venule sizes are widely variable; the smallest ones measure 20 – 40μm in diameter (Kaufmann *et al.*, 1988).

Finally, the intermediate villi branch into numerous terminal villi. These are grape-like terminal branches of the villous tree measuring 30 – 80μm (Benirschke *et al.*, 2006a).

They contain a loose stroma rich in highly coiled capillaries (Baergen, 2011c). The capillaries are bare endothelial tubes with no muscular layer (Kaufmann *et al.*, 1988). Their mean diameter range between 12 – 14μm, and they are characterised by areas of focal dilatation (sinusoids) measuring up to 50μm in diameter (Kaufmann *et al.*, 1988). The trophoblast layer is thinnest in the terminal villi such that the fetal capillaries are closer to the periphery of the villus. The cytotrophoblast joins with the syncytiotrophoblast to form a single layer of syncytial cells. This layer becomes very thin, especially near the fetal capillaries, forming the vasculo-syncytial membrane – a very thin membrane between the fetal capillaries and the maternal blood in the intervillous space (figure 1.6), improving gas and nutrient transfer between the mother and the fetus.
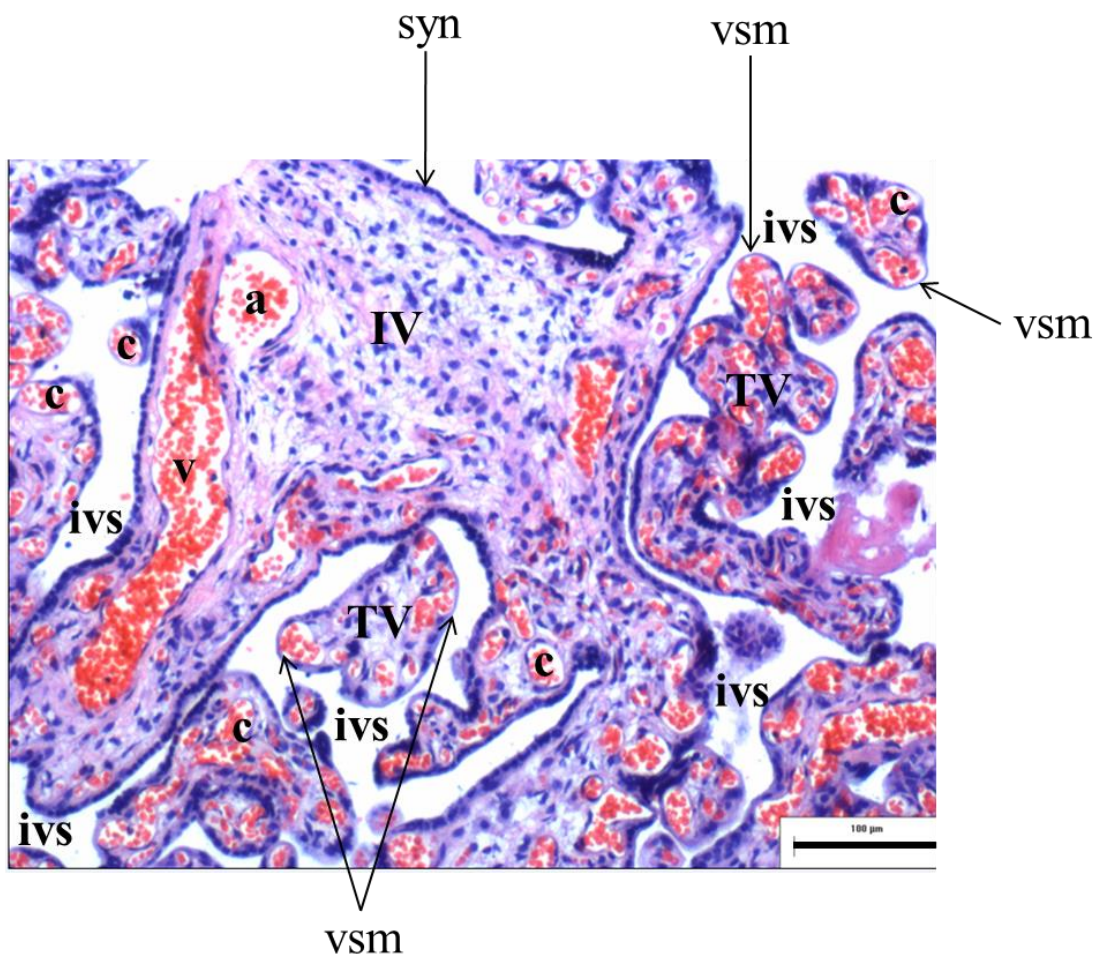
Figure 1.6: Hematoxylin and eosin-stained section of mature placental villi.

Syn, syncytiotrophoblast; vsm, vasculo-syncytial membrane; ivs, intervillous space; IV, intermediate villus; TV, terminal villus; a, arteriole; v, venule; c, capillary. The intermediate villus gives off several terminal villi. Arterioles and venules are found in the intermediate villus while the terminal villi contain the fetal capillaries. The syncytium is thin and, in the terminal villi, there is only a thin membrane (the vasculo-syncytial membrane) between the fetal capillaries and the intervillous space bringing the fetal circulation in close proximity to the maternal blood in the intervillous space to maximise exchange. Scale is 100µm.

1.2.2.2.2.2.3 The basal plate

The basal plate (figure 1.5B) is the maternal surface of the mature placenta. It is 100 – 1500µm thick and contains decidua cells from the outermost layer of the uterine endometrium as well as utero-placental vessels (spiral vessels) and fibrin (Baergen, 2011c). It therefore serves as the maternal interface to the embryo. The presence of fibrin, especially if in abundance, may suggest placenta damage due to an underlying pregnancy related pathology or complication.

1.2.3   Molecular regulation of placental vascularisation

The process of angiogenesis in the placenta is mediated by a complex interplay of growth factors, membrane-bound proteins, receptors and junctional adhesion molecules at cell-cell interactions and in the extracellular matrix. This section provides a brief review of some of the main players.

1.2.3.1   Angiogenic factors involved in placental angiogenesis

Several growth factors expressed in the human placenta (Table 1) play crucial roles in vascularisation. While some favour vessel formation and development (pro-angiogenic factors), others inhibit the angiogenic process (anti-angiogenic factors) creating an equilibrium that ensures adequate regulation of the process of angiogenesis.

1.2.3.1.1 Pro-angiogenic factors in the human placenta

1.2.3.1.1.1 The vascular endothelial growth factor (VEGF) family

In the human placenta, the VEGF family includes isoforms –A, –C, –E, –F and placental growth factor (PlGF). They are expressed in different sites within the human placenta (see Table 1), and act via specific receptors to promote endothelial cell proliferation, cell migration and vascular permeability. VEGF-A is expressed in trophoblast, macrophages and vascular smooth muscle cells (Charnock-Jones *et al.*, 2004; Vuorela *et al.*, 1997). The VEGFR-2 (kdr) receptor is specific for the VEGF-A ligand (Wu *et al.*, 2010) and expressed in the villous endothelial cells (Charnock-Jones *et al.*, 2004). VEGF-C, expressed in the decidua (Charnock-Jones *et al.*, 2004), interacts with the VEGFR-3 (flt-4) receptor which is expressed in the trophoblast (Wu *et al.*, 2010). The B and D isoforms of VEGF have not been detected in the placenta (Charnock-Jones *et al.*, 2004; Clark *et al.*, 1998).

PlGF and its receptor VEGFR-1 (flt-1), are expressed in trophoblast (Charnock-Jones *et al.*, 2004; Clark *et al.*, 1998; Vuorela *et al.*, 1997; Wu *et al.*, 2010). PlGF is biochemically and functionally similar to VEGFs (Gourvas *et al.*, 2012), both being paracrine factors performing synergistic actions in placental angiogenesis (Arroyo and Winn, 2008; Gourvas *et al.*, 2012; Beck and D'Amore, 1997; Demir *et al.*, 2006; Demir *et al.*, 2007; Hanahan, 1997; Vuorela *et al.*, 1997; Carmeliet *et al.*, 2001). PlGF interacts with VEGFR-1 to produce vessels that are more mature and stable (Vuorela *et al.*, 1997) compared to VEGF-induced vessels.

Maternal serum levels of PlGF are low in pregnancies complicated by FGR (Helske *et al.*, 2001; Wallner *et al.*, 2007; Benton *et al.*, 2016). This was suggested to be due to abundance of sVEGFR-1, a soluble form of VEGFR-1 which antagonises angiogenesis

by directly inhibiting cytotrophoblast invasion and binding to PlGF and VEGF-A to inhibit their interaction with their rightful receptors (Gourvas *et al.*, 2012).

1.2.3.1.1.2 The angiopoietin (Ang) family

Both angiopoietins, Ang-1 and Ang-2, are expressed in the placenta (Charnock-Jones *et al.*, 2004). Specifically, Ang-1 is expressed in the villous trophoblast and perivascular cells while Ang-2 is expressed solely in the villous trophoblast (see Table 1). They bind with equal affinity to their tyrosine kinase receptor Tie-2 but have different functions. Ang-1 maintains vessel integrity and plays a role in the later stages of vascular remodelling while Ang-2, a functional antagonist of Ang-1, functions to loosen cell-cell interactions and allow access to angiogenic inducers such as VEGF (Gourvas *et al.*, 2012). In other words, co-expression of Ang-2 and VEGF induces angiogenesis but Ang-2 alone results in vascular regression. Normal placental vascularisation, therefore, requires a balance in the Ang-1 to Ang-2 ratio.

1.2.3.1.1.3 Platelet-derived endothelial cell growth factor (PDGF/PD-ECGF)

PDGF is expressed in the villous stroma of the human placenta (Usuki *et al.*, 1990). It is a potent inducer of angiogenesis, signalling via two receptors (α and β) to stimulate growth and migration of endothelial cells (Bouis *et al.*, 2006; Ishikawa *et al.*, 1989). In addition, PDGF is involved in recruitment of pericytes required for stabilisation and maturation of blood vessels (Hellberg *et al.*, 2010; Gaengel *et al.*, 2009).

Table 1.1: Angiogenic growth factors, receptors and their location in the placenta

[Table adapted from (Charnock-Jones *et al.*, 2004)]

Angiogenic factors and receptors	Placental site
VEGF-A	Trophoblast, Hofbauer cells, vascular smooth muscle (Charnock-Jones *et al.*, 2004; Vuorela *et al.*, 1997)
VEGF-B	None detected (Charnock-Jones *et al.*, 2004)
VEGF-C	Decidual natural killer cells (Charnock-Jones *et al.*, 2004)
VEGF-D	None detected (Charnock-Jones *et al.*, 2004; Clark *et al.*, 1998)
PlGF	Trophoblast (Clark *et al.*, 1998; Vuorela *et al.*, 1997; Charnock-Jones *et al.*, 2004)
FGF-1 and FGF-2	Trophoblast and vascular smooth muscle (Charnock-Jones *et al.*, 2004; Shams and Ahmed, 1994; Ferriani *et al.*, 1994)
PDGF	Villous stroma (Usuki *et al.*, 1990)
Ang-1	Villous trophoblast and perivascular cells (Charnock-Jones *et al.*, 2004)
Ang-2	Villous trophoblast (Charnock-Jones *et al.*, 2004)
VEGFR-1 (flt-1): specific receptor for VEGF-B and PlGF ligands **(Wu *et al.*, 2010)**	Villous endothelial cells and trophoblast (Charnock-Jones *et al.*, 2004)
VEGFR-2 (kdr): specific receptor for VEGF-A ligand **(Wu *et al.*, 2010)**	Villous endothelial cells (Charnock-Jones *et al.*, 2004)
VEGFR-3 (flt-4): receptor for VEGF-C and VEGF-D ligands. Primarily mediates lymphangiogenesis **(Wu *et al.*, 2010)**	Trophoblast (Charnock-Jones *et al.*, 2004)
Tie-2: receptor for Ang-1 ligand	Villous endothelial cells and trophoblast (Charnock-Jones *et al.*, 2004)
Soluble VEGFR-1	Trophoblast (Charnock-Jones *et al.*, 2004)

1.2.3.1.1.4 The fibroblast growth factor (FGF) family

The FGF family is an eighteen member group of cytokines (Beenken and Mohammadi, 2009) which act via interaction with four receptors FGFR1-4. The FGF-1 (acidic FGF) and FGF-2 (basic FGF) are involved in fetal growth and development. FGF-1 and -2 are co-localised in first trimester cytotrophoblast cells and extravillous trophoblast and in the endothelial cells and smooth muscle cells of placental vessels by term (Shams and Ahmed, 1994; Ferriani *et al.*, 1994), suggesting a role in angiogenesis (Hamai *et al.*, 1998).

1.2.3.1.2 Anti-angiogenic factors in the human placenta

Anti-angiogenic agents are factors that inhibit the process of angiogenesis (Nyberg *et al.*, 2005). They have been extensively studied in tumorigenesis and include many matrix and non-matrix-derived factors that have been documented to play pivotal roles in the abnormal vascularisation seen in cancer cells (Hanahan and Folkman, 1996; Nyberg *et al.*, 2005; Colorado *et al.*, 2000). Some, such as endoglin, thrombospondin-1 (THBS-1 or TSP-1) and vascular endothelial growth factor receptor-1 (VEGFR-1; also known as flt-1, meaning fms-like tyrosine kinase-1) are expressed in the trophoblast cells of the placenta (Charnock-Jones *et al.*, 2004).

VEGFR-1 antagonises VEGF and PlGF resulting in endothelial cell dysfunction which interestingly can be corrected by exogenous administration of VEGF and PlGF (Maynard *et al.*, 2003). Endoglin, being a receptor for transforming growth factor beta 1 (TGFβ1), inhibits angiogenesis by impairing TGFβ1 signalling, the multifunctional cascade known to play prominent roles in the induction of angiogenesis (Jeyabalan *et al.*, 2008). Likewise, TSP-1 elicits signalling events that lead to programmed death in vascular endothelial cells (Volpert, 2000).

Several studies have linked changes in maternal serum concentrations of the soluble forms of endoglin (sENG) and VEGFR-1 (sVEGFR-1) to pregnancy complications such as preeclampsia and FGR (Jeyabalan *et al.*, 2008; Zhao *et al.*, 2010; Chaiworapongsa *et al.*, 2013; Ramma *et al.*, 2012; Petrozella *et al.*, 2012; Padavala *et al.*, 2006). Since both pregnancy complications are known to be associated with fetoplacental vascular pathologies, it is likely that the anti-angiogenic factors play a role in the disordered placental vascularisation associated with FGR and preeclampsia.

1.2.3.2 Signalling mechanisms involved in regulation of placental angiogenesis

1.2.3.2.1 The mitogen-activated protein kinase (MAPK) pathways

The protein kinases in the MAPK pathways induce signal transduction cascades involved in regulation of differentiation, proliferation and death of cells (Chen and Zheng, 2014). In the placenta, activation of the MAPK cascades regulates angiogenic responses *in vitro* i.e. endothelial cell proliferation, migration and tube formation by stimulating cellular responses to VEGF and FGF (Zheng *et al.*, 2008; Liao *et al.*, 2010; Feng *et al.*, 2012a; Feng *et al.*, 2012b). In knockout mice models, deficiency of specific protein kinases of the MAPK pathways have been shown to be associated with severe placental defects including poor vascularisation (Mudgett *et al.*, 2000; Okada *et al.*, 2007).

1.2.3.2.2 The endothelial nitric oxide synthase (eNOS) pathway

eNOS is the major isoform of nitric oxide synthase responsible for increased placental nitric oxide (NO) production during pregnancy (Zheng *et al.*, 2000; Myatt *et al.*, 1997). Placental NO is critical for vasodilation and angiogenesis at the maternal-fetal interface.

NO enhances angiogenesis by stimulating VEGF and FGF effects on villous endothelial cells (Cooke, 2003; Fukumura *et al.*, 2001). In addition, being a potent vasodilator, NO regulates feto-placental vascular resistance (Wareing *et al.*, 2005; Wareing *et al.*, 2002) and is a major player in the pathogenesis of pre-eclampsia (Leiva *et al.*, 2016). eNOS-/-mice are also known to have small pups (Kusinski *et al.*, 2012).

1.2.3.2.3 The NOTCH and the Wingless-related integration site (WNT) signalling pathways

NOTCH and *WNT* genes are transcriptional regulators of angiogenesis in humans. Notch signalling regulates endothelial cell proliferation and migration in angiogenesis (Phng and Gerhardt, 2009). When activated in the placenta, notch upregulates VEGFR-1 thereby increasing endothelial cell sensitivity to PlGF, stimulating vessel maturation and stability. In addition, notch activates WNT signalling in proliferating endothelial cells during branching angiogenesis (Phng *et al.*, 2009). When activated, WNT signal transduction promotes organisation and stabilisation of junctional adhesion molecules aiding endothelial cell-cell interactions during tube formation (Dejana, 2010). The WNT signalling pathway and its role in human placental vascularisation is discussed and investigated further in Chapter 4.

1.2.3.3 Oxygen effects on placental angiogenesis

Until the 10th week of gestation, the partial pressure of oxygen in the placenta's environment is as low as 17.9mmHg (Rodesch *et al.*, 1992; Aplin, 2000; Kingdom and Kaufmann, 1997; Wang and Zhao, 2010a). Early villi development and vascularisation therefore occurs at low oxygen tensions. However, as pregnancy advances, the partial pressure of oxygen progressively increases, reaching about 39.6mmHg by 12-13 weeks

gestation when flow is established to the placental bed. This increase triggers trophoblast invasion and remodelling of uterine spiral arteries (Rodesch *et al.*, 1992) to maximise utero-placental blood flow and ensure transfer of adequate concentration of oxygen to the developing fetus via the formed placental blood vessels. Fetal hypoxemia may result from failure of these physiological changes, and has been associated with complicated pregnancies, including FGR (Kingdom and Kaufmann, 1997; Pardi *et al.*, 1993).

Oxygen regulates expression of angiogenic factors and their interaction with their receptors. For instance, in human trophoblasts exposed to hypoxia, expression of VEGF was significantly higher and expression of PlGF lower than in trophoblasts cultured in normoxic conditions (Shore *et al.*, 1997; Groesch *et al.*, 2011).

The effects of oxygen on placental vascularisation and fetal growth are thought to be mediated by the transcription factor hypoxia-inducible factor (HIF) (Gourvas *et al.*, 2012). The HIF (1α, 1β, 2 and 3) are regulatory factors widely expressed throughout gestation in the syncytiotrophoblast, cytotrophoblast, and fetoplacental vasculature (Rajakumar and Conrad, 2000). They, however, have amplified action in early pregnancy when the partial pressure of oxygen is low, functioning to upregulate the expression of many genes vital for angiogenesis such as VEGF and erythropoietin (Patel *et al.*, 2010).

1.3   Pregnancy complications characterised by abnormal placental vascularity

Placental abnormalities, including defective placental vascularity, play key roles in the aetiopathogenesis of many adverse outcomes of pregnancy such as diabetes in pregnancy, pre-eclampsia, fetal growth restriction, early trimester loss and stillbirth. For example, placentas from pregnancies complicated by maternal diabetes are typically

hypervascularised (Lassance *et al.*, 2013; Jauniaux and Burton, 2006; Mayhew, 2002; Mayhew *et al.*, 1994) probably due to prolonged fetal hyperinsulinemia (Lassance *et al.*, 2013). Placental vascularity is however impoverished in pregnancies complicated by pre-eclampsia (Narasimha and Vasudeva, 2011; Plasencia *et al.*, 2015), pre-term delivery (Amir *et al.*, 2009), stillbirth (Ptacek *et al.*, 2016; Warrander *et al.*, 2012) and FGR (Junaid *et al.*, 2014; Chen *et al.*, 2002). Findings of further investigations on placental vascularity in FGR complicated pregnancies are presented in this thesis.

1.3.1 Fetal growth restriction

Fetal growth restriction (FGR), formerly called 'intrauterine growth restriction', is a serious obstetric complication resulting in impaired fetal growth velocity. Ultimately, this prevents the fetus from attaining its genetically endowed growth potential (Cox and Marton, 2009), manifesting clinically as estimated fetal weight or birth weight below the expected based on individualised growth assessments (Deter *et al.*, 2016).

Growth restricted fetuses are predisposed to several grave complications before, during and after birth. According to the ReCoDe system for classification of stillbirth by relevant condition at death, FGR is the single largest pathology associated with fetal death (Gardosi *et al.*, 2005). Of the 2,625 stillbirth cases considered in the population based cohort study over a seven year period, up to 43% of fetal deaths were linked to FGR. Those who survive are more likely to be born prematurely (Lackman *et al.*, 2001; Engineer and Kumar, 2010; Carreno *et al.*, 2011), by Caesarean section (Petersen *et al.*, 2009; Mullin, 2010) and are at increased risk of intrapartum asphyxia (Mullin, 2010), perinatal morbidity and/or death (Lackman *et al.*, 2001; Petersen *et al.*, 2009), childhood neurodevelopmental problems (Jarvis *et al.*, 2003; Edmonds *et al.*, 2010), and

metabolic as well as cardiovascular disorders later in life (Hales and Barker, 1992; Barker, 1995).

FGR is prevalent worldwide. According to the World Health Organisation (W.H.O), the prevalence of FGR varies widely among countries, complicating at least 5% of pregnancies in developed countries and significantly more (up to 40%) in developing countries (Kelly *et al.*, 1996).

Unfortunately, early prenatal diagnosis has remained challenging as fetal growth velocity naturally depends on several factors like parental size, race, parity, birth order, birth weight of previous babies, fetal gender and altitude (Mamelle *et al.*, 2006; Wills *et al.*, 2010; Tan *et al.*, 2004; Kinzler and Vintzileos, 2008; Gardosi *et al.*, 1992). Hence, there is no single universally adopted cut-off centile for diagnosis, the most popular in many centres being the 3rd, 5th or 10th centile. The lower the adopted centile, the lower the chances of having small-for-gestational-age babies (babies who are constitutionally but not pathologically small) misdiagnosed as being growth restricted but some true FGR cases may be missed. To address this overlap, birth centiles as well as abnormal umbilical artery Doppler velocimetry are usually considered when diagnosing FGR, although umbilical artery Doppler may be normal in some FGR cases.

The pathogenesis of FGR is complex. Fetal growth may be impaired by maternal, fetal or environmental factors (see table 1.2) (Peleg *et al.*, 1998; Bamfo and Odibo, 2011), but many cases are identified or suspected to be linked to placental abnormalities and consequent insufficiency (Warrander *et al.*, 2012). Placental insufficiency refers to a process associated with decrease in function of the placenta and consequent suboptimal transfer of nutrients to the growing fetus (Gagnon, 2003), resulting in complications such as FGR. Functions of the human placenta are listed in table 1.3. The impairment in placental function is detectable as abnormal umbilical artery waveforms on Doppler ultrasound (Harman and Baschat, 2003), reflecting elevated vascular resistance and

reduced blood flow through the fetal placental vessels in severe, early-onset FGR (Mitra *et al.*, 2000; Todros *et al.*, 1999; Jackson *et al.*, 1995).

Currently, there is no treatment to reverse FGR *in utero*. For affected pregnancies, management involves thorough prenatal surveillance to monitor the progression and severity of growth compromise as well as identify the appropriate time for delivery, which in severe cases, may be before the pregnancy attains full term.

Table 1.2: Etiological factors associated with fetal growth restriction

Causes of FGR (Peleg *et al.*, 1998; Bamfo and Odibo, 2011)

Maternal factors

- Chronic diseases: hypertension and other heart diseases, diabetes mellitus, chronic renal disease, protein-calorie malnutrition, autoimmune disorders, hemoglobinopathies, coagulopathies.

- Pregnancy complications: pre-eclampsia, gestational diabetes.

- Hormonal imbalance: growth hormone, thyroxine, parathyroid hormone, calcitonin, insulin.

- Smoking, substance and alcohol abuse.

- Medications: steroids, phenytoin, warfarin.

- Uterine disorders: malformations, intrauterine masses such as fibroids.

- Intrauterine infections: toxoplasmosis, cytomegalovirus, rubella, syphilis.

Fetal factors

- Multiple gestation.

- Twin-twin transfusion syndrome.

- Genetic and chromosomal abnormalities: Trisomies, Triploidy, family history.

- Congenital anomalies.

Placental factors

- Placental insufficiency.

- Placental anomalies: abnormal vascularisation, chronic abruption, infarction.

- Umbilical cord anomalies and accidents.

Environmental factors

- Hypoxia: following prolonged maternal exposure to high altitude.

Other: Idiopathic.

Table 1.3: Functions of the human placenta

Functions of the placenta (Gude *et al.*, 2004)
Transport and metabolism • Exchange and transfer of respiratory gases (oxygen and carbon dioxide) between the maternal and fetal circulations. • Materno-fetal absorption, metabolism and transport of nutrients necessary for fetal growth and development: water, proteins, amino acids, glucose, lipids, vitamins, minerals.
Endocrine • Production of several hormones and growth factors necessary for sustenance of pregnancy, and regulation of its own as well as fetal growth and development: placental lactogen, progesterone, oestrogen, chorionic gonadotrophin (hCG), growth hormone, insulin-like growth factor, epidermal growth factor. • Production of hormones necessary for initiation of labour at term: eicosanoids (prostaglandins and related compounds), chemokines, cytokines.
Excretion • Removal of carbon dioxide and other wastes from the fetus.
Protection • Able to prevent passage of some toxic substances from the maternal system to the fetus e.g xenobiotic molecules, microorganisms such as viruses. • Protects the fetus from antigen attack from the maternal system.

1.3.1.1 Feto-placental vascularity in FGR

An FGR fetus is most often accompanied by a defective placenta. Gross placental morphological abnormalities immediately noticeable at birth include small size, bizarre shape and anomalous cord insertion (Biswas and Ghosh, 2008). Placentas from FGR complicated pregnancies are likely to weigh less than those from gestational-age-matched uncomplicated pregnancies (Junaid *et al.*, 2014; Biswas and Ghosh, 2008; Mardi and Sharma, 2003), have elliptical rather than circular shape (Junaid *et al.*, 2014) and are more likely to have an eccentrically, marginally or even velamentously positioned cord (Biswas and Ghosh, 2008).

The other aberrant morphological feature of these placentas involves the vasculature. The chorionic plate of placentas from pregnancies complicated by FGR was described by Ullberg as "displaying a lower grade of complexity of arterial trees" (Ullberg, 2003) when he compared them with normal placentas using angiography and fractal dimension analysis techniques. Indeed, our recent study of the feto-placental vasculature by corrosion casting and histological techniques concurs with this view (Junaid *et al.*, 2014). In one aspect of the study, we compared the number of chorionic arterial branches in normal and FGR placental arterial casts and found significantly fewer branches in the FGR casts suggesting that the arteries branch less as they ramify across the chorionic plate. Not only that, first order branches in FGR casts were longer than similar branch order arteries in normal casts, and there were only ≤5 branch orders in FGR casts. In other words, arteries in FGR tend not to ramify far enough to reach the periphery of the placenta. In another aspect of the study, we quantified and compared villi vascularity in normal and FGR placentas using stereological approach. Stereology allows for extraction of three-dimensional information from two-dimensional sections permitting quantitative estimation of features of geometrical structures using sampled information (Dockery and Fraher, 2007; Mayhew and Lucocq, 2015). We found

significant hypovascularity in FGR placental villi. The hypovascularity was particularly worse in villi from the periphery of the FGR placentas suggesting differential vascularity in the organ. This interesting discovery, observed in the chorionic plate arteries as well as in the villi vessels, corroborates the findings from other studies of the placental vasculature, and may be a reflection of the decreased number and poor branching of the vessels. Using immunohistochemistry, Chen and colleagues reported abnormalities in the villous morphology including the number, area, structure and branching of peripheral villous capillaries (Chen *et al.*, 2002). In their study of cross sections of intermediate villi and terminal villi obtained from normal and FGR placentas, significant reductions were observed in the quantity of villi per unit placental cross-sectional area, number of capillaries per villous cross-section and capillary area to stromal area ratio of FGR samples. Likewise, many of the villi and capillaries lacked the usual looping, suggesting impoverished branching and vascularisation.

Similar alterations, including reduced volume density and surface area, sparse loops, longer, less branched and less coiled villi capillaries, were observed on electron microscopy of villi casts/profiles in placentas from preterm pregnancies complicated by FGR with abnormal umbilical artery Doppler waveforms (Mayhew *et al.*, 2004; Hitschold *et al.*, 1993; Krebs *et al.*, 1996; Todros *et al.*, 1999). In addition, *in vivo* placental volume and vascular indices were significantly reduced in FGR complicated pregnancies assessed by 3D power Doppler ultrasound (Abule *et al.*, 2016; Artunc Ulkumen *et al.*, 2015; Luria *et al.*, 2012; Noguchi *et al.*, 2009; Pomorski *et al.*, 2012).

Together, these evidences strongly suggest significant alterations in angiogenesis and consequent structural alterations in the FGR placental vasculature leading to a state of dysvascularity (abnormal vascularity). Currently, the evidences suggest the possibility of panhypovascularity – a state characterised by reduced vascularity at every vascular level, involving the arteries, veins, arterioles, venules and capillaries. Although existing

evidence on chorionic plate arteries and villous capillaries are in support of this hypothesis, the chorionic plate veins, arterioles and venules are still poorly studied.

1.3.1.2 Potential causes of defective vascularisation in the FGR placenta

There have been a few evidence based propositions, but the precise mechanism by which vascularisation becomes altered in the FGR placenta is still unknown. Being a heterogenous condition with multifactorial aetiopathogenesis, it is likely that the disordered placental vascularisation associated with FGR is also multifactorial.

Abnormal rotation of the blastocyst such that the embryonic and implantation poles are not aligned during implantation as early as 6dpc is possibly the earliest antecedent of abnormal placental morphology (Benirschke and Kaufmann, 2000) and consequent abnormal vascularisation. Consistent with this hypothesis of altered placental vascularisation originating early in development, morphologic changes such as abnormal shape and cord positions were seen in first trimester FGR placentas at 11 weeks gestation (Salafia *et al.*, 2012) and were found to correlate inversely with chorionic vascular surface density at delivery (Salafia *et al.*, 2012; Yampolsky *et al.*, 2009). In other words, the farther the cord inserts away from the centre during development, the poorer the chorionic vascular coverage at term. In the same vein, some researchers of the placental microvasculature have suggested the reduced villi vascularity associated with FGR to be developmental, following defects in the process of vascularisation very early in pregnancy (Macara *et al.*, 1995; Hitschold *et al.*, 1993; Jackson *et al.*, 1995). However, a few others have argued for vascular regression due to increased vessel fibrosis, atrophy and apoptosis following insults like hypoxia and upstream causes like thrombosis or infarction in the FGR placenta (Giles *et al.*, 1985; Fok *et al.*, 1990; Salafia *et al.*, 1997; Benirschke *et al.*, 2006b). Both the developmental

and the regression arguments are sound; disordered vascularity may arise *ab initio* from developmental defects, during the course of pregnancy from vascular regression and there may be a combination of both.

Another potential mechanism may be problems arising from molecular dysregulation of placental angiogenesis. The molecular mechanisms regulating placental angiogenesis, as well as the numerous factors involved, have been discussed in the sub-sections of section 1.2.3. Altered vascularisation may follow a loss of the physiological angiogenic equilibrium between pro- and anti-angiogenic factors, such that there is a tilt against angiogenesis (Nyberg *et al.*, 2005). This disruption in angiogenic balance could result from deficiency or inefficiency of pro-angiogenic factors and/or over-expression of anti-angiogenic factors in the placenta. Endothelial cells express receptors for the various angiogenic factors and signalling mechanisms required for their growth, proliferation, migration, tube formation and development into functional vessels (Demir *et al.*, 2006; Charnock-Jones *et al.*, 2004). Whether these cells are deficient, or express deficient or abnormal receptors or perhaps respond abnormally to angiogenic factors in the FGR placenta is still unknown. There is a wealth of literature on several investigations of most of these mechanisms and factors and how they alter human placental angiogenesis and vascularity; however, very little attention has been paid to WNT signalling. In this thesis, the behaviour of placental endothelial cells in the face of disrupted WNT signalling is reported in chapter 4. A detailed background on how abnormal WNT signalling may cause defective vascularisation is documented in the sub-sections of section 4.1.

1.4   Summary

The placenta is crucial for success of pregnancy and adequate fetal growth. It ensures efficient materno-fetal transfer of nutrient-rich blood through its blood vessels.

The placental vasculature develops by two distinct processes – vasculogenesis and angiogenesis – by progressive differentiation of vascular progenitors in the placental villi (Cogle and Scott, 2004; Arroyo and Winn, 2008; Hanahan, 1997; Demir *et al.*, 2006). These processes are initiated and modulated by several factors such as oxygen concentration, angiogenic factors, and receptors acting via various signalling pathways (Zheng *et al.*, 2008; Phng and Gerhardt, 2009; Cooke, 2003; Charnock-Jones *et al.*, 2004; Gourvas *et al.*, 2012). Stability of formed vessels is ensured by adequate perivascular structures such as the pericytes (Diaz-Flores *et al.*, 1991), a molecular balance between pro- and anti-angiogenic factors (Nyberg *et al.*, 2005), and regulation of signalling pathways involved in maintenance of endothelial cell-cell interactions.

Evidence has shown increased likelihood of alterations in placental vasculature to be associated with FGR. These alterations include reduction in number of vessels (Junaid *et al.*, 2014; Chen *et al.*, 2002), which is worse in the periphery of the placenta suggesting differential vascularity in the FGR placenta (Junaid *et al.*, 2014), impoverished branching (Junaid *et al.*, 2014; Krebs *et al.*, 1996), and loss of capillary looping in the villi (Krebs *et al.*, 1996). These findings suggest that the FGR placenta may be panhypovascular, although there is still limited evidence on veins and intermediate vessels.

Alterations in placental vascularisation may follow various mechanisms as discussed in section 1.3.1.2. Currently, therapeutic measures for FGR have been largely unsuccessful suggesting that these measures are not addressing the underlying mechanisms involved in the pathology. In the bigger picture, one of the outcomes of this project is to identify

whether enhancing vessel growth and development is an appropriate therapeutic consideration for FGR. However, it is important to first confirm whether the FGR placenta is panhypovascular and also investigate a candidate etiological factor that may underlie altered placental vascularity in FGR, as this may point to potential areas for more appropriate interventions.

1.5   Hypothesis, aims and research questions addressed in this thesis

We hypothesise that the placenta may be panhypovascular in FGR due to failed angiogenesis; and enhancing angiogenesis in the placenta may improve fetal growth.

The two main research questions addressed in this thesis are:

1.   Is the FGR placenta panhypovascular?

2.   Can angiogenesis be induced or enhanced to improve placental vascularity?

The overall aim of the studies in chapters 2 and 3 was to answer the first research question, while the study in chapter 4 was designed to address the second question. The specific aims of each study are stated in the corresponding chapter.

2   Chapter 2:   Holistic examination of the human placental vascular tree

reveals novel alterations associated with fetal growth restriction

2.1 Background

Successful development of the fetoplacental vasculature is essential to sustain healthy pregnancy. The feto-placental vessels are crucial for efficient materno-fetal transfer; hence they play a pivotal role in the pathogenesis of FGR. As discussed in chapter 1, there are evidences of the possibility of feto-placental panhypovascularity in FGR, though this is still inconclusive as feto-placental veins and intermediate vessels (the arterioles and venules) have been poorly studied. In the human placenta, the vessels that make up the feto-placental vasculature form two distinct tree-like networks – one arterial and the other venous (see details in Chapter 1). Although there are few reports of differences in the 'complexity' of some parts of these networks in FGR placentas (Ullberg, 2003), information on the entirety of both networks is lacking. A possible reason for this may be methodological. Many methods used to study feto-placental vessels do not take the entirety of the vasculature into account. For example, histology or electron microscopy studies have relied on random small samples, thus failing to reveal full network connectivity. Moreover, histology has been shown to be unreliable for interpretation of the three-dimensional (3D) structure of placental trees (Haeussner *et al.*, 2015). Each feto-placental vascular tree is a complex 3D entity with multiple branches and branch points/nodes. Due to the 3D nature, quantitative morphometry of the feto-placental trees requires 3D analysis like in other naturally occurring branching systems (Barker *et al.*, 1973).

Extraction of holistic information on the placental vascular network with intact connectivity is necessary to identify disease-associated changes [that are likely to be] of functional significance. For example, autism has been associated with changes in the 3D structure of dendritic trees and connectivity of neurones (Foldy *et al.*, 2013). As there are variations in vascularity of samples from different regions of the placenta (Junaid *et al.*, 2014), evaluation of the whole organ would better represent its entire vascularity.

To date, whole organ examination and quantification of the placental vascular tree remains an experimental challenge. As recently shown, corrosion casting of placental vessels permits 3D examination and quantification of the vessels (Junaid *et al.*, 2014; Gong *et al.*, 2011), but the small calibre vessels of the chorionic villi are difficult to quantify accurately from casts by direct measurement. Also, while the villous vessels are accessible by histology, 3D reconstruction analyses of histological sections limit obtainable data to small tissue samples hence do not represent the vascularity of the whole organ.

The aims of this study were

i.   To devise an effective and detailed technique for three-dimensional analyses of human placental vessels.

ii.   To apply the technique in the comparison of placental vessel networks in normal and fetal growth restriction (FGR) complicated pregnancies.

The problem was addressed using a combination of corrosion casting and microcomputed tomography (micro-CT) imaging to achieve a full account of placental vascular morphology. Micro-CT imaging permits 3D identification, reconstruction and quantification of anatomical trees. In animal studies, it has provided a detailed view of the kidney (Sled *et al.*, 2004; Bentley *et al.*, 2002), heart (Jorgensen *et al.*, 1998), brain (Vasquez *et al.*, 2011) and placental vasculature (Rennie *et al.*, 2007). To our knowledge the technique has yet to be used in the study of the human placental vascular tree in its entirety. Having performed micro-CT on vessel casts derived from human placentas we then went on to compare arterial and venous vessel networks in placentas from uncomplicated pregnancies and pregnancies complicated by fetal growth restriction (FGR) as case study. The study included examination of both the arterial and the venous networks of the human placenta.

2.2 Materials and methods

2.2.1 Specimen preparation

All placentas were obtained from women who delivered at St. Mary's Hospital, Manchester, United Kingdom, under Biobank ethical approval (REC 08/H1010/55). Informed consent was obtained prior to delivery and normal and FGR placentas were obtained within 30 minutes of delivery. FGR was defined as individualized birth ratio (IBR) $\leq 5^{th}$ centile (Table 1). Before imaging, all samples were processed in the Maternal and Fetal Health Research Centre Laboratory, Manchester, with appropriate licence for handling human tissue. Micro-CT imaging and Avizo analyses were performed in the Henry Moseley X-ray Imaging Facility, Manchester. Analyze analyses was performed in the Wolfson Molecular Imaging Centre, Manchester.

2.2.2 Pre imaging processing: Corrosion casting

The fetal membranes were trimmed off each placenta before weighing the placental disc. The umbilical cord was not trimmed off because it was required for vessel cannulation prior to corrosion casting. The fetal and maternal sides of each placental disc were photographed. Placental surface area (PA) was determined by uploading a photograph of each placental disc on Image Pro Plus software (Media Cybernetics Inc, USA) and tracing out an outline of the disc. The software computed the surface area for each outline.

The fetoplacental vasculature was perfused with a radiopaque methylmethacrylate-based casting material [Batson's No.17, Anatomical Corrosion Kit (Polysciences Inc, Germany)] as described in published corrosion casting protocols (Leiser *et al.*, 1997; Gordon *et al.*, 2007b; Junaid *et al.*, 2014). The cord was clamped immediately after

delivery to ensure the vessels remained dilated. For preparation of venous casts, the umbilical vein was cannulated within the cord, while for arterial casts, one of the umbilical arteries was cannulated (ahead of the Hyrtl's anastomosis, about 5cm before cord insertion) using a 20G cannula held in place with a suture. The two umbilical arteries are connected by the Hyrtl's anastomosis near the cord insertion in most human placentas (Ullberg *et al.*, 2001; Raio *et al.*, 2001). Therefore, cannulating one of the arteries ahead of the anastomosis permitted flow of perfusate into both arteries. About 20ml of 5000iu/L heparin in pre-warmed phosphate buffered saline (PBS) was infused to prevent intravascular coagulation. The PBS had been warmed to promote flow-mediated vasodilation. After 10 minutes, freshly prepared casting material (at room temperature) was manually injected through the cannula until back pressure prevented further injection. The cord was then clamped below the point of cannulation, to prevent leakage of the polymer. The placenta was left overnight on a polythene sheet on ice to lower the temperature, allowing polymerisation to occur at a more uniform rate. The following day, the whole cast placenta was immersed in 500ml of 20% w/v potassium hydroxide (KOH; Fisher Scientific, Lutterworth, UK) within a gasket-sealed tub in a water bath at 40°C. KOH solution was changed 6 hourly until the tissue was completely corroded. The solution was then replaced with distilled water for 6 hours to rinse off the KOH. The rinsed cast was air dried and photographed. A total of 12 normal (6 arterial, 6 venous) and 12 FGR (6 arterial, 6 venous) vascular casts were included in the study.

2.2.3   Image acquisition and processing

The principle of micro-CT imaging is illustrated in figure 2.1. 3D datasets were acquired for each cast using a high resolution micro-CT machine (Nikon metris XTH225, Nikon Metrology NV) fitted with a 225/320keV x-ray CT source, a rotating stage and a 2000 x 2000 Perkin Elmer detector, and controlled by Nikon's Inspect-X

software. The x-ray source was a microfocus tube emitting x-rays in cone beam geometry. The vessel cast, placed on the stage, was rotated over 360° at angular increments of 0.2° around the vertical axis with the whole cast within the field of view as scanning was performed with the x-ray source voltage set to 42kV. Maximum magnification and exposure time varied depending on each specimen's circumference, which had to be within the cone beam of irradiation. About 2000 slice views were generated for each cast. CT data acquired by Inspect-X were received via an application (CT Agent, Metris, UK) which wrote the files to disk, synchronising them with reconstruction software (CT Pro 2.0, Metris, UK). Reconstructed voxel sizes were in the range 0.08 to 0.1mm depending on the size of the cast. Vessels below 100μm in diameter were excluded from the analysis to be consistent across samples. The contrast to noise ratio of the CT data was sufficient to enable vessels down to 100μm diameter to be segmented automatically. Following 3D reconstruction of the CT projections into a single volume 3D virtual object on CT Pro, a MATLAB (MathWorks, Massachusetts, USA) algorithm was used to export the data into *.hx* and *.tiff* format compatible with volume rendering in Avizo (Avizo 8.0, FEI Visualization Sciences Group, Konrad-Zuse-Zentrum fur Informationstechnik Berlin (ZIB) and FEI, SAS) and Analyze (Analyze 12.0, AnalyzeDirect Inc, Biomedical Imaging Resource (BIR), Mayo Clinic, USA) 3D analysis software packages respectively. Images were examined for evidence of artefacts or breakages, none were found below 100μm.
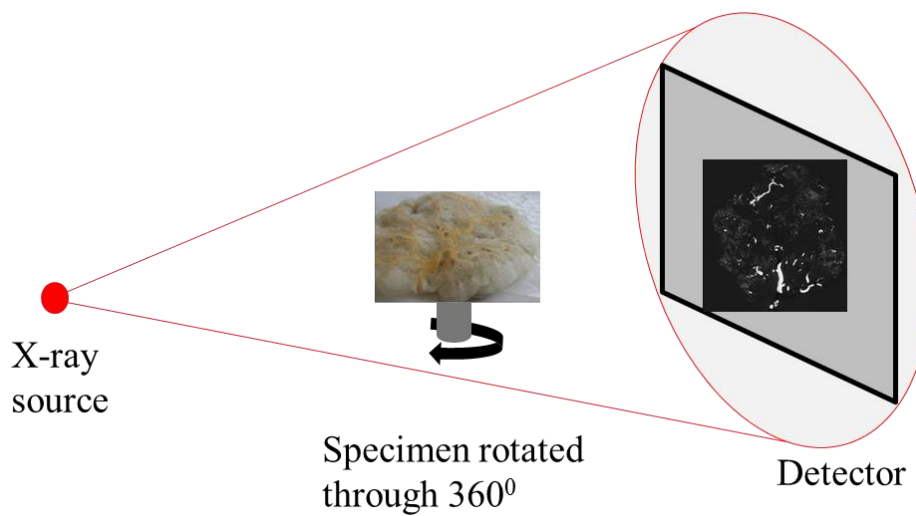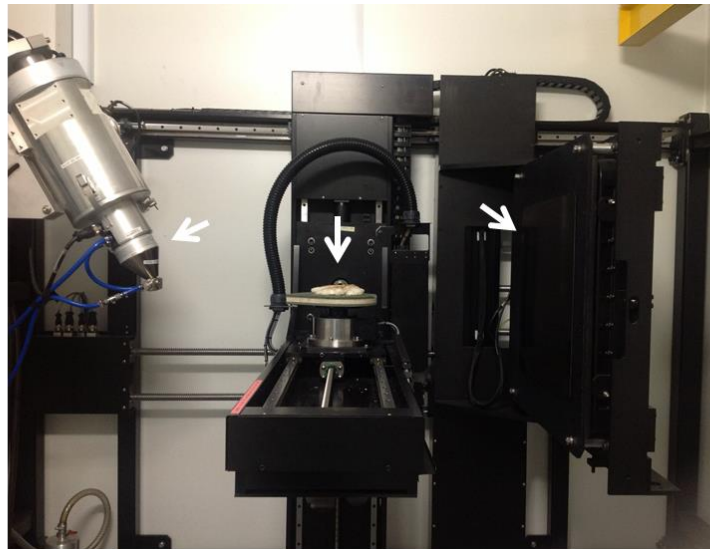
Figure 2.1: The principle of micro-CT imaging.

The left, middle and right arrows in the top image point to the x-ray source, vessel cast mounted on the rotating stage and the detector respectively. The source emits x-rays in cone beam geometry through the cast which is rotated over 360° to generate numerous slices of radiographs in the XY, XZ and YZ planes.

2.2.4 Image analyses

2.2.4.1 Three-dimensional vascular tree analyses in Avizo software

Each 3D dataset was volume-rendered in Avizo. Background noise was removed from the image using the 'orthoslice' tool and colourmap adjustments. The software was noted to crash when large casts were uploaded. Therefore, to ensure uniformity across all casts, analyses were performed in 800 x 500 x 300 voxel subvolumes. Depending on the size of each cast, 6-9 subvolumes were extracted per image (see example in figure 2.2). The vessels in each subvolume were segmented using the 'image segmentation' tool. Segmented vessels were skeletonised, rendering them in different colours based on their diameter (figure 2.3D). Nodes placed along the path of each vessel, representing a site of branching and/or any deviation of the vessel from a straight path, separated the vessels into various segments (figure 2.3E) from which measurements of morphological parameters such as vessel length, diameter and loopiness were derived. Data obtained from all subvolumes in each cast were added together. For the full protocol, see Appendix 1.
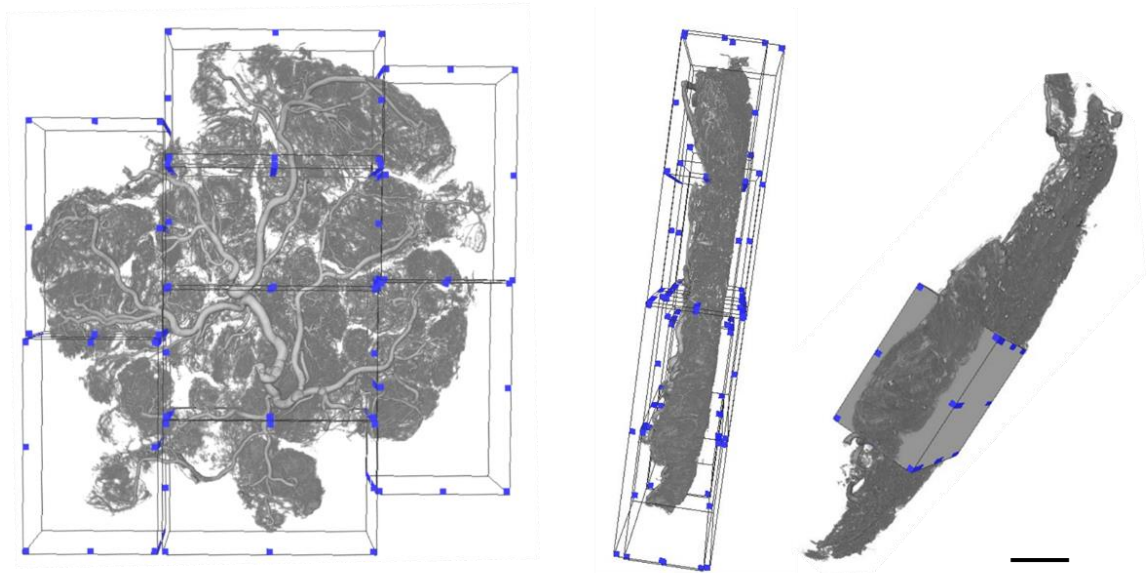
Figure 2.2: Reconstructed CT images of a vessel cast showing analyses subvolumes.

For this cast, eight 800 x 500 x 300 voxel subvolumes were extracted (left). Each subvolume spanned the entire thickness of the cast (middle and right) ensuring that all vessels in the subvolume are included in the analyses. Scale bar is 25mm.

2.2.4.2 Three-dimensional vascular tree analyses in Analyze software

For each vessel cast, all micro-CT image slices were imported as a single volume object into the Analyze workspace. Once loaded, the object was rendered for thresholding to generate a tree-like structure, which represents the skeleton of all the vessels in the original cast. The software placed blue nodes at branch points and red nodes at terminal points of branches in the tree. Terminal points represent the farthest extent of penetration of methacrylate into the respective capillary. From the generated trees, the total number of branches, number of true branches, number of branch levels and number of branches per branch level in each cast was extracted. For the full protocol, see Appendix 2.

2.2.5 Statistical analyses

Statistical analyses were conducted using GraphPad Prism® 6 (version 6.04 GraphPad Software, Inc., USA). Unless otherwise stated, data were represented as median and interquartile range (IQR), compared by Mann Whitney test and a p value of <0.05 was considered to be statistically significant. In all, twenty-four samples were analysed [12 normal (6 arterial, 6 venous) and 12 FGR (6 arterial, 6 venous)]. In previous investigations, we showed that differences in the human placental macrovasculature and microvasculature are detectable at similar sample size (Junaid *et al.*, 2014).

2.3 Results

2.3.1 Measured vessel biometry outputs

The casting material filled the vessels up to the level of capillaries measuring ~10μm (figure 2.4). Reconstruction of scan slices acquired by micro-CT of vessel casts permitted 3D visualisation of most of the placental vascular tree and production of a digital replica for analysis (figure 2.3). Vessel resolution differed based on the size of each vessel cast. The best resolution we achieved was ~60μm (diameter) from a whole vessel cast measuring ~15cm wide (figure 2.5). To ensure uniformity, only vessels ≥100μm in diameter were included in the analyses. Following segmentation and skeletonisation of reconstructed images using Avizo software (figure 2.3D and E), the number of vessel segments, length and diameter of each segment, and the total length of all vessel segments were generated.

Avizo places nodes at each branch and bend along the course of a vessel. Total node number therefore represents the sum of true branch points and vessel bends in the feto-placental circulation. A further analysis package, Analyze, was used to determine the number of true branch points. Skeleton tree maps (example shown in figure 2.6; for complete tree maps of all samples, see figures 5.1 – 5.24 in Appendix 3) demonstrating sequential branching levels for each microCT dataset were generated on Analyze. These demonstrated the total number of directional changes (branches plus bends), number of true branches, number of terminal branch points, number of branch levels and number of branches per branch level through the placental vascular tree. Analyze allowed determination of the tortuosity/loopiness of the vessels within the fetal arterial and venous trees. Loopiness was defined as total node number (Avizo) minus true branch number (Analyze).
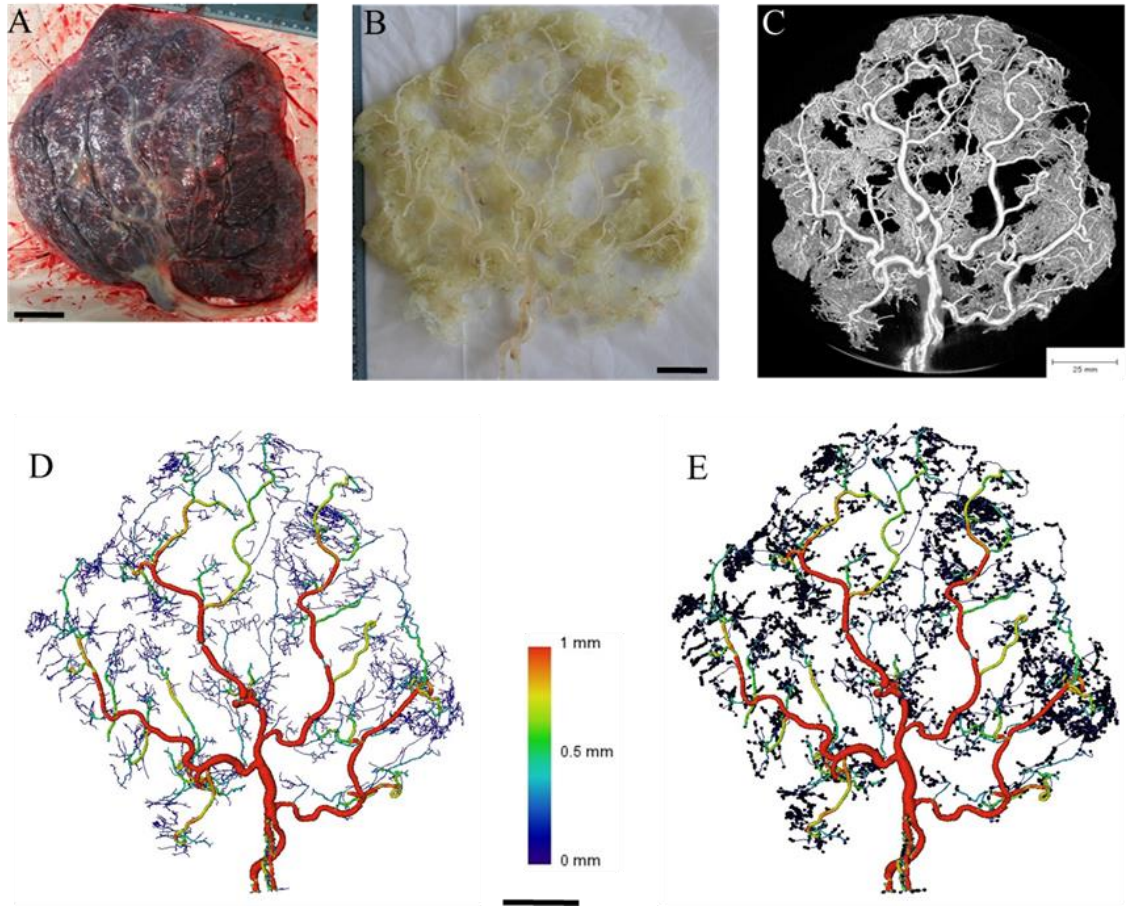
Figure 2.3: Example of an imaged and analysed placental vessel cast.

Images show an arterial cast (B) following corrosion casting of a normal placenta (A), a 3D reconstructed image of the arterial cast following micro-CT scanning (C) and analysis in Avizo (D and E). Vessels are coloured based on their diameter (D) and nodes are placed at bends and true branch points along the course of the vessels (E). Vessel diameter declined as the vascular tree branching progressed. Scale 25mm.
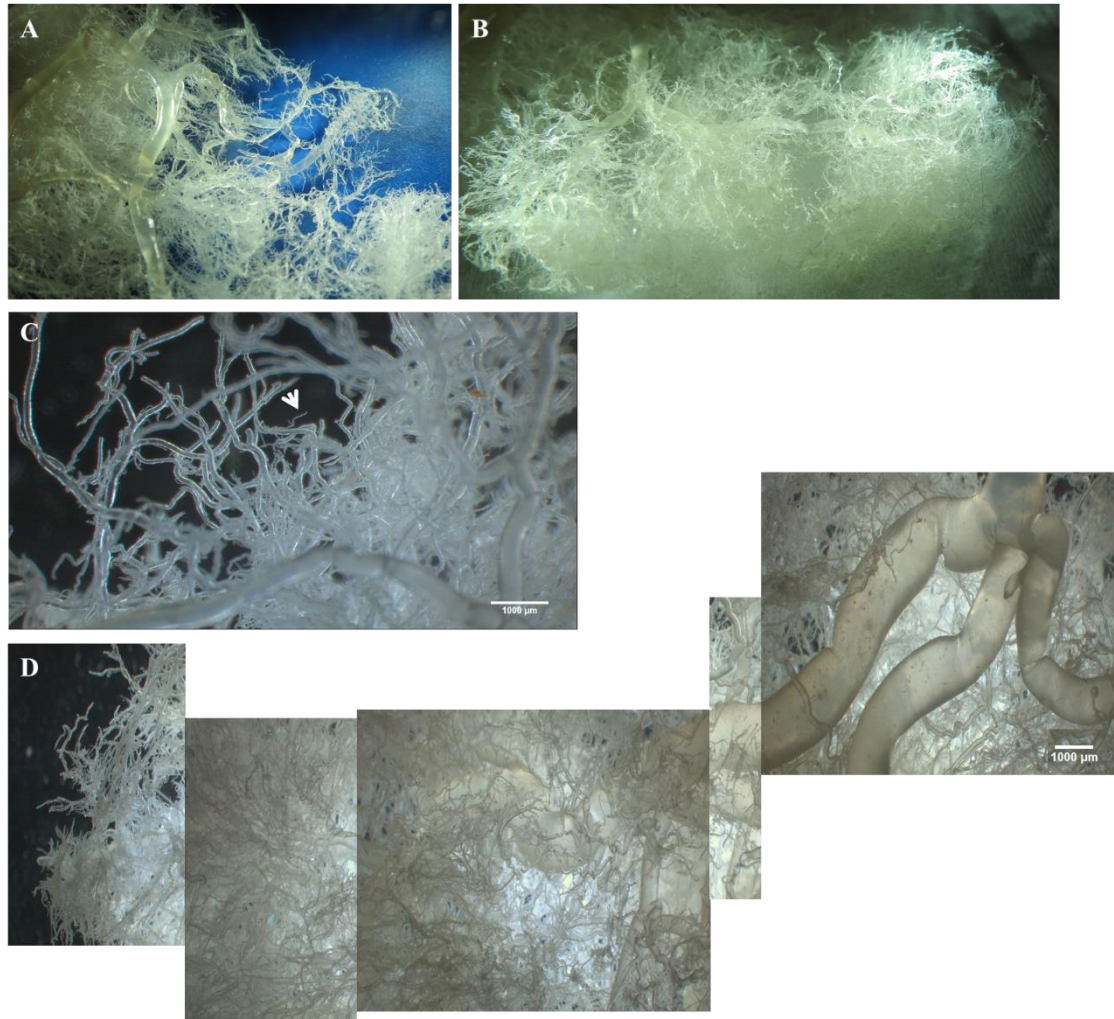
Figure 2.4: The extent of methacrylate penetration.

The smallest vessels on the casts (an example is pointed at by white arrowhead in C) measured ~10μm in diameter, proving that the casting material filled the vessels down to capillary level (A-D). In D, a reconstruction of images taken of a stem villous vessel traced as it branched and terminated in a bunch of capillaries is shown. A and B are photographs taken with a Canon EOS 350D digital camera, C and D are microscope images taken with a Zeiss Axiocam ERc camera attached to a Zeiss Discovery V20 stereomicroscope. Magnification is 20x and 10x in C and D respectively. Scale bars represent 1000μm.
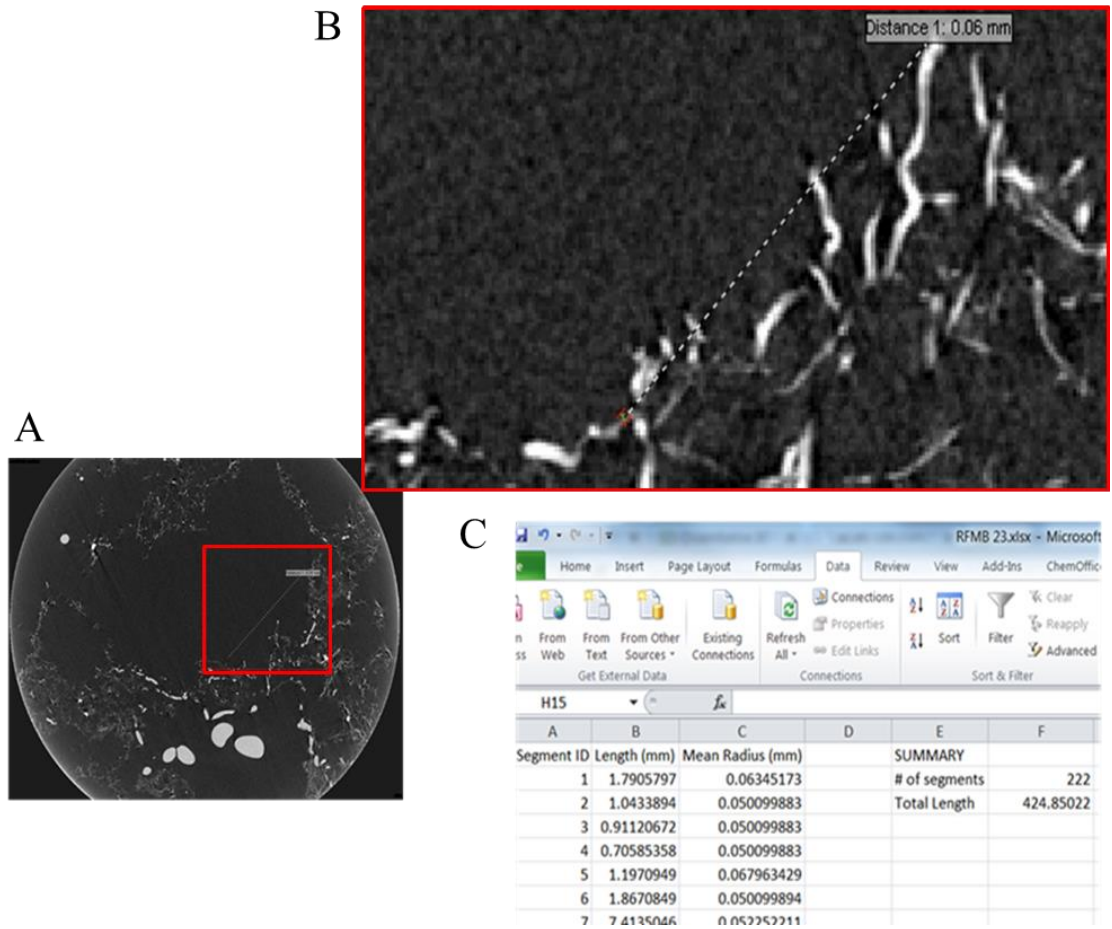
Figure 2.5: An example of a scan slice.

The area bounded by red box in A is zoomed in B to show the smallest voxel size of vessel (60µm) resolved in a scan of a 15cm wide placental vessel cast. C, screenshot of data obtained following segmentation and skeletonisation on Avizo software.
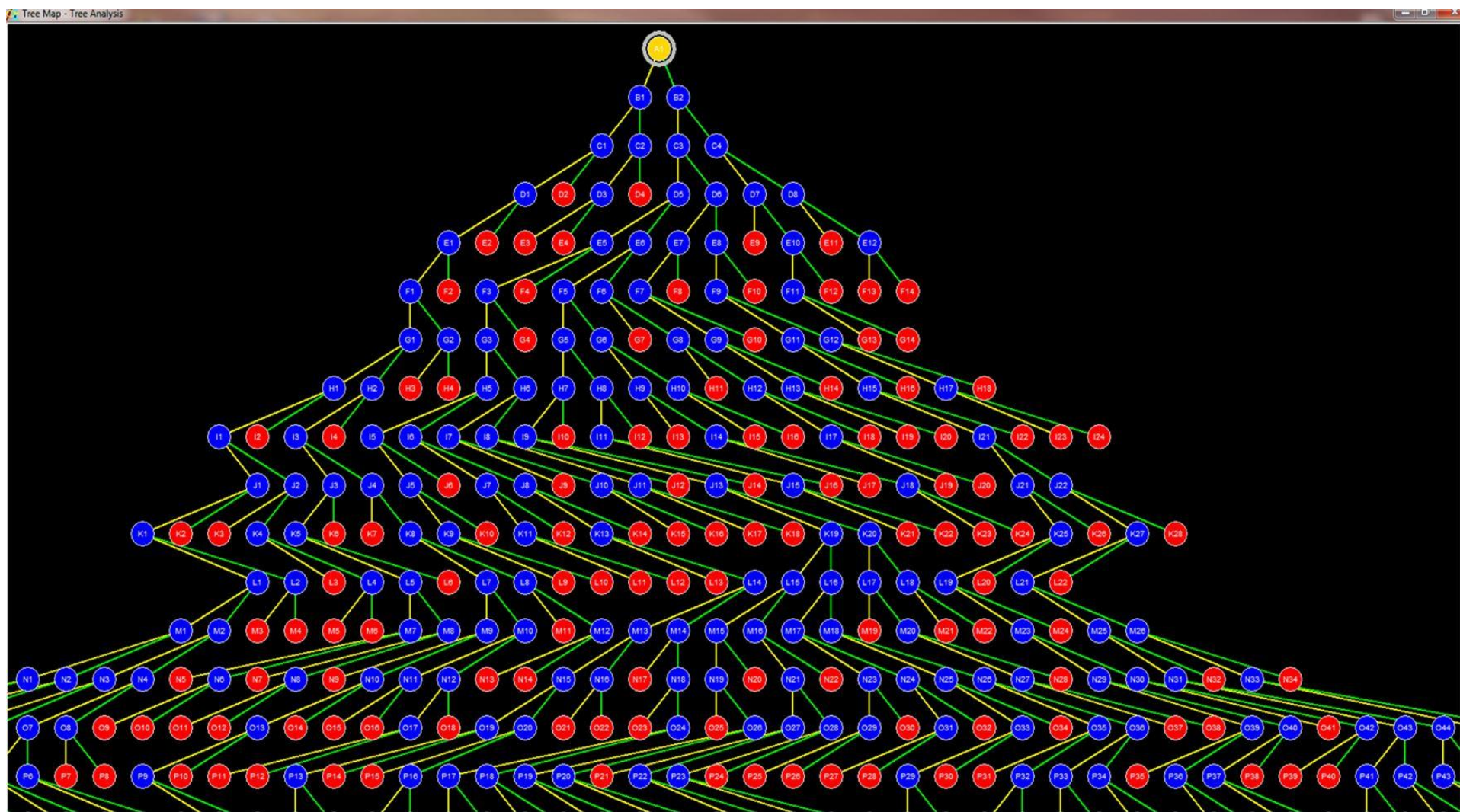
Figure 2.6: Screenshot showing part of a tree map of vessels generated on Analyze. The yellow dot at the top represents the root of all the vessels (umbilical cord insertion point). True branch points and terminal branch points are marked in blue and red dots respectively. Each point is labelled with alphabets designating the branch generation/level and numbers designating the number of branches at each level. Branching is mostly by bifurcation, with daughter vessels represented by coloured lines (one yellow and the other green). Occasionally, there were three branches from a parent vessel and a pink line represented the third vessel.

74

2.3.2 Demographic and gross placental features of samples studied

Having developed analysis tools to examine digital casts of placental fetal vasculature at a whole organ level, we compared vessel morphology in a selection of placentas from normal and FGR pregnancies. The demographic and clinical details of the women and newborns whose placentas were used are shown in Table 2.1. At delivery, the median gestational age, birth weight, individualized birth ratio (IBR), placental weight and placental surface area were significantly different between the normal and FGR-complicated clinical groups. Maternal age, body mass index, parity, smoking status, mode of delivery and early gestation Doppler findings were not different. There were no differences in the birth centile of the placentas used for arterial or venous casts for either the normal or FGR populations. Placentas from the normal and FGR clinical groups differed significantly. Although grossly, placental shape and cord insertion were not different, median surface area in normal placentas was $31362mm^2$ (IQR 29311 – $39234mm^2$) compared to $21238mm^2$ (IQR 18637 – $24966mm^2$) in FGR; p = 0.003. Similarly, median placental weight was 584.00g (IQR 504.60 – 668.50g) and 389.00g (IQR 304.30 – 446.00g); p = 0.0006 for the normal and FGR groups respectively.

2.3.3 Measurements of vascular morphology

2.3.3.1 The number of vessel segments in the normal and FGR casts

To correct for the effect of placental size on its vessel anatomy, vascular parameters measured for each placenta were divided by the individual placental surface area (PA) or alternatively placental weight (PW).

In Avizo, the part of a vessel between two nodes is a segment. Overall, the total number of vessel segments identified in the normal and FGR casts was not different (figure 2.7).

Table 2.1: Demographic, clinical and gross placental examination details of study participants.

	Normal (n = 12)	FGR (n = 12)	*p* value
Maternal age, *years*	31 (27 – 33)	31 (25 – 35)	0.7
Maternal BMI, *Kg/m²*	28 (22 – 32)	25 (20 – 28)	0.2
Smoking, *number (%)*	2/12 (17)	3/12 (25)	0.7
Parity	1 (0 – 2)	0 (0 – 1)	0.5
Gestational age at delivery, *days*	275 (270 – 288)	266 (253 – 268)	**0.002**
Birth weight, *g*	3544 (3300 – 4063)	2270 (2123 – 2515)	**<0.0001**
IBR, *centile*			
Arterial (n = 6)	62 (34 – 95) ⎤ *p* = 0.6	3.5 (1.5 – 5.0) ⎤ *p* = 0.2	
Venous (n = 6)	33 (19 – 66) ⎦	3.0 (0.0 – 5.0) ⎦	
All samples	46 (21 – 89)	3.5 (0.5 – 5.0)	**<0.0001**
Trimmed placental weight, *g*	584 (505 – 669)	389 (304 – 446)	**0.0006**
Placental surface area, *mm²*	31362 (29311- 39234)	21238 (18637- 24966)	**0.003**
Mode of delivery, *number (%)*			
Vaginal	5/12 (42)	8/12 (67)	0.2
Caesarean section	7/12 (58)	4/12 (33)	0.2
Umbilical artery Doppler, *number (%)*			
aEDF	0/12 (0)	1/12 (8)	0.4
Normal	10/12 (83)	8/12 (67)	0.4
Not done	2/12 (17)	3/12 (25)	0.7
Placental shape, *number (%)*			
Circular	1/12 (8)	0/12 (0)	0.4
Elliptical	11/12 (92)	12/12 (100)	0.4
Cord insertion, *number (%)*			
Central	1/12 (8)	0/12 (0)	0.4
Non central	11/12 (92)	12/12 (100)	0.4

Data shown are median and interquartile range (IQR) in parenthesis or in a number with percentage in paranthesis as appropriate. $p < 0.05$ is the chosen level of significance; Mann Whitney U test. BMI, IBR and aEDF represent body mass index, individualised birth weight ratio and absent end diastolic flow respectively. 'Arterial' and 'venous' refer to the vascular compartments casted for the respective placentas.

Adjusted for PA, the median number of vessel segments was 0.21 per mm^2 (IQR 0.15 – 0.36 per mm^2) and 0.16 per mm^2 (IQR 0.12 – 0.26 per mm^2) in the normal arterial and venous casts respectively, and 0.16 per mm^2 (IQR 0.11 – 0.22 per mm^2) and 0.23 per mm^2 (IQR 0.19 – 0.37 per mm^2) in the FGR arterial and venous casts respectively. Adjusted for PW, the median number of vessel segments was 10.86 per g (IQR 9.09 – 27.72 per g) and 10.76 per g (IQR 6.32 – 15.15 per g) in the normal arterial and venous casts respectively, and 9.23 per g (IQR 6.83 – 11.20 per g) and 13.01 per g (IQR 11.30 – 25.90 per g) in the FGR arterial and venous casts respectively.

In all casts, however, there was an expected progressive decline in the number of vessel segments from smaller to larger arteries and veins to the umbilical cord insertion (figure 2.8). In the normal casts, there were significantly fewer venule-size segments in the 100-200μm diameter range compared to similar sized arteriole segments (figure 2.8A). The median number was 1631 (IQR 1027 - 2085) venule-size segments compared to 4182 (IQR 3637 - 8887) arteriole-size segments; p = 0.002. As shown in figure 2.9, this difference persisted when controlling for variation in PA and PW [median 0.05 per mm^2 (IQR 0.03 – 0.06 per mm^2) venule-size segments compared to 0.14 per mm^2 (IQR 0.09 – 0.21 per mm^2) arteriole size segments; p = 0.009, and median 2.53 per g (IQR 1.77 – 4.58 per g) venule-size segments compared to 7.30 per g (IQR 5.78 – 15.30 per g) arteriole size segments; p = 0.004, adjusted for PA and PW respectively] but was not seen in the FGR casts (figure 2.10).

Figure 2.7: The number of vessel segments in normal and FGR vessel casts.

Adjusted for placental surface area (A) and weight (B), there was no demonstrable difference in the total number of vessel segments seen in the normal and FGR casts. n = 12 normal (6 arterial, 6 venous) and 12 FGR (6 arterial, 6 venous) casts. Data shown as median and IQR and compared by Mann Whitney test.
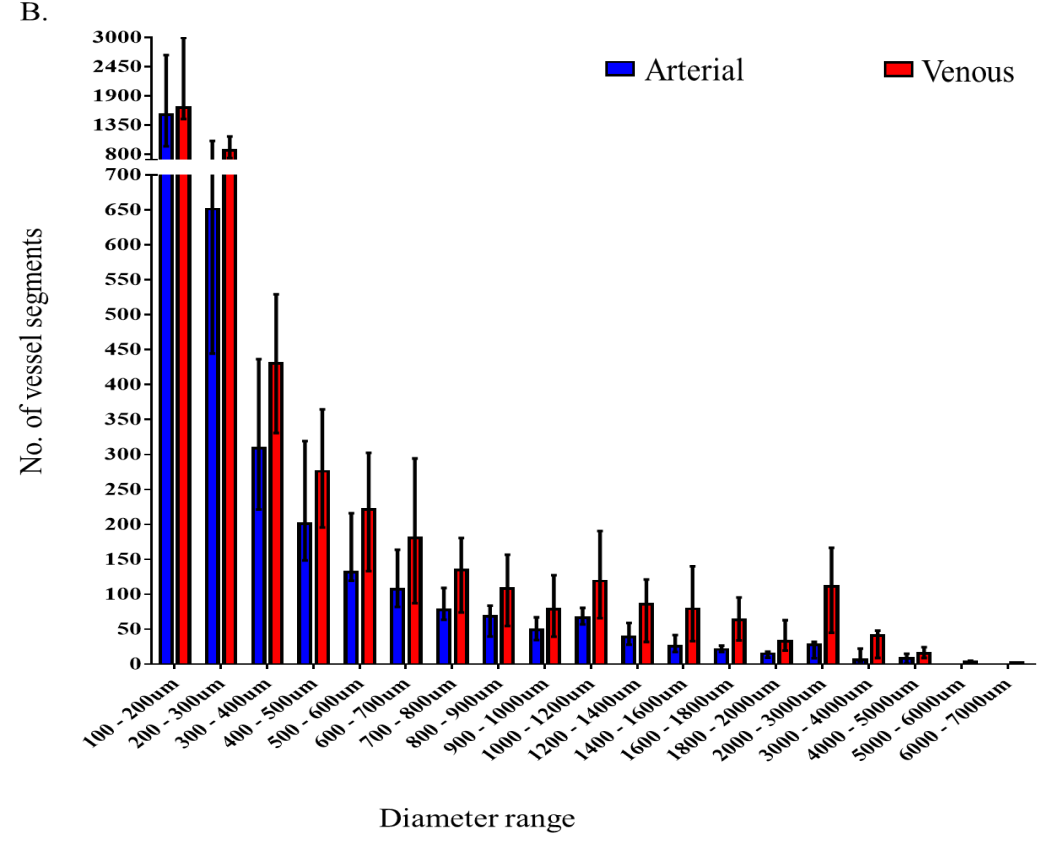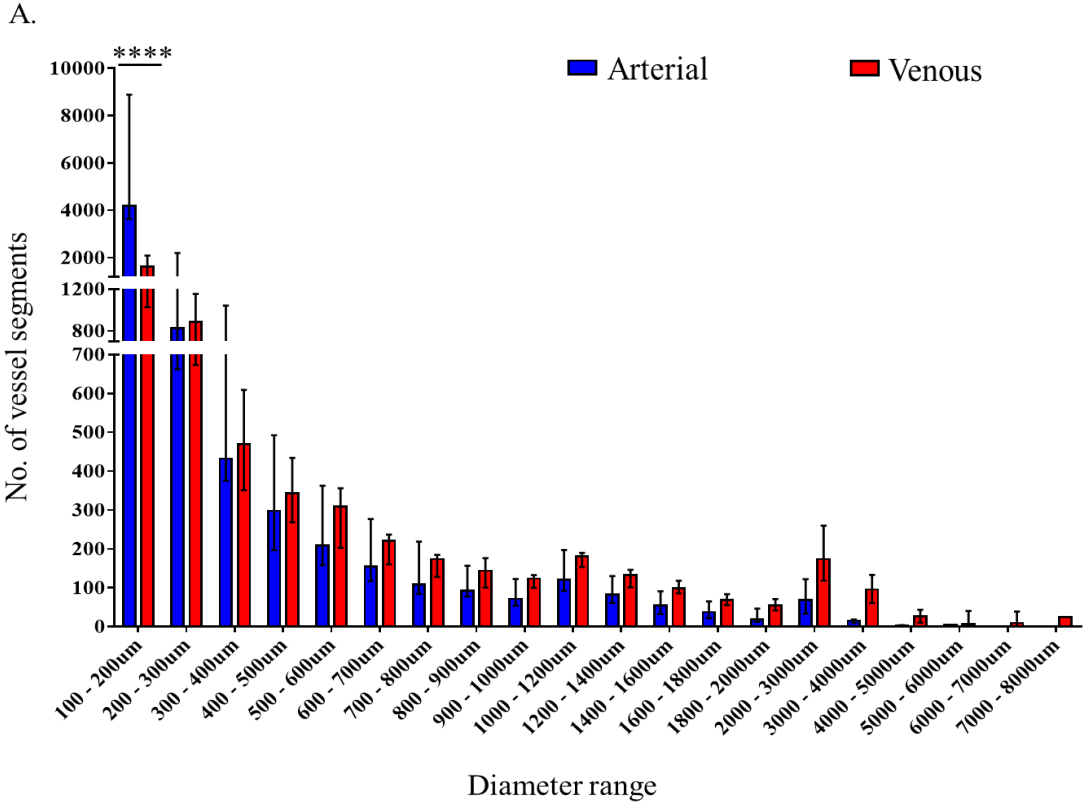
Figure 2.8: The number of vessel segments in different diameter ranges in normal and FGR vessel casts.

In both normal (A) and FGR (B) casts, the number of vessel segments declined progressively from the smallest to the largest diameter ranges. In the normal casts (A), there were significantly fewer segments within the 100 – 200μm diameter range in the venous compared to the arterial casts. Data is grouped by vessel diameter. Median + Interquartile range shown. Two-way RM Anova with Sidak's multiple comparison test. $p < 0.05$ is significant.
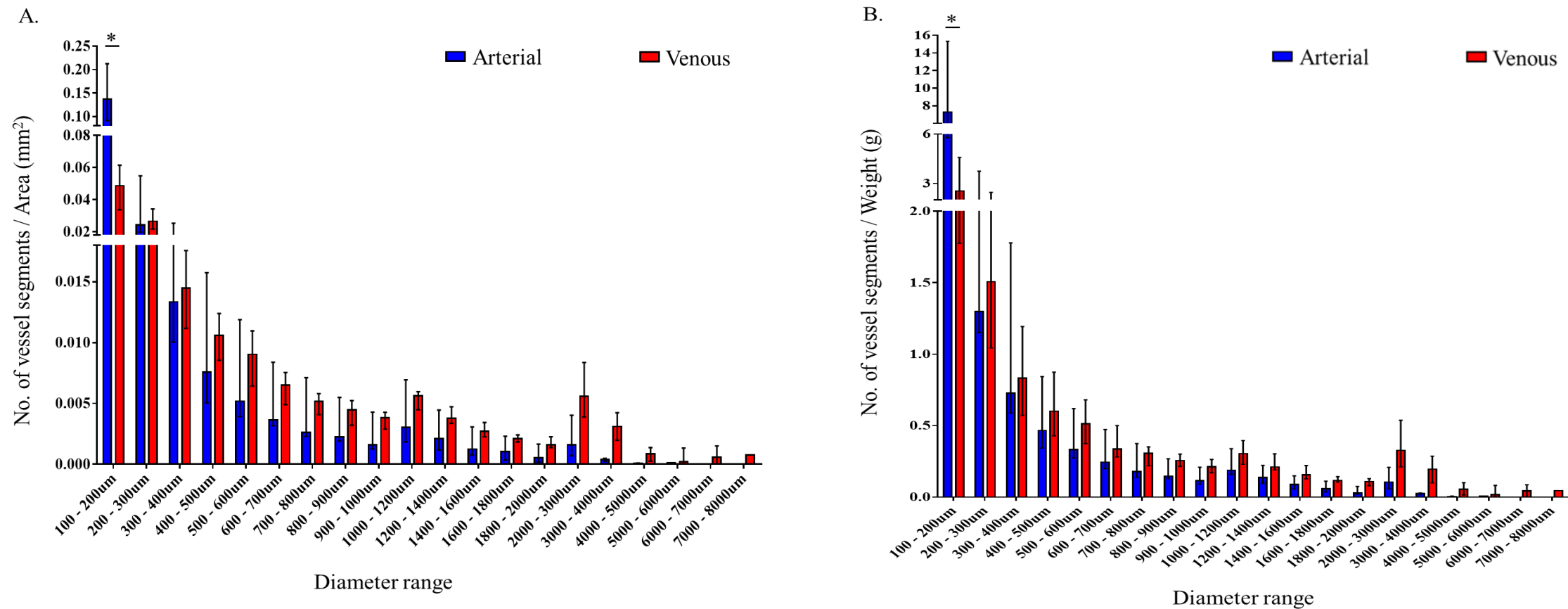
Figure 2.9: The number of vessel segments in the normal casts adjusted for the surface area and weight of the placentas.

The difference between the number of segments within 100 – 200µm diameter range in the normal arterial and normal venous casts persisted. Data adjusted for placental surface area (A) and placental weight (B). Median + Interquartile range shown. Two-way RM Anova with Sidak's multiple comparison test. $p < 0.05$ is significant.
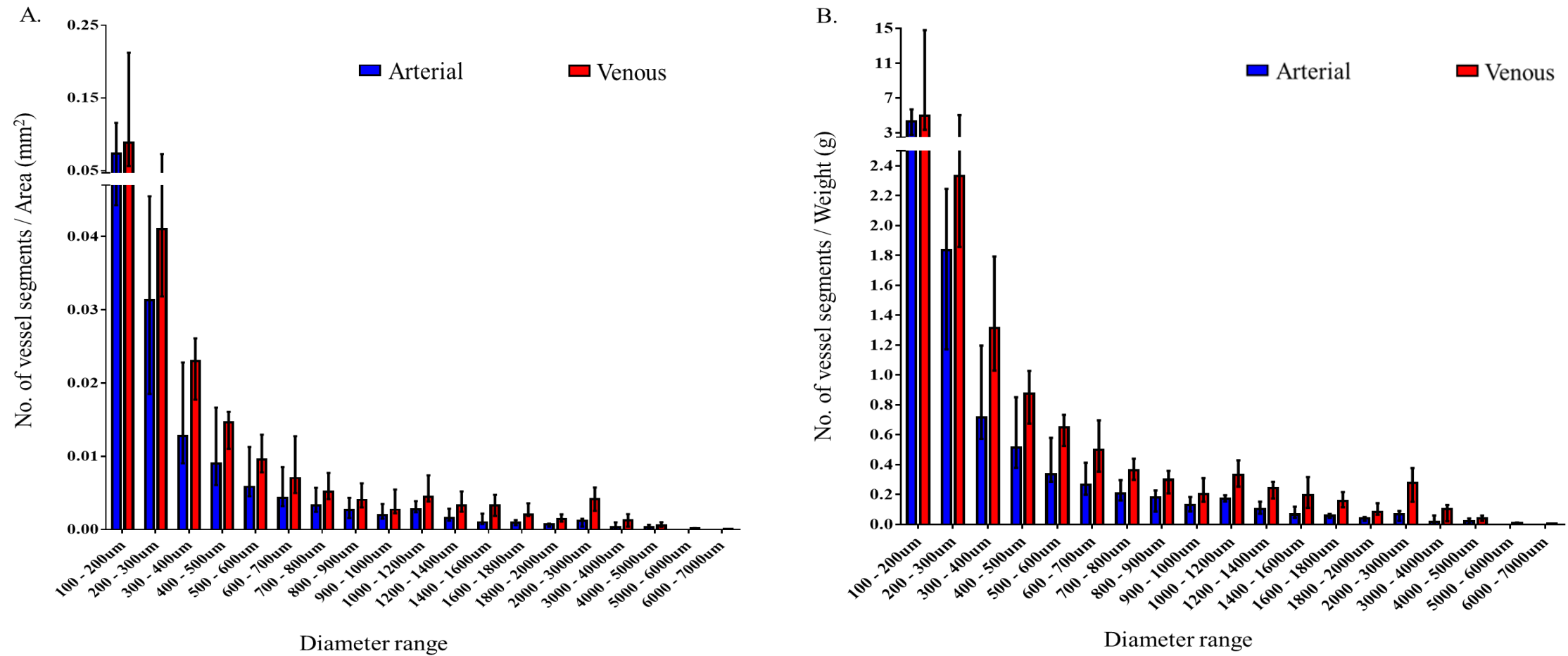
Figure 2.10: The number of vessel segments in the FGR casts adjusted for the surface area and weight of the placentas.

There was no difference between the number of segments in the arterial and venous casts at every diameter range. Data adjusted for placental surface area (A) and placental weight (B). Median + Interquartile range shown. Two-way RM Anova with Sidak's multiple comparison test.

2.3.3.2 Vessel length discrepancies were observed in both clinical groups

In normal placentas, the median arterial length per unit PA was 0.43mm/mm^2 (IQR 0.35 – 0.66mm/mm^2), greater than the median venous length of 0.26mm/mm^2 (IQR 0.20 – 0.33mm/mm^2); p = 0.03 (Figure 2.11A). Median arterial and venous length per unit PW in normal placentas was 27.29mm/g (IQR 19.65 – 42.44mm/g) and 13.39mm/g (IQR 12.18 – 22.94mm/g) respectively; p = 0.04 (Figure 2.11B).
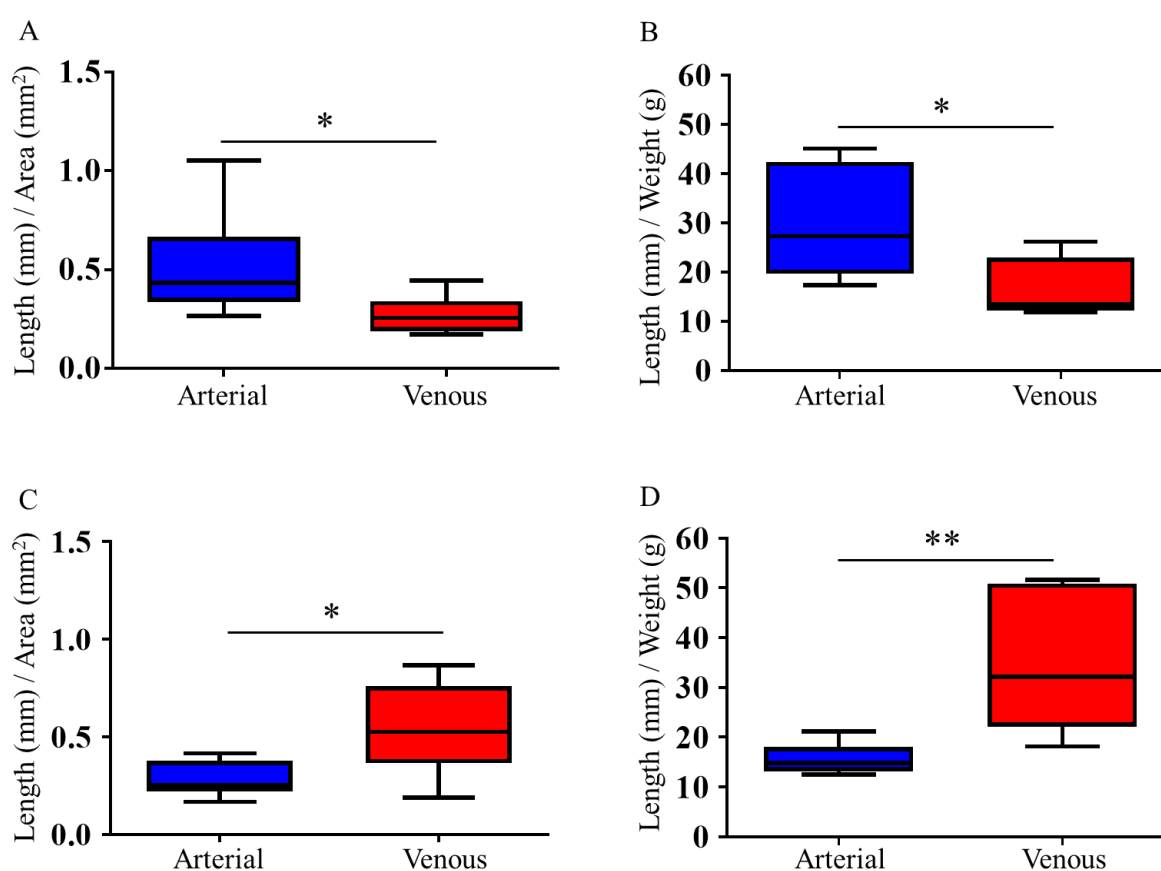
Figure 2.11: The length of arteries and veins in normal and FGR casts.

All data are adjusted for placental surface area and weight to eliminate the effect of placental size on vessel ramification. A and B represent normal while C and D represent FGR casts. In normal casts, arterial paths are longer than venous paths while venous paths are longer in FGR casts. Data presented as boxplots showing the median, range and interquartile range. n = 12 normal (6 arterial, 6 venous) and 12 FGR (6 arterial, 6 venous) casts. Mann Whitney test, p < 0.05 was taken as significant.

In FGR placentas the converse was noted: median arterial length was $0.25mm/mm^2$ (IQR $0.22 – 0.38mm/mm^2$), less than the median venous length of $0.53mm/mm^2$ (IQR $0.36 – 0.76mm/mm^2$); p = 0.04 and 14.82mm/g (IQR 13.13 – 18.10mm/g) compared to 32.10mm/g (IQR 22.08 – 50.92mm/g); p = 0.004 when adjusted for PA and PW respectively (Figure 2.11C and D).

2.3.3.3   FGR casts exhibit shorter arteries and longer veins than normal casts

Comparing FGR to normal placentas, arterial length per unit PA and PW was significantly shorter at $0.25mm/mm^2$ (IQR $0.22 – 0.38mm/mm^2$) versus $0.43mm/mm^2$ (IQR $0.35 – 0.66mm/mm^2$); p=0.03 and 14.82mm/g (IQR 13.13 – 18.10mm/g) versus 27.29mm/g (IQR 19.65 – 42.44mm/g); p=0.009 respectively, while venous length per PA and PW was significantly longer at $0.53mm/mm^2$ (IQR $0.36 – 0.76mm/mm^2$) versus $0.26mm/mm^2$ (IQR $0.20 – 0.33mm/mm^2$); p=0.05 and 32.10mm/g (IQR 22.08 – 50.92mm/g) versus 13.39mm/g (IQR 12.18 – 22.94mm/g); p=0.03 in the FGR group of placentas (Figure 2.12).
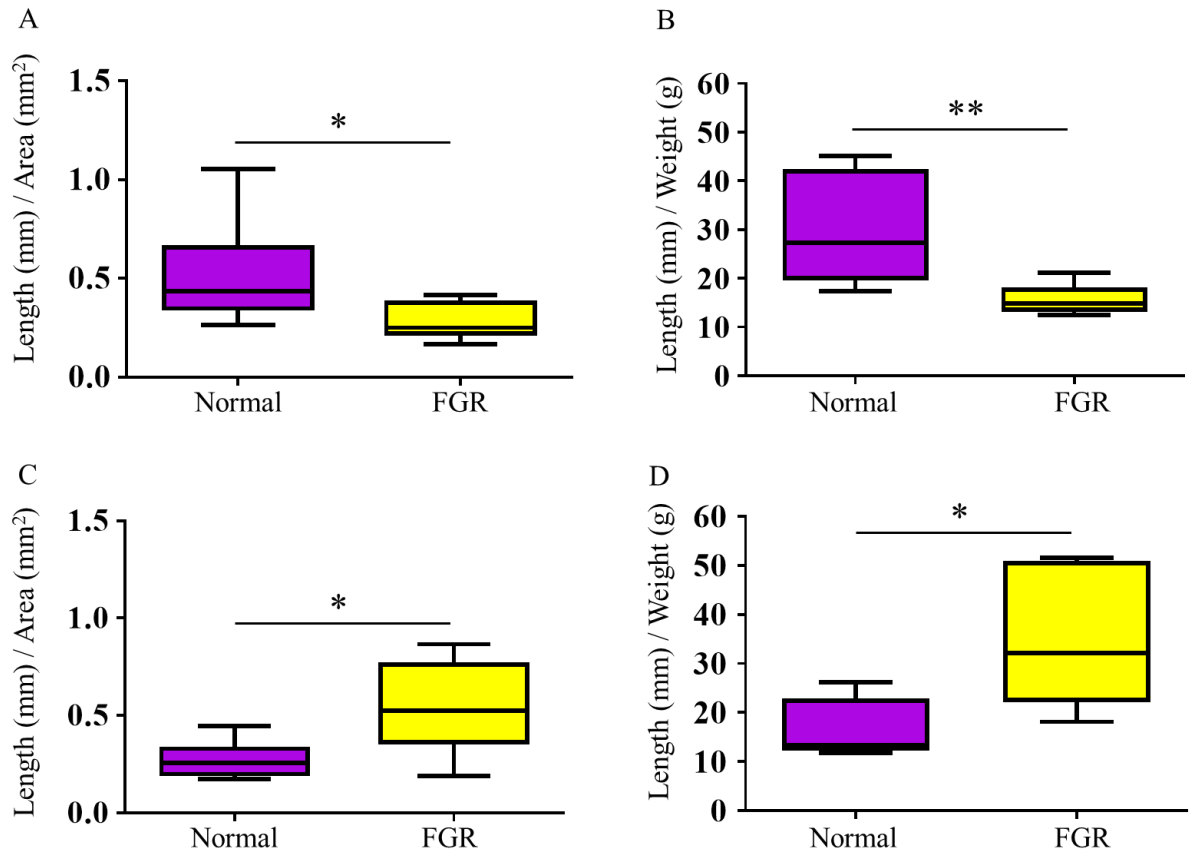
Figure 2.12: Arteries are shorter and veins are longer than normal in FGR casts.

All data are adjusted for placental surface area (PA) and weight (PW) to eliminate the effect of placental size on vessel ramification. Panels A and B represent the length of vessels in the arterial casts adjusted for PA and PW respectively. Panels C and D represent the length of vessels in the venous casts adjusted for PA and PW respectively. Compared to normal casts, arterial path was significantly shorter in FGR, with the surface area as well as the weight of the placenta adjusted for (A and B). However, the converse is true for the venous network (C and D). Data presented as boxplots showing the median, range and interquartile range. n = 12 normal (6 arterial, 6 venous) and 12 FGR (6 arterial, 6 venous) casts. Mann Whitney test, $p < 0.05$ is significant.

2.3.3.4 The number of vessel branches was similar in normal and FGR casts

The number of vessel branches in each cast was obtained on the Analyze software. Unlike the vessel segments derived on Avizo, which includes true vessel branches and false branches (bends falsely counted as branches), these represent true branches. As shown in figure 2.13, there was no significant difference between the number of branches in the normal and FGR casts. Adjusted for PA, the median number of branches was 0.03 per mm^2 (IQR 0.02 – 0.04) and 0.03 per mm^2 (IQR 0.02 – 0.04) in the normal arterial and venous casts respectively, and 0.03 per mm^2 (IQR 0.02 – 0.06) and 0.05 per mm^2 (IQR 0.03 – 0.06) in the FGR arterial and venous casts respectively. Adjusted for PW, the median number of vessel segments was 2.09 per g (IQR 1.15 – 2.83) and 2.06 per g (IQR 1.21 – 2.81) in the normal arterial and venous casts respectively, and 1.59 per g (IQR 1.15 – 3.25) and 2.89 per g (IQR 2.34 – 3.94) in the FGR arterial and venous casts respectively.

2.3.3.5 No difference in vessel tortuosity/loopiness in normal and FGR vessel casts.

As mentioned in section 2.3.1, the tortuosity/loopiness of the vessels in each cast was determined by subtracting the number of true vessel branches in a cast obtained on Analyze from the total number of vessel segments in the same cast obtained on Avizo [i.e. (true branches + bends/false branches) – true branches]. In other words, the false branches, which are areas of bends and twists along the course of the vessels, were adapted as a measure of loopiness of the vessels. There was no difference in vessel loopiness in the normal and FGR casts (figure 2.14). Adjusted for PA, the median loopiness was 0.18 per mm^2 (IQR 0.10 – 0.33) and 0.16 per mm^2 (IQR 0.12 – 0.21) in the normal arterial and venous casts respectively, and 0.11 per mm^2 (IQR 0.08 – 0.19) and 0.26 per mm^2 (IQR 0.19 – 0.89) in the FGR arterial and venous casts respectively.

Adjusted for PW, the median number of vessel segments was 9.66 per g (IQR 6.19 – 25.39) and 8.92 per g (IQR 6.66 – 13.89) in the normal arterial and venous casts respectively, and 7.52 per g (IQR 4.34 – 10.13) and 14.61 per g (IQR 10.64 – 32.02) in the FGR arterial and venous casts respectively.
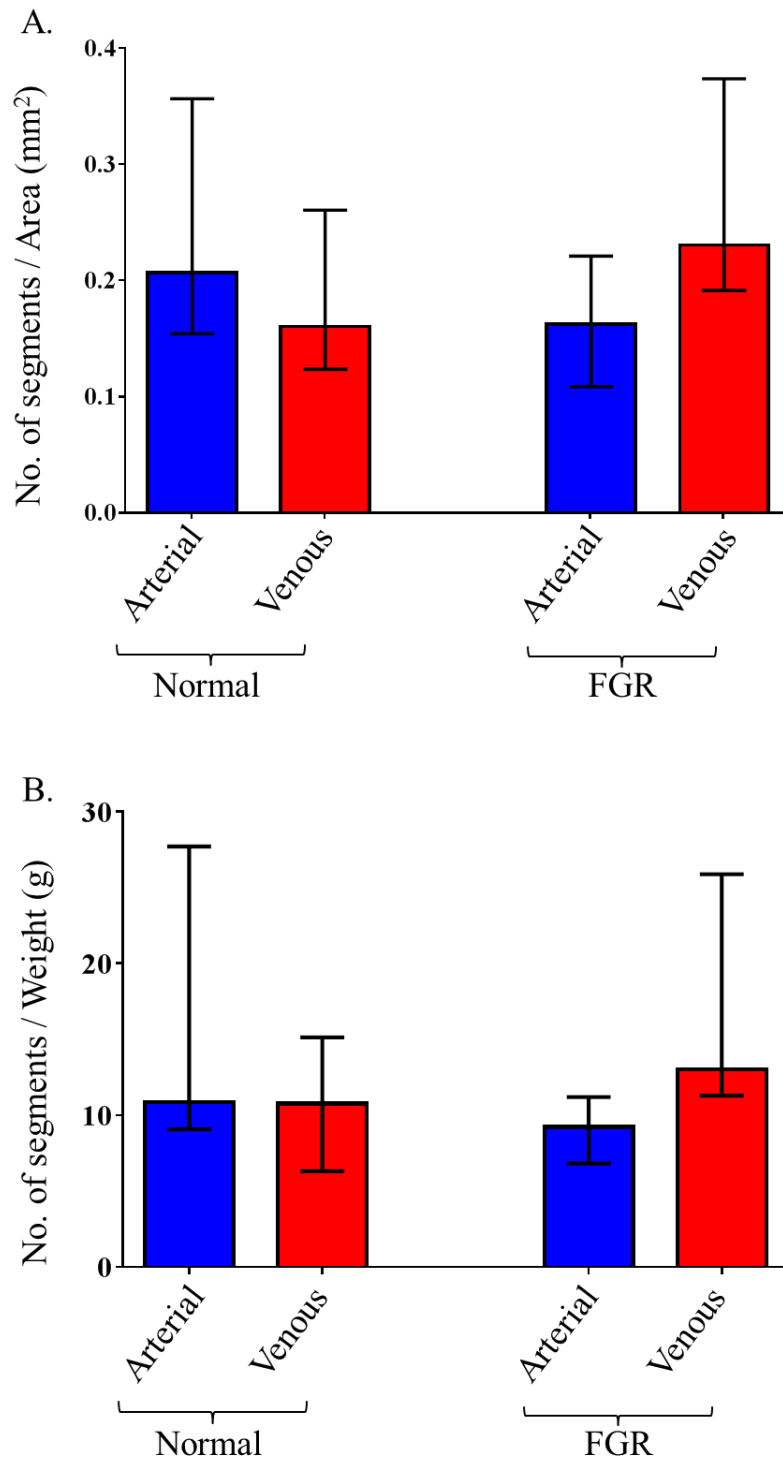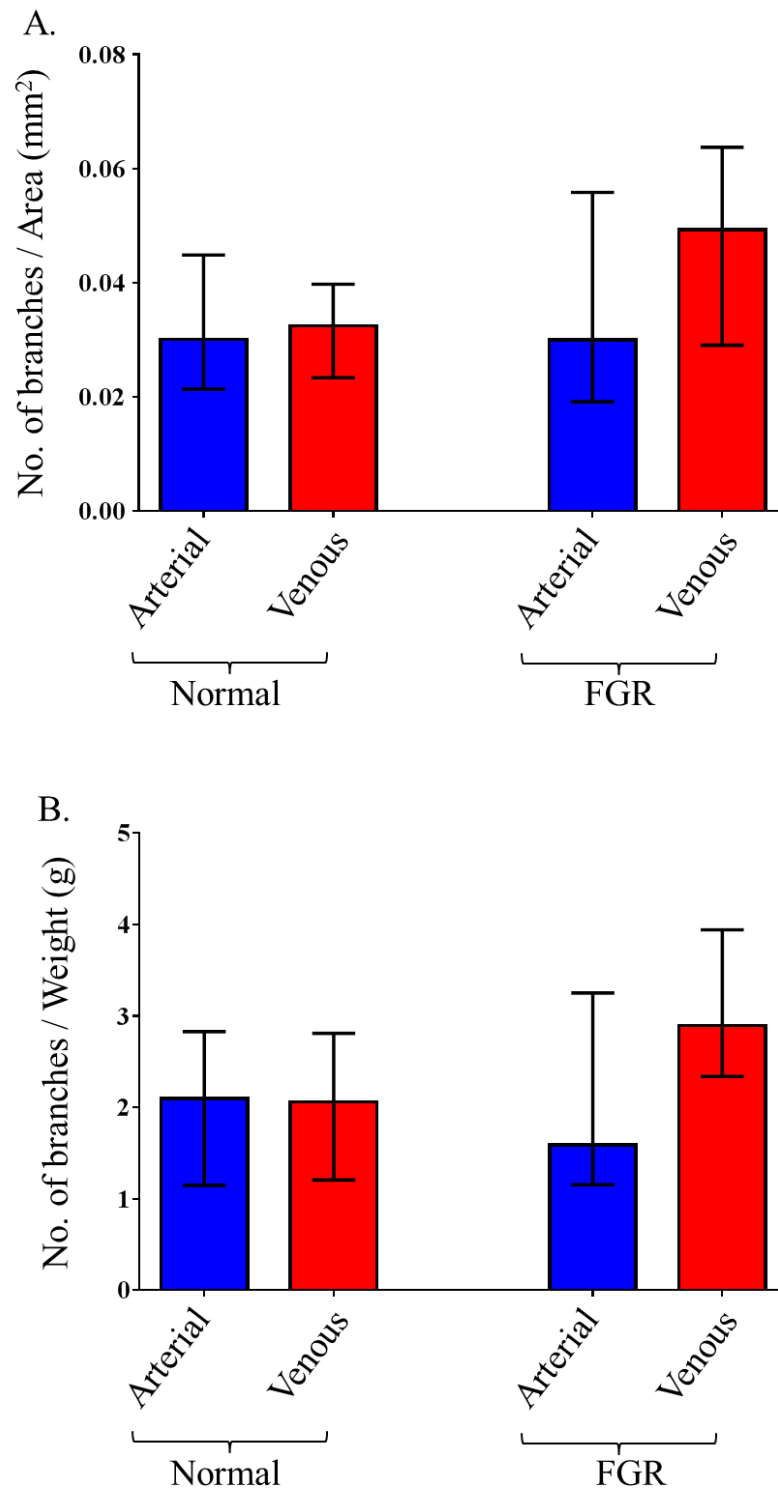
Figure 2.13: The number of vessel branches in normal and FGR vessel casts.

Adjusted for placental surface area (A) and weight (B), the number of vessel branches did not differ in the normal and FGR vessel casts. n = 12 normal (6 arterial, 6 venous) and 12 FGR (6 arterial, 6 venous) casts. Data shown as median and IQR and compared by Mann Whitney test.
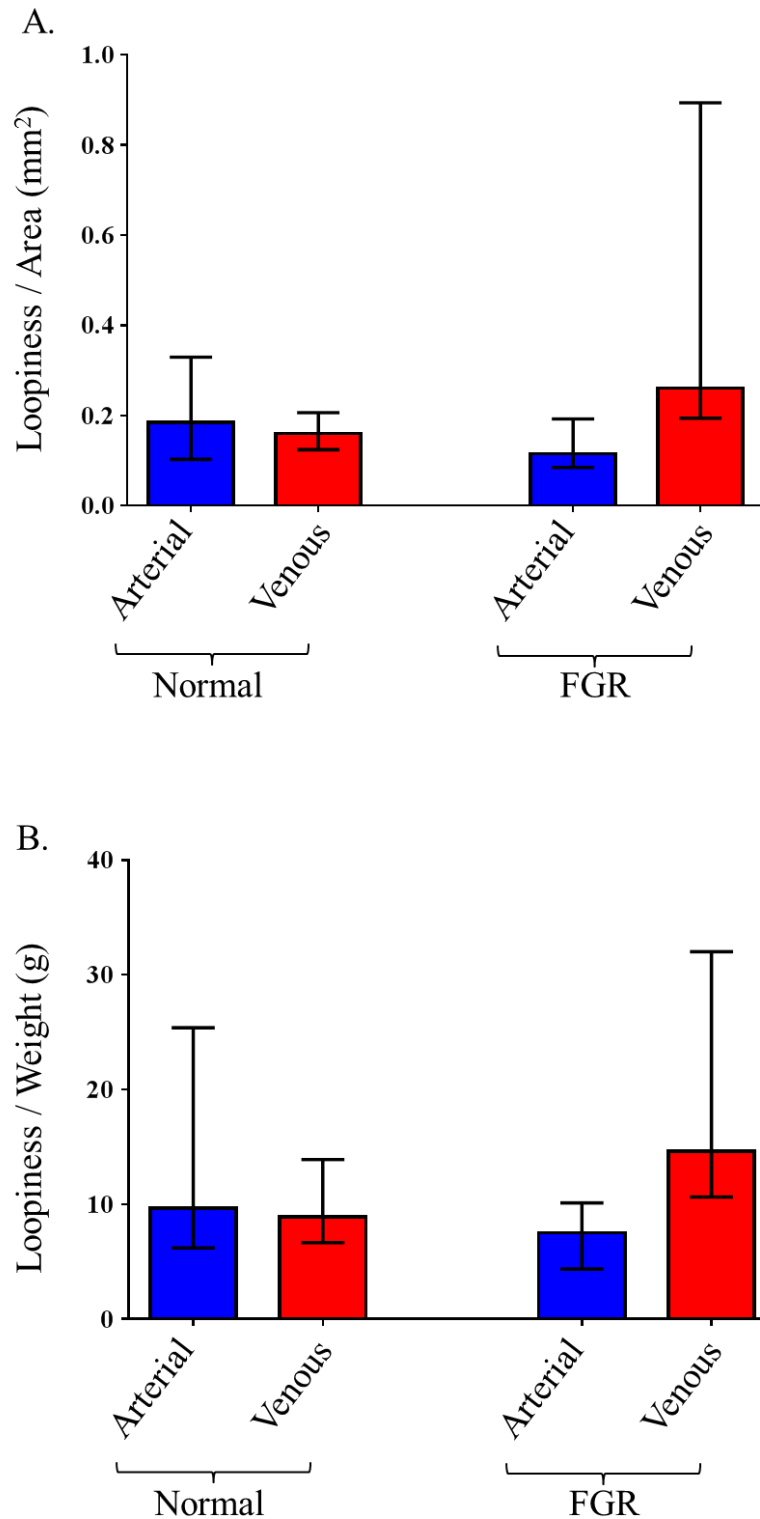
Figure 2.14: Tortuosity/loopiness of vessels in normal and FGR vessel casts.

Adjusted for placental surface area (A) and weight (B), there was no difference in vessel loopiness in the normal and FGR vessel casts. n = 12 normal (6 arterial, 6 venous) and 12 FGR (6 arterial, 6 venous) casts. Data shown as median and IQR and compared by Mann Whitney test.

2.3.3.6 Median vessel diameter was similar in normal and FGR vessel casts.

No significant differences were demonstrable in arterial or venous diameter in either normal or FGR vessel casts above the measurement threshold of 100μm (figure 2.15). Adjusted for PA, the median diameter was 0.06 per mm^2 (IQR 0.05 – 0.10) and 0.11 per mm^2 (IQR 0.07 – 0.17) in the normal arterial and venous casts respectively, and 0.11 per mm^2 (IQR 0.08 – 0.13) and 0.09 per mm^2 (IQR 0.06 – 0.13) in the FGR arterial and venous casts respectively. Adjusted for PW, the median number of vessel segments was 4.00 per g (IQR 3.12 – 4.73) and 5.68 per g (IQR 3.89 – 13.73) in the normal arterial and venous casts respectively, and 5.94 per g (IQR 4.11 – 8.29) and 5.97 per g (IQR 3.82 – 7.99) in the FGR arterial and venous casts respectively.
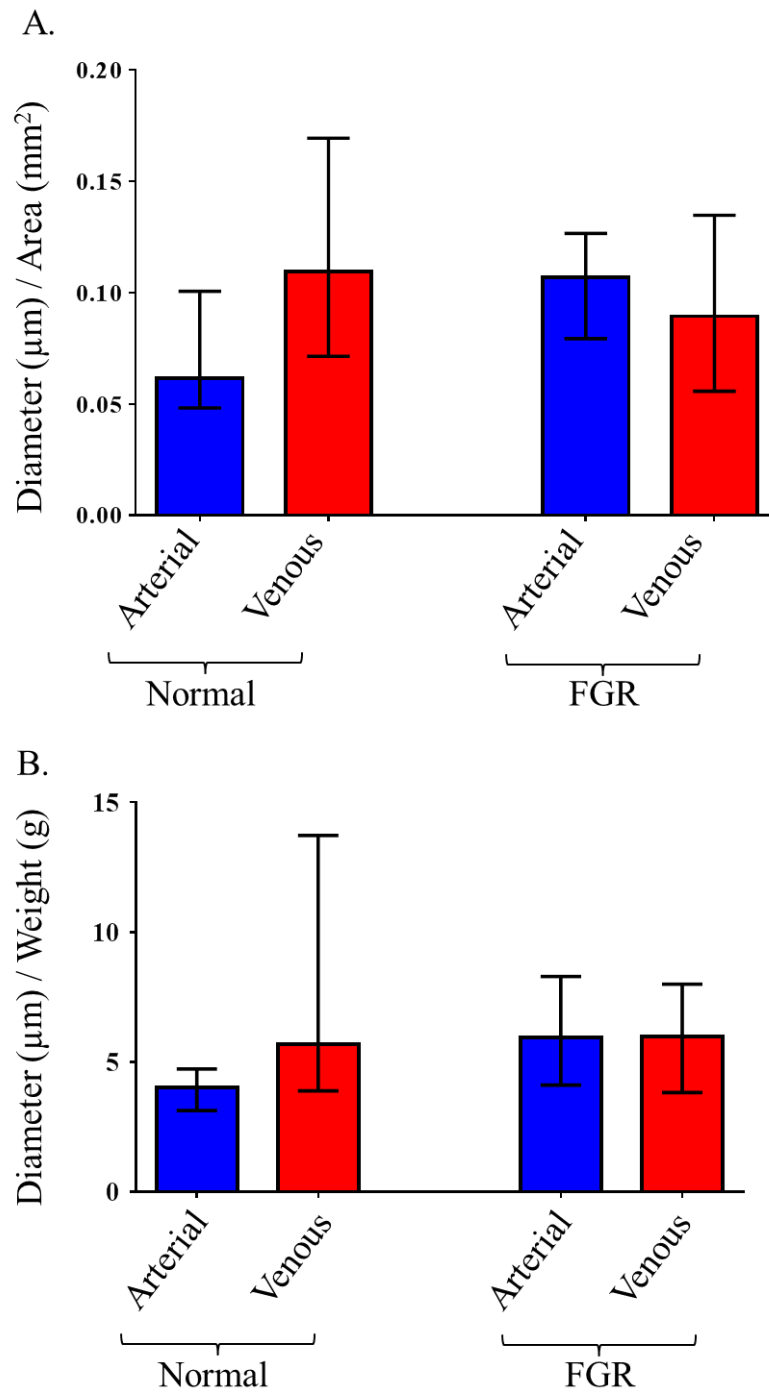
Figure 2.15: Median vessel diameter was similar in normal and FGR vessel casts.

Adjusted for placental surface area (A) and weight (B), there was no difference in the diameter of vessels in the normal and FGR vessel casts. n = 12 normal (6 arterial, 6 venous) and 12 FGR (6 arterial, 6 venous) casts. Data shown as median and IQR and compared by Mann Whitney test.

2.3.3.7 Mapping the branching level affected by variations in vessel length in the vessel casts.

In an attempt to identify the region where vascular lengths differ along the course of the vessels as they ramified in the FGR and normal placentas, we grouped the branch levels in the Analyze tree maps into deciles of branching and compared the number of branches at each decile level in the FGR trees to those in the normal trees (see example in figure 2.16). The number of branches in the arterial trees differed significantly at the eighth decile group (figure 2.17), in addition to a trend that suggests fewer branches from the fourth to the tenth decile group of branches in the FGR arterial trees. These differences were not seen when the venous trees were compared.
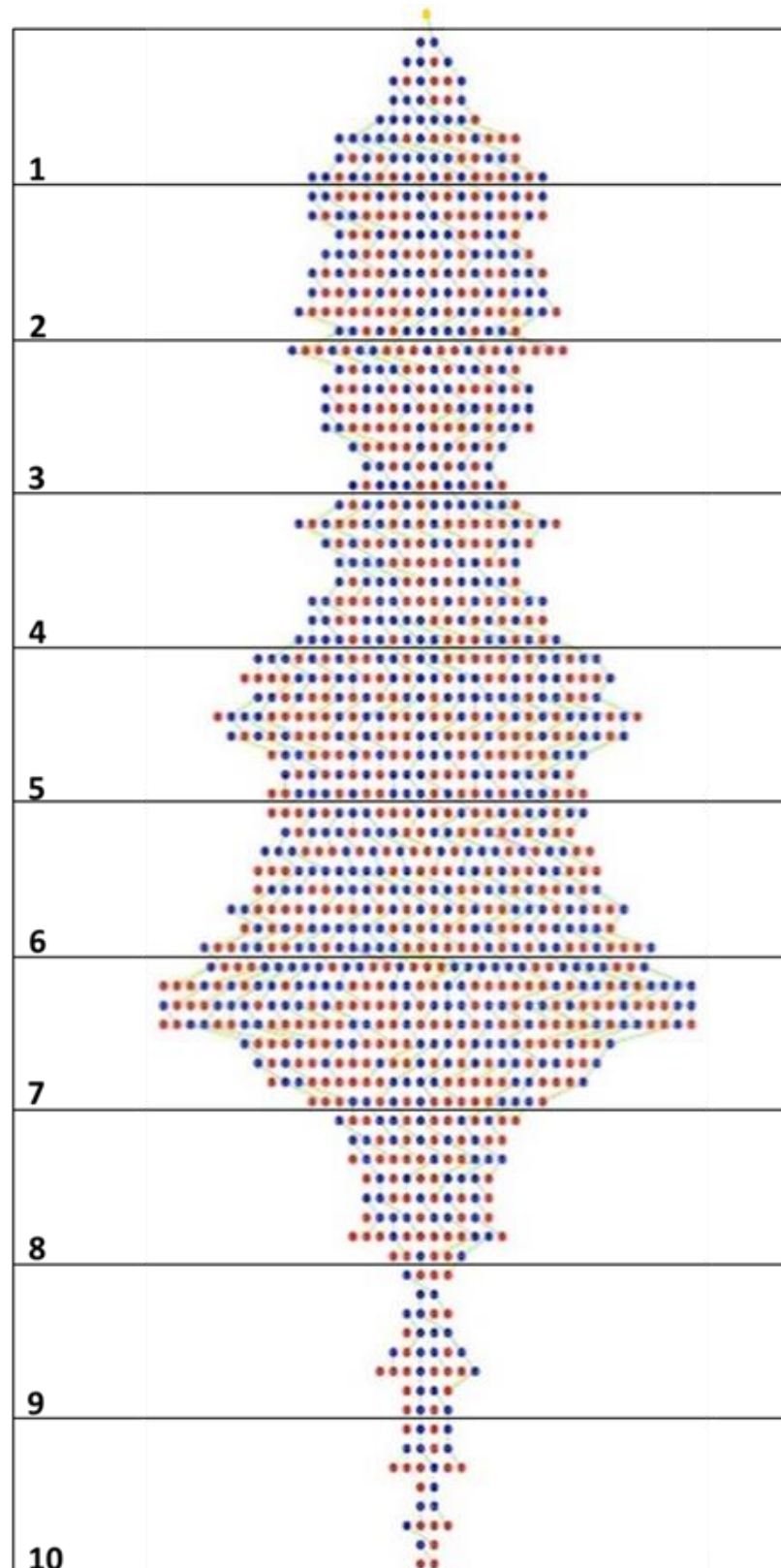
Figure 2.16: Example of a tree map grouped into decile (ten groups) of branching.

In this example, the total level of branching (excluding the root) was eighty. This was divided into ten groups containing eight levels each. For each group, the number of branches was counted and plotted. This was done for all the casts.
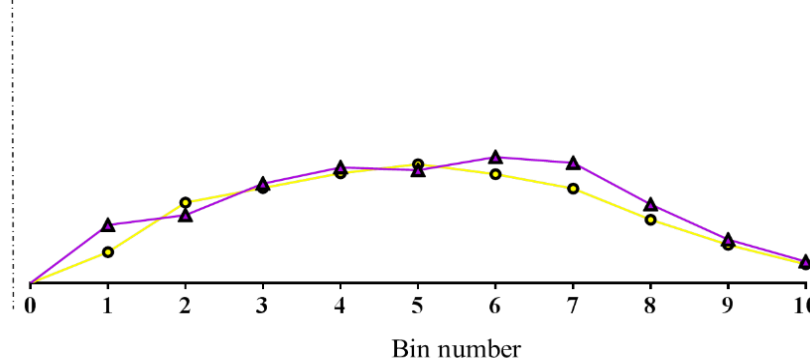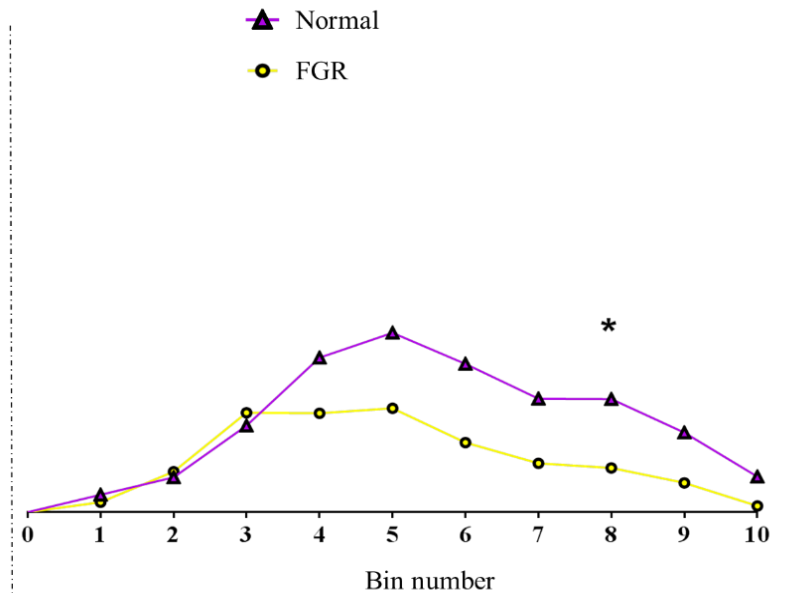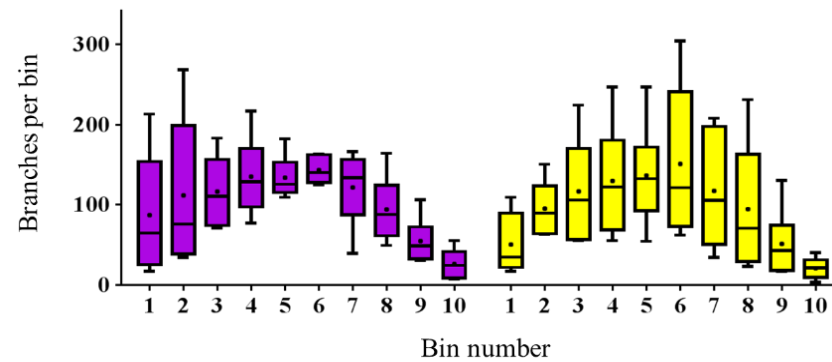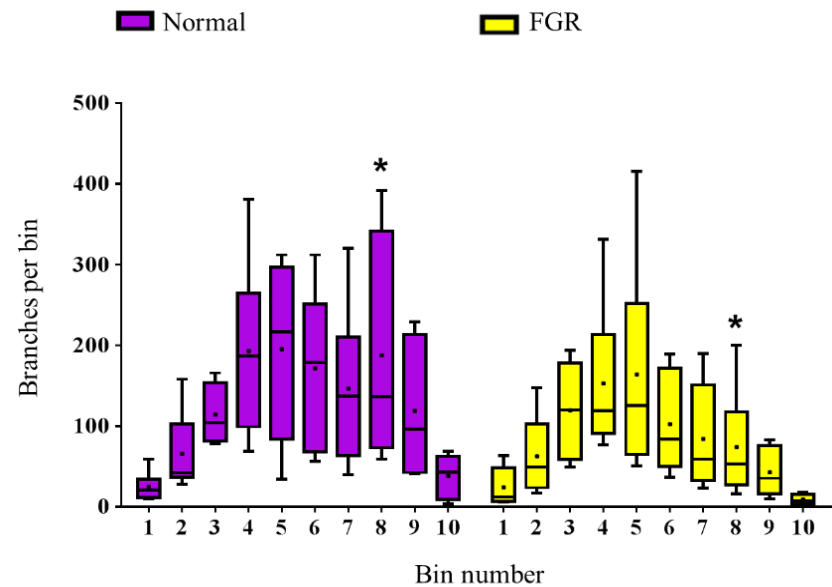
Figure 2.17: The number of branches in each of the ten bins in the tree maps.

Graphs represent arterial (top left) and venous (bottom left) tree maps. Line and dots within the boxes represent the median and mean respectively. There are significantly fewer branches in the FGR arterial trees around the level of the 8th bin of branches compared to normal while there is no difference in the number of branches in the venous trees. Curves on the top and bottom right represent the relationship between the median number of branches in the arterial and venous trees respectively. There is a trend suggesting fewer number of branches in the 4th – 10th bins of branches in the FGR arterial trees (top right). This trend is absent in the venous trees (bottom right). n = 6 samples per group. Two-way RM Anova with Sidak's multiple comparison test.

2.4 Discussion

2.4.1 Corrosion casting combined with micro-CT imaging is effective for holistic examination and quantification of the fetoplacental vasculature.

Possibly due to unavailability of suitable techniques, few studies have examined and quantified the human fetoplacental vasculature at whole organ level. Our successful creation of a three-dimensional digital representation of the human fetoplacental vascular tree is the first time, to our knowledge, that this has been achieved to address this issue. A variety of techniques have been utilised in previous studies of the structure of vascular trees. Direct visualisation and examination of the chorionic plate vessels, as well as other gross features of the placenta such as its shape and cord insertion, is perhaps the most popular, cheapest and easily accessible methodology. The large chorionic plate vessels are grossly visible at the surface. Arterial and venous branching patterns can be discriminated as the arteries are situated superficially, crossing over the veins. This approach, however, requires laborious examination of the placenta in a fresh or fixed state or taking photographs of the placenta for later analysis. It is also cumbersome and unreliable as many vessels, especially deep seated ones, are often obscure on photographic images.

Nearly eight decades ago, August Schummer (1902 – 1977) introduced the resin-casting and corrosion technique for studying vascular anatomy [for history see (Aharinejad, 1992; Vollmerhaus, 2002)]. The initial experiments were with a highly viscous polymer which limited the size of vessels that could be filled. Over the years, modifications and improvements have been made, and the technique is now widely used in the generation of three-dimensional durable casts of hollow anatomical structures including blood vessels of various organs (Aharinejad *et al.*, 1998; Gordon *et al.*, 2007a; Nettum, 1995; Razavi *et al.*, 2012; Gross *et al.*, 1993), including the glomeruli in the kidneys (Mondy

et al., 2009), the airway tree in the lungs (Jacob et al., 2013), the hepato-biliary tree in the liver (Kline et al., 2011), and the suprachoroidal space of the eyes (Krohn and Bertelsen, 1997), to mention a few.

In the placenta, the aim of corrosion casting is to allow visualisation of fetoplacental vessels up to the small terminal branches. The selected casting material must polymerise into a durable, biocompatible model as close as possible to the original vascular tree it was used to perfuse. Where further imaging of a cast is planned, as was the case in this study, the material must also possess contrast properties. Many commercially available perfusates cannot double as an agent for corrosion casting and a contrast agent. For example, radio-opaque media such as microfil, micropaque, barium sulphate and iodine solutions are low viscosity agents with excellent contrast properties but they do not polymerize, making them unsuitable for corrosion experiments. This implies that the perfused specimen would have to be radiographed in a fresh or fixed state, and visualisation of small vessel networks would be hampered by surrounding tissues. Corrosion casting overcomes this difficulty. Due to their high durability and radio-opaque properties, polymethylmethacrylate (PMMA)-based mixtures are popular for the production of bone cement prosthetic implants for hip replacement and several other orthopaedic procedures (Smith and Turner, 1973). The PMMA mixtures available for anatomical corrosion casting, such as mercox and Batson's no.17, are low viscosity perfusates with proven success in creating durable casts (Kanaujia et al., 1986; Kaufmann et al., 1985; Mondy et al., 2009). The PMMA mixture used in this study (Batson's no.17) was shown through scanning electron microscopy to fill capillaries as small as approximately 6µm in diameter (Gross et al., 1993); here, the smallest vessel identified measured approximately 10µm in diameter (see figure 2.4). The arterial and venous trees can be casted together in the same placenta, using coloured pigments to show how the branches relate to one another (Gordon et al., 2007a). In this study,

however, separate casts of the arteries and veins were made to ease analysis and allow for further imaging experiments on the casts.

Recent advances in technology and the advent of computer-aided analysis software launched the use of micro-CT imaging as an effective tool for resolving the fine architecture of small calibre vessels (Langheinrich *et al.*, 2004; Mondy *et al.*, 2009; Razavi *et al.*, 2012). The resolution obtainable is inversely related to the size of the specimen scanned. In other words, the smaller the specimen, the greater the resolution of its architecture will be after scanning. In this study, whole placental vessel casts were scanned with the aim of resolving the structure of the entire vascular tree, or at least down to the level of arterioles and venules. Scanning a whole vessel cast has advantages. Firstly, it creates a three-dimensional digital representation of the entirety of each vascular tree, allowing for visualisation and analyses of each vascular level in continuity with subsequent vascular levels in the tree (i.e, for instance, veins in continuity with venules). Secondly, it allows for objectivity in the morphometric analyses of the vessels. Thirdly, for analysis of the larger chorionic plate vessels, it is a suitable adjunct to the cast analysis model method we previously devised [described in (Junaid *et al.*, 2014)].

Micro-CT has been used in the study of anatomical beds such as the kidney glomeruli (Sled *et al.*, 2004; Bentley *et al.*, 2002), coronary branches in the heart (Jorgensen *et al.*, 1998) and mouse placental vasculature (Rennie *et al.*, 2007), as well as vessels in selected small regions of human placenta (Langheinrich *et al.*, 2004; Langheinrich *et al.*, 2008). In this study, we have demonstrated the potential of a combination of corrosion casting and microcomputed tomography (micro-CT) imaging to achieve a fuller account of human placental vascular morphology with high anatomical detail. We achieved resolution of vessels down to as small as 60μm when a whole arterial cast measuring ~15cm diameter was scanned. In the placenta, vessels at this diameter are at the terminal arteriole or post-capillary venule level. Below this level are the capillaries, known to

measure up to 50µm when visualised by microscopy of semithin sections (Benirschke *et al.*, 2006a). Typically, terminal placenta villi have a diameter of ~60µm when visualised by histology (Macara *et al.*, 1996) which can also provide more detailed information on surrounding tissues. However, histology is laborious and reliant on sampling of representative areas from what can often prove to be a heterogeneous vascular bed, especially in the context of placental pathology (Redline, 2015).

2.4.2 Previously unreported differences were observed in the vasculature of placentas from uncomplicated and FGR complicated pregnancies.

Micro-CT of the whole placenta demonstrates that above the level of terminal capillaries there are more small-diameter arteries than veins (figures 2.8 and 2.9). For the first time we have demonstrated longer venous and shorter arterial paths in FGR placentas. We have previously demonstrated the presence of fewer chorionic plate arteries (Junaid *et al.*, 2014) and sparse capillaries (Chen *et al.*, 2002; Junaid *et al.*, 2014), in addition to elongated capillaries reported by Krebs et al (Krebs *et al.*, 1996) in FGR placentas. Our Analyze generated branching trees identified differing vessel lengths between normal and FGR placentas in distal, but not terminal portions of the fetal arterial tree (8th decile of branching level, shown in figure 2.17). However, Analyze cannot identify the spatial distribution of vessel branches in placental casts and consequently we were unable to define exact vessel locations. This means that vessel diameters at different segment distributions cannot be identified and although the differences noted are clearly near the terminal end of the villous tree (figure 2.17), we cannot specify at which exact diameters this occurs. Previous studies examining human fetal placental venous structure are sparse, though some reports have linked alterations in umbilical vein structure to FGR (Peyter *et al.*, 2014; Rigano *et al.*, 2008). The

consequences of these previously unreported altered vessel path lengths on blood flow to the fetus are unknown. Given that placental veins convey oxygenated blood and nutrients to the fetus, it may be that longer venous return path in FGR pregnancies reduces the efficiency of materno-fetal nutrient and gas transfer, with more lost to the placenta itself.

We were also able to determine the tortuosity/loopiness of vessels in the networks. Capillaries in FGR placentas have been previously demonstrated to have poorly coiled, elongated loops (Krebs *et al.*, 1996), with reduced or similar tortuosity of individual villous branches compared to normal (Haeussner *et al.*, 2016). Our data adds that loopiness is found at all levels of the placental vascular tree (not just the villi), and overall, there are no differences in loopiness in normal and FGR placental vessels. This finding, together with our finding of similar total number of vessel branches in the normal and FGR vessel casts, suggests that the discrepancies we observed in vessel length were not due to variations in number of branches or loopiness of the vessels in the placentas. Whether arterial branching influences venous tree development, or vice versa, remains unclear.

Although delivery was significantly earlier in the FGR cases, seven of these cases attained term before delivery while five were delivered 10 - 14 days before term (between 252 - 256 days). It is unlikely for the placental vasculature to change significantly within this short period, therefore, we do not expect the difference in gestational age would impact on our findings.

2.4.3 Strengths and limitations of study

The strength of the study is the demonstration of vascular differences at whole organ level. There are, however, some limitations of the method employed. Vascular corrosion

casting is susceptible to technical problems such as breakage (especially of the tiny fragile parts) during the corrosion and washing steps, causing missing vessel segments. As shown in figure 2.4, the vessel casts created included vessels down to the smallest capillaries (~10μm diameter) in the placental vasculature. With micro-CT, because we aimed to scan the whole cast at once, resolution was limited, at best, to vessels measuring 60μm in diameter. The smaller capillaries could not be seen. Furthermore, in order to ensure uniformity in our analyses, we applied an analyses threshold excluding vessels ≤100μm. It may be possible to overcome this, by scanning small regions of the casts, and later reassembling the file but this would be cumbersome. Also, because resolution inversely correlates with the size of the sample, regional scanning would require breaking the casts into pieces, ruining the ability to examine the vasculature in its entirety and in continuity as we aimed. Scanning at nanoscale, rather than microscale, using advanced super-resolution imaging tools (Leahy *et al.*, 2016) may also be beneficial to overcome this limitation.

Secondly, using the current technique, arterial and venous networks cannot be examined simultaneously in the same placenta. Although, by adding different coloured pigments to the casting material, it is possible to create casts of both the arterial and venous networks of the same placenta together, it is impossible to differentiate the vessels after micro-CT imaging since colours do not show on radiographs. Experiments using other types of radio-opaque material, such as microfil, may address this.

Thirdly, although we were able to adapt the Avizo and Analyze software for analyses of placental vasculature, both software are not primarily designed for this purpose and so had limitations. Avizo has multiple programmes designed originally for use in material sciences, minerals, mining, cellular and structural biology while Analyze is primarily for medical imaging. This is a major challenge in 3D placental research as there is currently no placenta specific morphometric software. Other investigators of the

topology of placental vessels are faced with the same challenge. For example, investigators in Hans-Georg's laboratory are using Neurolucida software, originally designed for analysis of dendritic trees of neurones, for 3D analysis of the topology of placental villous trees (Haeussner *et al.*, 2016; Haeussner *et al.*, 2014). The branch trees generated by the Analyze programme are ineffective for anatomical localisation of vessels, which could help pin-point the exact vessels involved in the differences identified and heterogeneity of vascular ramification in relation to the position within the organ. We also were not able to examine branching angle distributions which, in terminal branches of villous trees, have been reported to relate inversely with feto-placental weight ratio (Haeussner *et al.*, 2014) and have been found to differ in normal and FGR terminal villi (Haeussner *et al.*, 2016).

Lastly, although the population studied was relatively tightly defined and statistical differences were observed, the cases were mostly late-onset FGR which may likely have included normal small fetuses and fetuses that are small due to non-vascular pathology.

2.4.4   Summary

In summary, the present study demonstrates further structural alterations in fetoplacental vessels of growth-restricted newborns, in addition to those we recently discovered (Junaid *et al.*, 2014). Further investigation is necessary to understand the implications for placental function.

3 Chapter 3: Bringing CLARITY to the human placenta: a potential technique for whole organ placental examination in intact state

3.1   Background

The potential of a combination of corrosion casting and micro-CT imaging to achieve a near-full account of vascular morphology have been described in chapter 2. While 3D casts of a significant proportion of placental vessel networks were created, analyses were limited to vessels ≥100µm in diameter; vessels smaller than that threshold remains incompletely documented. Here, the focus was to develop a technique that may allow fuller structural analyses of the entire human placental vascular network in an intact state.

The tissue clearing approach termed 'CLARITY' (Clear Lipidexchanged Acrylamide-hybridized Rigid Imaging/Immunostaining/In situ hybridization-compatible Tissue-hYdrogel), pioneered by Deisseroth's laboratory (Chung *et al.*, 2013) was used. The approach has been used successfully to examine individual cells and their interconnections in intact brain (Chung *et al.*, 2013; Chung and Deisseroth, 2013). It involves removal of lipid while providing a physical framework of hydrogel mesh to hold the tissue together in a state that preserves its structure and biological information. Lipid removal improves access of labelled markers allowing for immunostaining of deeper structures. We anticipated that, using this approach, human placental tissue can be preserved in a form that allows complete 3D analyses of vessel topology. In this pilot study, we specifically aimed to investigate the effectiveness of the tissue clearing technique as a tool for examining the placental vascular network in an intact state.

3.2 Materials and methods

3.2.1 Clearing of human placenta

Due to differences between brain and human placenta in terms of tissue composition and vascularity, some modifications had to be made to the original CLARITY protocol.

3.2.1.1 Sample preparation

Immediately after delivery of the placenta, the umbilical cord was clamped to keep all three umbilical vessels dilated by congested blood. The umbilical vessels were cannulated within the cord using a 20G cannula (BD Infusion Therapy, UK) held in place with silk 3.0 suture (Ethicon Inc, UK). About 20-40ml of 5000i.u heparin sulphate in phosphate buffered saline (PBS) was infused to prevent intravascular coagulation, followed by copious infusion of PBS (about 60 – 100ml) to thoroughly rinse out the vessels. This step was crucial as we observed that the presence of blood proteins in the tissue interfered with clearing. Due to New York State requirement for all delivered placentas to be sent for histology, only pieces of the placentas were obtained for clearing. Obtained heparinised samples were fixed for a week in freshly prepared 4% paraformaldehyde (PFA). Following fixation, samples were embedded overnight in hydrogel solution, containing 40% acrylamide and 2% bisacrylamide (Sigma-Aldrich, USA).

3.2.1.2 Electrophoretic clearing method

Fixed samples cut into 10x10mm pieces were washed in PBS, placed in custom designed filter eyelets in an electrophoretic chamber (chamber design and machine set up described in figure 3.1) placed on a stirrer. The chamber was filled (to the maximum

level) with clearing solution [8% sodium dodecyl sulfate (SDS) + 0.2M boric acid in distilled H_2O, pH 8.5] and connected to the power supply (50W, 1A, 45°C). Clearing solution was changed daily until samples were cleared, and then samples were washed in buffer (1% Triton-X in PBS).

3.2.1.3   Passive clearing method

After washing in PBS, samples were placed in a sealed tub containing the clearing solution (8% SDS + 0.2M boric acid, pH 8.5). Volume of clearing solution used depended on sample size, with up to 200ml for a placental lobule. The tub was left in an incubator shaker set to 120rpm, 55°C (Figure 3.2). Clearing solution was changed daily until samples were cleared (weeks – months depending on sample size/thickness). Once satisfactorily cleared, samples were bathed in half strength clearing solution (4% SDS + 0.2M boric acid, pH 8.5) at 55°C for a day, then washed in buffer (1% Triton-X in PBS). Wash buffer was changed half hourly for at least 10 washes. Samples were stored in wash buffer ready for immunostaining.
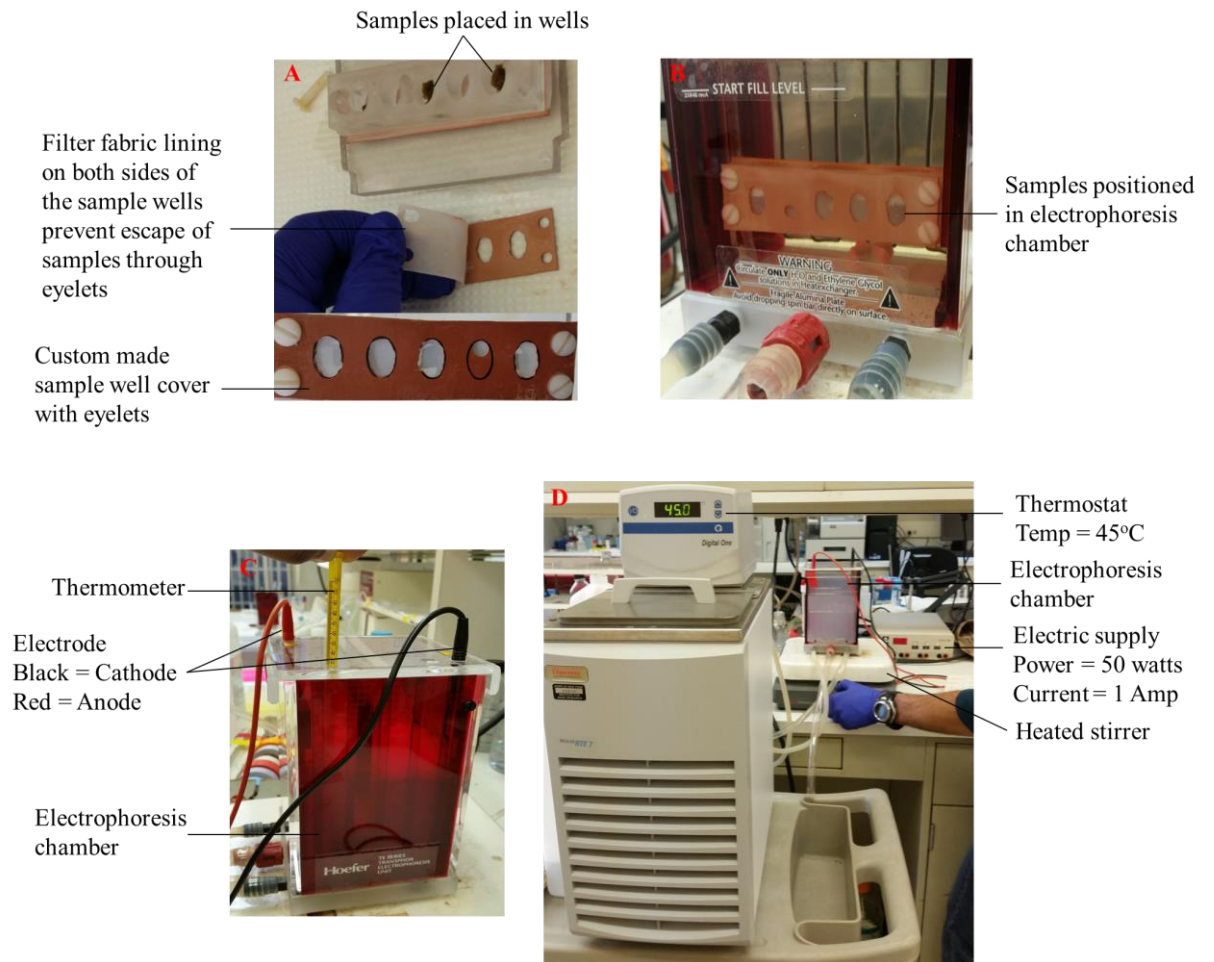
Figure 3.1: The electrophoretic clearing method.

The samples, ~1cm³, were placed in the sample wells sealed on both ends with filter lined custom built eyelets (A), then positioned in an electrophoresis chamber filled with clearing buffer (B). The chamber was sealed, electrodes connected and a thermometer inserted through the lid as shown in C. The chamber was placed on a heated stirrer and connected to the power supply and thermostat (D).
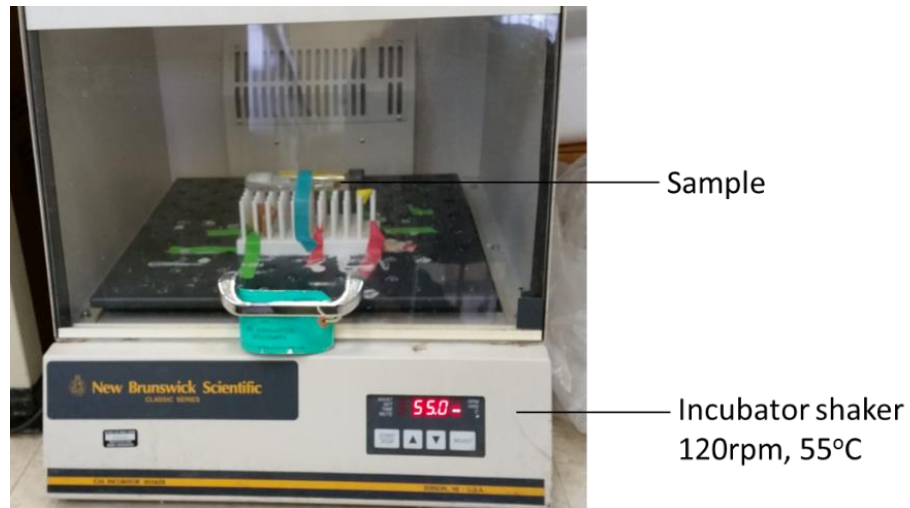
Figure 3.2: The passive clearing method.

The sample in a sealed tub filled with clearing buffer was placed in an incubator shaker.

3.2.1.4 Whole mount staining and imaging of cleared samples

Pieces of cleared samples, about 5mm^3, were rinsed thoroughly in wash buffer and suspended in 5ml of 99% Eosin Y (Sigma-Aldrich, Germany) for 10 minutes. For immunostaining, samples were washed in PBS and stained according to standard whole mount immunostaining protocol. This involved a protein blocking step with 2% bovine serum albumin (Sigma-Aldrich, Germany) in PBS before incubating samples overnight with a trophoblast marker (mouse anti-human cytokeratin 7 antibody; Dako, Denmark) used at 1:100 concentration, and subsequently with secondary antibody (goat anti-mouse IgG; Dako, Denmark) and a fluorescent dye (Acridine orange; Sigma-Aldrich, Germany). Stacks of the stained tissues were acquired with a laser scanning confocal microscope with water immersion objective lenses (Nikon Instruments Inc, USA), processed and rendered with Fiji Image J (Schindelin *et al.*, 2012).

3.3   Results

3.3.1   The effect of clearing on sample integrity

As clearing progressed, samples became increasingly pale and transparent (figures 3.3 and 3.4) such that the deeper structures including the vessels and smaller villi appeared more distinctively visible (figure 3.5) while the structure of the sample remained preserved. With the passive approach, samples cleared better and faster (Figure 3.4) compared to the electrophoretic method. Also, small pieces cleared within 14 days (Figure 3.4) while an intact placental lobule required more than double (~31 days) that amount of time (Figure 3.5). When not embedded in hydrogel before clearing, cleared samples felt extremely soft, slimy and fragile to touch. Samples embedded in hydrogel, on the other hand, were more resilient. As seen in figure 3.5, samples appeared to shrink as clearing progressed.

3.3.2   Clearing improved fluorescent dye penetration and imaging depth

To determine the effect of clearing on tissue permeability to fluorescent labels, samples were soaked in fluorescent dye as described in section 3.2.1.4 and the extent of dye penetration into the tissue was observed under a confocal microscope. In the uncleared (control) samples, the dye was visible only up to about 60µm depth. In the cleared samples, however, dye penetration was enhanced more than two fold (figure 3.6) such that the depth of fluorescence increased to 150µm.

3.3.3 Clearing had no substantial effect on villi structure

As described in section 3.2.1.4, samples were stained with an anti-cytokeratin-7 antibody, a known marker of trophoblasts. Villous trophoblast layers appeared not to be distorted by clearing; the cells remained well aligned around the villi and immunolabelling appeared better in the cleared tissue, showing and yielding bright localisation of the trophoblasts and also deeper structures within the villi (Figure 3.7).
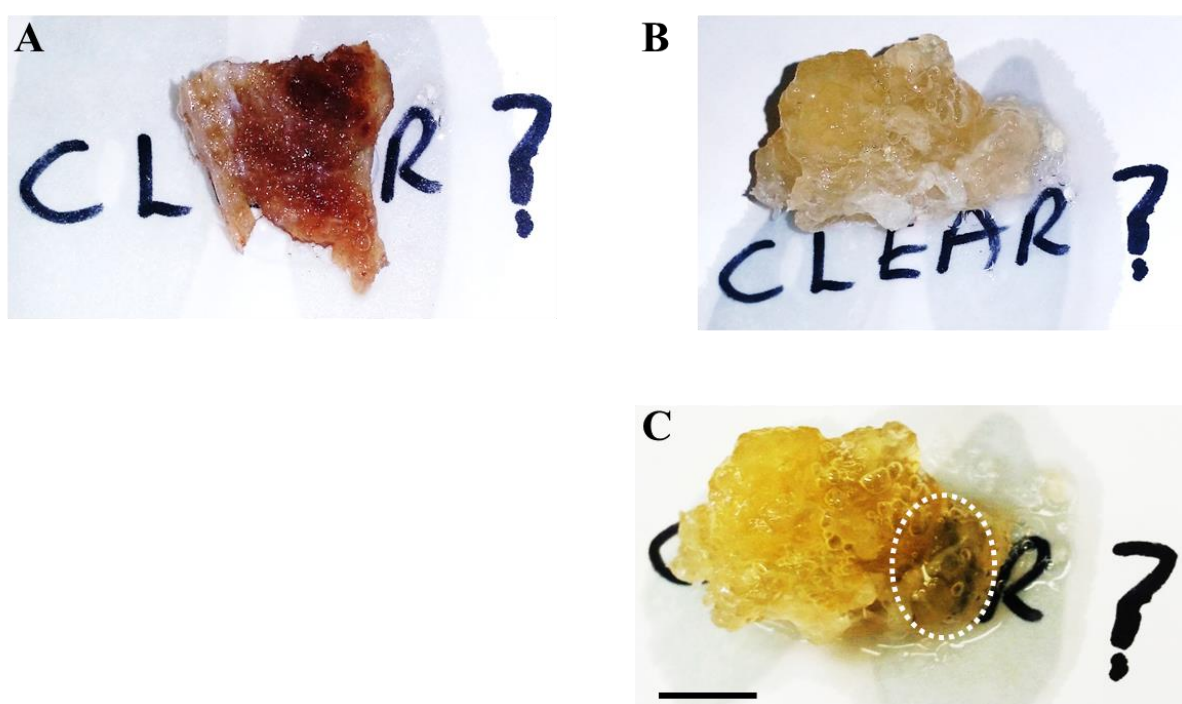
Figure 3.3: A piece of placenta specimen before and after clearing.

The piece shows transparency after clearing. A is control (uncleared), B and C are cleared specimens. In the encircled area in C, the underlying letter "A" is faintly visible. Scale bar represents 100mm.
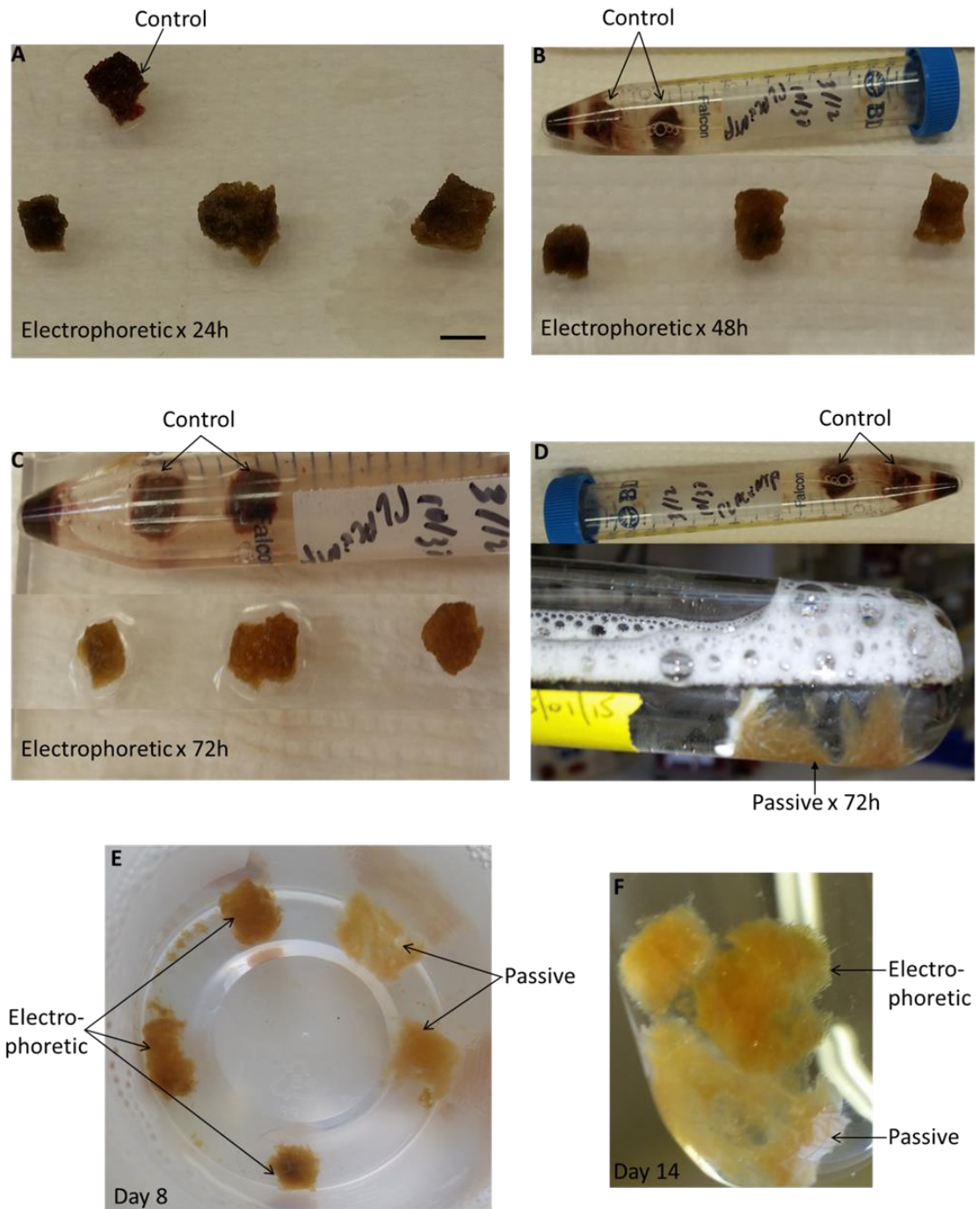
Figure 3.4: The progress of clearing over time.

Images shows samples following electrophoretic and passive clearing for 24h (A), 48h (B), 72h (C,D), 8 days (E) and 14 days (F). Scale bar represents 10mm.
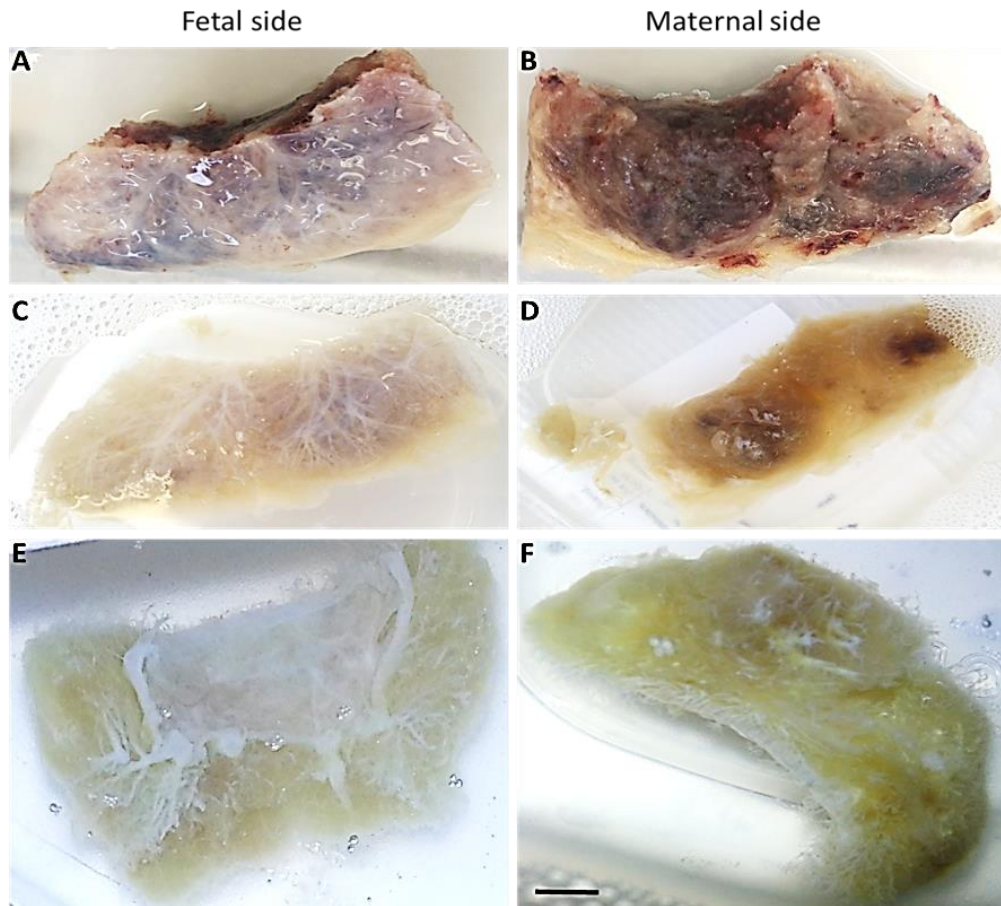
Figure 3.5: Progress of clearing in an intact placental lobule.

A placental lobule following passive clearing for 14 days (C, D) and 28 days (E, F). A and B are control. The sample appeared to shrink as clearing progressed. The chorionic plate can be seen shrunken in E. Scale bar represents 10mm.
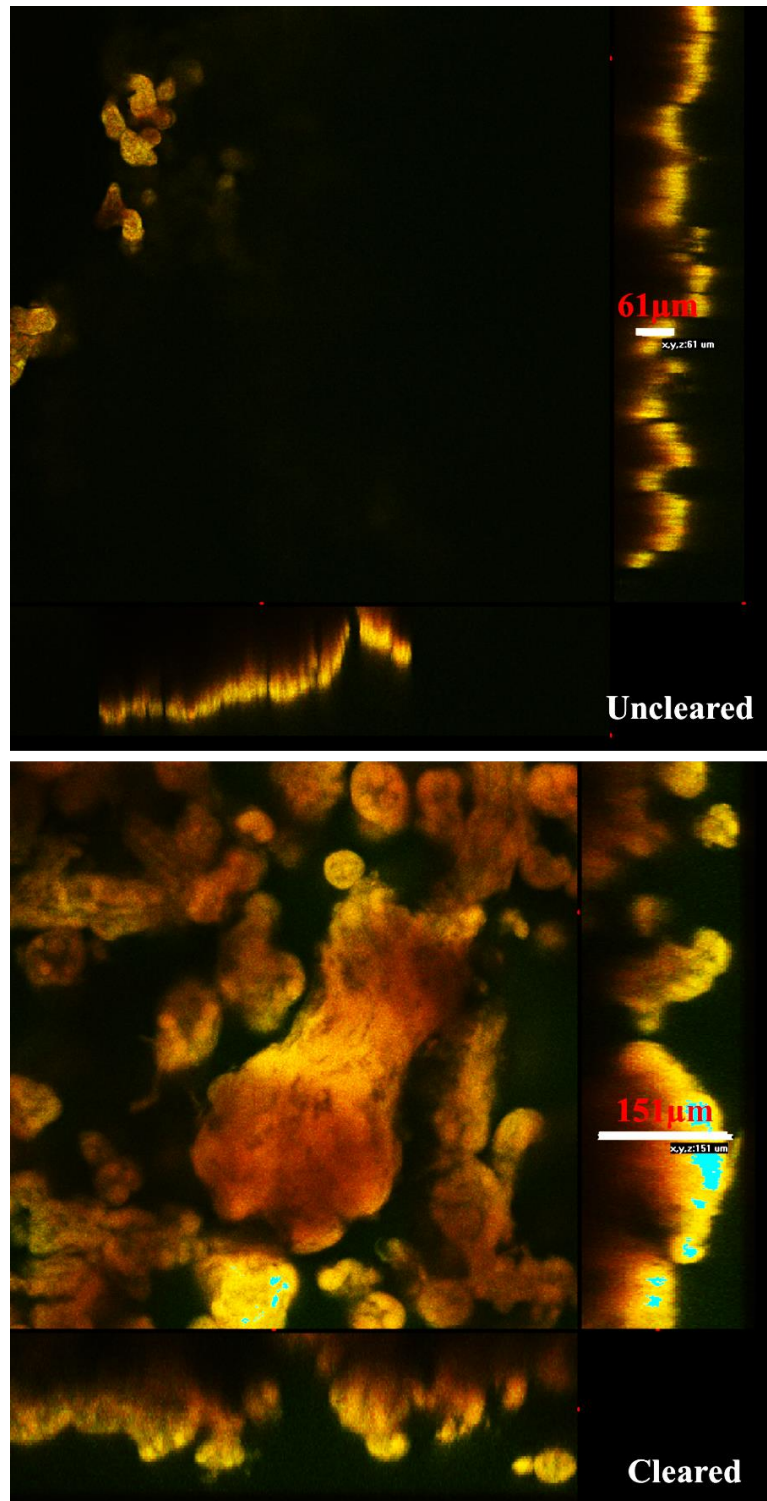
Figure 3.6: The effect of tissue clearing on depth of fluorescent dye penetration.

Confocal images with orthogonal projections depicting the depth of penetration of eosin in an uncleared (top) and a passively cleared (bottom) placental tissue. As shown by the scale bars, eosin penetration was deeper in the passively cleared than in the uncleared sample. In each image, the large, right and bottom panels represent the XY, XZ and YZ projections.
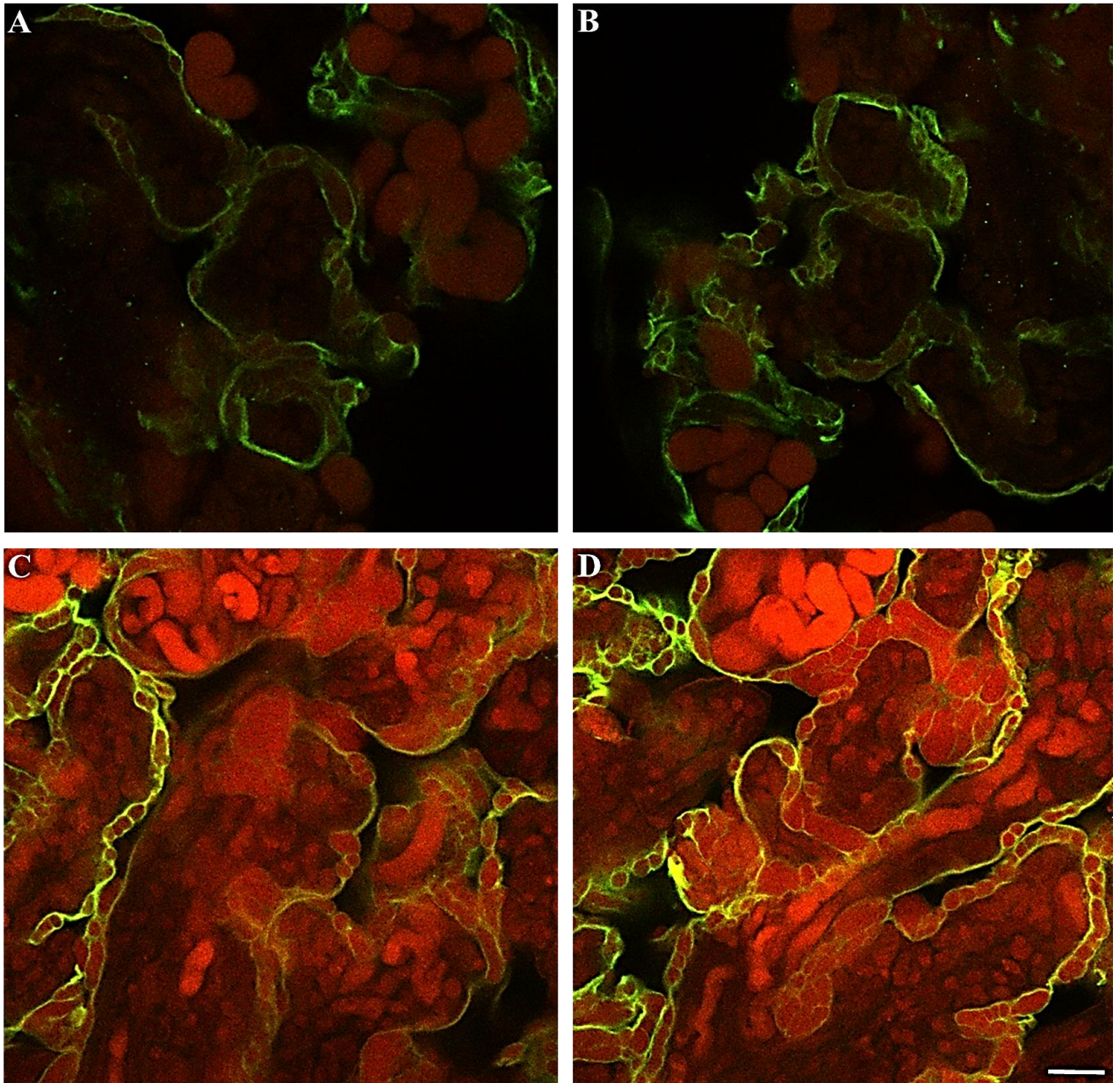
Figure 3.7: The effect of clearing on villous structure.

Representative images of uncleared (A and B) and cleared (C and D) placental tissue samples stained with trophoblast marker anti-cytokeratin 7 antibody (green) and fluorescent dye (acridine orange). Note the continuity of cytokeratin positivity in the trophoblast layer. Scale bar represents 100μm.

3.4 Discussion

3.4.1 Is the tissue clearing technique applicable in the study of the human placenta?

Approaches to investigate the morphological characteristics of the placental vasculature *ex vivo* have included histology (Junaid *et al.*, 2014; Chen *et al.*, 2002), electron microscopy (Krebs *et al.*, 1996), corrosion casting (Junaid *et al.*, 2014; Gordon *et al.*, 2007a) and mathematical modelling (Salafia *et al.*, 2010). None of these techniques has been suitable for extraction of information on the entire placental vascular network in an intact 3D state. While micro-CT imaging of corrosion cast specimens (described in chapter 2) gave a near-full account, vessels ≤100µm were excluded.

Tissue clearing techniques have mostly been used in examination of cells and their distribution and interconnections in intact specimens of, for example, mouse or human brains (Chung and Deisseroth, 2013; Chung *et al.*, 2013; Epp *et al.*, 2015; Hama *et al.*, 2011; Ke *et al.*, 2013; Liu *et al.*, 2015; Tomer *et al.*, 2014; Zheng and Rinaman, 2016). A variety of other tissues, such as skeletal muscle (Milgroom and Ralston, 2016), cartilage (Calve *et al.*, 2015), whole mouse (Yang *et al.*, 2014), liver (Lee *et al.*, 2014), kidney (Lee *et al.*, 2014), lung (Lee *et al.*, 2014), pancreas (Lee *et al.*, 2014) and intestine (Lee *et al.*, 2014) have all been successfully cleared but there have been no reports on the placenta. Two broad approaches to clearing biological specimens are described in the literature: the electrophoretic (Chung *et al.*, 2013) and the passive approach (Liu *et al.*, 2015; Tomer *et al.*, 2014). Here, both were adapted and tested for clearing human placental tissue, a larger and thicker organ with less lipid than brain and which is highly vascularised.

Differences in organ type necessitated modifications of the clearing protocol for the human placenta after several failed attempts. The process of clearing was observed to

occur gradually, and, depending on the sample size and method used, could be seen to advance over periods of several days or even weeks, as judged by the removal of blood residues. The high vascularity of the placenta and presence of blood proteins/haem impeded the rate of clearing and indeed it was difficult to achieve complete clearing. To overcome this, samples were first flushed with heparin to prevent intravascular coagulation and rinsed thoroughly with buffered saline before fixation and clearing.

Both the electrophoretic and passive methods have been shown to be effective for clearing, however, for placenta specimens, the passive method appeared more suitable particularly for large samples up to whole organ scale. The passive approach was cheaper, faster, and provided better clearing permitting better penetration of labelling probes. We observed that the duration of clearing was directly proportional to sample thickness, with placenta lobules taking more than twice as long as it took to clear smaller pieces of placenta (see figures 3.4 and 3.5). Also, tissue structure remained preserved following clearing and samples had better permeability as shown in figures 3.6 and 3.7.

3.4.2   Strengths and limitations of the study

This pilot study pioneered the utilisation of the tissue clearing technique in examination of human placenta specimens in an intact state. We endeavored to push the boundaries on tissue size with a view to eventual whole placental clearing and imaging. However, extracting information to characterise placental vascular network post-clearing remains a challenge. Also, immunostaining a sample the size of a whole intact placenta, if possible, will require large amounts of antibodies and dyes and will therefore be expensive. Furthermore, imaging depth of stained tissue samples depends on the working distance of the microscope objective and the thickness of the sample. We had

no access, if any exists, to an imaging tool able to handle a sample as large and thick as an intact human placenta. Advanced tools currently available allow imaging of specimens the size of a whole mouse (Pan *et al.*, 2016).

3.4.3   Summary

To summarise, we have demonstrated methods for successful clearing of human placenta samples to enhance the intensity of immunostaining in samples and improve imaging depth. While it is possible to clear large samples, the cost of immunostaining is a challenge, and imaging modality is limited by sample thickness. The technique was not suitable for our aim; however, going forward, there may be a role for the technique in placental studies that require small tissue samples. Also, future efforts should focus on developing analytical tools to extract information from cleared samples.

4   Chapter 4:   Altered placental vascularisation in FGR may be a sequela of

abnormal WNT signalling

4.1   Background

4.1.1   Placental vascularisation in human pregnancy

The processes involved in placental vascularisation are described in chapter 1. The precise mechanism by which vascularity becomes altered in FGR placenta is still unknown, but it may likely result from abnormalities in angiogenesis. Angiogenesis is regulated by interplay of several complex mechanisms involving several angiogenic factors, signalling molecules and receptors [for reviews see (Breier, 2000; Otrock *et al.*, 2007; Chen and Zheng, 2014; Carmeliet and Jain, 2011; Charnock-Jones *et al.*, 2004)]. It is not feasible to investigate all the mechanisms in a single project, hence, this study only focuses on one of the signalling mechanisms involved in endothelial cell-to-cell interactions during tube formation by placental endothelial cells [in physiological angiogenesis in the placenta].

4.1.2   Regulation of endothelial cell-to-cell interactions in placental angiogenesis

A crucial step in angiogenesis is adhesion of endothelial cells to one another via protein complexes and junctional adhesion molecules at adherens and tight junctions (Leach *et al.*, 2000). These contain the endothelial specific transmembrane protein vascular endothelial (VE) cadherin (Lampugnani *et al.*, 1992; Leach *et al.*, 1993), which, together with cytoplasmic proteins like β-catenin, form cadherin-catenin complexes responsible for gluing endothelial cells together (figure 4.1A) to form tubes (Lampugnani *et al.*, 1995; Dejana *et al.*, 1999). The cadherin-catenin complexes stabilise the tubes formed by linking the actin cytoskeleton of neighbouring endothelial cells together.

4.1.3 The role of WNT signalling in placental vascularisation disorders

The cytoplasmic protein β-catenin is a central player in a signalling pathway activated by wingless-related integration site (WNT) proteins, signalling molecules involved in the regulation of cell-to-cell interactions during development and in adult tissue homeostasis (Cadigan and Nusse, 1997; van Amerongen and Nusse, 2009). WNT signals are transduced via either a canonical or a non-canonical pathway. Canonical WNTs act by binding to co-receptor complexes comprising transmembrane G protein-coupled Frizzled (FZD) and low density lipoprotein receptor related proteins (LRP) on the cell surface to initiate a signal transduced to cytoplasmic β-catenin which migrates to the cell nucleus, inducing transcription of T-cell factor/lymphoid enhancer factor (TCF/LEF) complexes to activate WNT target genes (figure 4.1A) (Willert and Nusse, 1998; Komiya and Habas, 2008; Cadigan and Peifer, 2009; Macdonald *et al.*, 2007). Non-canonical WNTs on the other hand act by binding to FZDs independently of LRP5 or LRP6 and function independent of β-catenin (Komiya and Habas, 2008; Knofler and Pollheimer, 2013; Kohn and Moon, 2005; Semenov *et al.*, 2007). There are 19 *WNT* genes, 10 FZD and 2 LRP receptors in humans (Wodarz and Nusse, 1998; Hey *et al.*, 1998; Kim *et al.*, 1998; Massink *et al.*, 2015). Of these, 14 *WNT* genes, 8 FZD receptors (Sonderegger *et al.*, 2007) and both LRP receptors (Pollheimer *et al.*, 2006) exist in the human placenta (see Table 4.1).

Human endothelial cells *in-vivo* as well as in culture have been shown to possess an autogenous ability to activate the canonical WNT signalling pathway, in addition to expressing several receptors and modulators of WNT signalling (Goodwin *et al.*, 2006). Canonical WNTs are believed to support angiogenesis by organising and stabilising cadherins at adherens junctions thereby aiding cell-to-cell adhesions (figure 4.1A) (Dejana, 2010). Many studies now propose that developmental angiogenesis in organs such as the placenta (Ishikawa *et al.*, 2001; Herr *et al.*, 2014; Monkley *et al.*, 1996;

Chen *et al.*, 2016), lungs (Yuan *et al.*, 2015), retina (Huang *et al.*, 2016; Wang *et al.*, 2012; Ye *et al.*, 2009; Zhou *et al.*, 2014) and brain (Daneman *et al.*, 2009; Stenman *et al.*, 2008) require WNT signalling. Similarly, many suggest that an angiogenic switch secondary to abnormal WNT signalling is a major culprit involved in tumour progression in carcinogenesis (Yeo *et al.*, 2014; Ekstrom *et al.*, 2014; Pate *et al.*, 2014; Yao *et al.*, 2014; Planutis *et al.*, 2014; Ji *et al.*, 2015). Thus, WNT signalling pathway alterations alter endothelial cell behaviour leading to vascular defects. In the mouse placenta, WNT2 deficiency was shown to result in catastrophic defects in vessel development such as decrease in the number of fetal capillaries, oedema from accumulation of maternal blood, and increase in the amount of fibrinoid material (Monkley *et al.*, 1996). Also, homozygous offspring of FZD5 knockout mice were plagued with fatally defective vasculogenesis in the placenta due to markedly reduced endothelial cell proliferation, disorganised capillary plexus, and defects in yolk sac angiogenesis as a result of WNT5A/FZD signalling failure (Ishikawa *et al.*, 2001). Homozygous WNT7B mutant mice do not survive past mid gestation due to placental abnormalities including failure of chorio-allantoic fusion, abnormally shaped chorion, decrease in the size of the chorion and alterations in the organisation of the chorion (Parr *et al.*, 2001).
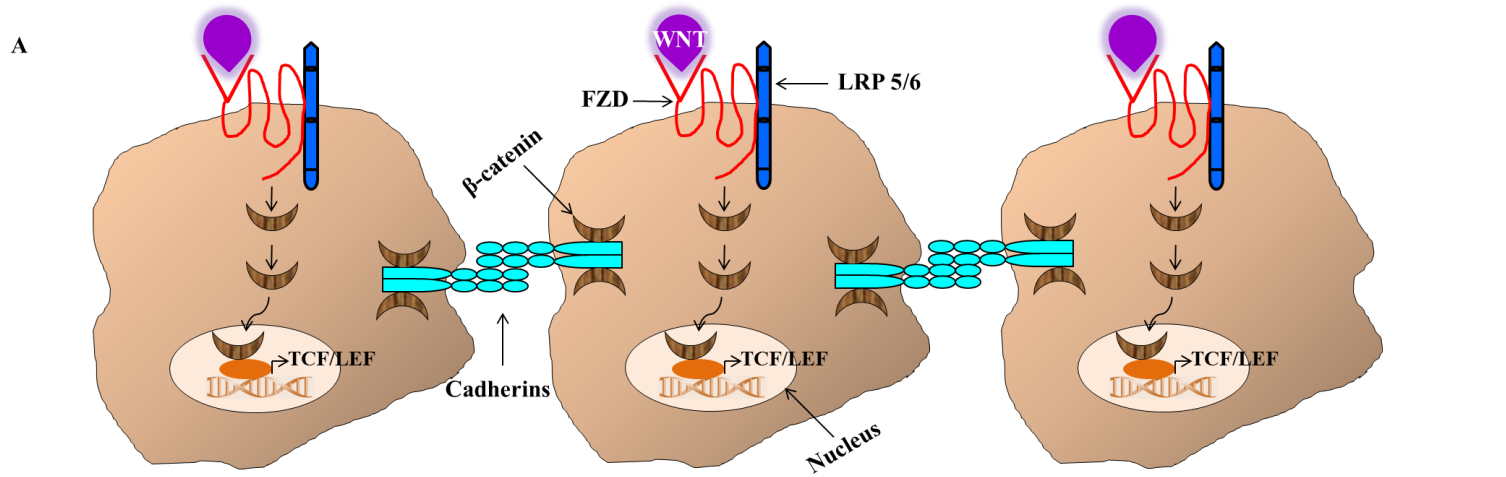
Figure 4.1: Canonical WNT signalling in endothelial cells.

When the pathway is active (A), WNTs bind to the FZD-LRP5/6 receptor complexes on the cell membrane to activate stabilisation and translocation of cytoplasmic β-catenin to the cell nucleus where β-catenin activates transcription of TCF/LEF complexes to activate WNT target genes. β-catenin also migrate to the adherens junctions where, by forming cadherin-catenin complexes with the endothelial specific transmembrane protein VE-cadherin, they stabilise and organise the adherens junctions to foster cell-cell adhesion. In the absence of WNT (B), when WNT gets inhibited by WIF or sFRP for example, cytoplasmic β-catenins become unstable and gets ubiquitinated and degraded by proteasomes. Adherens junctions become unstable and disorganised due to lack of cadherin-catenin complexes. Redrawn and modified from Dejana 2010 (Dejana, 2010).
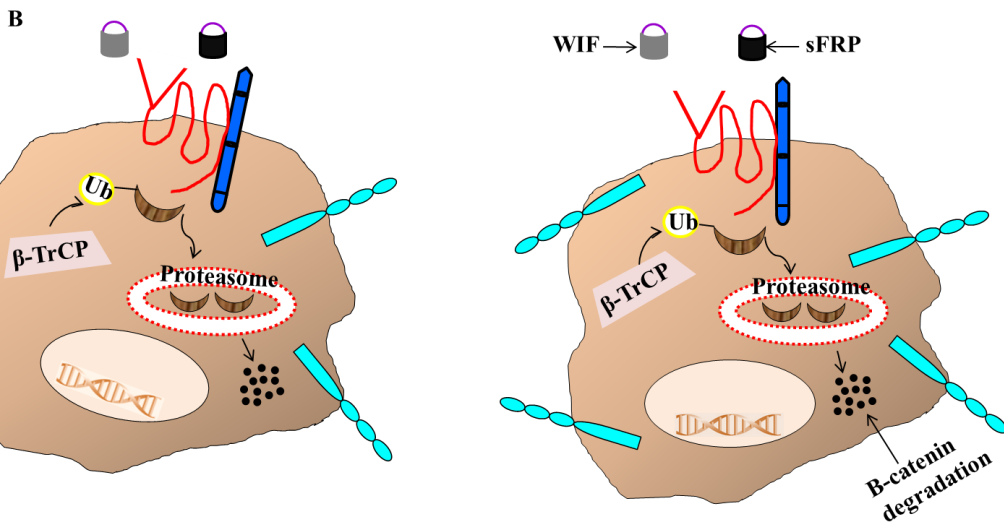
Table 4.1: Human *WNT* genes and receptors.

Human *WNT* genes	Present in placenta?
WNT1	Yes
WNT2	Yes
WNT2B (WNT13)	Yes
WNT3	Yes
WNT3A	No
WNT4	Yes
WNT5A	Yes
WNT5B	Yes
WNT6	Yes
WNT7A	Yes
WNT7B	Yes
WNT8A	No
WNT8B	No
WNT9A (**Previously** *WNT14*)	No
WNT9B (**Previously** *WNT15*)	Yes
WNT10A	Yes
WNT10B	Yes
WNT11	Yes
WNT16	No
Human FZD receptors	**Present in placenta?**
FZD1	Yes
FZD2	Yes
FZD3	Yes
FZD4	Yes
FZD5	Yes
FZD6	Yes
FZD7	Yes
FZD8	No
FZD9	No
FZD10	Yes
Human LRP receptors	**Present in placenta?**
LRP5	Yes
LRP6	Yes

4.1.4 Hypothesis/Aims

Here, we hypothesize that endothelial cell behaviour is altered in FGR placentas due to instability and disorganisation of adherens junctions following abnormal WNT signalling. A successful attempt to correct WNT signalling impairment may therefore prove effective in enhancing placental angiogenesis and, in effect, improve placental vascularity.

We aimed to

i. Determine the effect of WNT inhibition on human placental endothelial cells in culture

ii. Determine the response of human endothelial cells to withdrawal of WNT inhibition following exposure

iii. Compare the effect(s) of WNT signalling inhibition on endothelial cell behaviour in placentas from normal and FGR complicated pregnancies

iv. Compare the response of normal and FGR endothelial cells to withdrawal of WNT inhibition following exposure

To achieve these aims, it was important to understand the normal behaviour of endothelial cells in culture and how to inhibit WNT signalling.

4.1.5 Endothelial cell behaviour in *in-vitro* angiogenesis

The main cells involved in angiogenesis are the endothelial cells. In culture, when endothelial cells of the same origin are incubated together in favourable conditions and fed with essential growth factors, they spontaneously sprout outgrowths towards one another to form three-dimensional tube-like structures [TLS; otherwise known as

capillary-like structures] (Auerbach *et al.*, 2003). Their TLS formation potential may be further enhanced by culture on collagen- or fibrin-coated plates. The process involves interplay of proteins and complex mechanisms including several angiogenic growth factors, WNTs, integrins, chemokines, proteases, junctional molecules and receptors (Carmeliet and Jain, 2011).

4.1.6 How to inhibit WNT signalling in endothelial cells in culture

Canonical WNT signalling is regulated by secreted proteins that can antagonise and turn off the pathway. There are natural WNT inhibitors such as WNT inhibitory factor (WIF) and secreted frizzled-related protein (sFRP) that can bind WNTs (figure 4.1B), preventing WNT interaction with receptors (Hsieh *et al.*, 1999; Ng *et al.*, 2014; Cruciat and Niehrs, 2013); Dickkopf (DKK) proteins which disrupt FZD-LRP complex formation (Semenov *et al.*, 2001); and beta transducing repeat-containing E3 ubiquitin protein ligase (β-TrCP) which mediates ubiquitination and degradation of β-catenin by proteasomes (figure 4.1B) (Aberle *et al.*, 1997; Marikawa and Elinson, 1998).

In culture, WNT signalling can be inhibited by targeting various levels of the pathway. Examples of pharmacologic compounds that have been shown to effectively inhibit WNT signalling are listed in Table 4.2.

Here, niclosamide (2',5-dichloro-4'-nitrosalicylanilide), an anti-helminthic drug used for treatment of tapeworm infection in humans, was used to inhibit WNT signalling in human placental endothelial cells. Niclosamide is known to exert multiple inhibitory effects on the WNT pathway by promoting endocytosis of FZD receptors (Chen *et al.*, 2009b), degrading LRP5 and LRP6 (Lu *et al.*, 2011), and inhibiting stabilisation of β-catenin (Chen *et al.*, 2009b). These inhibitory effects on WNT signalling are now identified as mechanisms for its potential as a cancer therapeutic agent (Arend *et al.*,

2014; Lu *et al.*, 2011; Ono *et al.*, 2014). Its ability to inhibit WNT signalling at multiple levels, thereby non-specifically blocking all types of WNT action, makes it a suitable WNT inhibitor in human placenta-derived cells known to express many *WNT* genes and receptors.

By treating human placenta-derived endothelial cells with niclosamide, it is anticipated that the drug will inhibit WNT signalling, causing instability of cadherins, disorganisation of adherens junctions and failure of TLS formation. Primary endothelial cells derived from placentas from FGR complicated placentas may be especially affected. And reversing WNT inhibition (by removing niclosamide) may rescue cells affected by impaired WNT signalling. Also, if WNT signalling in FGR endothelium is altered, the corresponding endothelial cells may be differentially sensitive to pharmacological modulators of the WNT pathway.

Table 4.2: Pharmacological inhibitors of WNT signalling in culture

Compound	Mechanism of action	Reference
Ant1.4Br/Ant 1.4Cl	Inhibits free WNT (no effect on membrane bound WNT)	(Morrell *et al.*, 2008)
C59	Inhibits WNT secretion Inhibits WNT activation of β-catenin	(Proffitt *et al.*, 2013)
Inhibitor of WNT production (IWP)	Inhibits WNT secretion	(Chen *et al.*, 2009a)
Niclosamide	Inhibits WNT-stimulated β-catenin stabilisation Promotes FZD endocytosis Degrades LRP-5/6	(Chen *et al.*, 2009b; Lu *et al.*, 2011)
Apicularen	Inhibits WNT-receptor complexes	(Cruciat *et al.*, 2010)
Bafilomycin	Inhibits WNT-receptor complexes	(George *et al.*, 2007)
2,4-diamino-quinazoline	Inhibits β-catenin transcriptional activity	(Chen *et al.*, 2009c)
Vitamin D (1-alpha, 25-dihydroxyvitamin D3)	Inhibits β-catenin transcriptional activity	(Pendas-Franco *et al.*, 2008)
Quercetin	Inhibits β-catenin transcriptional activity	(Park *et al.*, 2005)
Shizokaol D	Inhibits endogenous WNT target genes	(Tang *et al.*, 2016)
OMP-18R5	Inhibits WNT signalling by interacting with multiple FZD receptors	(Gurney *et al.*, 2012)

4.2 Materials and methods

4.2.1 Cell culture

All culture experiments were performed in a sterile microbiological safety cabinet.

4.2.1.1 Cell types/lines

Two types of human placenta-derived endothelial cells were used. Human umbilical vessel endothelial cells (HUVECs) were purchased from Lonza, USA. Human placental artery endothelial cells (HPAECs) were donated by Dr Paul Brownbill. These primary endothelial cells had been isolated from human placental chorionic plate arteries from normal and FGR placentas, and confirmed to be endothelial cells by immunohistochemical staining for endothelial specific markers (Jones *et al.*, 2015).

All HUVECs and HPAECs were used between the second and fifth passages.

4.2.1.2 Growing cells to confluency

For HUVECs, the cells were grown in $75cm^2$ cell culture flasks (Corning Inc, USA). To each flask, 15ml of pre-warmed culture media [endothelial basal medium-2 supplemented with endothelial growth medium-2 (EBM-2 and EGM-2; Lonza, bullet kit catalogue number CC-3162)] was added, then left in incubator for 15 minutes. A vial of HUVECs was removed from cryogenic storage, the cells were quickly thawed by adding 1ml of warm serum-containing media to the vial. Thawed cells were added at 1×10^6 cells/flask and mixed gently for even distribution. Flasks were left in an incubator (21% O_2, 5% CO_2, 37^0C) until cells had grown to 60% confluency.

Due to a smaller quantity of cells available and extremely sparse distribution, hence poor survival, of HPAECs when cultured in $75cm^2$ flasks, the cells were grown in

$25cm^2$ flasks. To each flask, 4ml of pre-warmed culture media [endothelial basal medium supplemented with endothelial growth medium-microvascular (EBM and EGM-MV; Lonza, bullet kit catalogue number CC-3125), vascular endothelial growth factor (VEGF; Lonza, catalogue number CC-4114A) and recombinant human fibroblast growth factor basic 146 amino acids (rhFGF basic; R&D Systems, catalogue number 233-FB-025)] was added and incubated for 15 minutes. A vial of HPAECs was removed from cryogenic storage, the cells were quickly thawed by adding 1ml of warm serum-containing medium to the vial. Thawed cells were spun down in a centrifuge for 5 minutes at 800rpm, re-suspended in 1ml of culture medium, added to each flask at 0.5 x 10^6 cells/flask and mixed gently for even distribution. Flasks were left in an incubator (21% O_2, 5% CO_2, 37^0C) until 60% confluent.

4.2.1.3   The tube-forming assay

A schematic of the experimental set-up for the tube-forming assay is shown in figure 4.2. Sterilised 12mm diameter coverslips (Thermoscientific Inc, UK) were placed in 18 wells of a sterile 24 well cell culture plate (Corning Inc, USA) and coated with a thin homogenous spread of 80% matrigel basement membrane matrix (Corning B.V, The Netherlands). Plates were placed in a 37^0C incubator (21% O_2, 5% CO_2, 37^0C) for the gel to set. A flask of cells was washed thrice with sterile Hank's balanced salt solution without Ca^{2+}/Mg^{2+} (HBSS; Invitrogen) and trypsinised (Trypsin-EDTA; Lonza, catalogue number CC-5012) for few minutes to detach the cells (2ml trypsin per $75cm^2$ flask, 1ml trypsin per $25cm^2$ flask). Serum-containing media [Dulbecco's modified eagle's medium (DMEM; Lonza) with fetal calf serum (FCS; Lonza)] was added to neutralise trypsin. Cells were spun down for 10 minutes at 1000rpm, then re-suspended in the appropriate culture media for the cell type. Cells were counted in haemocytometer, then seeded on matrigel-coated coverslips (figure 4.2A) at 10,000 cells/well and

incubated (21% O_2, 5% CO_2, 37^0C). By 6h post-seeding when cells had attached to matrigel (figure 4.4), 1µM niclosamide, dissolved in dimethyl sulfoxide (DMSO), was added to 6 wells, and equal concentration of DMSO (vehicle) was added to another 6 wells (figure 4.2B). The final concentration of DMSO in each of these 12 wells was 0.001% (1µl per 1000µl of culture media). The remaining 6 wells had only cells growing on matrigel. By 24h (36-48h for FGR HPAECs) post treatment when appropriate tubes had formed in the wells, images were captured with the x10 objective on a digital microscope (EVOS XL Core, AMG, ThermoFisher scientific, UK). For each coverslip, three images were captured using a random systematic approach and excluding the edges of the wells. Coverslips from three wells each in the untreated, niclosamide-treated and vehicle-treated cell groups were transferred into a new 24 well plate and the cells fixed as described in section 4.2.1.4 (figure 4.2C). The remaining three wells each of untreated, niclosamide-treated and vehicle-treated cells were rescued (figure 4.2C) by aspirating media and replacing with fresh warm culture media appropriate for the cell type. Rescued cells were cultured for a further 24 hours, imaged and fixed as in section 4.2.1.4.

4.2.1.4 Fixation of cells

Media was removed from each well by aspiration. Coverslips were washed thrice with PBS to completely remove media. Cells were fixed by adding 1ml of 4% PFA to each well for 30 minutes at room temperature. Subsequently, each coverslip was washed thrice with PBS to remove PFA, then each coverslip was covered with 1ml of PBS. Plates were sealed with parafilm to prevent evaporation and stored at 4^oC.
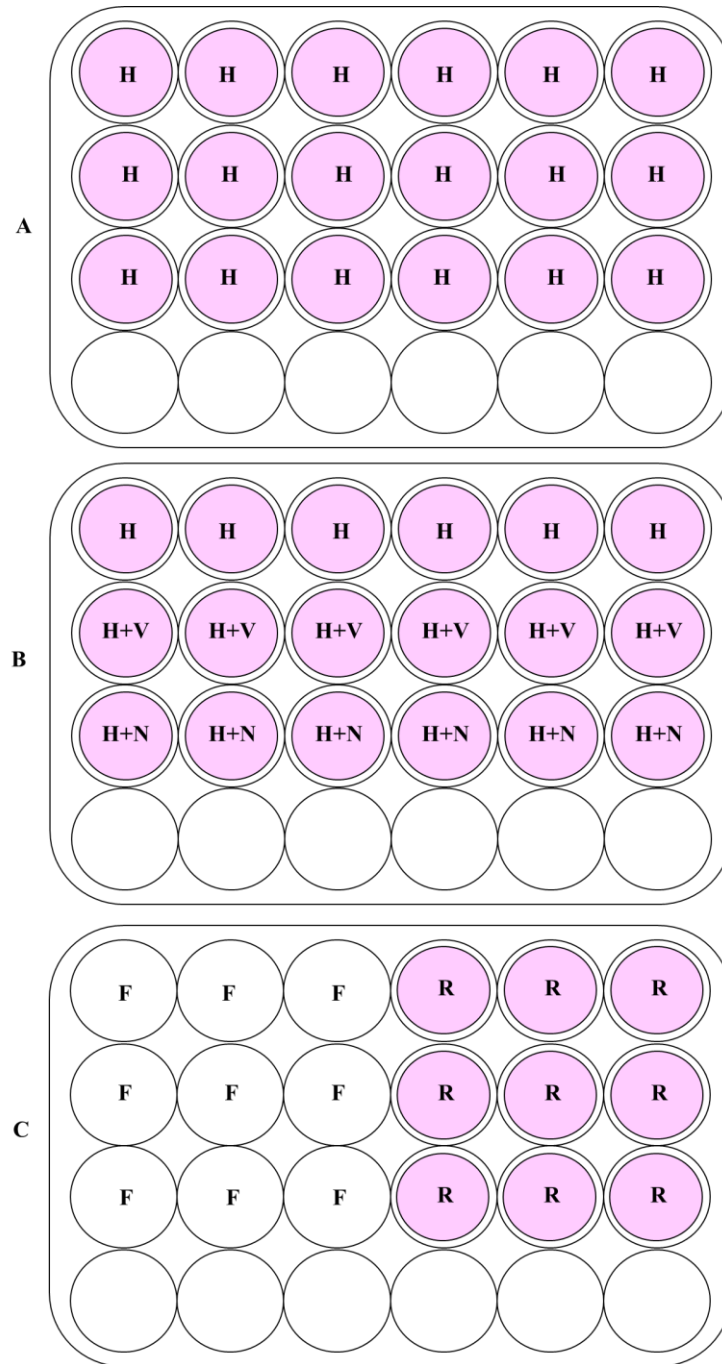
Figure 4.2: Experimental set-up for tube-forming assay.

For each experiment, sterilised coverslips were placed in 18 wells in a 24-well plate and coated with 80% matrigel (pink) before seeding the endothelial cells (H) on them as shown in A. Once the cells attached to matrigel, niclosamide (N) was added to 6 wells and the vehicle (V) was added to 6 wells as shown in B. At 24h post treatment, coverslips from 3 wells in each group were transferred into a new plate and fixed (F). Cells in the remaining wells were 'rescued' (R) by changing the culture media, shown in C.

4.2.1.5 Immunocytochemistry

Cells on coverslips were placed in ammonium chloride (2.6mg/L in PBS) for 10 minutes to quench auto-fluorescence and enhance antigenicity, then washed thrice in PBS and permeabilised in 0.5% Triton-X for 15 minutes at room temperature. The coverslips were washed again thrice in PBS and placed on a labelled sheet of parafilm in a dark humid chamber, with the cell covered surface facing up. Primary antibody, diluted in 1% BSA, was pipetted at 50µl/coverslip followed by overnight incubation at 4°C. The primary antibodies used for the separate staining experiments included polyclonal rabbit cleaved caspace 3 (CC3; Abiob Biotechnology Inc, Germany) to mark apoptotic cells, monoclonal mouse anti-Ki67 (Dako, Denmark) to mark proliferating cells, and monoclonal rabbit anti-β-catenin (Sigma Aldrich, Germany) to demonstrate the effect of WNT inhibition by niclosamide on the cells. Cells were then incubated for 2 hours at room temperature with the appropriate secondary antibody (an anti-species of the first antibody) conjugated with fluorescent dye (Alexa fluor 488; ThermoFisher Scientific, UK) and conjugated phalloidin (Alexa 568 phalloidin, ThermoFisher Scientific, UK) to mark actin filaments. Secondary antibody was washed off, followed by a 4′,6-diamidino-2-phenylindole (DAPI; ThermoFisher Scientific, UK) wash to mark nuclear DNA before cells were mounted on labelled slides using fluorescent mounting medium (Dako, Denmark). Stained coverslips were stored in the dark at 4°C ready for imaging.

4.2.1.6 Microscopy

Cells were imaged on a Zeiss Axio Observer Z1 inverted fluorescence microscope (Carl Zeiss Microimaging GmbH, Germany), using the attached Apotome accessory and Zen software to reduce background fluorescence and edit the images respectively.

4.2.1.7 Histochemical assessment for cellular senescence

Niclosamide-treated cells were assessed using the senescent cells histochemical staining kit (Sigma Aldrich Inc, USA). The method is based on detection of SA-β-gal activity, which has been extensively used as a biomarker for senescence (Heo *et al.*, 2013; Dimri *et al.*, 1995). Following treatment, cells were fixed for 6 minutes at room temperature in 20% formaldehyde, 2% glutaraldehyde, 70.4mM Na_2HPO_4, 14.7mM KH_2PO_4, 1.37M NaCl, and 26.8mM KCl. Fixed cells were washed with PBS, and incubated overnight with freshly prepared staining mixture (staining solution + potassium ferricyanide + potassium ferrocyanide + X-gal solution + distilled H_2O) at 37^oC in non-CO_2 incubator. Cells positive for senescence stained blue. Images were captured with the x10 objective on a digital microscope (EVOS XL Core, AMG, ThermoFisher scientific, UK). For each coverslip, three images were captured using a random systematic approach and excluding the edges of the wells. Cells were overlaid with 70% glycerol solution and stored at 4^oC. The experiment was repeated 5 times, each performed in triplicate.

4.2.2 Data analysis

4.2.2.1 Analysis of tube assay images

Tube assay images were analysed using the Wimtube programme for tube formation assay (Wimasis Image Analysis, Germany) to quantify the cell covered area, tube length, number of tubes and branch points in each image (figure 4.3).
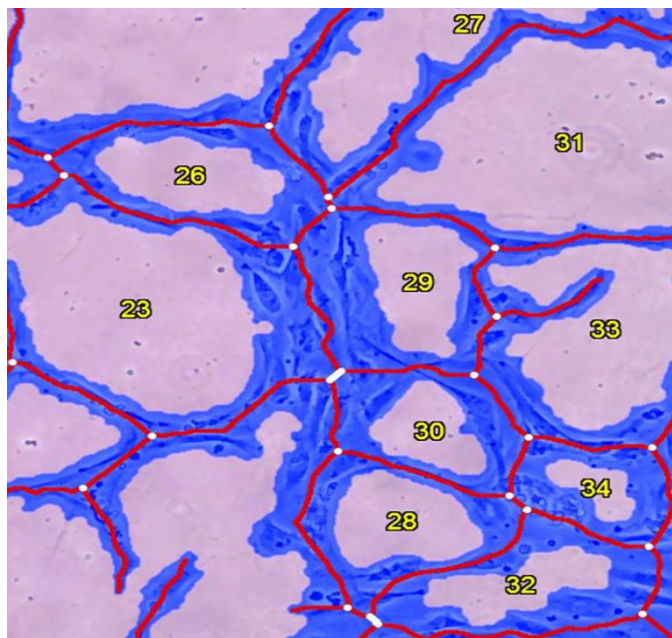
Figure 4.3: Example of an image analysed by the Wimtube programme.

Cell covered areas are marked in blue, tubes marked in red, branching points marked in white and loops (completely connected tubes) numbered in yellow.

4.2.2.2   Analysis of senescence images

For quantification of senescence, the total number of cells and the number of cells positive for senescence (blue) in each image was counted. The mean number from the three fields from each experiment and the mean percentage of positive cells were calculated.

4.2.2.3   Statistical analysis

Statistical analyses were conducted using GraphPad Prism® 6 (version 6.04 GraphPad Software, Inc., USA). Normality of data distribution was tested by D'Agostino & Pearson omnibus normality test. Where data passed normality test, they were

represented as mean ± standard error of mean (SEM) and compared by t test, unless otherwise stated. Non-parametric data were presented as median and interquartile range (IQR) and compared by Mann Whitney test and Wilcoxon matched-pairs signed rank test for unpaired and paired data sets respectively, unless otherwise stated. A p value of <0.05 was considered to be statistically significant.

4.3   Results

4.3.1   Placental endothelial cell behaviour in *in-vitro* angiogenesis

As expected, the endothelial cells attached and formed TLS on matrigel after few hours of incubation (Figure 4.4). By 3h, seeded HUVECs were attached to matrigel beginning the process of tube formation. HUVECs formed TLS by 24h post seeding. Normal HPAECs were attached by 4h and formed tubes by 24h. FGR HPAECs, on the other hand, were slower. They required up to 6h and 36-48h to attach and form tubes respectively.
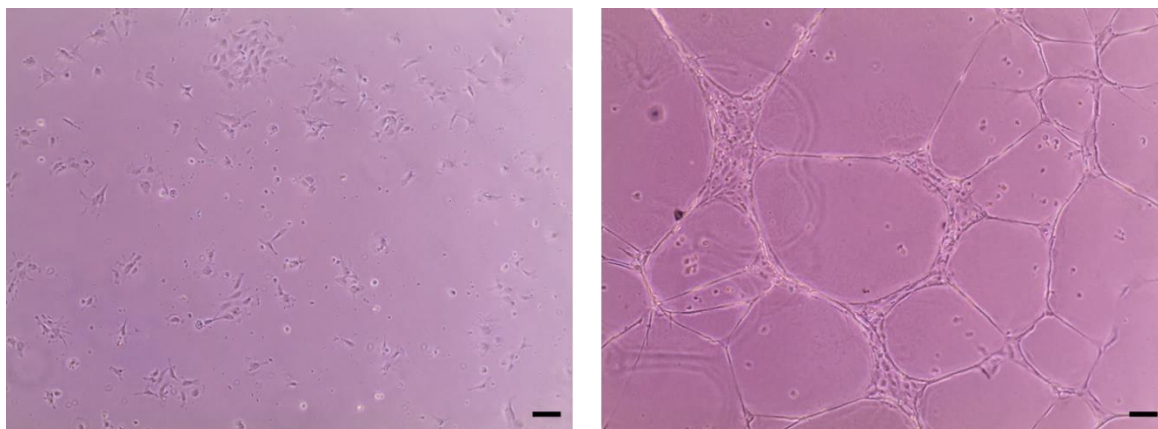
Figure 4.4: Behaviour of HUVECs in *in-vitro* angiogenesis.

When seeded on matrigel, human umbilical vein endothelial cells (HUVECs) attached to the underlying matrigel within 3h (left) and networked with one another to form tube-like structures (right) by 24h post seeding. Scale bar represents 1000µm.

4.3.2 The effect(s) of WNT signalling inhibition on human placental endothelial cells in culture

4.3.2.1 The vehicle (DMSO) had no effect on the behaviour of HUVECs in culture

The vehicle used for dissolving niclosamide in this experiment was DMSO. Cells cultured with DMSO were compared with cells cultured alone on matrigel (control). As shown in figure 4.5, DMSO had no significant effect on the behaviour of HUVECs, including their ability to form TLS, compared to control. The mean percentage area of coverslip covered by cells was $23.66 \pm 2.79\%$ in the control group, similar to $22.49 \pm 2.71\%$ in the vehicle group, $p = 0.77$. A mean of 108.40 ± 11.60 TLS were formed by cells in the control group, compared to 128.20 ± 12.85 TLS in the vehicle group, $p = 0.26$; number of branch points was 33.02 ± 5.44 and 43.26 ± 7.46 in the control and vehicle groups respectively, $p = 0.28$; and tube length was only slightly longer in the vehicle group (16863 ± 1579mm compared to 14607 ± 1368mm in controls, $p = 0.29$). Having established this, data showing the effect of niclosamide treatment on the cells were represented on graphs as a percentage of the appropriate vehicle.
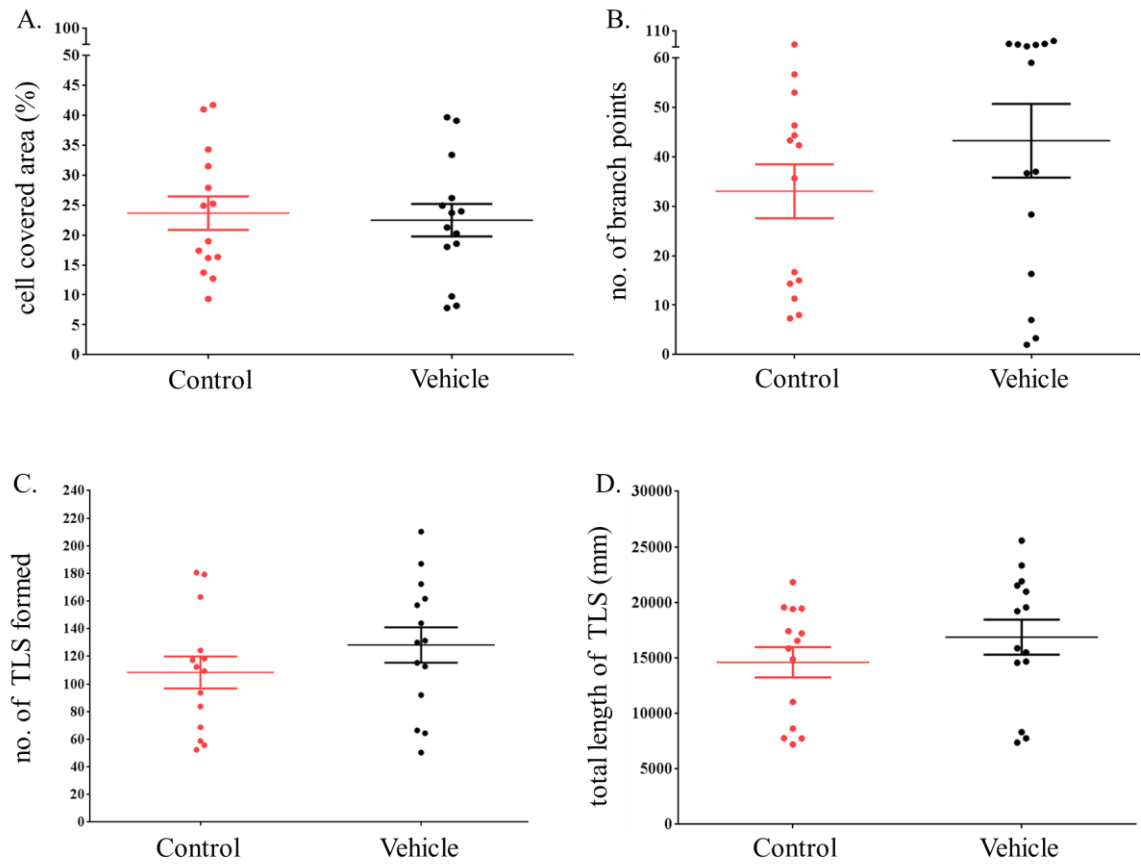
Figure 4.5: The effect of DMSO (vehicle) on HUVEC behaviour in culture.

DMSO had no appreciable effect on the cells' ability to form TLS. Control refers to cells cultured alone, vehicle refers to cells cultured with 1μM of DMSO. Data represents the mean ± SEM of n = 14 experiments. Each experiment was performed in triplicate. Normality of data tested and confirmed by D'Agostino & Pearson omnibus normality test. Comparison by Unpaired t test with Welch's correction. P value considered significant if <0.05.

4.3.2.2 Niclosamide alters endothelial cell behaviour and inhibits TLS formation

The ability of placenta-derived endothelial cells to form TLS on matrigel following treatment with Niclosamide was assessed to determine whether WNT inhibition affects placental angiogenesis. TLS was visibly reduced in wells containing niclosamide-treated cells. Niclosamide's effect was noticeable from 1μM concentration above which varying concentrations impaired TLS formation in a dose dependent manner, with ≥2μM being toxic to the cells (figure 4.6).

Vehicle

Niclosamide treated

0.1μM

0.1μM

0.5μM

0.5μM

1μM

1μM

1.5μM

1.5μM
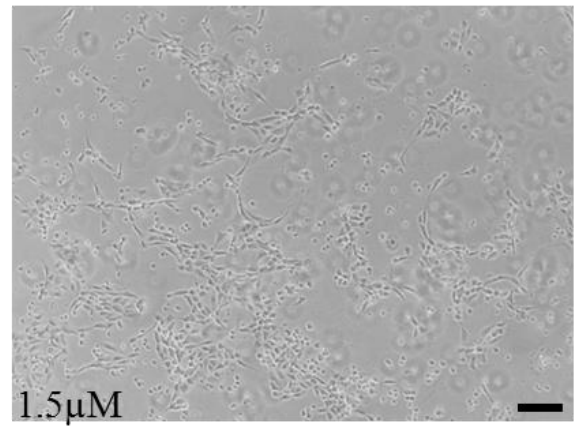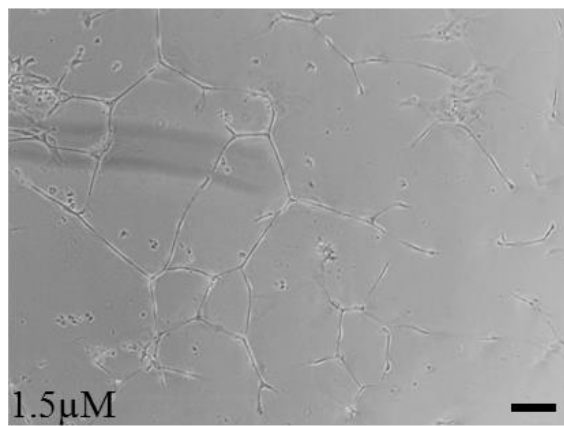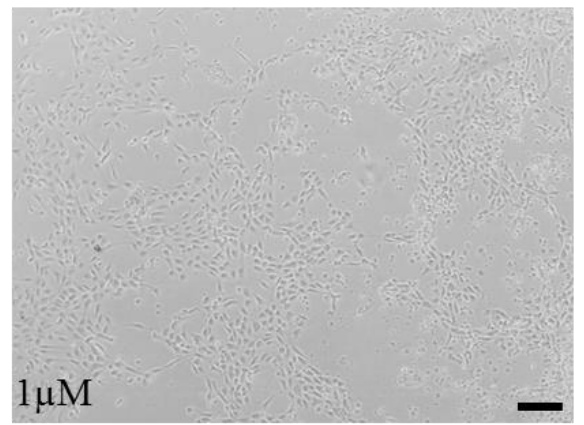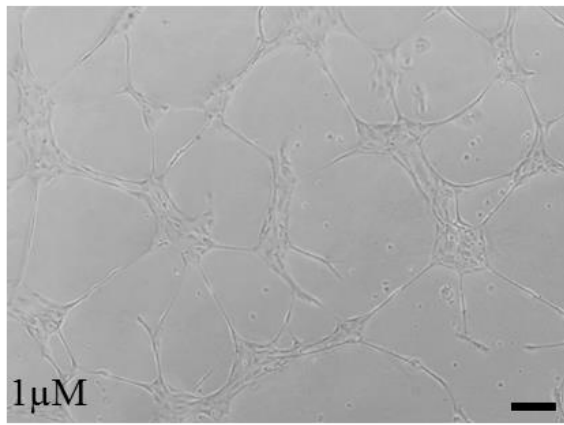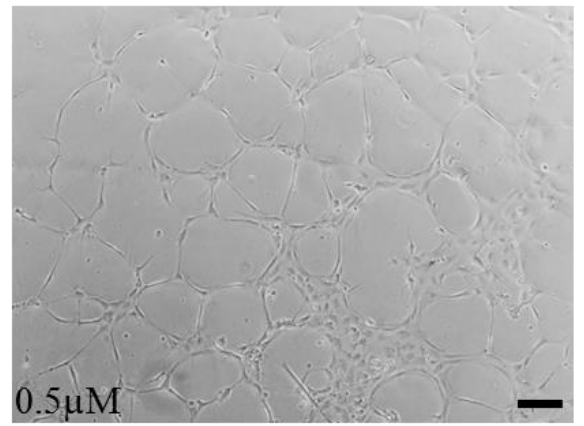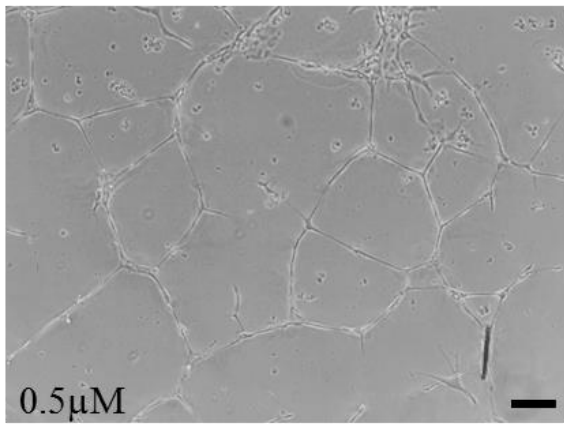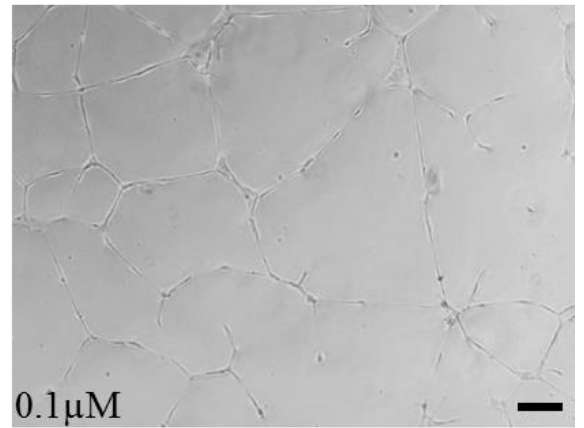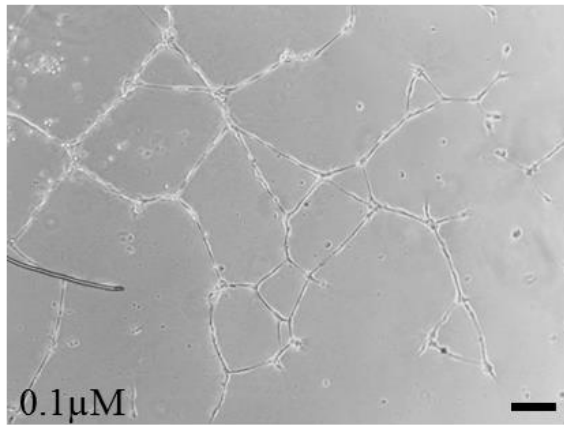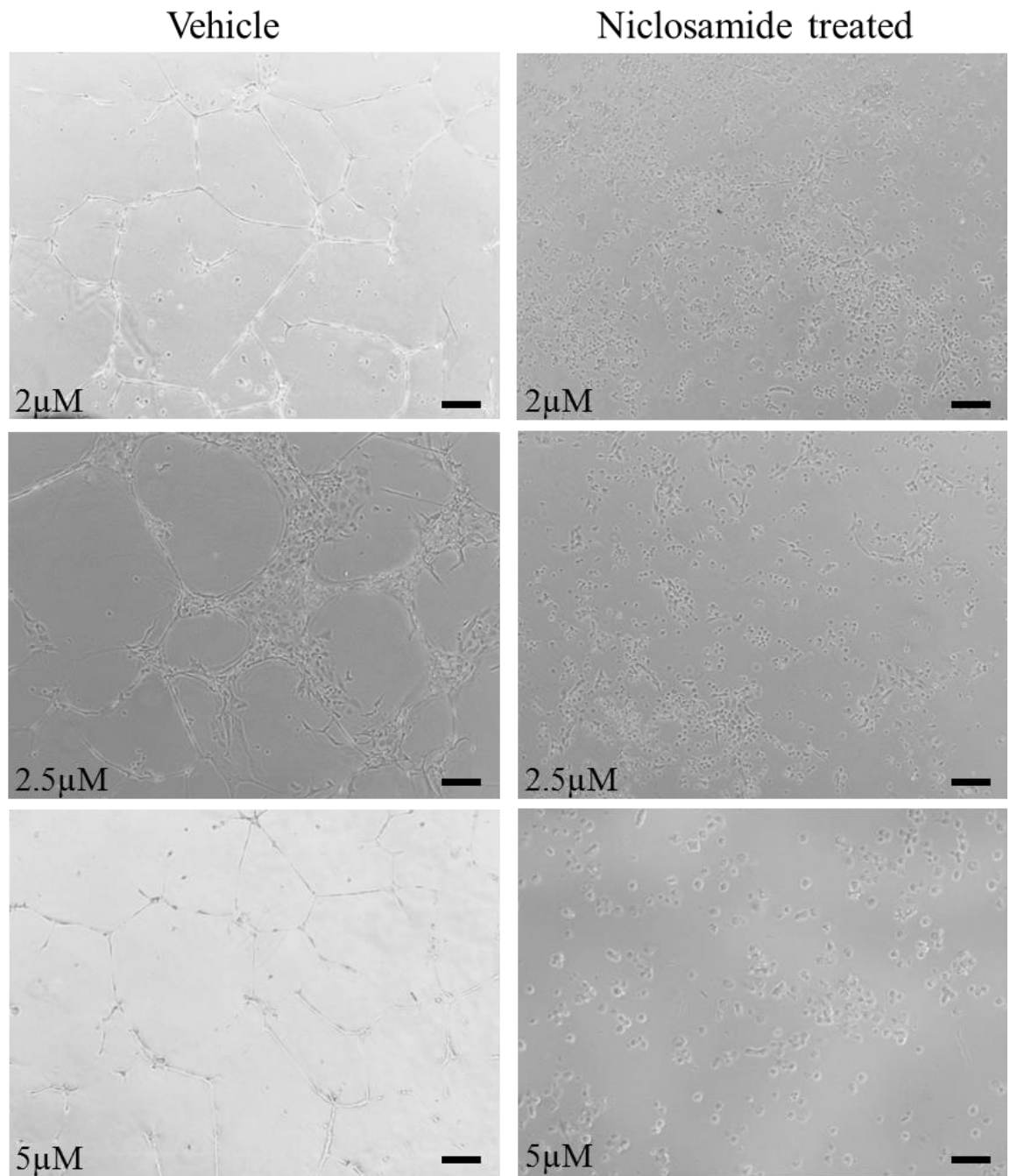
Figure 4.6: Representative images showing the effect of varying concentrations of niclosamide on TLS formation by HUVECs in culture.

Niclosamide visibly inhibited TLS formation in wells. The inhibitory effect was dose dependent; doses ≥1μM caused significant disorganisation of the cells and loss of their TLS formation ability. At doses ≥2μM, the cells were severely inhibited and a majority were rounded when treated with 5μM of niclosamide. Each scale bar represents 1000μm.

A. Vehicle

B. Niclosamide (1µM) treated

C.

D.

E.

F.
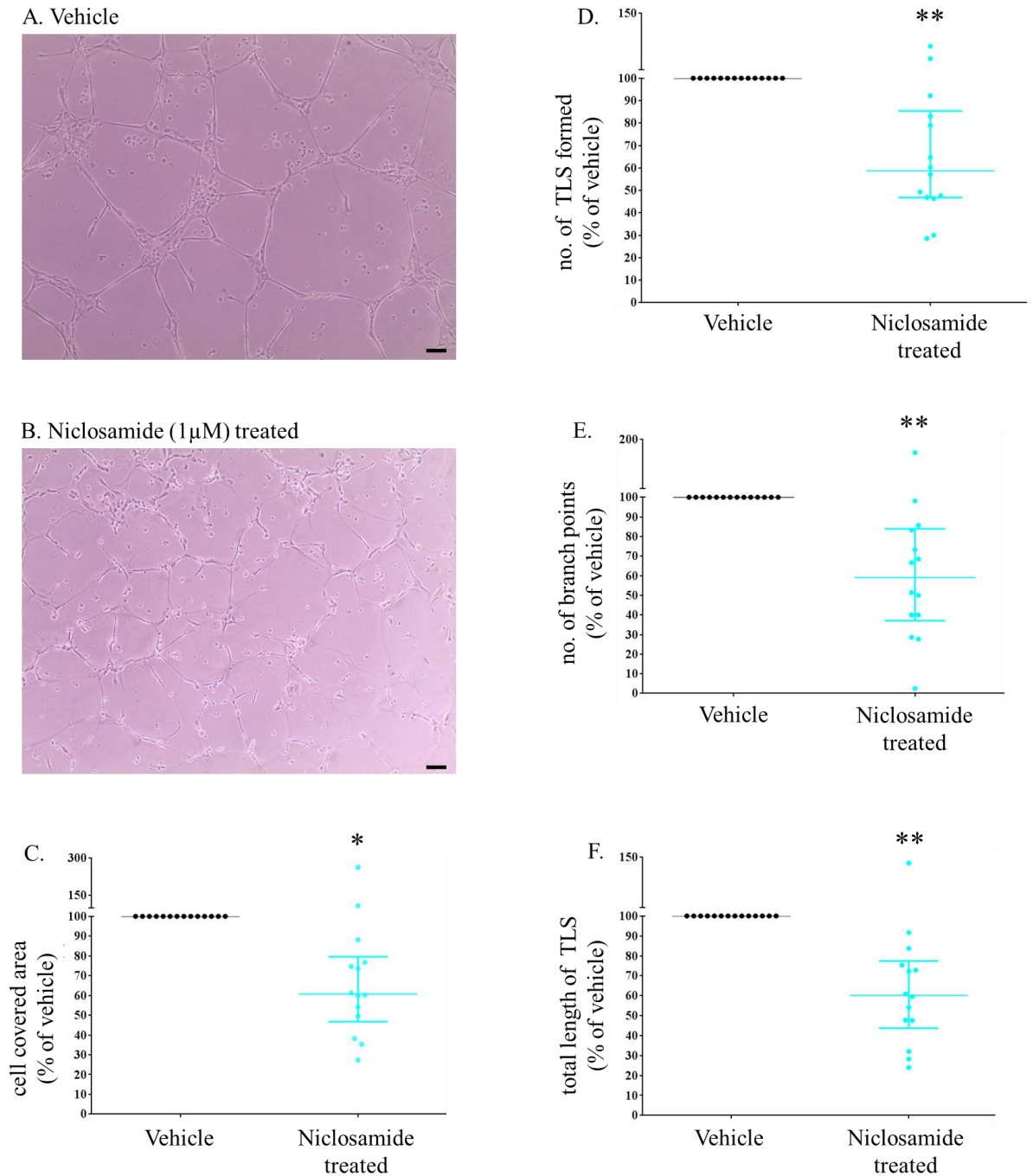
Figure 4.7: The effect(s) of niclosamide on the behaviour of HUVECs in culture.

Representative images showing poorer TLS formation by HUVECs treated with 1µM of niclosamide (B) compared with untreated HUVECs (A). Niclosamide had a significant negative impact on TLS formation (C, D, E and F). Data not normally distributed based on D'Agostino & Pearson omnibus normality test. Median + IQR of n = 14 experiments shown. Each experiment was performed in triplicate. Data analysed by Wilcoxon signed rank test, *$p \leq 0.05$, **$p \leq 0.01$. Scale bars in A and B represent 1000µm.

In this study, niclosamide was used at 1µM concentration. At this concentration, treated cells were observed to be poor at forming TLS (figure 4.7A and B) but remained otherwise viable. In wells containing niclosamide treated cells, median cell covered area was 60.69% (IQR 46.78 – 79.62%) of vehicle, $p = 0.02$ (figure 4.7C); median number of TLS formed was 58.73% (IQR 46.78 – 85.37%) of vehicle, $p = 0.002$ (figure 4.7D); median number of branch points was 59.04% (IQR 37.14 – 83.93%) of vehicle, $p = 0.01$ (figure 4.7E); and the median length of tubes formed was 60.20% (IQR 43.75 – 77.47%) of vehicle, $p = 0.003$ (figure 4.7F).

4.3.2.3 Niclosamide at 1µM dose does not affect endothelial cell survival

4.3.2.3.1 Niclosamide treatment did not halt endothelial cell proliferation

Like the untreated cells, niclosamide treated cells did show evidence of proliferation. The cells demonstrated positivity for the nuclear protein Ki67 (Figure 4.8), signifying that the cells were in active phases of the cell cycle. Also, in the untreated cells, actin filaments appeared stretched and continuous with one another (figure 4.8B), demonstrating networking in the cells to form TLS. In niclosamide-treated cells, however, actin filaments were short and did not network with neighbouring cells (Figure 4.8E).
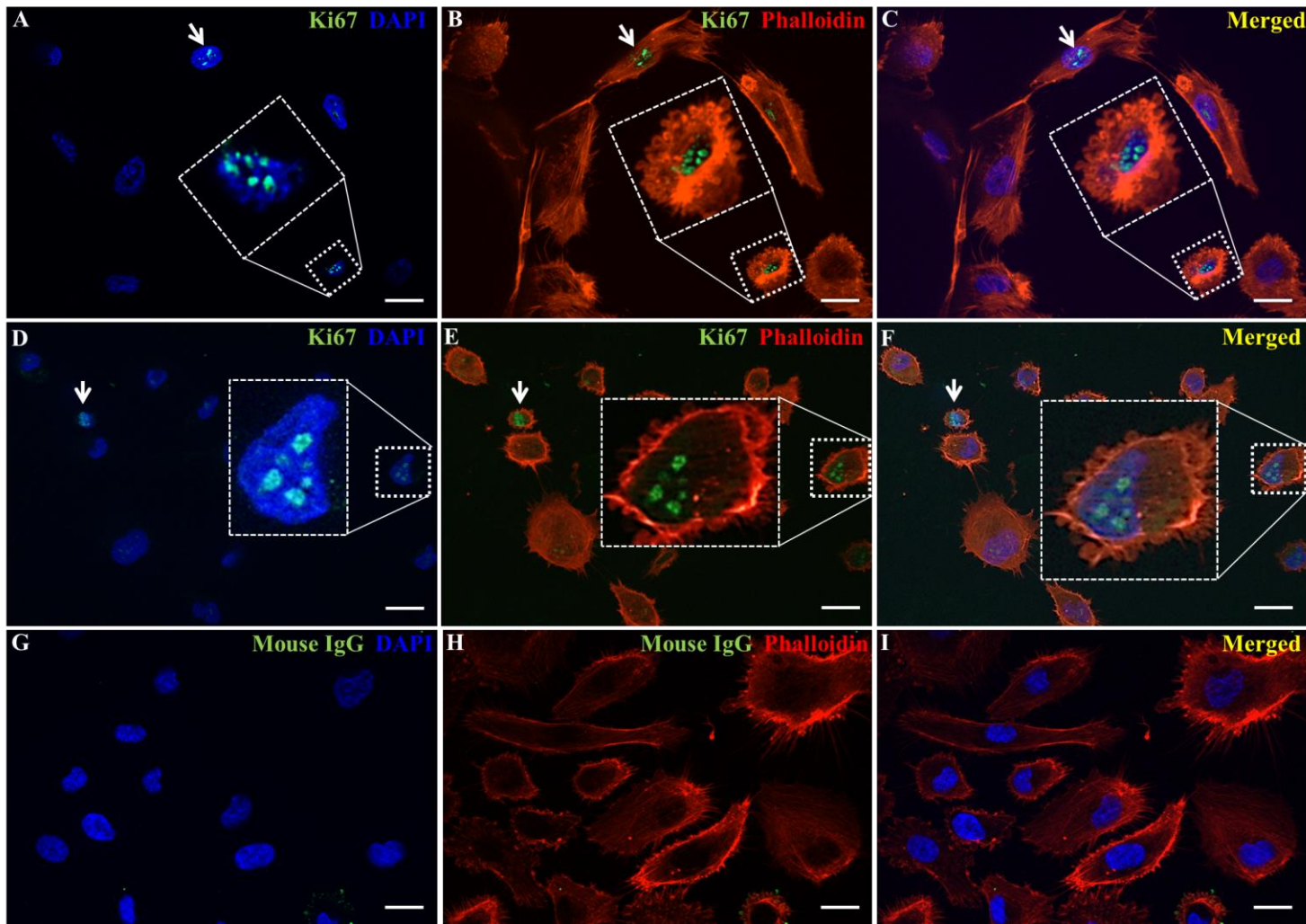
Figure 4.8: Niclosamide-treated cells showed evidence of retained ability to proliferate.

Representative images showing Ki67 positivity (green, inset and white arrows) which demonstrates proliferation in untreated as well as niclosamide-treated HUVECs. Cell nuclei are marked with DAPI (blue) and actin filaments around the cells which aid networking of the cells with one another during TLS formation are marked with phalloidin (red). Images A-C show the vehicle, D-F show niclosamide treated cells and G-I show isotype-matched negative control (mouse IgG). Actin filaments are clearly short in niclosamide-treated cells (E-F), suggesting inhibition of the cells' ability to network with one another. Scale bars in each image represent 20µm.

4.3.2.3.2 Niclosamide treatment did not cause apoptosis in treated endothelial cells

To determine whether the inhibition of TLS formation by niclosamide at the dose used (1µM) led to cell death, the cells were stained with antibody for cleaved caspase 3 (CC3), a known marker of apoptosis. For positive control, cells treated with 5µM staurosporine, a known inducer of cell apoptosis via activation of caspase 3 (Chae *et al.*, 2000) were used. Apoptotic cells are characterised by changes in cell morphology such as DNA condensation and compacted nuclei, cells becoming spherical and clumping together in aggregates, and CC3 positivity. There was no appreciable difference in the quantity of CC3 positive cells in the niclosamide-treated and untreated cells (Figure 4.9).

4.3.2.3.3 Niclosamide treatment did not increase senescence rate in treated endothelial cells

To determine whether niclosamide induced senescence in the treated cells, causing loss of their ability to grow, divide and migrate, the rate of cellular senescence in treated and untreated cells was compared by the histochemical method. In all experiments, a few cells were observed to stain positive for senescence (blue stained cells in figure 4.10A and B) in both the treated and the untreated groups. The number of senescent cells was expressed as a percentage of the total cell population (figure 4.10C) and as a percentage of the number of senescent cells in the untreated group (figure 4.10D). In the untreated and treated cell populations respectively, the median percentage of senescent cells was 11.96% (IQR 8.31 – 17.70%) and 11.76% (IQR 4.55 – 17.66%), p = 0.7. Median senescence positivity in niclosamide-treated cells was 59.09% (IQR 17.00 – 102.10%) of vehicle, p = 0.3.
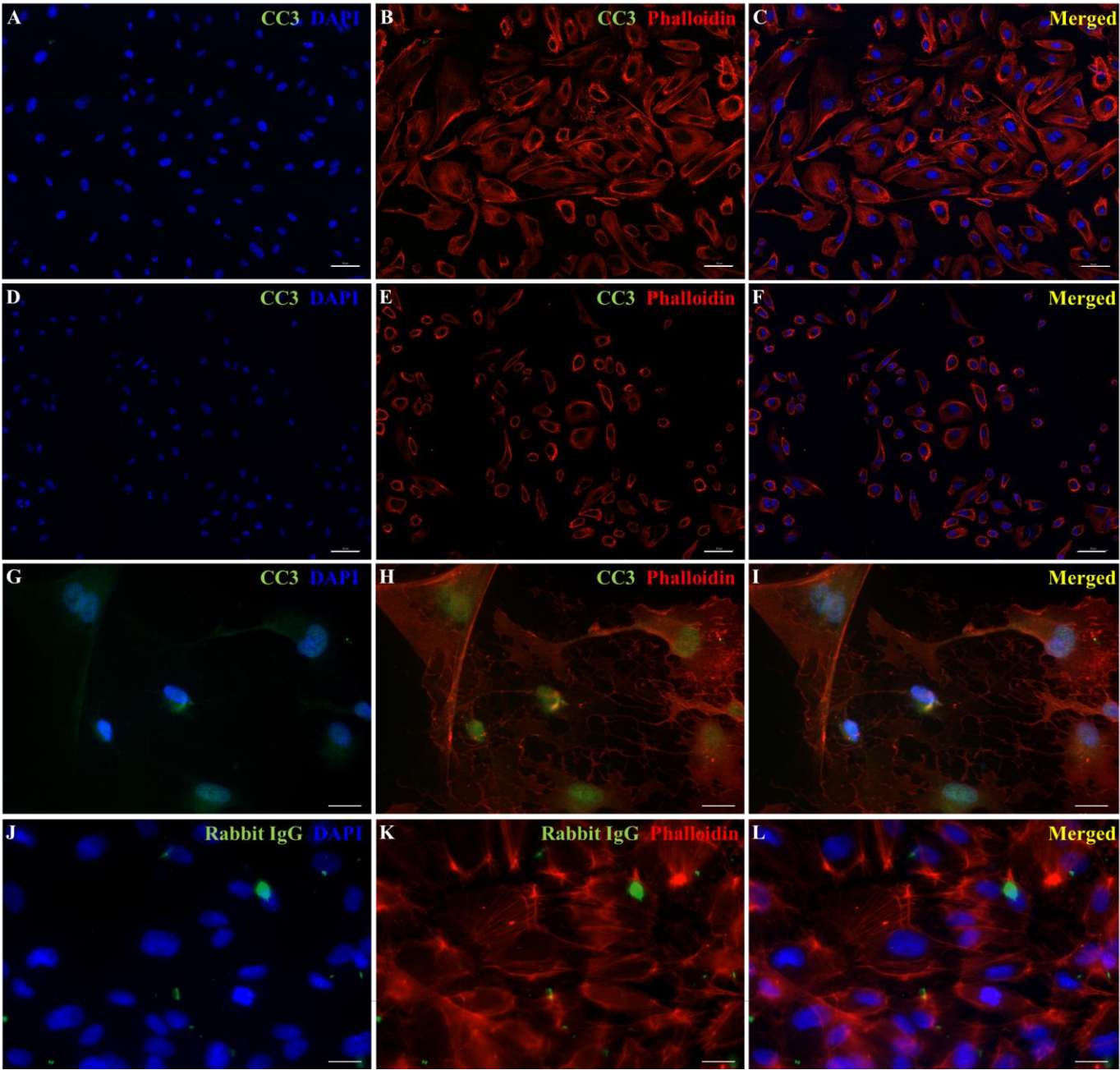
Figure 4.9: Niclosamide-treated cells showed no evidence suggestive of apoptosis induction following treatment.

Representative images showing niclosamide-treated and untreated HUVECs stained with cleaved caspace-3 (CC3) antibody to check for cell apoptosis. Niclosamide treated cells were predominantly negative for CC3 suggesting that niclosamide at 1μM concentration does not cause apoptosis in the cells. Cell nuclei are marked with DAPI (blue), actin filaments are marked with phalloidin (red) and CC3 are marked with alexa 488 (green). Images A-C shows the vehicle, D-F shows niclosamide-treated cells, G-I shows positive control (cells treated with 5μM staurosporine, a known inducer of cell apoptosis via activation of caspase 3) and J-L shows isotype-matched negative control (rabbit IgG). Image scale is 10μm in A-F and 20μm in G-L.
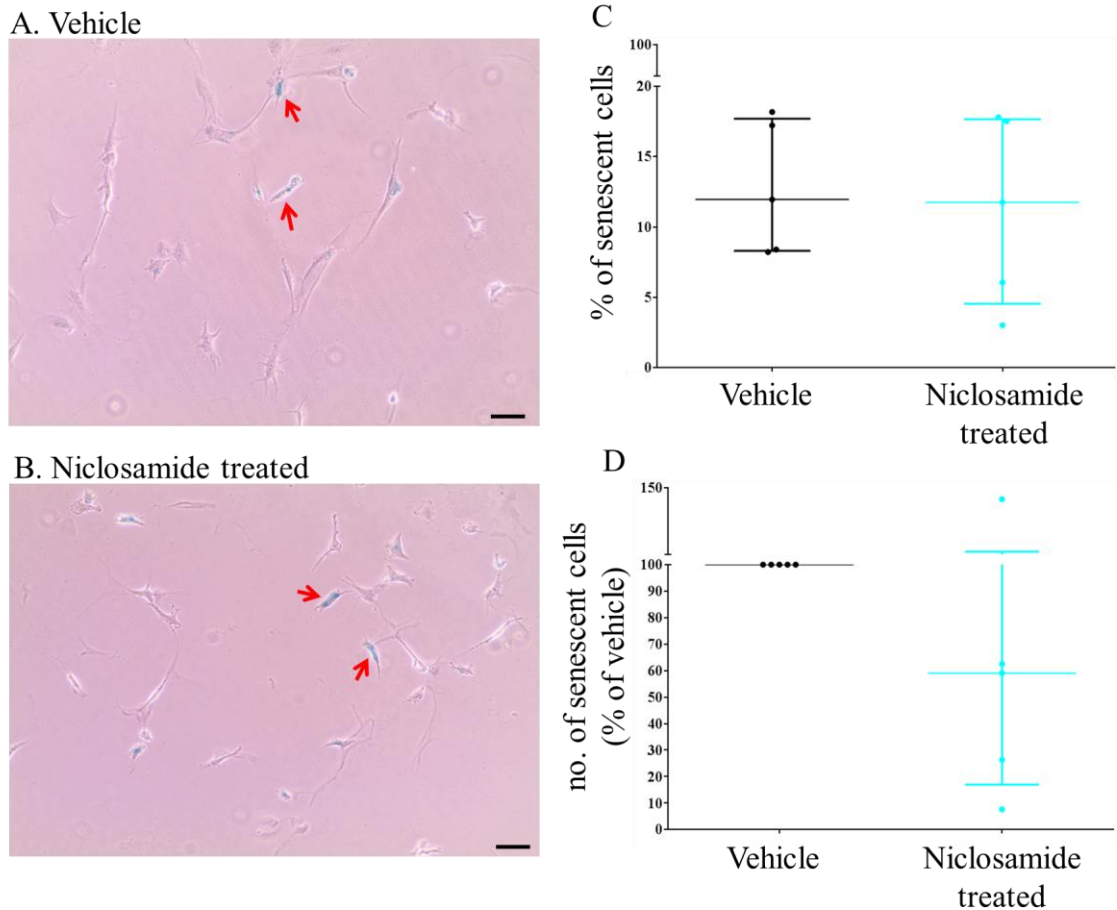
Figure 4.10: Niclosamide-treated cells showed no evidence of excessive senescence.

Representative images showing presence of senescent cells among niclosamide-treated (B) as well as untreated (A) HUVECs populations. The percentage of senescent cells in both groups was similar (C) and the number of senescent cells among the treated cells did not differ from the untreated (D). Data represents the median and IQR of n = 5 experiments. Each experiment was performed in triplicate. Comparison by Mann-Whitney test in C and Wilcoxon signed rank test in D. Scale bars in A and B represent 1000μm.

4.3.3 The response of endothelial cells to withdrawal of WNT inhibition post exposure to niclosamide

To determine the response of the cells to withdrawal of WNT inhibition, niclosamide containing media was replaced with fresh media. As shown in figures 4.11 and 4.12, the cells were observed to have recovered from the WNT inhibitory effects of niclosamide by 24h post rescue. The cells regained their TLS forming ability (figure 4.11D), and neighbouring cells proceeded towards networking evidenced by their actin filaments extending towards one another (figure 4.12D), albeit haphazardly.

By 24h post rescue, the median cell-covered area increased from 60.16% (IQR 43.95 – 75.72%) to 101.6% (IQR 72.00 – 150.20%) of vehicle, $p = 0.01$ (figure 4.13A); median number of TLS increased from 57.11% (IQR 46.64 – 81.04%) of vehicle to 77.05% (66.79 – 123.90%) of vehicle, $p = 0.03$ (figure 4.13C); median number of branch points increased from 51.41% (IQR 34.29 – 78.33%) of vehicle to 75.71% (IQR 48.92 – 183.50%) of vehicle, $p = 0.03$ (figure 4.13B); and median length of TLS increased from 59.54% (IQR 39.86 – 74.11%) of vehicle to 84.54% (IQR 73.71 – 135.00%) of vehicle, $p = 0.003$ (figure 4.13D).
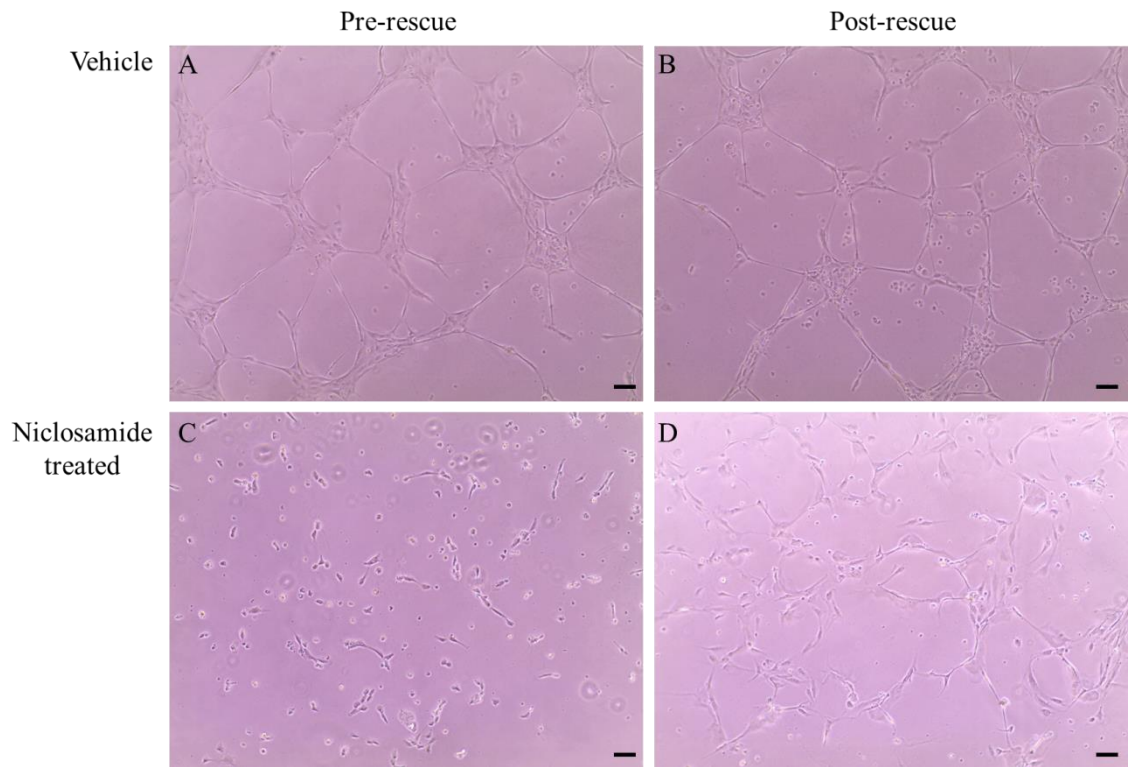
Figure 4.11: The response of niclosamide-treated endothelial cells to withdrawal of WNT inhibition.

Representative images showing the behaviour of endothelial cells following withdrawal of niclosamide. Cells in A and C were treated with DMSO only and 1μM niclosamide dissolved in DMSO respectively for 24h (pre-rescue), then culture media was changed and the cells cultured for a further 24h (B and D; post rescue). Niclosamide treatment impaired TLS formation in the cells but did not kill them (C). Following removal of niclosamide, the cells resumed TLS forming activity although they appeared disorganised (D). Scale bar 1000μm.
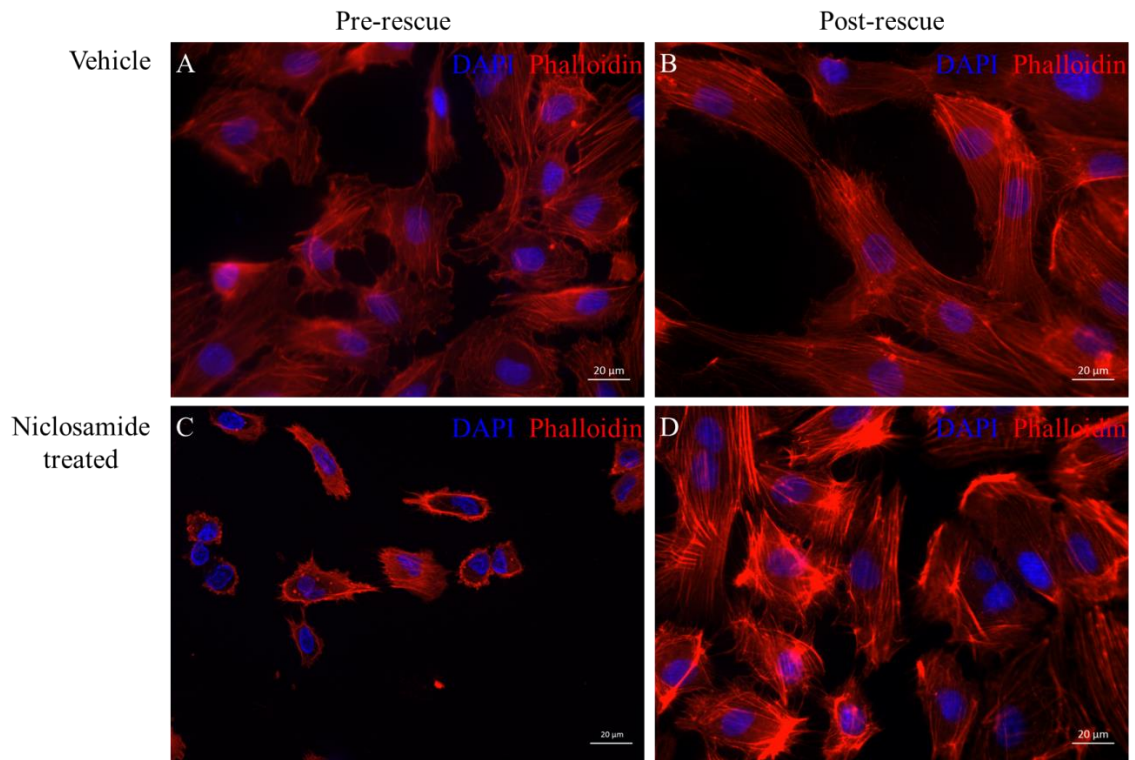
Figure 4.12: Endothelial cell behaviour following rescue from WNT inhibition.

Representative images showing the behaviour of endothelial cells in the presence and absence of niclosamide. Cell nuclei are stained with DAPI (blue) and actin filaments with phalloidin (red). Actin filaments appeared stunted in the niclosamide treated cells pre-rescue, characteristic of a lack of networking between the cells (C). Post rescue, the cells showed evidence of recovery. Actin filaments of each cell extended towards neighbouring cells, although the cells appeared disorganised compared to control. Scale bar 20µm.
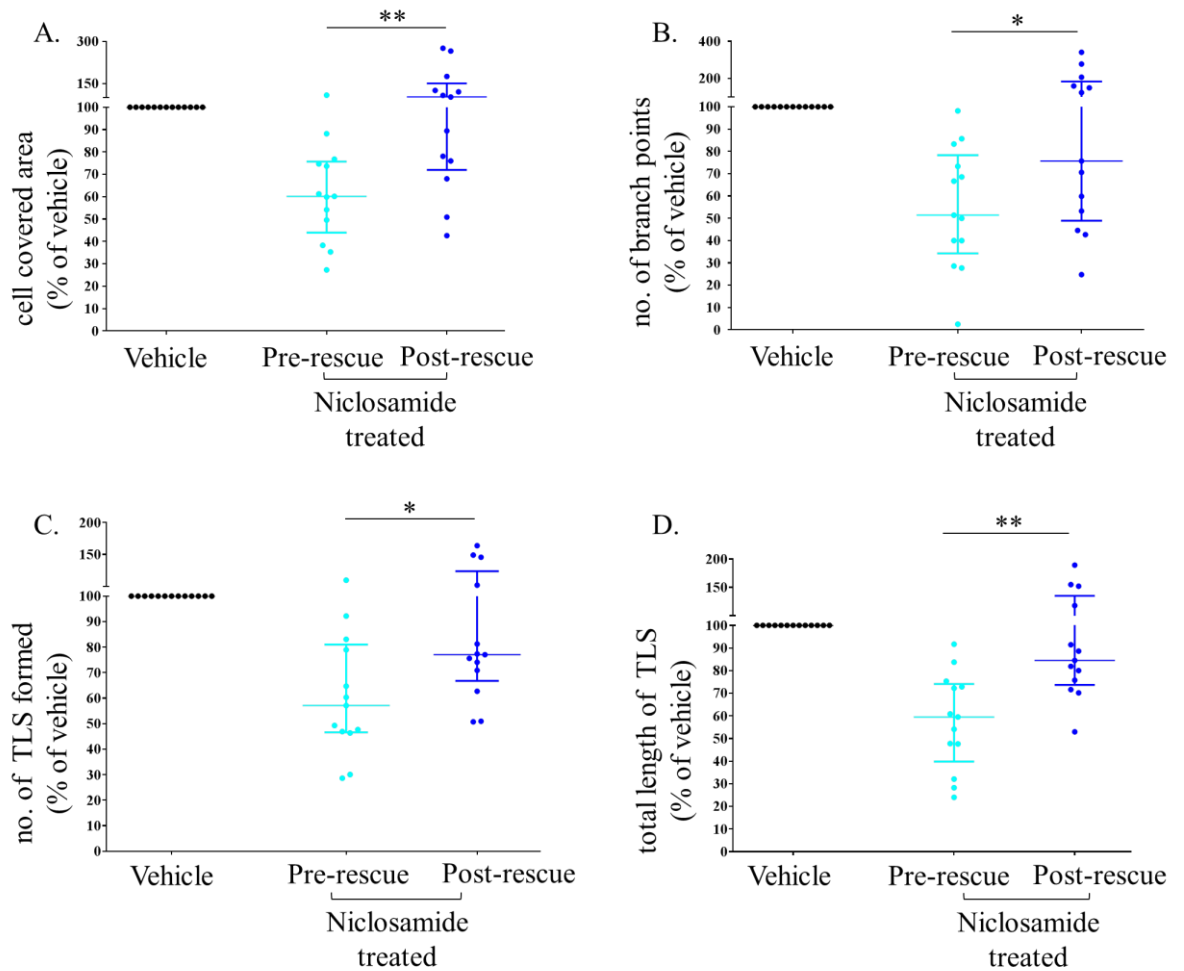
Figure 4.13: Endothelial cells recovered from niclosamide-induced WNT inhibition.

Pre-rescue bars represent cells cultured with niclosamide while post-rescue bars represent the same cells 24h after changing the culture medium. When the WNT inhibitory effect of niclosamide was removed, the cells showed strong evidence of recovery, with significant increases in the cell covered area (A), branch points (B), TLS formation (C) and TLS length (D). Data not normally distributed based on D'Agostino & Pearson omnibus normality test. Median + IQR of n = 13 experiments shown. Each experiment was performed in triplicate. Data analysed by Wilcoxon matched-pairs signed rank test, *p ≤ 0.05, **p ≤ 0.01.

4.3.4 The effect(s) of WNT signalling inhibition on endothelial cell behaviour in placentas from normal and FGR complicated pregnancies

Having used HUVECs to validate the suitability of the tube forming assay to effectively study the effect of WNT inhibition on endothelial cells and how the cells respond to withdrawal of WNT inhibition, primary endothelial cells isolated from human placentas were studied using the assay. The human placental artery endothelial cells (HPAECs) were isolated from placentas donated by five women who had uncomplicated pregnancies and five women whose pregnancies were complicated by FGR.

4.3.4.1 Demographic and clinical details of study participants

The demographic and clinical details of the women and newborns whose placentas were used are shown in Table 4.3. At delivery, as expected, the median birth weight and individualized birth ratio (IBR) were significantly different between the normal and FGR-complicated clinical groups. Maternal age, body mass index, parity, smoking status, mode of delivery, gestational age at delivery and early gestation Doppler findings were not different.

Table 4.3: Demographic and clinical details of study participants

	Normal (n = 5)	FGR (n = 5)	*p* value
Maternal age, *years*	26 (26 – 3031)	26 (23 – 33)	0.79
Maternal BMI, *Kg/m²*	25 (24 – 28)	23 (22 – 27)	0.42
Smoking, *number (%)*	0/5 (0)	0/5 (0)	> 0.99
Parity	2 (2 – 3)	1 (1 – 3)	0.71
Gestational age at delivery, *days*	273 (270 – 276)	271 (252 – 276)	0.52
Birth weight, *g*	3740 (3590 – 3825)	1980 (1890 – 2719)	**0.008**
IBR, *centile*	75 (50 – 87)	1 (0.5 – 2.5)	**0.008**
Mode of delivery, *number (%)*			
Vaginal	0/5 (0)	1/5 (20)	> 0.99
Caesarean section	5/5 (100)	4/5 (80)	> 0.99
Umbilical artery Doppler			
EDF present? *number (%)*	5/5 (100)	5/5 (100)	> 0.99
PI	1.0 (1.0 – 1.1)	1.2 (0.9 – 1.4)	0.69

Data shown are median and interquartile range (IQR) in parenthesis or in a number with percentage in parenthesis as appropriate. Comparisons by Mann Whitney U test; $p \leq$ 0.05 is significant. BMI, IBR, EDF and PI represent body mass index, individualised birth weight ratio, end diastolic flow and pulsatility index respectively.

4.3.4.2 Niclosamide altered TLS formation in primary placental endothelial cells

As expected, niclosamide-treated HPAECs, both normal and FGR, showed evidence of WNT inhibition compared to vehicle. In the normal and FGR HPAECs respectively, the median cell covered area was 67.05% (IQR 33.57 – 87.21%), $p < 0.05$ of vehicle and 59.67% (IQR 32.23 – 94.75%), $p < 0.05$ of vehicle (figure 4.14A); total branch points was 37.08% (IQR 19.25 – 68.49%), $p < 0.05$ of vehicle and 31.93% (IQR 12.72 – 41.73%), $p < 0.01$ of vehicle (figure 4.14B); median number of TLS formed was 54.05% (IQR 33.72 – 70.89%), $p < 0.05$ of vehicle and 52.11% (IQR 34.74 – 66.00%), $p < 0.01$ of vehicle (figure 4.14C); and total length of TLS was 54.83% (IQR 33.07 – 70.71%) of vehicle and 52.30% (IQR 38.40 – 77.12%), $p < 0.05$ of vehicle (figure 4.14D).

Comparing the effects of niclosamide treatment on the normal and FGR HPAECs (see table 4.4), there was no significant difference in the cell-covered area ($p = 0.67$), total branch points ($p = 0.41$), number of TLS formed ($p = 0.67$) and total length of TLS ($p = 0.94$).
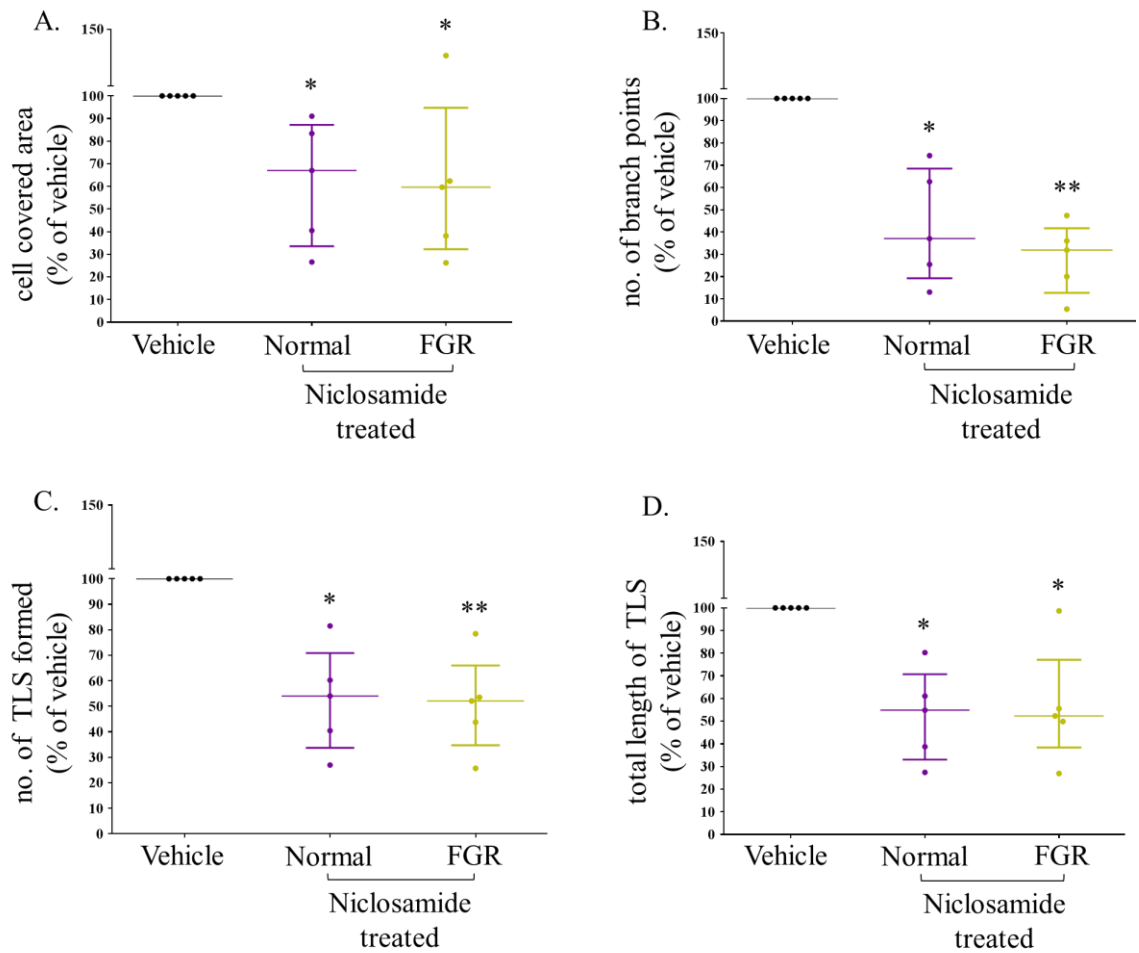
Figure 4.14: Normal and FGR HPAECs showed evidences of WNT inhibition following niclosamide treatment.

In both normal and FGR HPAECs, there were significantly less cell covered area (A), fewer branch points (B), poorer TLS formation (C), and reduced length of TLS (D), compared to vehicle. Data represents the median and IQR of n = 5 experiments each for normal and FGR HPAECs. Each experiment was performed in triplicate. Analysis by Kruskal-Wallis followed by Dunn's test, $*p \leq 0.05$, $**p \leq 0.01$.

Table 4.4: Effects of niclosamide treatment on normal and FGR HPAECs.

	Normal	FGR	p value
Cell-covered area (% of vehicle)	67.05 (33.57 – 87.21)	59.67 (32.23 – 94.75)	0.67
Branch points (% of vehicle)	37.08 (19.25 – 68.49)	31.93 (12.72 – 41.73)	0.41
Number of TLS (% of vehicle)	54.05 (33.72 – 70.89)	52.11 (34.74 – 66.00)	0.67
Total length of TLS (% of vehicle)	54.83 (33.07 – 70.71)	52.30 (38.40 – 77.12)	0.94

Data shown are median and interquartile range (IQR). Comparisons by Mann Whitney test; $p \leq 0.05$ is significant. TLS represents tube like structures.

4.3.5 Normal and FGR placental endothelial cells showed evidence suggestive of differential recovery from the WNT inhibitory effects of niclosamide

As depicted in figure 4.15, TLS formation in both the normal and the FGR HPAECs showed an upward trend post rescue, particularly significantly in the FGR HPAECs, suggesting that the cells recovered from WNT inhibition following withdrawal of niclosamide. The median cell covered area by the normal HPAECs increased slightly from 67.05% (IQR 33.57 – 87.21%) to 70.68% (IQR 58.85 – 108.20%) of vehicle while that covered by the FGR HPAECs increased significantly from 59.67% (IQR 32.23 – 94.75%) to 104.70% (52.71 – 225.60%) of vehicle (figure 4.15A); total branch points increased from 37.08% (IQR 19.25 – 68.49%) to 57.50% (IQR 49.69 – 127.00%) of vehicle in normal HPAECs and from 31.93% (IQR 12.72 – 41.73%) to 76.24% (38.35 – 257.10%) of vehicle in the FGR HPAECs (figure 4.15B); median number of TLS formed by the normal HPAECs increased from 54.05% (IQR 33.72 – 70.89%) to 78.24% (IQR 69.03 – 111.40%) of vehicle and TLS formed by FGR HPAECs increased from 52.11% (IQR 34.74 – 66.00%) to 107.70% (IQR 52.61 – 186.30%) of vehicle (figure 4.15C); and total length of TLS increased from 54.83% (IQR 33.07 – 70.71%) to 81.04% (IQR 72.69 – 111.20%) of vehicle and from 52.30% (IQR 38.40 – 77.12%) to 102.90% (IQR 55.34 – 179.50%) of vehicle in the normal and FGR HPAECs respectively (figure 4.15D).
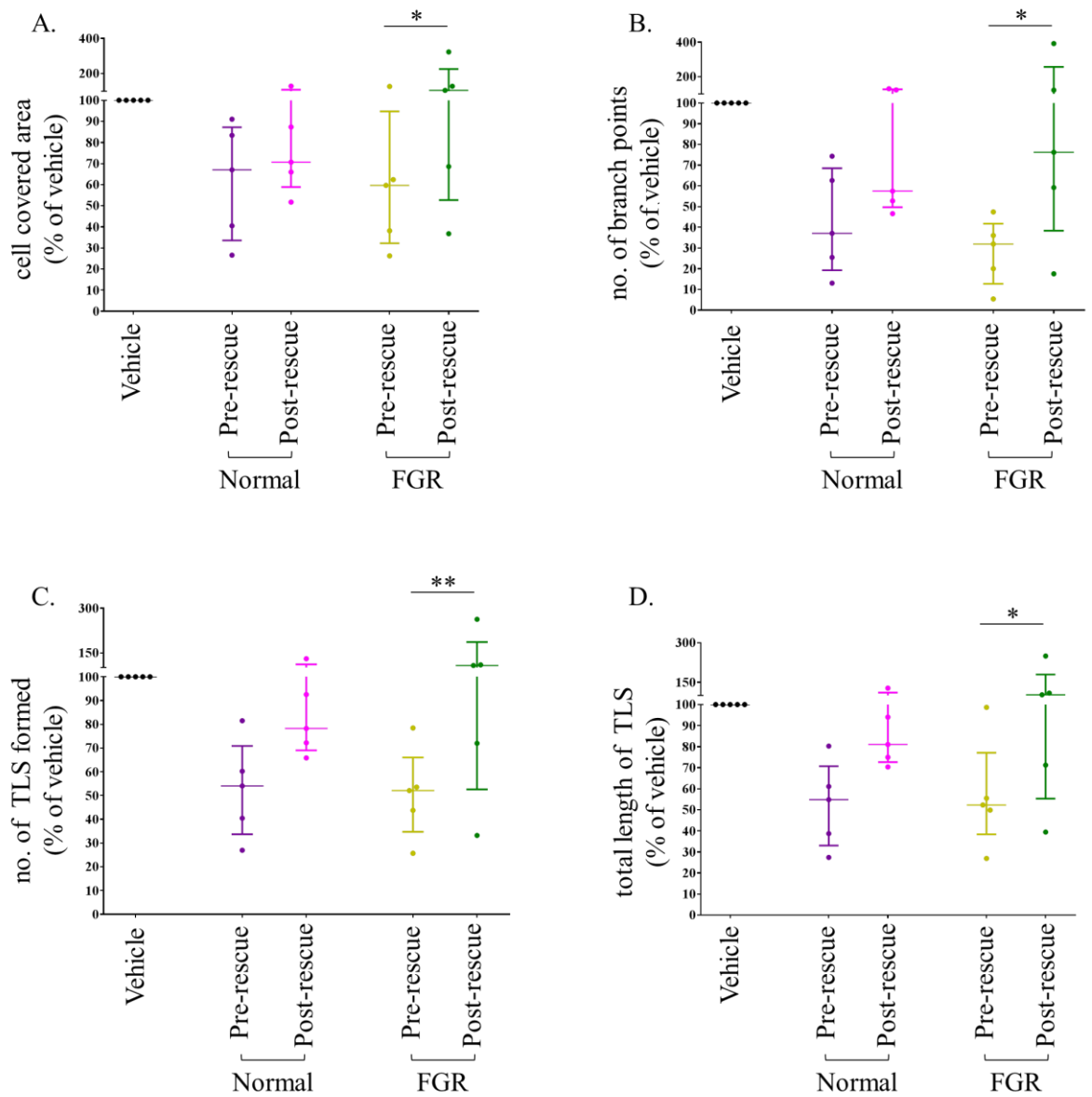
Figure 4.15: Normal and FGR HPAECs showed evidence of recovery following withdrawal of WNT inhibition.

Pre-rescue bars represent cells cultured with niclosamide while post-rescue bars represent the same cells 24h after changing the culture media. Post rescue from niclosamide, the cell covered area, number of branch points, number of TLS and length of TLS in both groups increased. These increases were statistically significant in the FGR HPAECs. Data represents the median and IQR of n = 5 experiments each for normal and FGR HPAECs. Each experiment was performed in triplicate. Analysis by Friedman followed by Dunn's test, *p ≤ 0.05, **p ≤ 0.01.

4.4 Discussion

Despite evidence of the detrimental effects of abnormal WNT signalling on mouse placental vascularisation (Monkley *et al.*, 1996; Ishikawa *et al.*, 2001; Parr *et al.*, 2001), investigation of the role of WNT signalling in human placental vascularisation is still lacking. Although it is unknown whether the placental vascular abnormalities found to be associated with FGR (described in the earlier chapters of this thesis) precede or follow the onset of growth failure in the fetus, a possible aetiology is impaired angiogenesis.

4.4.1 Optimisation of the tube forming assay for WNT signalling investigation

Formation of interconnected TLS is a highly specific characteristic of endothelial cells when plated on reconstituted basement membrane matrix such as matrigel (Kleinman and Martin, 2005; Kubota *et al.*, 1988). In many *in-vitro* studies of both physiological and pathological angiogenesis, using a variety of endothelial cell lines, the tube-forming assay has been employed to replicate the steps involved in the natural process [see (Menden *et al.*, 2015; Liao *et al.*, 2012; Kawasaki *et al.*, 2000; Li *et al.*, 2016; Zhang *et al.*, 2016; Ramaesh *et al.*, 2010) to mention a few]. Tube assays are extensively used to investigate how angiogenic and anti-angiogenic factors affect angiogenesis. In addition, the assay is reproducible, and the formed TLS are quantifiable.

In this study, an experimental model based on tube formation was designed to investigate how WNT signalling may be involved in altering human placental vascularisation in FGR. The designed experiment was initially tested on endothelial cells derived from human umbilical vein (HUVECs) because these have been widely shown to form TLS on matrigel. However, demographic and clinical details of samples from which commercial HUVECs are derived are unknown. This necessitated the use of

a more suitable endothelial cell model for the comparison required in this study. Hence, primary endothelial cells isolated from chorionic plate arteries (HPAECs) from normal and FGR human placentas, with known donors, were used.

Precautionary measures were taken to ensure maximum tube formation: firstly, cells were plated between the second and the fifth passages because following replicative passaging, usually after the fifth passage, endothelial cells begin undergoing senescence (AbuBakar *et al.*, 2014). Secondly, pilot experiments were performed to optimise the cell seeding density for both cells lines used. For both HUVECs and HPAECs, maximal response was established using ~10,000 cells per well in a 24-well plate.

There are many *WNT* genes and receptors involved in human placental angiogenesis. The choice of niclosamide as WNT signalling inhibitor was based on its ability to non-specifically antagonise the pathway at multiple levels – degrading LRP5 and LRP6 (Lu *et al.*, 2011), endocytosis of FZD receptors (Chen *et al.*, 2009b) and destabilisation of β-catenin (Chen *et al.*, 2009b).

4.4.2   Impaired WNT signalling hinders tube formation during human placental angiogenesis

Angiogenesis involves multiple steps, including cell proliferation, migration and tube formation. In the current study, we investigated whether niclosamide-induced WNT signalling inhibition alters endothelial cell behaviour, more precisely their tube formation activity. The results demonstrate that niclosamide significantly inhibits tube formation in human placental endothelial cells *in-vitro*. The vehicle was demonstrated to have no appreciable effect on the cells.

Niclosamide is known to inhibit migration and proliferation of cancer cells (Osada *et al.*, 2011; Satoh *et al.*, 2016) and was, in a very recent study, shown to suppress chemotactic migration, proliferation as well as formation of TLS in HUVECs (Huang *et al.*, 2015). Our findings agree with this latest report and add that niclosamide also inhibits angiogenesis in chorionic artery-derived endothelial cells (HPAECs). In our study, the endothelial cells did not lose their ability to proliferate following niclosamide treatment, neither did they become apoptotic or senescent. This suggests that niclosamide had no effect on the viability and survival of the cells, as similarly shown in a recent assessment of HUVEC cell viability after niclosamide treatment (Huang *et al.*, 2015).

FGR HPAECs demonstrated an innate slower ability to form tubes than normal, requiring up to double the 24h it took normal HPAECs and HUVECs to form tubes. However, the eventual impact of niclosamide on the cells was not different. While TLS formation was significantly inhibited in both normal and FGR HPAECs treated with niclosamide compared to those untreated, there were no differences between the effects of niclosamide on the FGR HPAECs compared to the normal HPAECs.

4.4.3 The effects of WNT signalling impairment on angiogenesis can be halted and reversed in placental endothelial cells

We further investigated the responses of the endothelial cells to withdrawal of niclosamide-induced WNT signalling antagonism. We found that all the placental endothelial cells were capable of regaining their TLS-forming potential once the WNT inhibitory stimulus was removed. This further confirms that the cells were not forced into biological aging, or killed by niclosamide, but they probably became quiescent, with reduced networking behaviour. FGR HPAECs in particular showed a significant trend of recovery that suggests that they responded better than normal HPAECs when

rescued. The reason for this is unclear, but the rebound response may be an indication of chronic WNT signalling dysfunction in the FGR HPAECs. A repeat of the recovery experiments using agonists of the WNT signalling pathway may be useful to confirm this phenomenon. Also, it may be that the FGR HPAECs have an inherent ability to cope with and recover from stress due to their prolonged exposure to the disease state *in vivo*. Indeed, these cells (the same FGR HPAECs used in our experiments) have been shown to exhibit increase in endothelial nitric oxide synthase expression as well as increased flow-mediated shear stress-induced nitric oxide production compared to the normal HPAECs (Jones *et al.*, 2015).

4.4.4   Strengths and limitations of the study

To our knowledge, this study is the first to show that human placental endothelial cells can recover from abnormal WNT signalling-induced inhibition of angiogenesis. Also novel was the use of HPAECs to compare the effects of WNT signalling inhibition on angiogenesis in normal and FGR placentas, as well as the responses of the cells to withdrawal of WNT inhibition. Many previous placenta-related angiogenesis studies have used HUVECs as these are commercially available. However, HUVECs are derived from the umbilical vein, and so are representative of umbilical cord rather than placental vessels. In addition, the demographic or clinical details of donors of commercial HUVECs are usually not available, making HPAECs more appropriate for the comparisons in this study.

Human placental vein endothelial cells (HPVECs) are structurally not similar to HPAECs. While HPAECs are polygonal with smooth surfaces, HPVECs are spindle-shaped with rough surfaces (due to presence of numerous microvilli) and are more difficult to isolate (Lang *et al.*, 2008). In addition, at confluence, HPAECs are arranged

in loose monolayers having a cobblestone appearance while HPVECs form tighter bonds with one another with a swirl-like morphology (Lang *et al.*, 2008). Also, chorionic endothelial cells are more stable compared to villi endothelial cells (personal communication with Dr Paul Brownbill, July 2016). These differences raise the suspicion that the endothelial cells may behave differently. While we have shown really interesting discoveries with the HPAECs, it will be further interesting to investigate WNT signalling in HPVECs, to compare responses of HPAECs and HPVECs, and also examine endothelial cells from every vascular level in the placental vascular tree down to the capillaries.

A factor that may have affected responses of the cells is that they had been in cryogenic storage prior to these experiments. Very recently, TLS formation was shown to be lower in previously cryopreserved compared to fresh HUVECs (Marquez-Curtis *et al.*, 2016). However, the cells used in this study formed appropriate TLS and were capable of eliciting the responses and differences we aimed to investigate.

4.4.5   Summary

To summarise, we have demonstrated an *in-vitro* model of WNT signalling in human placental endothelial cells. Our findings show that WNT signalling inhibition causes endothelial quiescence, which is completely reversible. The possibility of successfully correcting WNT signalling impairment in human placental endothelial cells, especially in FGR cells, may provide a new focus for developing therapeutic agents to enhance placental vascularity in FGR complicated pregnancies.

5 Chapter 5:   General discussion

5.1   Overview

The goal of the three studies reported in this thesis was to address two major research questions:

1.   Is the FGR placenta panhypovascular?

2.   Can angiogenesis be induced or enhanced to improve placental vascularity?

Here in this final chapter, the main points from each study are brought together for a concluding discussion.

5.1.1   Is the placenta panhypovascular in FGR?

Although our preceding studies and those of other research groups provided substantial evidence of intravillous hypovascularity [or more appropriately, hypocapillarity] and hypovascularity at chorionic arterial level in FGR placentas (Junaid *et al.*, 2014; Chen *et al.*, 2002; Krebs *et al.*, 1996; Almasry and Elfayomy, 2012; Mayhew *et al.*, 2004), the main feto-placental vascular abnormalities identified to be associated with FGR in the current studies are vessel length discrepancies and altered endothelial cell behaviour. While these add to the growing evidence of dysvascularity in the FGR placenta, our finding of similar total number of vessels in the normal and FGR casts, as well as comparable degree of tortuosity discounts our panhypovascularity hypothesis. This implies that although hypovascularity involves specific vascular levels, there may be compensation at other levels and this may explain the observation of differential vascularity at the stem, intermediate and terminal levels of the villi [specifically, hypovascularity in stem and intermediate villi but hypervascularity in terminal villi] in some FGR placentas (Todros *et al.*, 1999). Altered vessel lengths, particularly increased venous length, may be a reflection of such underlying compensation.

It is worthy to restate here that the findings reported in this thesis involves vessels at vascular levels ≥100µm in diameter i.e. excludes the capillaries and many arterioles and venules smaller than 100µm. While the casts did include all vascular levels (down to 10µm which is definitely at the capillary level), our imaging and analyses approach permitted limited examination. We tried to develop the clearing method (reported in chapter 3) so we could see the intermediate vessels more clearly and potentially study vessel topology with more depth but the approach was unsuccessful. The applicability, strengths and limitations of the techniques are detailed in the corresponding chapters.

In principle, vessel length discrepancies could be because of altered angiogenesis; however, whether the longer venous path is a well-disseminated even increase in venous length or is focussed on specific area(s) of the placenta is unknown. A key fact to remember is that more doesn't necessarily imply better. While vessel elongation may suggest adequate coverage of the placenta, predictions from mathematical models of villous geometry are that increased vessel length has a non-linear or even inverse relationship with oxygen uptake at the distal villi (Lin *et al.*, 2016).

Furthermore, we observed alterations in the behaviour and response of FGR placental-derived endothelial cells to addition and withdrawal of stress stimulus in static culture (see chapter 4). This may indicate that the parent vessels from which the cells were isolated respond abnormally to similar stress *in vivo*, with consequences for materno-fetal nutrient exchange and transfer.

In light of these findings, available evidence so far rules out panhypovascularity but strongly supports dysvascularity in FGR placentas.

5.1.2 Can angiogenesis be induced or enhanced to improve placental vascularity?

Therapeutic approaches for FGR in human pregnancy have hitherto been largely unsuccessful although there are some promising reports from preclinical studies using animal models (Dilworth *et al.*, 2013; Stanley *et al.*, 2012; Richter *et al.*, 2009; Lassala *et al.*, 2010) and few small-scale clinical trials (von Dadelszen *et al.*, 2011; Xiao and Li, 2005) while some large-scale clinical trials are still ongoing (Ganzevoort *et al.*, 2014; Alers *et al.*, 2013; Hobson *et al.*, 2013). This suggests that current measures may not be addressing the underlying mechanisms involved in the pathology. Our findings of altered angiogenic behaviour/response of human placental endothelial cells following *in-vitro* pharmacological manipulation suggests that impairment of WNT signalling may play a role in defective angiogenesis and consequent dysvascularity in the FGR placenta. Likewise, the demonstrated ability of the endothelial cells to recover, regaining their angiogenic potential following withdrawal of WNT inhibition provides compelling evidence that impaired WNT signalling may indeed underlie defective vascularisation in FGR placentas. More importantly, these evidences suggest the need to explore the WNT pathway as a potential new target for therapeutic interventions to correct placental dysvascularity in FGR. Therapeutic angiogenesis (administration of exogenous agents to induce angiogenesis and restore vascularity *in vivo*) is an on-going focus of many studies aimed at developing alternative, non-surgical, non- or minimally-invasive treatment options for conditions such as limb ischemia (Deev *et al.*, 2015; Makinen *et al.*, 2002), ischemic renal injury (Logue *et al.*, 2016), and myocardial infarction (Awada *et al.*, 2015; Garbern *et al.*, 2011). Indeed, a recent report on how pravastatin ameliorated placental vascular defects and improved fetal growth in mouse models of FGR with glucocorticoid-excess-induced underdevelopment of the placental vasculature (Wyrwoll *et al.*, 2016) provides persuasive indication of the potential of WNT-signalling-modulating therapeutics in the management of fetal growth restriction.

It is worthy to note that pravastatin, though primarily a lipid-lowering drug, is a known activator of WNT signalling (Jiang *et al.*, 2014). Therefore, administration of pharmacological, human placenta-specific agonists of WNT signalling to stimulate neovascularisation may be an exciting new target for consideration in management of the pregnancy complication.

5.2 Physiological relevance: potential effect(s) of placental dysvascularity on fetal growth

Fetal growth depends critically on sufficient blood flow through the placental vessels. The physical laws regulating flow through conduits, such as blood vessels, are that the rate of flow is inversely proportional to the resistance to flow within the vessels, as long as the pressure at which the blood is propelled remains controlled (Clark *et al.*, 2015). As an equation,

$$F \ \alpha \ \frac{\Delta P}{R}$$

where F is the rate of flow, ΔP is the change in pressure and R is the resistance to flow within the vessels. This implies that in a hemodynamically stable state, blood flow through the network of placental vessels, and by extension fetal growth, depends ultimately on the resistance of the vessels to the flow of blood within them. While the radius of a vessel is the major determinant of resistance to flow within the vessel, other important determinants include vessel length, spatial arrangement of the vessels, and the viscosity of the blood. All these factors have combined effects on vessel resistance, as explained by Hagen-Poiseuille's equation

$$R \ \alpha \ \frac{8\eta L}{\pi \, r^4}$$

which implies that the resistance (R) within a vessel is directly proportional to the length (L) of the vessel and the viscosity of the blood (η) flowing through the vessel, and inversely proportional to the radius of the vessel to the 4th power (r^4) (Clark *et al.*, 2015).

Thus, in the dysvascular FGR placenta, the sparse vascular network, length discrepancies and impoverished vascularity may contribute to worsen the vascular resistance, causing poor blood flow to and from the fetus. Indeed, in *ex vivo* perfusion studies, FGR placental vessels demonstrated high resistance and poor flow-mediated vasodilation (Jones *et al.*, 2015) and there are predictions that suggest that features of placental dysvascularity (such as abnormal vessel length) have negative implications for materno-fetal oxygen exchange and transfer (Lin *et al.*, 2016).

5.3   Conclusion

This thesis has advanced our understanding of the state of feto-placental vascularity in FGR complicated pregnancies. The most significant results from this project may be summarised as follows:

1. The FGR placenta is dysvascular but not panhypovascular

2. Potentially, placental vascularity may be improved by inducing/enhancing angiogenesis in the FGR placenta

The possibility of improving vascularity in a diseased placenta implies the possibility of improving placental blood flow and, by extension, nutrient and oxygen delivery to the fetus. This is a potential area to explore further and target for development of more appropriate interventions for fetal growth restriction.

5.4   Recommendations for future research

Some scientific gaps were identified in the course of this project as requiring further investigation.

<u>Improved definition of altered feto-placental vascularity in FGR</u>

- Develop technique for full account/examination of the entire feto-placental vessel networks in an intact state. The techniques and analyses employed in this thesis only permitted a near-full account (we had a $\geq 100\mu m$ threshold). Imaging in a more advanced scanner with higher resolution may allow a more complete account.

- We encountered many challenges with the clearing technique, but the approach may be productive given funding to cover the costs of the large amounts of reagents and antibodies required for a whole placenta. Also, imaging, analyses and quantification methods for the technique need to be developed.

- Perform cell biology to find out why venous circuit is longer and investigate possible intrinsic differences in angiogenic responses in the arterial and venous systems.

- It will be interesting to determine the exact week (gestational age) that placental vascular alterations begin during pregnancy, and to correlate this with the time of onset of growth restriction.

Further investigation of WNT signalling in FGR

- We have tested response of endothelial cells to withdrawal of WNT signalling, it will be interesting to go further by observing the response of these cells to activation of the pathway by agonists.

- Since chorionic and villi vessels differ in origin and function, there is a need to compare WNT signalling in chorionic vessel endothelial cells (HPAECs and HPVECs) and endothelial cells from villi vessels. For the villi vessels, there is need to develop a method to differentiate arterioles from venules. During the course of this project, this was attempted by staining villi samples with EphB4 antibody but the approach was not successful (see appendix 4 and figures 5.25 – 5.27).

Implications for placental function

- It will be necessary to investigate the specific impact of each abnormality observed in the FGR feto-placental vasculature on placental function.

Bibliography

Aberle, H., Bauer, A., Stappert, J., Kispert, A. & Kemler, R. (1997) beta-catenin is a target for the ubiquitin-proteasome pathway. *Embo Journal,* 16(13)**,** 3797-3804.

AbuBakar, S., Shu, M. H., Johari, J. & Wong, P. F. (2014) Senescence affects endothelial cells susceptibility to dengue virus infection. *Int J Med Sci,* 11(6)**,** 538-44.

Abule, R. M., Bernardes, L. S., Doro, G. F., Miyadahira, S. & Francisco, R. P. (2016) Reduced placental volume and flow in severe growth restricted fetuses. *Clinics (Sao Paulo),* 71(6)**,** 332-7.

Aharinejad, S., Schreiner, W. & Neumann, F. (1998) Morphometry of human coronary arterial trees. *Anat Rec,* 251(1)**,** 50-9.

Aharinejad, S. H., Lametschwandtner, A. (1992) Corrosion Casting - A Historical Review. *Microvascular Corrosion Casting in Scanning Electron Microscopy.* Austria: Springer Vienna.

Alers, N. O., Jenkin, G., Miller, S. L. & Wallace, E. M. (2013) Antenatal melatonin as an antioxidant in human pregnancies complicated by fetal growth restriction--a phase I pilot clinical trial: study protocol. *BMJ Open,* 3(12)**,** e004141.

Almasry, S. M. & Elfayomy, A. K. (2012) Morphometric analysis of terminal villi and gross morphological changes in the placentae of term idiopathic intrauterine growth restriction. *Tissue Cell,* 44(4)**,** 214-9.

Amir, H., Weintraub, A., Aricha-Tamir, B., Apel-Sarid, L., Holcberg, G. & Sheiner, E. (2009) A piece in the puzzle of intrauterine fetal death: Pathological findings in placentas from term and preterm intrauterine fetal death pregnancies. *Journal of Maternal-Fetal & Neonatal Medicine,* 22(9)**,** 759-764.

Ananth, C. V., Kaminsky, L., Getahun, D., Kirby, R. S. & Vintzileos, A. M. (2009) Recurrence of fetal growth restriction in singleton and twin gestations. *J Matern Fetal Neonatal Med,* 22(8)**,** 654-61.

Aplin, J. D. (2000) Hypoxia and human placental development. *Journal of Clinical Investigation,* 105(5)**,** 559-560.

Aplin, J. D. & Jones, C. J. P. (2008) *Human placental development* (second ed.). United Kingdom: Informa Healthcare.

Aplin, J. D., Whittaker, H., Jana Lim, Y. T., Swietlik, S., Charnock, J. & Jones, C. J. (2015) Hemangioblastic foci in human first trimester placenta: Distribution and gestational profile. *Placenta,* 36(10)**,** 1069-77.

Arend, R. C., Londono-Joshi, A. I., Samant, R. S., Li, Y., Conner, M., Hidalgo, B., Alvarez, R. D., Landen, C. N., Straughn, J. M. & Buchsbaum, D. J. (2014) Inhibition of Wnt/beta-catenin pathway by niclosamide: a therapeutic target for ovarian cancer. *Gynecol Oncol,* 134(1)**,** 112-20.

Arroyo, J. A. & Winn, V. D. (2008) Vasculogenesis and angiogenesis in the IUGR placenta. *Seminars in Perinatology,* 32(3)**,** 172-177.

Artunc Ulkumen, B., Pala, H. G., Uyar, Y., Koyuncu, F. M. & Bulbul Baytur, Y. (2015) The alteration in placental volume and placental mean grey value in growth-restricted pregnancies assessed by 3D ultrasound (Growth Restriction & 3D Ultrasonography). *J Obstet Gynaecol,* 35(5)**,** 447-50.

Auerbach, R., Lewis, R., Shinners, B., Kubai, L. & Akhtar, N. (2003) Angiogenesis assays: a critical overview. *Clin Chem,* 49(1)**,** 32-40.

Auguste, P., Lemiere, S., Larrieu-Lahargue, F. & Bikfalvi, A. (2005) Molecular mechanisms of tumor vascularization. *Crit Rev Oncol Hematol,* 54(1)**,** 53-61.

Awada, H. K., Johnson, N. R. & Wang, Y. (2015) Sequential delivery of angiogenic growth factors improves revascularization and heart function after myocardial infarction. *J Control Release,* 207**,** 7-17.

Baergen, R. N. (2011a) Chorionic villi: histology and villous development. *In:* Baergen, R. N. (ed.) *Manual of Pathology of the Human Placenta.* New York, USA: Springer Science.

Baergen, R. N. (2011b) Evaluation of the first trimester products of conception. *In:* Baergen, R. N. (ed.) *Manual of Pathology of the Human Placenta.* Second ed. New York, USA: Springer Science.

Baergen, R. N. (2011c) Overview and microscopic survey of the placenta. *In:* Baergen, R. N. (ed.) *Manual of Pathology of the Human Placenta.* New York, USA: Springer Science.

Bamfo, J. E. & Odibo, A. O. (2011) Diagnosis and management of fetal growth restriction. *J Pregnancy,* 2011**,** 640715.

Barker, D. J. (1995) Fetal origins of coronary heart disease. *BMJ,* 311(6998)**,** 171-4.

Barker, S. B., Cumming, G. & Horsfield, K. (1973) Quantitative morphometry of the branching structure of trees. *J Theor Biol,* 40(1)**,** 33-43.

Baron, M. H. (2003) Embryonic origins of mammalian hematopoiesis. *Exp Hematol,* 31(12)**,** 1160-9.

Beck, L., Jr. & D'Amore, P. A. (1997) Vascular development: cellular and molecular regulation. *FASEB J,* 11(5)**,** 365-73.

Beenken, A. & Mohammadi, M. (2009) The FGF family: biology, pathophysiology and therapy. *Nat Rev Drug Discov,* 8(3)**,** 235-53.

Benirschke, K. & Kaufmann, P. (1990) Nonvillous parts of the placenta. *In:* Benirschke, K., Kaufmann, P. (ed.) *Pathology of the human placenta.* Second ed. New York: Springer Science & Business Media.

Benirschke, K. & Kaufmann, P. (2000) Early Development of the Human Placenta. *Pathology of the Human Placenta.* 4th ed.: Springer.

Benirschke, K., Kaufmann, P. & Baergen, R. N. (2006a) Architecture of normal villous trees. *In:* Benirschke, K., Kaufmann, P., Baergen, R. N. (ed.) *Pathology of the human placenta.* 5th ed. USA: Springer.

Benirschke, K., Kaufmann, P. & Baergen, R. N. (2006b) Classification of villous maldevelopment. *In:* Benirschke, K., Kaufmann, P., Baergen, R.N. (ed.) *Pathology of the human placenta.* 5th ed. USA: Springer.

Benirschke, K., Kaufmann, P. & Baergen, R. N. (2006c) Macroscopic features of the delivered placenta. *In:* Benirschke, K., Kaufmann, P., Baergen, R.N. (ed.) *Pathology of the human placenta.* 5th ed.: Springer.

Benirschke, K., Kaufmann, P. & Baergen, R. N. (2006d) Microscopic survey. *In:* Benirschke, K., Kaufmann, P., Baergen, R.N. (ed.) *Pathology of the human placenta.* 5th ed. USA: Springer.

Bentley, M. D., Ortiz, M. C., Ritman, E. L. & Romero, J. C. (2002) The use of microcomputed tomography to study microvasculature in small rodents. *American Journal of Physiology-Regulatory Integrative and Comparative Physiology,* 282(5)**,** R1267-R1279.

Benton, S. J., McCowan, L. M., Heazell, A. E., Grynspan, D., Hutcheon, J. A., Senger, C., Burke, O., Chan, Y., Harding, J. E., Yockell-Lelievre, J., Hu, Y., Chappell, L. C., Griffin, M. J., Shennan, A. H., Magee, L. A., Gruslin, A. & von Dadelszen, P. (2016) Placental growth factor as a marker of fetal growth restriction caused by placental dysfunction. *Placenta,* 42**,** 1-8.

Berdahl, D. M., Blaine, J., Van Voorhis, B. & Dokras, A. (2010) Detection of enlarged yolk sac on early ultrasound is associated with adverse pregnancy outcomes. *Fertil Steril,* 94(4)**,** 1535-7.

Berghella, V. (2007) Prevention of recurrent fetal growth restriction. *Obstet Gynecol,* 110(4)**,** 904-12.

Biswas, S. & Ghosh, S. K. (2008) Gross morphological changes of placentas associated with intrauterine growth restriction of fetuses: a case control study. *Early Hum Dev,* 84(6)**,** 357-62.

Bouis, D., Kusumanto, Y., Meijer, C., Mulder, N. H. & Hospers, G. A. (2006) A review on pro- and anti-angiogenic factors as targets of clinical intervention. *Pharmacol Res,* 53(2)**,** 89-103.

Breier, G. (2000) Angiogenesis in embryonic development--a review. *Placenta,* 21 Suppl A**,** S11-5.

Burton, G. J., Kaufmann, P., Huppertz, B. (2006) Anatomy and Genesis of the Placenta. *In:* Neill, J. D. (ed.) *Knobil and Neill's Physiology of Reproduction.* Third ed. USA: Elsevier Academic Press.

Cadigan, K. M. & Nusse, R. (1997) Wnt signaling: a common theme in animal development. *Genes Dev,* 11(24)**,** 3286-305.

Cadigan, K. M. & Peifer, M. (2009) Wnt signaling from development to disease: insights from model systems. *Cold Spring Harb Perspect Biol,* 1(2)**,** a002881.

Calve, S., Ready, A., Huppenbauer, C., Main, R. & Neu, C. P. (2015) Optical clearing in dense connective tissues to visualize cellular connectivity in situ. *PLoS One,* 10(1)**,** e0116662.

Carmeliet, P. & Jain, R. K. (2011) Molecular mechanisms and clinical applications of angiogenesis. *Nature,* 473(7347)**,** 298-307.

Carmeliet, P., Moons, L., Luttun, A., Vincenti, V., Compernolle, V., De Mol, M., Wu, Y., Bono, F., Devy, L., Beck, H., Scholz, D., Acker, T., DiPalma, T., Dewerchin, M., Noel, A., Stalmans, I., Barra, A., Blacher, S., VandenDriessche, T., Ponten, A., Eriksson, U., Plate, K. H., Foidart, J. M., Schaper, W., Charnock-Jones, D. S., Hicklin, D. J., Herbert, J. M., Collen, D. & Persico, M. G. (2001) Synergism between vascular endothelial growth factor and placental growth factor contributes to angiogenesis and plasma extravasation in pathological conditions. *Nat Med,* 7(5)**,** 575-83.

Carreno, C. A., Costantine, M. M., Holland, M. G., Ramin, S. M., Saade, G. R. & Blackwell, S. C. (2011) Approximately one-third of medically indicated late preterm births are complicated by fetal growth restriction. *American Journal of Obstetrics and Gynecology,* 204(3).

Castellucci, M., Scheper, M., Scheffen, I., Celona, A. & Kaufmann, P. (1990) The development of the human placental villous tree. *Anat Embryol (Berl),* 181(2)**,** 117-28.

Chae, H. J., Kang, J. S., Byun, J. O., Han, K. S., Kim, D. U., Oh, S. M., Kim, H. M., Chae, S. W. & Kim, H. R. (2000) Molecular mechanism of staurosporine-induced apoptosis in osteoblasts. *Pharmacol Res,* 42(4)**,** 373-81.

Chaiworapongsa, T., Romero, R., Korzeniewski, S. J., Kusanovic, J. P., Soto, E., Lam, J., Dong, Z., Than, N. G., Yeo, L., Hernandez-Andrade, E., Conde-Agudelo, A. & Hassan, S. S. (2013) Maternal plasma concentrations of angiogenic/antiangiogenic factors in the third trimester of pregnancy to identify the patient at risk for stillbirth at or near term and severe late preeclampsia. *Am J Obstet Gynecol,* 208(4)**,** 287 e1-287 e15.

Charnock-Jones, D. S., Kaufmann, P. & Mayhew, T. M. (2004) Aspects of human fetoplacental vasculogenesis and angiogenesis. I. Molecular regulation. *Placenta,* 25(2-3)**,** 103-13.

Chen, B., Dodge, M. E., Tang, W., Lu, J., Ma, Z., Fan, C. W., Wei, S., Hao, W., Kilgore, J., Williams, N. S., Roth, M. G., Amatruda, J. F., Chen, C. & Lum, L. (2009a) Small molecule-mediated disruption of Wnt-dependent signaling in tissue regeneration and cancer. *Nat Chem Biol,* 5(2)**,** 100-7.

Chen, C. P., Bajoria, R. & Aplin, J. D. (2002) Decreased vascularization and cell proliferation in placentas of intrauterine growth-restricted fetuses with abnormal umbilical artery flow velocity waveforms. *Am J Obstet Gynecol,* 187(3)**,** 764-9.

Chen, D. B. & Zheng, J. (2014) Regulation of placental angiogenesis. *Microcirculation,* 21(1)**,** 15-25.

Chen, M., Wang, J., Lu, J., Bond, M. C., Ren, X. R., Lyerly, H. K., Barak, L. S. & Chen, W. (2009b) The anti-helminthic niclosamide inhibits Wnt/Frizzled1 signaling. *Biochemistry,* 48(43)**,** 10267-74.

Chen, Y., Zhang, Y., Deng, Q., Shan, N., Peng, W., Luo, X., Zhang, H., Baker, P. N., Tong, C. & Qi, H. (2016) Inhibition of Wnt Inhibitory Factor 1 Under Hypoxic Condition in Human Umbilical Vein Endothelial Cells Promoted Angiogenesis in Vitro. *Reprod Sci.*

Chen, Z. C., Venkatesan, A. M., Dehnhardt, C. M., Dos Santos, O., Delos Santos, E., Ayral-Kaloustian, S., Chen, L., Geng, Y., Arndt, K. T., Lucas, J., Chaudhary, I. & Mansour, T. S. (2009c) 2,4-Diamino-quinazolines as inhibitors of beta-catenin/Tcf-4 pathway: Potential treatment for colorectal cancer. *Bioorganic & Medicinal Chemistry Letters,* 19(17)**,** 4980-4983.

Chung, K. & Deisseroth, K. (2013) CLARITY for mapping the nervous system. *Nat Methods,* 10(6)**,** 508-13.

Chung, K., Wallace, J., Kim, S. Y., Kalyanasundaram, S., Andalman, A. S., Davidson, T. J., Mirzabekov, J. J., Zalocusky, K. A., Mattis, J., Denisin, A. K., Pak, S., Bernstein, H., Ramakrishnan, C., Grosenick, L., Gradinaru, V. & Deisseroth, K. (2013) Structural and molecular interrogation of intact biological systems. *Nature,* 497(7449)**,** 332-7.

Clark, A. R., Lin, M., Tawhai, M., Saghian, R. & James, J. L. (2015) Multiscale modelling of the feto-placental vasculature. *Interface Focus,* 5(2)**,** 20140078.

Clark, D. E., Smith, S. K., Licence, D., Evans, A. L. & Charnock-Jones, D. S. (1998) Comparison of expression patterns for placenta growth factor, vascular endothelial growth factor (VEGF), VEGF-B and VEGF-C in the human placenta throughout gestation. *J Endocrinol,* 159(3)**,** 459-67.

Cogle, C. R. & Scott, E. W. (2004) The hemangioblast: cradle to clinic. *Exp Hematol,* 32(10)**,** 885-90.

Colorado, P. C., Torre, A., Kamphaus, G., Maeshima, Y., Hopfer, H., Takahashi, K., Volk, R., Zamborsky, E. D., Herman, S., Sarkar, P. K., Ericksen, M. B., Dhanabal, M., Simons, M., Post, M., Kufe, D. W., Weichselbaum, R. R., Sukhatme, V. P. & Kalluri, R. (2000) Anti-angiogenic cues from vascular basement membrane collagen. *Cancer Research,* 60(9)**,** 2520-6.

Cooke, J. P. (2003) NO and angiogenesis. *Atherosclerosis Supplements,* 4(4)**,** 53-60.

Cox, P. & Marton, T. (2009) Pathological assessment of intrauterine growth restriction. *Best Pract Res Clin Obstet Gynaecol,* 23(6)**,** 751-64.

Cruciat, C. M. & Niehrs, C. (2013) Secreted and Transmembrane Wnt Inhibitors and Activators. *Cold Spring Harb Perspect Biol,* 5(3).

Cruciat, C. M., Ohkawara, B., Acebron, S. P., Karaulanov, E., Reinhard, C., Ingelfinger, D., Boutros, M. & Niehrs, C. (2010) Requirement of prorenin receptor and vacuolar H+-ATPase-mediated acidification for Wnt signaling. *Science,* 327(5964)**,** 459-63.

Daneman, R., Agalliu, D., Zhou, L., Kuhnert, F., Kuo, C. J. & Barres, B. A. (2009) Wnt/beta-catenin signaling is required for CNS, but not non-CNS, angiogenesis. *Proceedings of the National Academy of Sciences of the United States of America,* 106(2)**,** 641-646.

Deev, R. V., Bozo, I. Y., Mzhavanadze, N. D., Voronov, D. A., Gavrilenko, A. V., Chervyakov, Y. V., Staroverov, I. N., Kalinin, R. E., Shvalb, P. G. & Isaev, A. A. (2015) pCMV-vegf165 Intramuscular Gene Transfer is an Effective Method of Treatment for Patients With Chronic Lower Limb Ischemia. *Journal of Cardiovascular Pharmacology and Therapeutics,* 20(5)**,** 473-482.

Dejana, E. (2010) The role of wnt signaling in physiological and pathological angiogenesis. *Circ Res,* 107(8)**,** 943-52.

Dejana, E., Bazzoni, G. & Lampugnani, M. G. (1999) Vascular endothelial (VE)-cadherin: only an intercellular glue? *Exp Cell Res,* 252(1)**,** 13-9.

Demir, R., Kayisli, U. A., Cayli, S. & Huppertz, B. (2006) Sequential steps during vasculogenesis and angiogenesis in the very early human placenta. *Placenta,* 27(6-7)**,** 535-9.

Demir, R., Seval, Y. & Huppertz, B. (2007) Vasculogenesis and angiogenesis in the early human placenta. *Acta Histochem,* 109(4)**,** 257-65.

Deter, R. L., Levytska, K., Melamed, N., Lee, W. & Kingdom, J. C. (2016) Classifying neonatal growth outcomes: use of birth weight, placental evaluation and individualized growth assessment. *J Matern Fetal Neonatal Med***,** 1-11.

Diaz-Flores, L., Gutierrez, R., Varela, H., Rancel, N. & Valladares, F. (1991) Microvascular pericytes: a review of their morphological and functional characteristics. *Histol Histopathol,* 6(2)**,** 269-86.

Dilworth, M. R., Andersson, I., Renshall, L. J., Cowley, E., Baker, P., Greenwood, S., Sibley, C. P. & Wareing, M. (2013) Sildenafil citrate increases fetal weight in a mouse model of fetal growth restriction with a normal vascular phenotype. *PLoS One,* 8(10)**,** e77748.

Dimri, G. P., Lee, X. H., Basile, G., Acosta, M., Scott, C., Roskelley, C., Medrano, E. E., Linskens, M., Rubelj, I., Pereirasmith, O., Peacocke, M. & Campisi, J. (1995) A Biomarker That Identifies Senescent Human-Cells in Culture and in Aging Skin in-Vivo. *Proceedings of the National Academy of Sciences of the United States of America,* 92(20)**,** 9363-9367.

Dockery, P. & Fraher, J. (2007) The quantification of vascular beds: a stereological approach. *Exp Mol Pathol,* 82(2)**,** 110-20.

Edmonds, C. J., Isaacs, E. B., Cole, T. J., Rogers, M. H., Lanigan, J., Singhal, A., Birbara, T., Gringras, P., Denton, J. & Lucas, A. (2010) The effect of intrauterine growth on verbal IQ scores in childhood: a study of monozygotic twins. *Pediatrics,* 126(5)**,** e1095-101.

Ekstrom, E. J., Bergenfelz, C., von Bulow, V., Serifler, F., Carlemalm, E., Jonsson, G., Andersson, T. & Leandersson, K. (2014) WNT5A induces release of exosomes containing pro-angiogenic and immunosuppressive factors from malignant melanoma cells. *Mol Cancer,* 13**,** 88.

Engineer, N. & Kumar, S. (2010) Perinatal variables and neonatal outcomes in severely growth restricted preterm fetuses. *Acta Obstet Gynecol Scand,* 89(9)**,** 1174-81.

Epp, J. R., Niibori, Y., Liz Hsiang, H. L., Mercaldo, V., Deisseroth, K., Josselyn, S. A. & Frankland, P. W. (2015) Optimization of CLARITY for Clearing Whole-Brain and Other Intact Organs(1,2,3). *eNeuro,* 2(3).

Falo, A. P. (2009) Intrauterine growth retardation (IUGR): prenatal diagnosis by imaging. *Pediatr Endocrinol Rev,* 6 Suppl 3**,** 326-31.

Feng, L., Liao, W. X., Luo, Q., Zhang, H. H., Wang, W., Zheng, J. & Chen, D. B. (2012a) Caveolin-1 orchestrates fibroblast growth factor 2 signaling control of angiogenesis in placental artery endothelial cell caveolae. *J Cell Physiol,* 227(6)**,** 2480-91.

Feng, L., Zhang, H. H., Wang, W., Zheng, J. & Chen, D. B. (2012b) Compartmentalizing proximal FGFR1 signaling in ovine placental artery endothelial cell caveolae. *Biol Reprod,* 87(2)**,** 40.

Ferriani, R. A., Ahmed, A., Sharkey, A. & Smith, S. K. (1994) Colocalization of acidic and basic fibroblast growth factor (FGF) in human placenta and the cellular effects of bFGF in trophoblast cell line JEG-3. *Growth Factors,* 10(4)**,** 259-68.

Fok, R. Y., Pavlova, Z., Benirschke, K., Paul, R. H. & Platt, L. D. (1990) The Correlation of Arterial Lesions with Umbilical Artery Doppler Velocimetry in the Placentas of Small-for-Dates Pregnancies. *Obstetrics and Gynecology,* 75(4)**,** 578-583.

Foldy, C., Malenka, R. C. & Sudhof, T. C. (2013) Autism-associated neuroligin-3 mutations commonly disrupt tonic endocannabinoid signaling. *Neuron,* 78(3)**,** 498-509.

Fukumura, D., Gohongi, T., Kadambi, A., Izumi, Y., Ang, J., Yun, C. O., Buerk, D. G., Huang, P. L. & Jain, R. K. (2001) Predominant role of endothelial nitric oxide synthase in vascular endothelial growth factor-induced angiogenesis and vascular permeability. *Proceedings of the National Academy of Sciences of the United States of America,* 98(5)**,** 2604-2609.

Gaengel, K., Genove, G., Armulik, A. & Betsholtz, C. (2009) Endothelial-mural cell signaling in vascular development and angiogenesis. *Arterioscler Thromb Vasc Biol,* 29(5)**,** 630-8.

Gagnon, R. (2003) Placental insufficiency and its consequences. *Eur J Obstet Gynecol Reprod Biol,* 110 Suppl 1**,** S99-107.

Ganzevoort, W., Alfirevic, Z., von Dadelszen, P., Kenny, L., Papageorghiou, A., van Wassenaer-Leemhuis, A., Gluud, C., Mol, B. W. & Baker, P. N. (2014) STRIDER: Sildenafil Therapy In Dismal prognosis Early-onset intrauterine growth Restriction--a protocol for a systematic review with individual participant data and aggregate data meta-analysis and trial sequential analysis. *Syst Rev,* 3**,** 23.

Garbern, J. C., Minami, E., Stayton, P. S. & Murry, C. E. (2011) Delivery of basic fibroblast growth factor with a pH-responsive, injectable hydrogel to improve angiogenesis in infarcted myocardium. *Biomaterials,* 32(9)**,** 2407-16.

Gardosi, J., Chang, A., Kalyan, B., Sahota, D. & Symonds, E. M. (1992) Customised antenatal growth charts. *Lancet,* 339(8788)**,** 283-7.

Gardosi, J., Kady, S. M., McGeown, P., Francis, A. & Tonks, A. (2005) Classification of stillbirth by relevant condition at death (ReCoDe): population based cohort study. *British Medical Journal,* 331(7525)**,** 1113-1117.

George, A., Leahy, H., Zhou, J. & Morin, P. J. (2007) The vacuolar-ATPase inhibitor bafilomycin and mutant VPS35 inhibit canonical Wnt signaling. *Neurobiol Dis,* 26(1)**,** 125-33.

Giles, W. B., Trudinger, B. J. & Baird, P. J. (1985) Fetal umbilical artery flow velocity waveforms and placental resistance: pathological correlation. *Br J Obstet Gynaecol,* 92(1)**,** 31-8.

Gong, S. P., Zhao, Y. T. & Yu, Y. H. (2011) Vascular network modeling reveals significant differences in vascular morphology in growth-restricted placentas. *Rev Obstet Gynecol,* 4(3-4)**,** 103-8.

Goodwin, A. M., Sullivan, K. M. & D'Amore, P. A. (2006) Cultured endothelial cells display endogenous activation of the canonical Wnt signaling pathway and

express multiple ligands, receptors, and secreted modulators of Wnt signaling. *Dev Dyn,* 235(11)**,** 3110-20.

Gordon, Z., Elad, D., Almog, R., Hazan, Y., Jaffa, A. J. & Eytan, O. (2007a) Anthropometry of fetal vasculature in the chorionic plate. *J Anat,* 211(6)**,** 698-706.

Gordon, Z., Eytan, O., Jaffa, A. J. & Elad, D. (2007b) Hemodynamic analysis of Hyrtl anastomosis in human placenta. *Am J Physiol Regul Integr Comp Physiol,* 292(2)**,** R977-82.

Gourvas, V., Dalpa, E., Konstantinidou, A., Vrachnis, N., Spandidos, D. A. & Sifakis, S. (2012) Angiogenic factors in placentas from pregnancies complicated by fetal growth restriction (Review). *Molecular Medicine Reports,* 6(1)**,** 23-27.

Groesch, K. A., Torry, R. J., Wilber, A. C., Abrams, R., Bieniarz, A., Guilbert, L. J. & Torry, D. S. (2011) Nitric oxide generation affects pro- and anti-angiogenic growth factor expression in primary human trophoblast. *Placenta,* 32(12)**,** 926-31.

Gross, P. M., Joneja, M. G., Pang, J. J., Polischuk, T. M., Shaver, S. W. & Wainman, D. S. (1993) Topography of short portal vessels in the rat pituitary gland: a scanning electron-microscopic and morphometric study of corrosion cast replicas. *Cell Tissue Res,* 272(1)**,** 79-88.

Gude, N. M., Roberts, C. T., Kalionis, B. & King, R. G. (2004) Growth and function of the normal human placenta. *Thromb Res,* 114(5-6)**,** 397-407.

Gurney, A., Axelrod, F., Bond, C. J., Cain, J., Chartier, C., Donigan, L., Fischer, M., Chaudhari, A., Ji, M., Kapoun, A. M., Lam, A., Lazetic, S., Ma, S., Mitra, S., Park, I. K., Pickell, K., Sato, A., Satyal, S., Stroud, M., Tran, H., Yen, W. C., Lewicki, J. & Hoey, T. (2012) Wnt pathway inhibition via the targeting of Frizzled receptors results in decreased growth and tumorigenicity of human tumors. *Proc Natl Acad Sci U S A,* 109(29)**,** 11717-22.

Haeussner, E., Aschauer, B., Burton, G. J., Huppertz, B., Edler von Koch, F., Muller-Starck, J., Salafia, C., Schmitz, C. & Frank, H. G. (2015) Does 2D-Histologic identification of villous types of human placentas at birth enable sensitive and reliable interpretation of 3D structure? *Placenta,* 36(12)**,** 1425-32.

Haeussner, E., Buehlmeyer, A., Schmitz, C., von Koch, F. E. & Frank, H. G. (2014) Novel 3D microscopic analysis of human placental villous trees reveals unexpected significance of branching angles. *Sci Rep,* 4**,** 6192.

Haeussner, E., Schmitz, C., Frank, H. G. & Edler von Koch, F. (2016) Novel 3D light microscopic analysis of IUGR placentas points to a morphological correlate of compensated ischemic placental disease in humans. *Sci Rep,* 6**,** 24004.

Hales, C. N. & Barker, D. J. (1992) Type 2 (non-insulin-dependent) diabetes mellitus: the thrifty phenotype hypothesis. *Diabetologia,* 35(7)**,** 595-601.

Hama, H., Kurokawa, H., Kawano, H., Ando, R., Shimogori, T., Noda, H., Fukami, K., Sakaue-Sawano, A. & Miyawaki, A. (2011) Scale: a chemical approach for fluorescence imaging and reconstruction of transparent mouse brain. *Nat Neurosci,* 14(11)**,** 1481-8.

Hamai, Y., Fujii, T., Yamashita, T., Kozuma, S., Okai, T. & Taketani, Y. (1998) Evidence for basic fibroblast growth factor as a crucial angiogenic growth factor, released from human trophoblasts during early gestation. *Placenta,* 19(2-3)**,** 149-55.

Hanahan, D. (1997) Signaling vascular morphogenesis and maintenance. *Science,* 277(5322)**,** 48-50.

Hanahan, D. & Folkman, J. (1996) Patterns and emerging mechanisms of the angiogenic switch during tumorigenesis. *Cell,* 86(3)**,** 353-64.

Harman, C. R. & Baschat, A. A. (2003) Comprehensive assessment of fetal wellbeing: which Doppler tests should be performed? *Curr Opin Obstet Gynecol,* 15(2)**,** 147-57.

Hellberg, C., Ostman, A. & Heldin, C. H. (2010) PDGF and vessel maturation. *Recent Results Cancer Res,* 180**,** 103-14.

Helske, S., Vuorela, P., Carpen, O., Hornig, C., Weich, H. & Halmesmaki, E. (2001) Expression of vascular endothelial growth factor receptors 1, 2 and 3 in placentas from normal and complicated pregnancies. *Molecular Human Reproduction,* 7(2)**,** 205-10.

Heo, J. I., Cho, J. H. & Kim, J. R. (2013) HJURP Regulates Cellular Senescence in Human Fibroblasts and Endothelial Cells Via a p53-Dependent Pathway. *Journals of Gerontology Series a-Biological Sciences and Medical Sciences,* 68(8)**,** 914-925.

Herr, F., Horndasch, M., Howe, D., Baal, N., Goyal, P., Fischer, S., Zygmunt, M. & Preissner, K. T. (2014) Human placenta-derived Wnt-5a induces the expression of ICAM-1 and VCAM-1 in CD133(+)CD34(+)-hematopoietic progenitor cells. *Reproductive Biology,* 14(4)**,** 262-275.

Hey, P. J., Twells, R. C., Phillips, M. S., Yusuke, N., Brown, S. D., Kawaguchi, Y., Cox, R., Guochun, X., Dugan, V., Hammond, H., Metzker, M. L., Todd, J. A. & Hess, J. F. (1998) Cloning of a novel member of the low-density lipoprotein receptor family. *Gene,* 216(1)**,** 103-11.

Hitschold, T., Weiss, E., Beck, T., Hunterfering, H. & Berle, P. (1993) Low target birth weight or growth retardation? Umbilical Doppler flow velocity waveforms and histometric analysis of fetoplacental vascular tree. *Am J Obstet Gynecol,* 168(4)**,** 1260-4.

Hobson, S. R., Lim, R., Gardiner, E. E., Alers, N. O. & Wallace, E. M. (2013) Phase I pilot clinical trial of antenatal maternally administered melatonin to decrease the level of oxidative stress in human pregnancies affected by pre-eclampsia (PAMPR): study protocol. *BMJ Open,* 3(9)**,** e003788.

Hsieh, J. C., Kodjabachian, L., Rebbert, M. L., Rattner, A., Smallwood, P. M., Samos, C. H., Nusse, R., Dawid, I. B. & Nathans, J. (1999) A new secreted protein that binds to Wnt proteins and inhibits their activities. *Nature,* 398(6726)**,** 431-436.

Huang, M., Qiu, Q., Zeng, S., Xiao, Y., Shi, M., Zou, Y., Ye, Y., Liang, L., Yang, X. & Xu, H. (2015) Niclosamide inhibits the inflammatory and angiogenic activation of human umbilical vein endothelial cells. *Inflamm Res,* 64(12)**,** 1023-32.

Huang, W., Li, Q., Amiry-Moghaddam, M., Hokama, M., Sardi, S. H., Nagao, M., Warman, M. L. & Olsen, B. R. (2016) Critical Endothelial Regulation by LRP5 during Retinal Vascular Development. *PLoS One,* 11(3)**,** e0152833.

Ishikawa, F., Miyazono, K., Hellman, U., Drexler, H., Wernstedt, C., Hagiwara, K., Usuki, K., Takaku, F., Risau, W. & Heldin, C. H. (1989) Identification of angiogenic activity and the cloning and expression of platelet-derived endothelial cell growth factor. *Nature,* 338(6216)**,** 557-62.

Ishikawa, T., Tamai, Y., Zorn, A. M., Yoshida, H., Seldin, M. F., Nishikawa, S. & Taketo, M. M. (2001) Mouse Wnt receptor gene Fzd5 is essential for yolk sac and placental angiogenesis. *Development,* 128(1)**,** 25-33.

Jackson, M. R., Walsh, A. J., Morrow, R. J., Mullen, J. B., Lye, S. J. & Ritchie, J. W. (1995) Reduced placental villous tree elaboration in small-for-gestational-age pregnancies: relationship with umbilical artery Doppler waveforms. *Am J Obstet Gynecol,* 172(2 Pt 1)**,** 518-25.

Jacob, R. E., Colby, S. M., Kabilan, S., Einstein, D. R. & Carson, J. P. (2013) In situ casting and imaging of the rat airway tree for accurate 3D reconstruction. *Exp Lung Res,* 39(6)**,** 249-57.

Jarvis, S., Glinianaia, S. V., Torrioli, M. G., Platt, M. J., Miceli, M., Jouk, P. S., Johnson, A., Hutton, J., Hemming, K., Hagberg, G., Dolk, H. & Chalmers, J. (2003) Cerebral palsy and intrauterine growth in single births: European collaborative study. *Lancet,* 362(9390)**,** 1106-11.

Jauniaux, E. & Burton, G. J. (2006) Villous histomorphometry and placental bed biopsy investigation in type I diabetic pregnancies. *Placenta,* 27(4-5)**,** 468-474.

Jeyabalan, A., McGonigal, S., Gilmour, C., Hubel, C. A. & Rajakumar, A. (2008) Circulating and placental endoglin concentrations in pregnancies complicated by intrauterine growth restriction and preeclampsia. *Placenta,* 29(6)**,** 555-63.

Ji, T., Guo, Y., Kim, K., McQueen, P., Ghaffar, S., Christ, A., Lin, C., Eskander, R., Zi, X. L. & Hoang, B. H. (2015) Neuropilin-2 expression is inhibited by secreted Wnt antagonists and its down-regulation is associated with reduced tumor growth and metastasis in osteosarcoma. *Mol Cancer,* 14.

Jiang, Y., Zhang, Y., Zhang, H., Zhu, B., Li, P., Lu, C., Xu, Y., Chen, W. & Lin, N. (2014) Pravastatin prevents steroid-induced osteonecrosis in rats by suppressing PPARgamma expression and activating Wnt signaling pathway. *Exp Biol Med (Maywood),* 239(3)**,** 347-55.

Jones, S., Bischof, H., Lang, I., Desoye, G., Greenwood, S. L., Johnstone, E. D., Wareing, M., Sibley, C. P. & Brownbill, P. (2015) Dysregulated flow-mediated vasodilatation in the human placenta in fetal growth restriction. *J Physiol,* 593(14)**,** 3077-92.

Jorgensen, S. M., Demirkaya, O. & Ritman, E. L. (1998) Three-dimensional imaging of vasculature and parenchyma in intact rodent organs with X-ray micro-CT. *American Journal of Physiology-Heart and Circulatory Physiology,* 275(3)**,** H1103-H1114.

Junaid, T. O., Brownbill, P., Chalmers, N., Johnstone, E. D. & Aplin, J. D. (2014) Fetoplacental vascular alterations associated with fetal growth restriction. *Placenta,* 35(10)**,** 808-15.

Kanaujia, R. R., Miyamoto, Y., Hatano, E. & Ikuta, Y. (1986) Resin corrosion cast (Mercox) in experimental evaluation of small vessel anastomosis. *J Reconstr Microsurg,* 2(4)**,** 213-20.

Kaufmann, P., Bruns, U., Leiser, R., Luckhardt, M. & Winterhager, E. (1985) The fetal vascularisation of term human placental villi. II. Intermediate and terminal villi. *Anat Embryol (Berl),* 173(2)**,** 203-14.

Kaufmann, P., Luckhardt, M. & Leiser, R. (1988) Three dimensional representation of the fetal vessel system in the human placenta. *In:* Kaufmann, P., Miller, R.K. (ed.) *Placental vascularization and blood flow* New York, USA: Plenum medical book company.

Kaufmann, P., Mayhew, T. M. & Charnock-Jones, D. S. (2004) Aspects of human fetoplacental vasculogenesis and angiogenesis. II. Changes during normal pregnancy. *Placenta,* 25(2-3)**,** 114-26.

Kawasaki, J., Hirano, K., Hirano, M., Nishimura, J., Nakatsuka, A., Fujishima, M. & Kanaide, H. (2000) Dissociation between the Ca2+ signal and tube formation induced by vascular endothelial growth factor in bovine aortic endothelial cells. *European Journal of Pharmacology,* 398(1)**,** 19-29.

Ke, M. T., Fujimoto, S. & Imai, T. (2013) SeeDB: a simple and morphology-preserving optical clearing agent for neuronal circuit reconstruction. *Nat Neurosci,* 16(8)**,** 1154-61.

Kelly, A., Kevany, J., de Onis, M. & Shah, P. M. (1996) A WHO Collaborative Study of Maternal Anthropometry and Pregnancy Outcomes. *Int J Gynaecol Obstet,* 53(3)**,** 219-33.

Kim, D. H., Inagaki, Y., Suzuki, T., Ioka, R. X., Yoshioka, S. Z., Magoori, K., Kang, M. J., Cho, Y., Nakano, A. Z., Liu, Q., Fujino, T., Suzuki, H., Sasano, H. & Yamamoto, T. T. (1998) A new low density lipoprotein receptor related protein, LRP5, is expressed in hepatocytes and adrenal cortex, and recognizes apolipoprotein E. *J Biochem,* 124(6)**,** 1072-6.

Kingdom, J., Huppertz, B., Seaward, G. & Kaufmann, P. (2000) Development of the placental villous tree and its consequences for fetal growth. *Eur J Obstet Gynecol Reprod Biol,* 92(1)**,** 35-43.

Kingdom, J. C. & Kaufmann, P. (1997) Oxygen and placental villous development: origins of fetal hypoxia. *Placenta,* 18(8)**,** 613-21; discussion 623-6.

Kinzler, W. L. & Vintzileos, A. M. (2008) Fetal growth restriction: a modern approach. *Curr Opin Obstet Gynecol,* 20(2)**,** 125-31.

Kleinman, H. K. & Martin, G. R. (2005) Matrigel: basement membrane matrix with biological activity. *Semin Cancer Biol,* 15(5)**,** 378-86.

Kline, T. L., Zamir, M. & Ritman, E. L. (2011) Relating function to branching geometry: a micro-CT study of the hepatic artery, portal vein, and biliary tree. *Cells Tissues Organs,* 194(5)**,** 431-42.

Knofler, M. & Pollheimer, J. (2013) Human placental trophoblast invasion and differentiation: a particular focus on Wnt signaling. *Front Genet,* 4**,** 190.

Kohn, A. D. & Moon, R. T. (2005) Wnt and calcium signaling: beta-catenin-independent pathways. *Cell Calcium,* 38(3-4)**,** 439-46.

Komiya, Y. & Habas, R. (2008) Wnt signal transduction pathways. *Organogenesis,* 4(2)**,** 68-75.

Krebs, C., Macara, L. M., Leiser, R., Bowman, A. W., Greer, I. A. & Kingdom, J. C. (1996) Intrauterine growth restriction with absent end-diastolic flow velocity in the umbilical artery is associated with maldevelopment of the placental terminal villous tree. *Am J Obstet Gynecol,* 175(6)**,** 1534-42.

Krohn, J. & Bertelsen, T. (1997) Corrosion casts of the suprachoroidal space and uveoscleral drainage routes in the pig eye. *Acta Ophthalmol Scand,* 75(1)**,** 28-31.

Kubota, Y., Kleinman, H. K., Martin, G. R. & Lawley, T. J. (1988) Role of laminin and basement membrane in the morphological differentiation of human endothelial cells into capillary-like structures. *J Cell Biol,* 107(4)**,** 1589-98.

Kusinski, L. C., Stanley, J. L., Dilworth, M. R., Hirt, C. J., Andersson, I. J., Renshall, L. J., Baker, B. C., Baker, P. N., Sibley, C. P., Wareing, M. & Glazier, J. D. (2012) eNOS knockout mouse as a model of fetal growth restriction with an impaired uterine artery function and placental transport phenotype. *American Journal of Physiology-Regulatory Integrative and Comparative Physiology,* 303(1)**,** R86-R93.

Lackman, F., Capewell, V., Richardson, B., daSilva, O. & Gagnon, R. (2001) The risks of spontaneous preterm delivery and perinatal mortality in relation to size at birth according to fetal versus neonatal growth standards. *Am J Obstet Gynecol,* 184(5)**,** 946-53.

Lakshmi-Devi, C. K., Raghupathy, N.S. (2013) The Histological Findings in Human Placenta at Different Gestational Ages. *IOSR Journal of Dental and Medical Sciences* 6(1)**,** 29 - 31.

Lampugnani, M. G., Corada, M., Caveda, L., Breviario, F., Ayalon, O., Geiger, B. & Dejana, E. (1995) The molecular organization of endothelial cell to cell junctions: differential association of plakoglobin, beta-catenin, and alpha-catenin with vascular endothelial cadherin (VE-cadherin). *J Cell Biol,* 129(1)**,** 203-17.

Lampugnani, M. G., Resnati, M., Raiteri, M., Pigott, R., Pisacane, A., Houen, G., Ruco, L. P. & Dejana, E. (1992) A novel endothelial-specific membrane protein is a marker of cell-cell contacts. *J Cell Biol,* 118(6)**,** 1511-22.

Lang, I., Schweizer, A., Hiden, U., Ghaffari-Tabrizi, N., Hagendorfer, G., Bilban, M., Pabst, M. A., Korgun, E. T., Dohr, G. & Desoye, G. (2008) Human fetal placental endothelial cells have a mature arterial and a juvenile venous phenotype with adipogenic and osteogenic differentiation potential. *Differentiation,* 76(10)**,** 1031-43.

Langheinrich, A. C., Vorman, S., Seidenstucker, J., Kampschulte, M., Bohle, R. M., Wienhard, J. & Zygmunt, M. (2008) Quantitative 3D micro-CT imaging of the human feto-placental vasculature in intrauterine growth restriction. *Placenta,* 29(11)**,** 937-41.

Langheinrich, A. C., Wienhard, J., Vormann, S., Hau, B., Bohle, R. M. & Zygmunt, M. (2004) Analysis of the fetal placental vascular tree by X-ray micro-computed tomography. *Placenta,* 25(1)**,** 95-100.

Lassala, A., Bazer, F. W., Cudd, T. A., Datta, S., Keisler, D. H., Satterfield, M. C., Spencer, T. E. & Wu, G. (2010) Parenteral administration of L-arginine prevents fetal growth restriction in undernourished ewes. *J Nutr,* 140(7)**,** 1242-8.

Lassance, L., Miedl, H., Absenger, M., Diaz-Perez, F., Lang, U., Desoye, G. & Hiden, U. (2013) Hyperinsulinemia Stimulates Angiogenesis of Human Fetoplacental Endothelial Cells: A Possible Role of Insulin in Placental Hypervascularization in Diabetes Mellitus. *Journal of Clinical Endocrinology & Metabolism,* 98(9)**,** E1438-E1447.

Leach, L., Clark, P., Lampugnani, M. G., Arroyo, A. G., Dejana, E. & Firth, J. A. (1993) Immunoelectron characterisation of the inter-endothelial junctions of human term placenta. *J Cell Sci,* 104 (Pt 4)**,** 1073-81.

Leach, L., Lammiman, M. J., Babawale, M. O., Hobson, S. A., Bromilou, B., Lovat, S. & Simmonds, M. J. (2000) Molecular organization of tight and adherens junctions in the human placental vascular tree. *Placenta,* 21(5-6)**,** 547-57.

Leahy, M., Thompson, K., Zafar, H., Alexandrov, S., Foley, M., O'Flatharta, C. & Dockery, P. (2016) Functional imaging for regenerative medicine. *Stem Cell Res Ther,* 7(1)**,** 57.

Lee, H., Park, J. H., Seo, I., Park, S. H. & Kim, S. (2014) Improved application of the electrophoretic tissue clearing technology, CLARITY, to intact solid organs including brain, pancreas, liver, kidney, lung, and intestine. *BMC Dev Biol,* 14**,** 48.

Leiser, R., Krebs, C., Ebert, B. & Dantzer, V. (1997) Placental vascular corrosion cast studies: A comparison between ruminants and humans. *Microscopy Research and Technique,* 38(1-2)**,** 76-87.

Leiva, A., Fuenzalida, B., Barros, E., Sobrevia, B., Salsoso, R., Saez, T., Villalobos, R., Silva, L., Chiarello, I., Toledo, F., Gutierrez, J., Sanhueza, C., Pardo, F. & Sobrevia, L. (2016) Nitric Oxide is a Central Common Metabolite in Vascular Dysfunction Associated with Diseases of Human Pregnancy. *Current Vascular Pharmacology,* 14(3)**,** 237-259.

Li, Z., Ren, W., Zeng, Q., Chen, S., Zhang, M., Zhao, Y., Cheng, J. & Wang, X. (2016) Effects of survivin on angiogenesis in vivo and in vitro. *Am J Transl Res,* 8(2)**,** 270-83.

Liao, C. H., Lin, F. Y., Wu, Y. N. & Chiang, H. S. (2012) Androgens inhibit tumor necrosis factor-alpha-induced cell adhesion and promote tube formation of human coronary artery endothelial cells. *Steroids,* 77(7)**,** 756-64.

Liao, W. X., Feng, L., Zheng, J. & Chen, D. B. (2010) Deciphering mechanisms controlling placental artery endothelial cell migration stimulated by vascular endothelial growth factor. *Endocrinology,* 151(7)**,** 3432-44.

Lin, M., Mauroy, B., James, J. L., Tawhai, M. H. & Clark, A. R. (2016) A multiscale model of placental oxygen exchange: The effect of villous tree structure on exchange efficiency. *J Theor Biol*.

Liu, A. K., Hurry, M. E., Ng, O. T., DeFelice, J., Lai, H. M., Pearce, R. K., Wong, G. T., Chang, R. C. & Gentleman, S. M. (2015) Bringing CLARITY to the human brain: visualisation of Lewy pathology in three-dimensions. *Neuropathol Appl Neurobiol*.

Logue, O. C., McGowan, J. W., George, E. M. & Bidwell, G. L., 3rd. (2016) Therapeutic angiogenesis by vascular endothelial growth factor supplementation for treatment of renal disease. *Curr Opin Nephrol Hypertens*.

Lu, W., Lin, C., Roberts, M. J., Waud, W. R., Piazza, G. A. & Li, Y. (2011) Niclosamide suppresses cancer cell growth by inducing Wnt co-receptor LRP6 degradation and inhibiting the Wnt/beta-catenin pathway. *PLoS One,* 6(12)**,** e29290.

Luckhardt, M., Leiser, R., Kingdom, J., Malek, A., Sager, R., Kaisig, C. & Schneider, H. (1996) Effect of physiologic perfusion-fixation on the morphometrically evaluated dimensions of the term placental cotyledon. *J Soc Gynecol Investig,* 3(4)**,** 166-71.

Luria, O., Barnea, O., Shalev, J., Barkat, J., Kovo, M., Golan, A. & Bar, J. (2012) Two-dimensional and three-dimensional Doppler assessment of fetal growth restriction with different severity and onset. *Prenat Diagn,* 32(12)**,** 1174-80.

Macara, L., Kingdom, J. C., Kaufmann, P., Kohnen, G., Hair, J., More, I. A., Lyall, F. & Greer, I. A. (1996) Structural analysis of placental terminal villi from growth-restricted pregnancies with abnormal umbilical artery Doppler waveforms. *Placenta,* 17(1)**,** 37-48.

Macara, L., Kingdom, J. C., Kohnen, G., Bowman, A. W., Greer, I. A. & Kaufmann, P. (1995) Elaboration of stem villous vessels in growth restricted pregnancies with abnormal umbilical artery Doppler waveforms. *Br J Obstet Gynaecol,* 102(10)**,** 807-12.

Macdonald, B. T., Semenov, M. V. & He, X. (2007) SnapShot: Wnt/beta-catenin signaling. *Cell,* 131(6)**,** 1204.

Makinen, K., Manninen, H., Hedman, M., Matsi, P., Mussalo, H., Alhava, E. & Yla-Herttuala, S. (2002) Increased vascularity detected by digital subtraction angiography after VEGF gene transfer to human lower limb artery: a randomized, placebo-controlled, double-blinded phase II study. *Mol Ther,* 6(1)**,** 127-33.

Mamelle, N., Boniol, M., Riviere, O., Joly, M. O., Mellier, G., Maria, B., Rousset, B. & Claris, O. (2006) Identification of newborns with Fetal Growth Restriction (FGR) in weight and/or length based on constitutional growth potential. *Eur J Pediatr,* 165(10)**,** 717-25.

Mardi, K. & Sharma, J. (2003) Histopathological evaluation of placentas in IUGR pregnancies. *Indian J Pathol Microbiol,* 46(4)**,** 551-4.

Marikawa, Y. & Elinson, R. P. (1998) beta-TrCP is a negative regulator of the Wnt/beta-catenin signaling pathway and dorsal axis formation in Xenopus embryos. *Mechanisms of Development,* 77(1)**,** 75-80.

Marquez-Curtis, L. A., Billal Sultani, A., McGann, L. E. & Elliott, J. A. (2016) Beyond membrane integrity: Assessing the functionality of human umbilical vein endothelial cells after cryopreservation. *Cryobiology*.

Massink, M. P., Creton, M. A., Spanevello, F., Fennis, W. M., Cune, M. S., Savelberg, S. M., Nijman, I. J., Maurice, M. M., van den Boogaard, M. J. & van Haaften, G. (2015) Loss-of-Function Mutations in the WNT Co-receptor LRP6 Cause Autosomal-Dominant Oligodontia. *American Journal of Human Genetics,* 97(4)**,** 621-6.

Mayhew, T. M. (2002) Enhanced fetoplacental angiogenesis in pre-gestational diabetes mellitus: the extra growth is exclusively longitudinal and not accompanied by microvascular remodelling. *Diabetologia,* 45(10)**,** 1434-1439.

Mayhew, T. M. & Lucocq, J. M. (2015) From gross anatomy to the nanomorphome: stereological tools provide a paradigm for advancing research in quantitative morphomics. *J Anat,* 226(4)**,** 309-21.

Mayhew, T. M., Sorensen, F. B., Klebe, J. G. & Jackson, M. R. (1994) Growth and Maturation of Villi in Placentae from Well-Controlled Diabetic Women. *Placenta,* 15(1)**,** 57-65.

Mayhew, T. M., Wijesekara, J., Baker, P. N. & Ong, S. S. (2004) Morphometric evidence that villous development and fetoplacental angiogenesis are compromised by intrauterine growth restriction but not by pre-eclampsia. *Placenta,* 25(10)**,** 829-833.

Maynard, S. E., Min, J. Y., Merchan, J., Lim, K. H., Li, J., Mondal, S., Libermann, T. A., Morgan, J. P., Sellke, F. W., Stillman, I. E., Epstein, F. H., Sukhatme, V. P. & Karumanchi, S. A. (2003) Excess placental soluble fms-like tyrosine kinase 1 (sFlt1) may contribute to endothelial dysfunction, hypertension, and proteinuria in preeclampsia. *Journal of Clinical Investigation,* 111(5)**,** 649-58.

Menden, H., Welak, S., Cossette, S., Ramchandran, R. & Sampath, V. (2015) Lipopolysaccharide (LPS)-mediated angiopoietin-2-dependent autocrine angiogenesis is regulated by NADPH oxidase 2 (Nox2) in human pulmonary microvascular endothelial cells. *J Biol Chem,* 290(9)**,** 5449-61.

Milgroom, A. & Ralston, E. (2016) Clearing skeletal muscle with CLARITY for light microscopy imaging. *Cell Biol Int,* 40(4)**,** 478-83.

Mitra, S. C., Seshan, S. V. & Riachi, L. E. (2000) Placental vessel morphometry in growth retardation and increased resistance of the umbilical artery Doppler flow. *J Matern Fetal Med,* 9(5)**,** 282-6.

Mondy, W. L., Cameron, D., Timmermans, J. P., De Clerck, N., Sasov, A., Casteleyn, C. & Piegl, L. A. (2009) Micro-CT of Corrosion Casts for Use in the Computer-Aided Design of Microvasculature. *Tissue Engineering Part C-Methods,* 15(4)**,** 729-738.

Monkley, S. J., Delaney, S. J., Pennisi, D. J., Christiansen, J. H. & Wainwright, B. J. (1996) Targeted disruption of the Wnt2 gene results in placentation defects. *Development,* 122(11)**,** 3343-53.

Morrell, N. T., Leucht, P., Zhao, L., Kim, J. B., ten Berge, D., Ponnusamy, K., Carre, A. L., Dudek, H., Zachlederova, M., McElhaney, M., Brunton, S., Gunzner, J., Callow, M., Polakis, P., Costa, M., Zhang, X. M., Helms, J. A. & Nusse, R. (2008) Liposomal packaging generates Wnt protein with in vivo biological activity. *PLoS One,* 3(8)**,** e2930.

Mudgett, J. S., Ding, J., Guh-Siesel, L., Chartrain, N. A., Yang, L., Gopal, S. & Shen, M. M. (2000) Essential role for p38alpha mitogen-activated protein kinase in placental angiogenesis. *Proc Natl Acad Sci U S A,* 97(19)**,** 10454-9.

Mullin, P. M., Incerpi, M.H. (2010) *Fetal growth restriction* (5th ed.). united kingdom: Wiley-Blackwell.

Myatt, L., Eis, A. L., Brockman, D. E., Greer, I. A. & Lyall, F. (1997) Endothelial nitric oxide synthase in placental villous tissue from normal, pre-eclamptic and intrauterine growth restricted pregnancies. *Hum Reprod,* 12(1)**,** 167-72.

Narasimha, A. & Vasudeva, D. S. (2011) Spectrum of changes in placenta in toxemia of pregnancy. *Indian Journal of Pathology and Microbiology,* 54(1)**,** 15-20.

Nettum, J. A. (1995) Combined Vascular Bronchoalveolar Casting Using Formalin-Fixed Canine Lungs and a Low-Viscosity Silicone-Rubber. *Anatomical Record,* 243(4)**,** 479-482.

Ng, R. C. L., Matsumaru, D., Ho, A. S. H., Garcia-Barcelo, M. M., Yuan, Z. W., Smith, D., Kodjabachian, L., Tam, P. K. H., Yamada, G. & Lui, V. C. H. (2014) Dysregulation of Wnt inhibitory factor 1 (Wif1) expression resulted in aberrant Wnt-beta-catenin signaling and cell death of the cloaca endoderm, and anorectal malformations. *Cell Death and Differentiation,* 21(6)**,** 978-989.

Noguchi, J., Hata, K., Tanaka, H. & Hata, T. (2009) Placental vascular sonobiopsy using three-dimensional power Doppler ultrasound in normal and growth restricted fetuses. *Placenta,* 30(5)**,** 391-7.

Nyberg, P., Xie, L. & Kalluri, R. (2005) Endogenous inhibitors of angiogenesis. *Cancer Research,* 65(10)**,** 3967-79.

Okada, Y., Ueshin, Y., Isotani, A., Saito-Fujita, T., Nakashima, H., Kimura, K., Mizoguchi, A., Oh-Hora, M., Mori, Y., Ogata, M., Oshima, R. G., Okabe, M. & Ikawa, M. (2007) Complementation of placental defects and embryonic lethality by trophoblast-specific lentiviral gene transfer. *Nat Biotechnol,* 25(2)**,** 233-7.

Ono, M., Yin, P., Navarro, A., Moravek, M. B., Coon, V. J., Druschitz, S. A., Gottardi, C. J. & Bulun, S. E. (2014) Inhibition of canonical WNT signaling attenuates human leiomyoma cell growth. *Fertil Steril,* 101(5)**,** 1441-9.

Osada, T., Chen, M., Yang, X. Y., Spasojevic, I., Vandeusen, J. B., Hsu, D., Clary, B. M., Clay, T. M., Chen, W., Morse, M. A. & Lyerly, H. K. (2011) Antihelminth compound niclosamide downregulates Wnt signaling and elicits antitumor responses in tumors with activating APC mutations. *Cancer Research,* 71(12)**,** 4172-82.

Otrock, Z. K., Mahfouz, R. A., Makarem, J. A. & Shamseddine, A. I. (2007) Understanding the biology of angiogenesis: review of the most important molecular mechanisms. *Blood Cells Mol Dis,* 39(2)**,** 212-20.

Padavala, S., Pope, N., Baker, P. & Crocker, I. (2006) An imbalance between vascular endothelial growth factor and its soluble receptor in placental villous explants of intrauterine growth-restricted pregnancies. *Journal of the Society for Gynecologic Investigation,* 13(1)**,** 40-47.

Pan, C., Cai, R., Quacquarelli, F. P., Ghasemigharagoz, A., Lourbopoulos, A., Matryba, P., Plesnila, N., Dichgans, M., Hellal, F. & Erturk, A. (2016) Shrinkage-mediated imaging of entire organs and organisms using uDISCO. *Nat Methods*.

Pardi, G., Cetin, I., Marconi, A. M., Lanfranchi, A., Bozzetti, P., Ferrazzi, E., Buscaglia, M. & Battaglia, F. C. (1993) Diagnostic value of blood sampling in fetuses with growth retardation. *N Engl J Med,* 328(10)**,** 692-6.

Park, C. H., Chang, J. Y., Hahm, E. R., Park, S., Kim, H. K. & Yang, C. H. (2005) Quercetin, a potent inhibitor against beta-catenin/Tcf signaling in SW480 colon cancer cells. *Biochemical and Biophysical Research Communications,* 328(1)**,** 227-234.

Parr, B. A., Cornish, V. A., Cybulsky, M. I. & McMahon, A. P. (2001) Wnt7b regulates placental development in mice. *Developmental Biology,* 237(2)**,** 324-332.

Pate, K. T., Stringari, C., Sprowl-Tanio, S., Wang, K., TeSlaa, T., Hoverter, N. P., McQuade, M. M., Garner, C., Digman, M. A., Teitell, M. A., Edwards, R. A., Gratton, E. & Waterman, M. L. (2014) Wnt signaling directs a metabolic program of glycolysis and angiogenesis in colon cancer. *EMBO J,* 33(13)**,** 1454-73.

Patel, J., Landers, K., Mortimer, R. H. & Richard, K. (2010) Regulation of hypoxia inducible factors (HIF) in hypoxia and normoxia during placental development. *Placenta,* 31(11)**,** 951-7.

Peleg, D., Kennedy, C. M. & Hunter, S. K. (1998) Intrauterine growth restriction: identification and management. *Am Fam Physician,* 58(2)**,** 453-60, 466-7.

Pendas-Franco, N., Aguilera, O., Pereira, F., Gonzalez-Sancho, J. M. & Munoz, A. (2008) Vitamin D and Wnt/beta-catenin pathway in colon cancer: role and regulation of DICKKOPF genes. *Anticancer Res,* 28(5A)**,** 2613-23.

Petersen, S. G., Wong, S. F., Urs, P., Gray, P. H. & Gardener, G. J. (2009) Early onset, severe fetal growth restriction with absent or reversed end-diastolic flow

velocity waveform in the umbilical artery: Perinatal and long-term outcomes. *Australian & New Zealand Journal of Obstetrics & Gynaecology,* 49(1)**,** 45-51.

Petrozella, L., Mahendroo, M., Timmons, B., Roberts, S., McIntire, D. & Alexander, J. M. (2012) Endothelial microparticles and the antiangiogenic state in preeclampsia and the postpartum period. *Am J Obstet Gynecol,* 207(2)**,** 140 e20-6.

Peyter, A. C., Delhaes, F., Baud, D., Vial, Y., Diaceri, G., Menetrey, S., Hohlfeld, P. & Tolsa, J. F. (2014) Intrauterine growth restriction is associated with structural alterations in human umbilical cord and decreased nitric oxide-induced relaxation of umbilical vein. *Placenta,* 35(11)**,** 891-899.

Phng, L. K. & Gerhardt, H. (2009) Angiogenesis: A Team Effort Coordinated by Notch. *Developmental Cell,* 16(2)**,** 196-208.

Phng, L. K., Potente, M., Leslie, J. D., Babbage, J., Nyqvist, D., Lobov, I., Ondr, J. K., Rao, S., Lang, R. A., Thurston, G. & Gerhardt, H. (2009) Nrarp Coordinates Endothelial Notch and Wnt Signaling to Control Vessel Density in Angiogenesis. *Developmental Cell,* 16(1)**,** 70-82.

Planutis, K., Planutiene, M. & Holcombe, R. F. (2014) A novel signaling pathway regulates colon cancer angiogenesis through Norrin. *Sci Rep,* 4**,** 5630.

Plasencia, W., Gonzalez-Davila, E., Lorenzo, A. G., Armas-Gonzalez, M., Padron, E. & Gonzalez-Gonzalez, N. L. (2015) First trimester placental volume and vascular indices in pregnancies complicated by preeclampsia. *Prenatal Diagnosis,* 35(12)**,** 1247-1254.

Pollheimer, J., Loregger, T., Sonderegger, S., Saleh, L., Bauer, S., Bilban, M., Czerwenka, K., Husslein, P. & Knofler, M. (2006) Activation of the canonical wingless/T-cell factor signaling pathway promotes invasive differentiation of human trophoblast. *Am J Pathol,* 168(4)**,** 1134-47.

Pomorski, M., Zimmer, M., Florjanski, J., Michniewicz, J., Wiatrowski, A., Fuchs, T. & Milnerowicz-Nabzdyk, E. (2012) Comparative analysis of placental vasculature

and placental volume in normal and IUGR pregnancies with the use of three-dimensional Power Doppler. *Arch Gynecol Obstet,* 285(2)**,** 331-7.

Proffitt, K. D., Madan, B., Ke, Z., Pendharkar, V., Ding, L., Lee, M. A., Hannoush, R. N. & Virshup, D. M. (2013) Pharmacological inhibition of the Wnt acyltransferase PORCN prevents growth of WNT-driven mammary cancer. *Cancer Research,* 73(2)**,** 502-7.

Ptacek, I., Smith, A., Garrod, A., Bullough, S., Bradley, N., Batra, G., Sibley, C. P., Jones, R. L., Brownbill, P. & Heazell, A. E. P. (2016) Quantitative assessment of placental morphology may identify specific causes of stillbirth. *Bmc Clinical Pathology,* 16.

Raio, L., Ghezzi, F., di Naro, E., Franchi, M., Balestreri, D., Durig, P. & Schneider, H. (2001) In-utero characterization of the blood flow in the Hyrtl anastomosis. *Placenta,* 22(6)**,** 597-601.

Rajakumar, A. & Conrad, K. P. (2000) Expression, ontogeny, and regulation of hypoxia-inducible transcription factors in the human placenta. *Biol Reprod,* 63(2)**,** 559-69.

Ramaesh, T., Logie, J. J., Roseweir, A. K., Millar, R. P., Walker, B. R., Hadoke, P. W. & Reynolds, R. M. (2010) Kisspeptin-10 inhibits angiogenesis in human placental vessels ex vivo and endothelial cells in vitro. *Endocrinology,* 151(12)**,** 5927-34.

Ramma, W., Buhimschi, I. A., Zhao, G., Dulay, A. T., Nayeri, U. A., Buhimschi, C. S. & Ahmed, A. (2012) The elevation in circulating anti-angiogenic factors is independent of markers of neutrophil activation in preeclampsia. *Angiogenesis,* 15(3)**,** 333-40.

Razavi, H., Dusch, M. N., Zarafshar, S. Y., Taylor, C. A. & Feinstein, J. A. (2012) A method for quantitative characterization of growth in the 3-D structure of rat pulmonary arteries. *Microvasc Res,* 83(2)**,** 146-53.

Redline, R. W. (2015) Classification of placental lesions. *Am J Obstet Gynecol,* 213(4 Suppl)**,** S21-8.

Reilly, F. D. & Russell, P. T. (1977) Neurohistochemical evidence supporting an absence of adrenergic and cholinergic innervation in the human placenta and umbilical cord. *Anat Rec,* 188(3)**,** 277-86.

Rennie, M. Y., Whiteley, K. J., Kulandavelu, S., Adamson, S. L. & Sled, J. G. (2007) 3D visualisation and quantification by microcomputed tomography of late gestational changes in the arterial and venous feto-placental vasculature of the mouse. *Placenta,* 28(8-9)**,** 833-40.

Reynolds, L. P., Caton, J. S., Redmer, D. A., Grazul-Bilska, A. T., Vonnahme, K. A., Borowicz, P. P., Luther, J. S., Wallace, J. M., Wu, G. & Spencer, T. E. (2006) Evidence for altered placental blood flow and vascularity in compromised pregnancies. *J Physiol,* 572(Pt 1)**,** 51-8.

Richter, H. G., Hansell, J. A., Raut, S. & Giussani, D. A. (2009) Melatonin improves placental efficiency and birth weight and increases the placental expression of antioxidant enzymes in undernourished pregnancy. *J Pineal Res,* 46(4)**,** 357-64.

Rigano, S., Bozzo, M., Padoan, A., Mustoni, P., Bellotti, M., Galan, H. L. & Ferrazzi, E. (2008) Small size-specific umbilical vein diameter in severe growth restricted fetuses that die in utero. *Prenatal Diagnosis,* 28(10)**,** 908-913.

Rodesch, F., Simon, P., Donner, C. & Jauniaux, E. (1992) Oxygen measurements in endometrial and trophoblastic tissues during early pregnancy. *Obstet Gynecol,* 80(2)**,** 283-5.

Sadler, T. W. (2012) Third month to birth: the fetus and placenta. *Langman's Medical Embryology.* 12th ed. USA: Wolters Kluwer / Lippincott Williams & Wilkins.

Salafia, C. M., Pezzullo, J. C., Minior, V. K. & Divon, M. Y. (1997) Placental pathology of absent and reversed end-diastolic flow in growth-restricted fetuses. *Obstet Gynecol,* 90(5)**,** 830-6.

Salafia, C. M., Yampolsky, M., Misra, D. P., Shlakhter, O., Haas, D., Eucker, B. & Thorp, J. (2010) Placental surface shape, function, and effects of maternal and fetal vascular pathology. *Placenta,* 31(11)**,** 958-62.

Salafia, C. M., Yampolsky, M., Shlakhter, A., Mandel, D. H. & Schwartz, N. (2012) Variety in placental shape: when does it originate? *Placenta,* 33(3)**,** 164-70.

Satoh, K., Zhang, L., Zhang, Y., Chelluri, R., Boufraqech, M., Nilubol, N., Patel, D., Shen, M. & Kebebew, E. (2016) Identification of Niclosamide as a Novel Anticancer Agent for Adrenocortical Carcinoma. *Clin Cancer Res*.

Schindelin, J., Arganda-Carreras, I., Frise, E., Kaynig, V., Longair, M., Pietzsch, T., Preibisch, S., Rueden, C., Saalfeld, S., Schmid, B., Tinevez, J. Y., White, D. J., Hartenstein, V., Eliceiri, K., Tomancak, P. & Cardona, A. (2012) Fiji: an open-source platform for biological-image analysis. *Nat Methods,* 9(7)**,** 676-82.

Semenov, M. V., Habas, R., Macdonald, B. T. & He, X. (2007) SnapShot: Noncanonical Wnt Signaling Pathways. *Cell,* 131(7)**,** 1378.

Semenov, M. V., Tamai, K., Brott, B. K., Kuhl, M., Sokol, S. & He, X. (2001) Head inducer Dickkopf-1 is a ligand for Wnt coreceptor LRP6. *Current Biology,* 11(12)**,** 951-961.

Shams, M. & Ahmed, A. (1994) Localization of mRNA for basic fibroblast growth factor in human placenta. *Growth Factors,* 11(2)**,** 105-11.

Shore, V. H., Wang, T. H., Wang, C. L., Torry, R. J., Caudle, M. R. & Torry, D. S. (1997) Vascular endothelial growth factor, placenta growth factor and their receptors in isolated human trophoblast. *Placenta,* 18(8)**,** 657-65.

Sled, J. G., Marxen, M. & Henkelman, R. M. (2004) Analysis of micro-vasculature in whole kidney specimens using micro-CT. *Developments in X-Ray Tomography Iv,* 5535**,** 53-64.

Smith, R. E. & Turner, R. J. (1973) Total Hip-Replacement Using Methylmethacrylate Cement Analysis of Data from 3,482 Cases. *Clinical Orthopaedics and Related Research,* (95)**,** 231-238.

Sonderegger, S., Husslein, H., Leisser, C. & Knofler, M. (2007) Complex expression pattern of Wnt ligands and frizzled receptors in human placenta and its trophoblast subtypes. *Placenta,* 28 Suppl A**,** S97-102.

Standring, S., Borley, N.R., Collins, P., Crossman, A.R., Gatzoulis, M.A., Healy, J.C., Johnson, D., Mahadevan, V., Newell, R.L.M., and Wigley, C. (2008) Implantation and placentation. *In:* Standring, S. (ed.) *Gray's Anatomy: The Anatomical Basis of Clinical Practice.* Fortieth edition ed. Spain: Churchill Livingstone, Elsevier.

Stanley, J. L., Andersson, I. J., Hirt, C. J., Moore, L., Dilworth, M. R., Chade, A. R., Sibley, C. P., Davidge, S. T. & Baker, P. N. (2012) Effect of the anti-oxidant tempol on fetal growth in a mouse model of fetal growth restriction. *Biol Reprod,* 87(1)**,** 25, 1-8.

Stenman, J. M., Rajagopal, J., Carroll, T. J., Ishibashi, M., McMahon, J. & McMahon, A. P. (2008) Canonical Wnt Signaling Regulates Organ-Specific Assembly and Differentiation of CNS Vasculature. *Science,* 322(5905)**,** 1247-1250.

Tan, H., Wen, S. W., Walker, M. & Demissie, K. (2004) Parental race, birth weight, gestational age, and fetal growth among twin infants in the United States. *Early Hum Dev,* 80(2)**,** 153-60.

Tang, L., Zhu, H., Yang, X., Xie, F., Peng, J., Jiang, D., Xie, J., Qi, M. & Yu, L. (2016) Shizukaol D, a Dimeric Sesquiterpene Isolated from Chloranthus serratus, Represses the Growth of Human Liver Cancer Cells by Modulating Wnt Signalling Pathway. *PLoS One,* 11(3)**,** e0152012.

Todros, T., Sciarrone, A., Piccoli, E., Guiot, C., Kaufmann, P. & Kingdom, J. (1999) Umbilical Doppler waveforms and placental villous angiogenesis in pregnancies complicated by fetal growth restriction. *Obstet Gynecol,* 93(4)**,** 499-503.

Tomer, R., Ye, L., Hsueh, B. & Deisseroth, K. (2014) Advanced CLARITY for rapid and high-resolution imaging of intact tissues. *Nat Protoc,* 9(7)**,** 1682-97.

Ullberg, U. (2003) *The Human Placenta: an Angiographic Study.* Ph.D, Kongl Carolinska Medico Chirurgiska Institutet.

Ullberg, U., Sandstedt, B. & Lingman, G. (2001) Hyrtl's anastomosis, the only connection between the two umbilical arteries. A study in full term placentas from AGA infants with normal umbilical artery blood flow. *Acta Obstet Gynecol Scand,* 80(1)**,** 1-6.

Usuki, K., Norberg, L., Larsson, E., Miyazono, K., Hellman, U., Wernstedt, C., Rubin, K. & Heldin, C. H. (1990) Localization of platelet-derived endothelial cell growth factor in human placenta and purification of an alternatively processed form. *Cell Regul,* 1(8)**,** 577-84.

van Amerongen, R. & Nusse, R. (2009) Towards an integrated view of Wnt signaling in development. *Development,* 136(19)**,** 3205-14.

Vasquez, S. X., Gao, F., Su, F., Grijalva, V., Pope, J., Martin, B., Stinstra, J., Masner, M., Shah, N., Weinstein, D. M., Farias-Eisner, R. & Reddy, S. T. (2011) Optimization of microCT imaging and blood vessel diameter quantitation of preclinical specimen vasculature with radiopaque polymer injection medium. *PLoS One,* 6(4)**,** e19099.

Vollmerhaus, B. (2002) August Schummer (1902-1977): Pioneer of a modern anatomy of corrosion. *Anatomia Histologia Embryologia-Journal of Veterinary Medicine Series C,* 31(6)**,** 326-330.

Volpert, O. V. (2000) Modulation of endothelial cell survival by an inhibitor of angiogenesis thrombospondin-1: a dynamic balance. *Cancer Metastasis Rev,* 19(1-2)**,** 87-92.

von Dadelszen, P., Dwinnell, S., Magee, L. A., Carleton, B. C., Gruslin, A., Lee, B., Lim, K. I., Liston, R. M., Miller, S. P., Rurak, D., Sherlock, R. L., Skoll, M. A., Wareing, M. M., Baker, P. N., Research into Advanced Fetal, D. & Therapy, G. (2011) Sildenafil citrate therapy for severe early-onset intrauterine growth restriction. *BJOG,* 118(5)**,** 624-8.

Vuorela, P., Hatva, E., Lymboussaki, A., Kaipainen, A., Joukov, V., Persico, M. G., Alitalo, K. & Halmesmaki, E. (1997) Expression of vascular endothelial growth factor and placenta growth factor in human placenta. *Biol Reprod,* 56(2)**,** 489-94.

Wallner, W., Sengenberger, R., Strick, R., Strissel, P. L., Meurer, B., Beckmann, M. W. & Schlembach, D. (2007) Angiogenic growth factors in maternal and fetal serum in pregnancies complicated by intrauterine growth restriction. *Clin Sci (Lond),* 112(1)**,** 51-7.

Wang, Y. & Zhao, S. (2010a) Oxygen Tension and Placental Vascular Development. *In:* Granger, D. N., Granger, J. (ed.) *Vascular Biology of the Placenta.* San Rafael (CA): Morgan and Claypool Life Science.

Wang, Y. & Zhao, S. (2010b) Placental Blood Circulation. *In:* Granger, D. N., Granger, J. (ed.) *Vascular Biology of the Placenta.* San Rafael (CA): Morgan & Claypool Life Sciences.

Wang, Y. S., Rattner, A., Zhou, Y. L., Williams, J., Smallwood, P. M. & Nathans, J. (2012) Norrin/Frizzled4 Signaling in Retinal Vascular Development and Blood Brain Barrier Plasticity. *Cell,* 151(6)**,** 1332-1344.

Wareing, M., Akef, H., Greenwood, S. L., Bugg, G., Baker, P. N., Maternal & Fetal Health Research Centre, U. o. M. S. M. s. H. U. K. M. W. m. a. u. (2005) Umbilical artery Doppler waveform indices from normal pregnant women are related to vasodilatation of placental chorionic plate small arteries. *J Obstet Gynaecol,* 25(3)**,** 248-52.

Wareing, M., Crocker, I. P., Warren, A. Y., Taggart, M. J. & Baker, P. N. (2002) Characterization of small arteries isolated from the human placental chorionic plate. *Placenta,* 23(5)**,** 400-9.

Warrander, L. K., Batra, G., Bernatavicius, G., Greenwood, S. L., Dutton, P., Jones, R. L., Sibley, C. P. & Heazell, A. E. (2012) Maternal perception of reduced fetal movements is associated with altered placental structure and function. *PLoS One,* 7(4)**,** e34851.

Weber, K. (1982) [Morphologic studies on the venous blood drainage of the human placenta]. *Z Mikrosk Anat Forsch,* 96(3)**,** 407-32.

Willert, K. & Nusse, R. (1998) Beta-catenin: a key mediator of Wnt signaling. *Curr Opin Genet Dev,* 8(1)**,** 95-102.

Wills, A. K., Chinchwadkar, M. C., Joglekar, C. V., Natekar, A. S., Yajnik, C. S., Fall, C. H. & Kinare, A. S. (2010) Maternal and paternal height and BMI and patterns of fetal growth: the Pune Maternal Nutrition Study. *Early Hum Dev,* 86(9)**,** 535-40.

Wodarz, A. & Nusse, R. (1998) Mechanisms of Wnt signaling in development. *Annu Rev Cell Dev Biol,* 14**,** 59-88.

Wolman, I., Gull, I., Fait, G., Amster, R., Kupferminc, M. J., Lessing, J. B. & Jaffa, A. J. (2002) Persistent right umbilical vein: incidence and significance. *Ultrasound Obstet Gynecol,* 19(6)**,** 562-4.

Wu, F. T., Stefanini, M. O., Mac Gabhann, F., Kontos, C. D., Annex, B. H. & Popel, A. S. (2010) A systems biology perspective on sVEGFR1: its biological function, pathogenic role and therapeutic use. *J Cell Mol Med,* 14(3)**,** 528-52.

Wyrwoll, C. S., Noble, J., Thomson, A., Tesic, D., Miller, M. R., Rog-Zielinska, E. A., Moran, C. M., Seckl, J. R., Chapman, K. E. & Holmes, M. C. (2016) Pravastatin ameliorates placental vascular defects, fetal growth, and cardiac function in a model of glucocorticoid excess. *Proc Natl Acad Sci U S A,* 113(22)**,** 6265-70.

Xiao, X. M. & Li, L. P. (2005) L-Arginine treatment for asymmetric fetal growth restriction. *Int J Gynaecol Obstet,* 88(1)**,** 15-8.

Yampolsky, M., Salafia, C. M., Shlakhter, O., Haas, D., Eucker, B. & Thorp, J. (2009) Centrality of the umbilical cord insertion in a human placenta influences the placental efficiency. *Placenta,* 30(12)**,** 1058-64.

Yang, B., Treweek, J. B., Kulkarni, R. P., Deverman, B. E., Chen, C. K., Lubeck, E., Shah, S., Cai, L. & Gradinaru, V. (2014) Single-cell phenotyping within transparent intact tissue through whole-body clearing. *Cell,* 158(4)**,** 945-58.

Yao, L., Sun, B., Zhao, X., Zhao, X., Gu, Q., Dong, X., Zheng, Y., Sun, J., Cheng, R., Qi, H. & An, J. (2014) Overexpression of Wnt5a promotes angiogenesis in NSCLC. *Biomed Res Int,* 2014**,** 832562.

Ye, X., Wang, Y. S., Cahill, H., Yu, M. Z., Badea, T. C., Smallwood, P. M., Peachey, N. S. & Nathans, J. (2009) Norrin, Frizzled-4, and Lrp5 Signaling in Endothelial Cells Controls a Genetic Program for Retinal Vascularization. *Cell,* 139(2)**,** 285-298.

Yeo, E. J., Cassetta, L., Qian, B. Z., Lewkowich, I., Li, J. F., Stefater, J. A., 3rd, Smith, A. N., Wiechmann, L. S., Wang, Y., Pollard, J. W. & Lang, R. A. (2014) Myeloid WNT7b mediates the angiogenic switch and metastasis in breast cancer. *Cancer Research,* 74(11)**,** 2962-73.

Yuan, K., Orcholski, M. E., Panaroni, C., Shuffle, E. M., Huang, N. F., Jiang, X. U., Tian, W., Vladar, E. K., Wang, L. L., Nicolls, M. R., Wu, J. Y. & Perez, V. A. D. (2015) Activation of the Wnt/Planar Cell Polarity Pathway Is Required for Pericyte Recruitment during Pulmonary Angiogenesis. *American Journal of Pathology,* 185(1)**,** 69-84.

Zhang, J., Liu, C., Shi, W., Yang, L., Zhang, Q., Cui, J., Fang, Y., Li, Y., Ren, G., Yang, S. & Xiang, R. (2016) The novel VEGF receptor 2 inhibitor YLL545 inhibits angiogenesis and growth in breast cancer. *Oncotarget*.

Zhao, W., Qiao, J., Zhang, Q., Zhao, Y. & Chen, Q. (2010) Levels of antiangiogenic factors in preeclamptic pregnancies. *Growth Factors,* 28(4)**,** 293-8.

Zheng, H. & Rinaman, L. (2016) Simplified CLARITY for visualizing immunofluorescence labeling in the developing rat brain. *Brain Struct Funct,* 221(4)**,** 2375-83.

Zheng, J., Li, Y., Weiss, A. R., Bird, I. M. & Magness, R. R. (2000) Expression of endothelial and inducible nitric oxide synthases and nitric oxide production in ovine placental and uterine tissues during late pregnancy. *Placenta,* 21(5-6)**,** 516-24.

Zheng, J., Wen, Y., Song, Y., Wang, K., Chen, D. B. & Magness, R. R. (2008) Activation of multiple signaling pathways is critical for fibroblast growth factor 2- and vascular endothelial growth factor-stimulated ovine fetoplacental endothelial cell proliferation. *Biol Reprod,* 78(1)**,** 143-50.

Zhou, K. K., Benyajati, S., Le, Y., Cheng, R., Zhang, W. B. & Ma, J. X. (2014) Interruption of Wnt Signaling in Muller Cells Ameliorates Ischemia-Induced Retinal Neovascularization. *PLoS One,* 9(10).

Appendices

Appendix 1: <u>Protocol for analysis of micro-CT data on Avizo</u>

Steps involved

1. Obtain voxel size of the data

2. Open data in Avizo

3. Volume rendering of data

4. Cropping

5. Apply scale bars & grids

6. Segmentation of data

7. Measurements 1: Volume and Area

8. Skeletonisation

9. Measurements 2: Length, number of branch points

10. Measurements 3: Diameter, Length, manual measures

11. Taking snapshots

1. Obtain voxel size of data

- Locate the .vgi file of the data e.g RFMB29.vgi

- Right click the file

- Open with notepad

- Scroll down to resolution, note the value (the 3 values represent the X, Y & Z planes respectively)

- Scroll further down to verify the unit e.g mm

2. Open data in avizo

- Start Avizo standard

- Click "open data" in project view

- Locate and open the data stored in .tif format

- Copy all the .tif files (Ctrl A), then click open

- Type in the voxel size obtained in section 1 above (in the 3 boxes)

- Click ok

3. Volume rendering of data

- Right click the imported data in project view

- Click volume rendering

- Adjust the colourmap to get rid of background grey scale/noise (change numbers until you achieve a desirable view)

- Click view on the top pane, choose "background", choose "uniform" and change colour as desired, then click ok

4. Cropping

- Right click the data

- Go to "compute"

- Go to "volume edit"

- Change from "Draw" to "Tadbox"

- Change from "Box" to "Cylinder"

- Change axis to "Z axis"

- Click the "outside" box on "cut"

- Click apply

- This creates another data in the project view with the suffix "modif*"

- Deactivate the former data

- Do volume rendering for the new data (as in section 3 above)

- Rotate the new 3D image to view its base/background and crop any background noise as follows:

  - Right click the data, choose orthoslice

  - Move the slice line to separate the data from the background noise (move slice number)

  - Click the "clip" tool to crop off the noise

  - Deactivate orthoslice

- Rotate the data back to position

5. **Apply scale bars & grids**

- Right click data

- Click "annotate"

- Choose "scale bars" or "local axis" (whichever is required)

- Change colour from the background/default colour (default is white)

- Change unit to what is desired e.g mm

- Change font and select its colour as desired

- Adjust scale bars as desired

- Apply grids if necessary

6. **Segmentation of data**

- Right click data, scroll to "image segmentation", choose "edit new label field"

- View in 4 viewers mode (viewers 0, 1, 2 & 3)

0	1
2	3

0 = 3D view

1 = XY

2 = XZ   } slice planes

3 = YZ

- Choose the XY slice, change to 2 viewer mode

- Tick show in 3D

- Tick all slices

- Use zoom tools to zoom in to show a perfect circle of slice XY (whole data in view)

- Set "data window" to 37 & 100 (or whichever values you've been working with from the beginning)

- Use magic wand tool or threshold tool to select data to segment

- Selected data turns red, adjust slider to create your selection

- Use eraser tool to clean off errors

- Tick "all slices"

- Click the ⊕ sign to add the selection for analysis

- You can change the title "inside" to whatever you want to use

7. Measurements 1: volume and area

- Click segmentation at the top pane

- Click material statistics

- You will obtain the volume in mm^3 and area in mm^2 (use the inside data, ignore the exterior ones)

8. Skeletonisation

- Right click labels (green in project view)

- Scroll down to image morphology

- Click autoskeleton

- Click apply at the bottom of the page

- Click spatial graph view on project view to modify parameters as follows:

  - Turn nodes on or off

  - Change node colour

  - Change segment styles – choose tubes

  - Change colour of segments/tubes

  - Change tube scale from "constant" to "thickness"

  - Adjust tube scale factor

  - Change segment colouring from "constant" to "thickness"

  - Change segment colourmap to physics.icol (click edit and choose physics.icol)

  - Double click the colour gradient shown, physics.icol data will appear in project view. Right click the physics.icol data, choose annotate, choose colourmap legend

  - Tick custom text

  - Change font colour to black (default is white)

  - Type in values with desired unit in apostrophe e.g 0/"0 mm" 0.5/"0.5 mm" 1/"1 mm" to replace the low, medium and high in the default settings

9. **Measurements 2: length, number of branch points**

- Right click spatial graph data in project view

- Choose measure

- Click spatial graph statistics

- Click apply

- Right click on the resultant green data "Smt.statistics" in project view

- Scroll to compute and click "spreadsheet filter"

- Click "show spreadsheet"

10. **Measurements 3: diameter, length, manual measures**

- Convert spatial graph to line set

  - Right click the Smt.SptGraph data

  - Scroll to "convert" and click "spatial graph to line set"

  - Click apply

  - Click on the resultant data in project view

  - Click the ruler icon in the top pane

  - Draw line to measure

11. Taking snapshots

- Take snapshots at any point by clicking on the camera icon in the top pane (put scale bars or colourmap legend, as in sections 5 and 8 respectively, before taking snapshot, if necessary)

Appendix 2: <u>Protocol for analysis of micro-CT data on Analyze</u>

Steps involved

1. Load data on Analyze workspace

2. Pre-process/Segment/Threshold

3. Generate tree map

1. Load data on Analyze workspace

- Open Analyze and click file

- Choose import/export
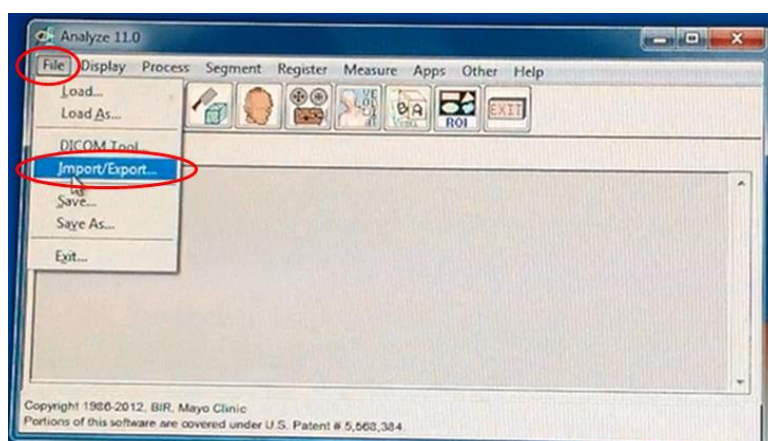
- On import/export page, click tools and choose volume tool
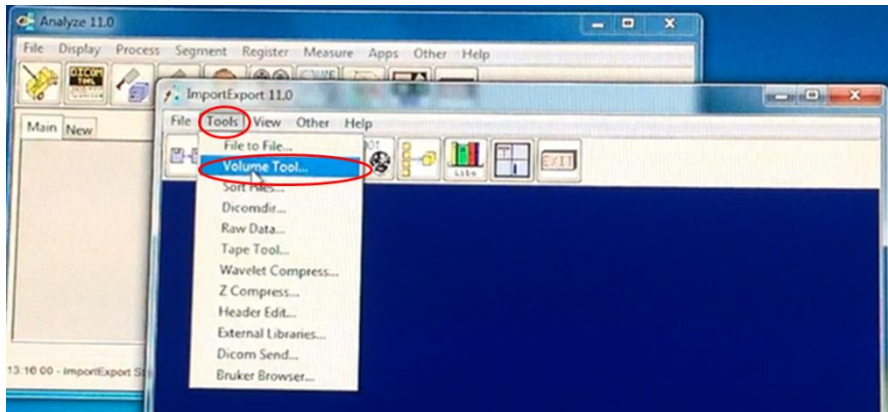
- Click wild cards
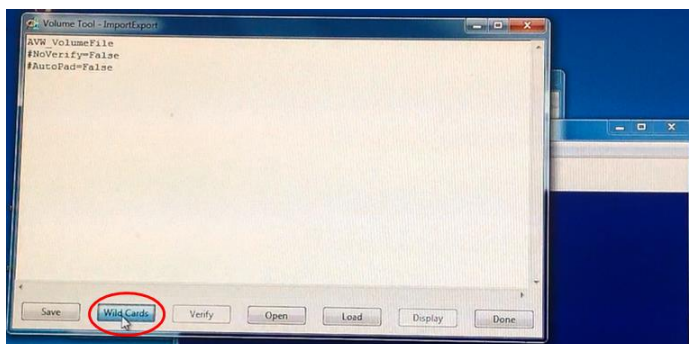
- Find the CT slices (in .tiff format) in your directory

- Click apply and save as .vol file.
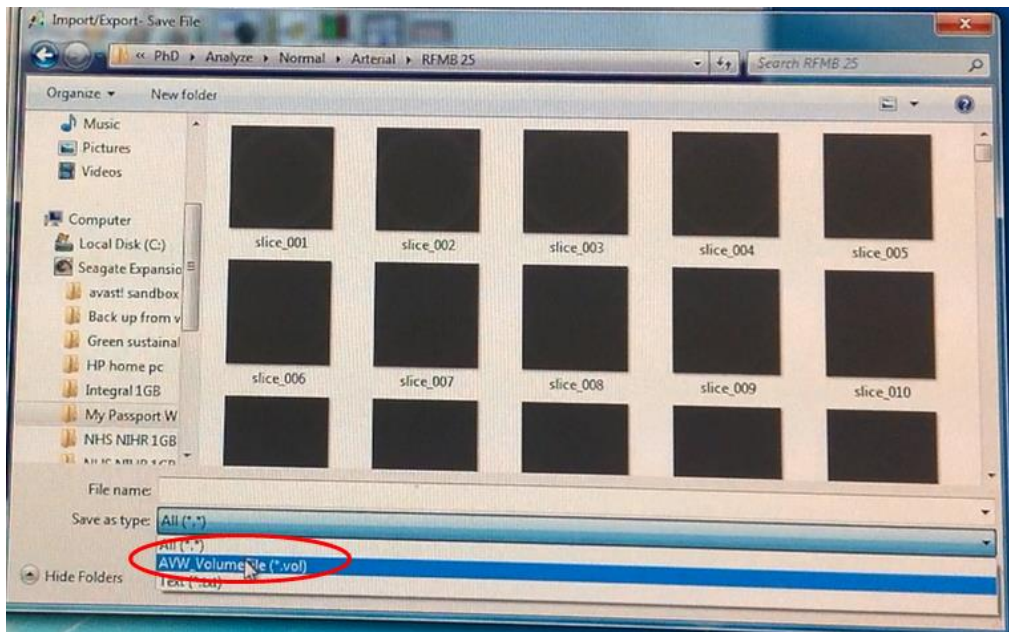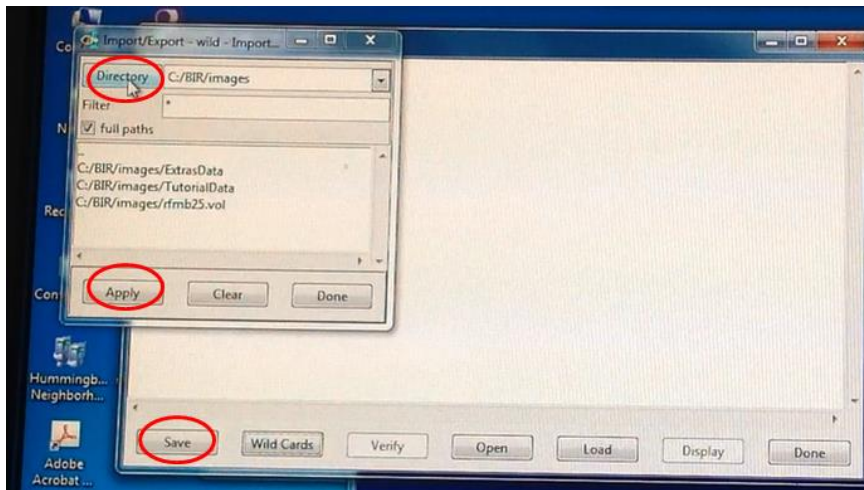
- Close import/export page

- Back in Analyze workspace, click "file" and choose "load as"
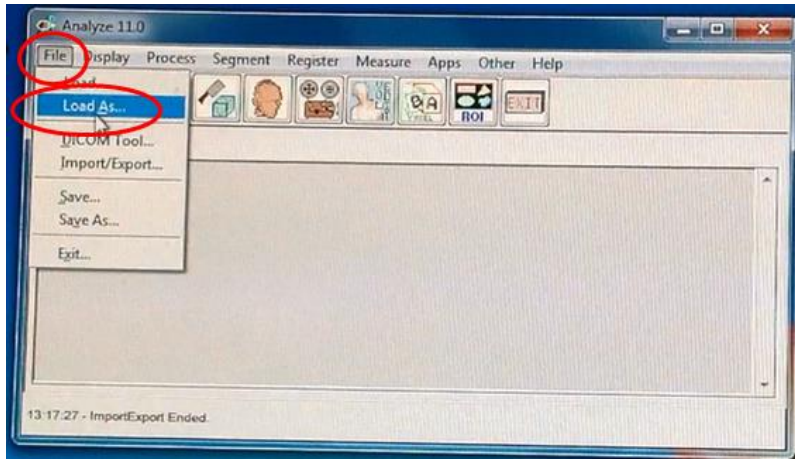
- Find and load the .vol file you just saved

- Click subregion (at the top), then click interactive (below)

- Choose the slices you wish to load from the image viewer that appears and click done
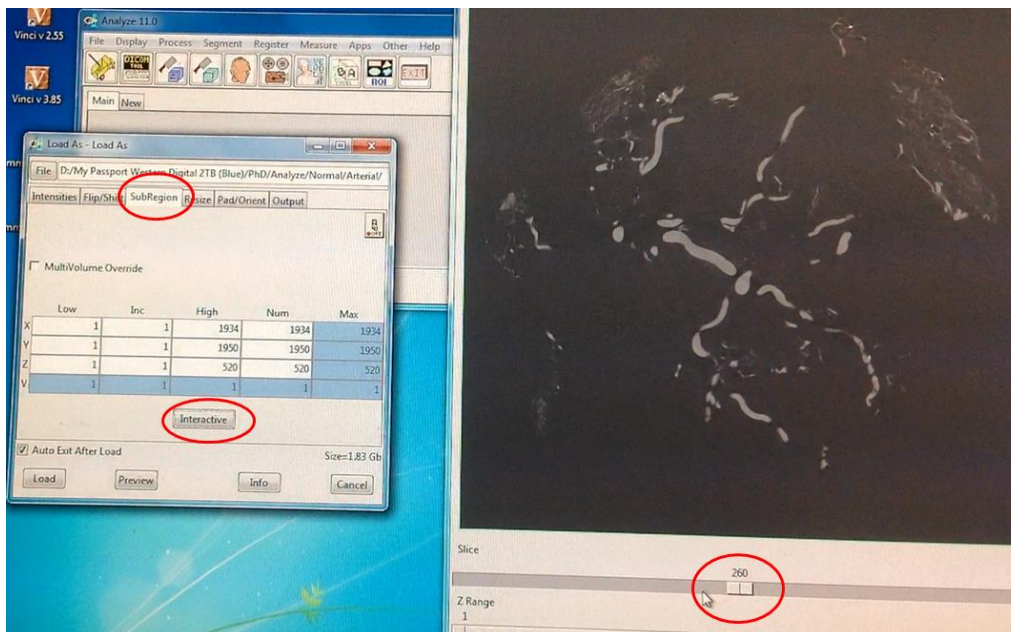
- Click resize, tick force cubic, change voxel size from 1 to 2

- Click load and wait for the .vol to load into the workspace.
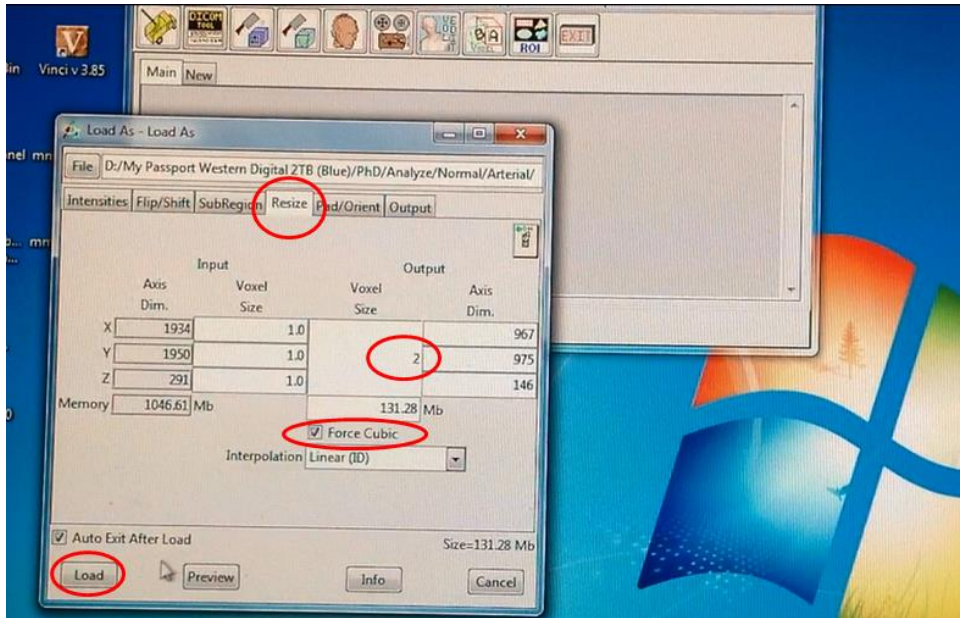
2. **Pre-process/Segment/Threshold**

- Click segment and choose volume edit
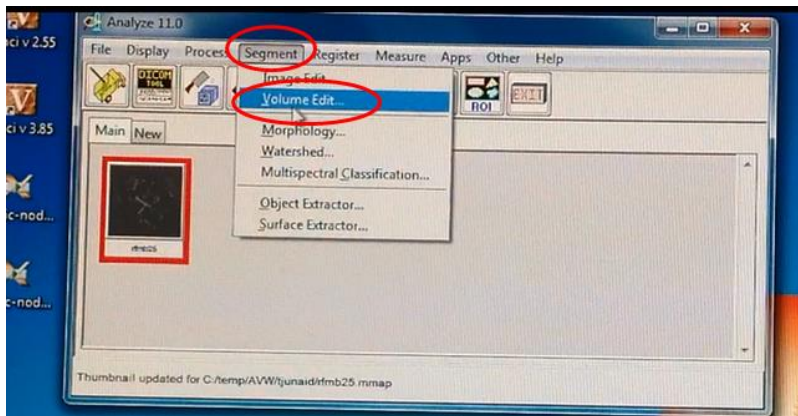
- On the new page that opens, tick display, click semi-automatic and tick threshold

- Then threshold by adjusting the slider on the page

- When you finish with thresholding, click define object (save object map here if you want – click file and choose save object map)
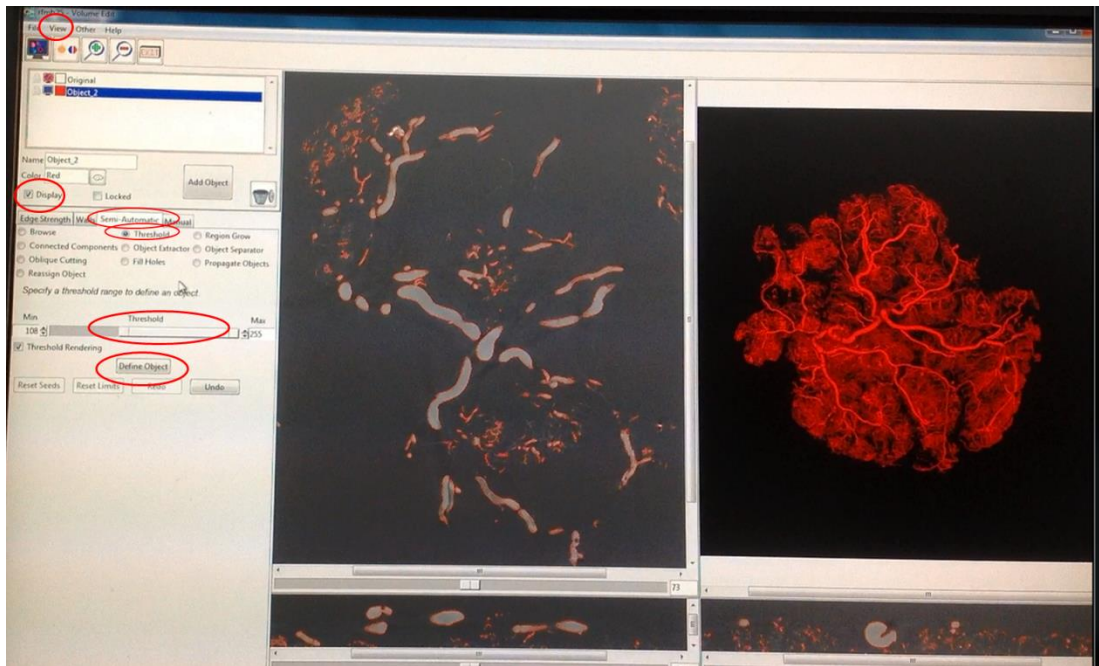
- Click view, then objects, save as binary, save to disk in your format of choice, then save to analyze workspace (this must be done) and click done.
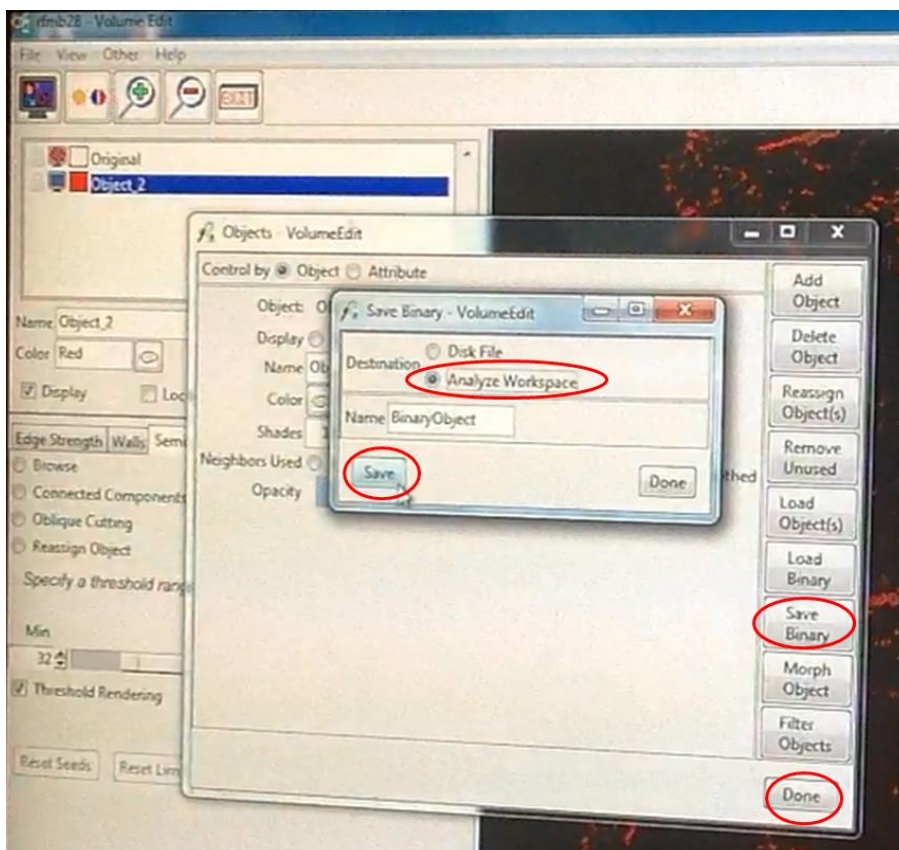
3. **Generate tree map**

- Choose the binary object you saved on Analyze workspace

- Click measure

- Choose tree analysis
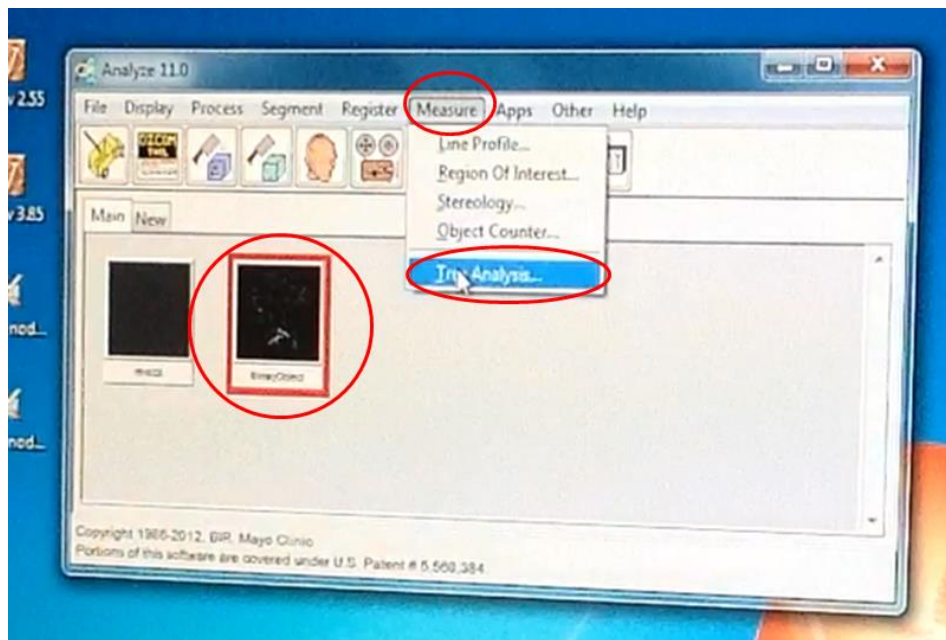
- Click other

- Click options and untick display obliques, then click done

- Click generate

- Click slice, you can look at the slices by sliding the slice slider (don't touch the increment and number sliders)

- Click done
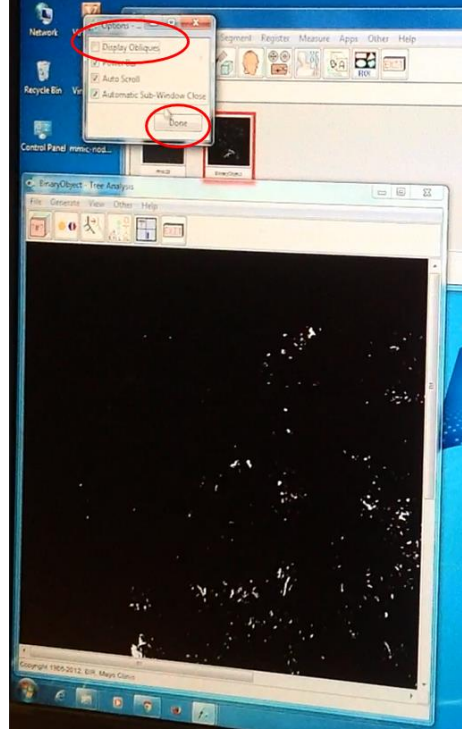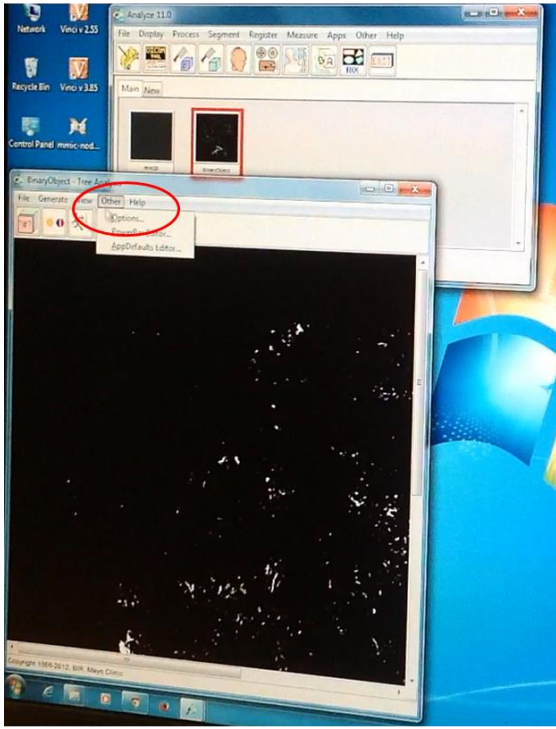
- Click generate, generate tree, then generate tree again

- Once tree(s) open, combine the trees as necessary

- Tick map, when tree map loads, save as pdf (right click, choose print, choose save as pdf)

- Click stats and calculate stats for analyses results.
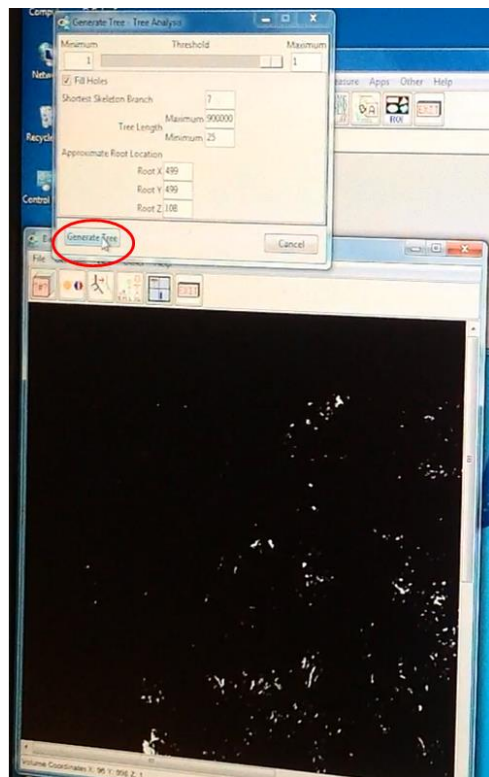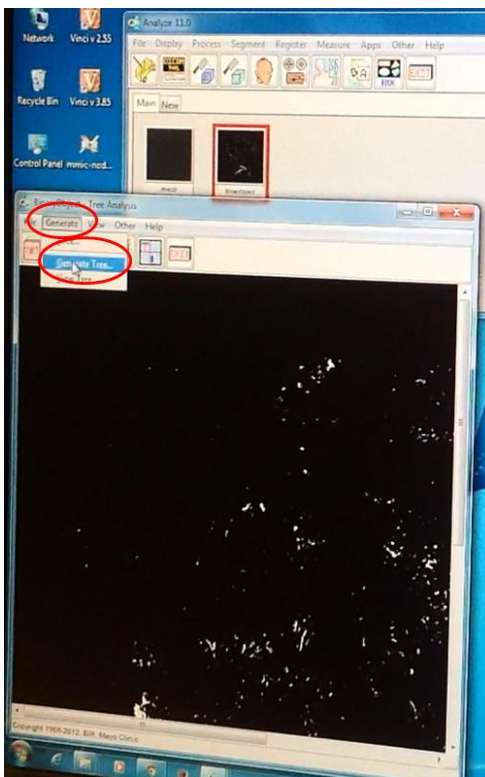
Appendix 3: <u>Analyze tree maps for all samples</u>

The tree maps generated from all twenty-four casts are shown in figures 5.1 – 5.24. Each tree has been compressed and resized to fit on the pages of this thesis. A screenshot of part of an original tree is shown in chapter 2 (figure 2.6). As explained in figure 2.6, the yellow dot at the top of each tree represents the root of all the vessels (umbilical cord insertion point). True branch points and terminal branch points are marked in blue and red dots respectively. Branching is mostly by bifurcation, with daughter vessels represented by coloured lines (one yellow and the other green). Occasionally, there were three branches from a parent vessel and a pink line represented the third vessel.
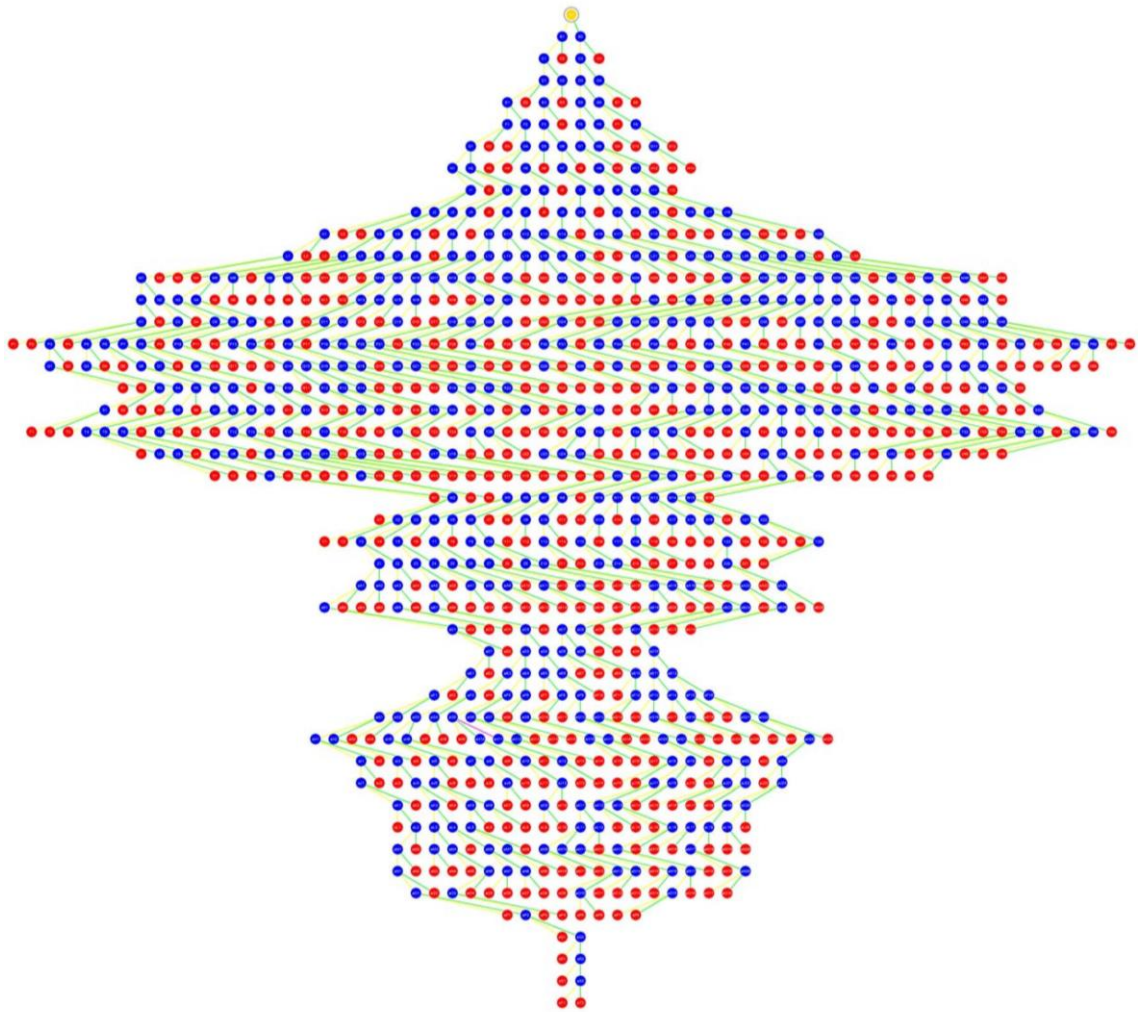
Figure 5.1: Normal arterial tree 1
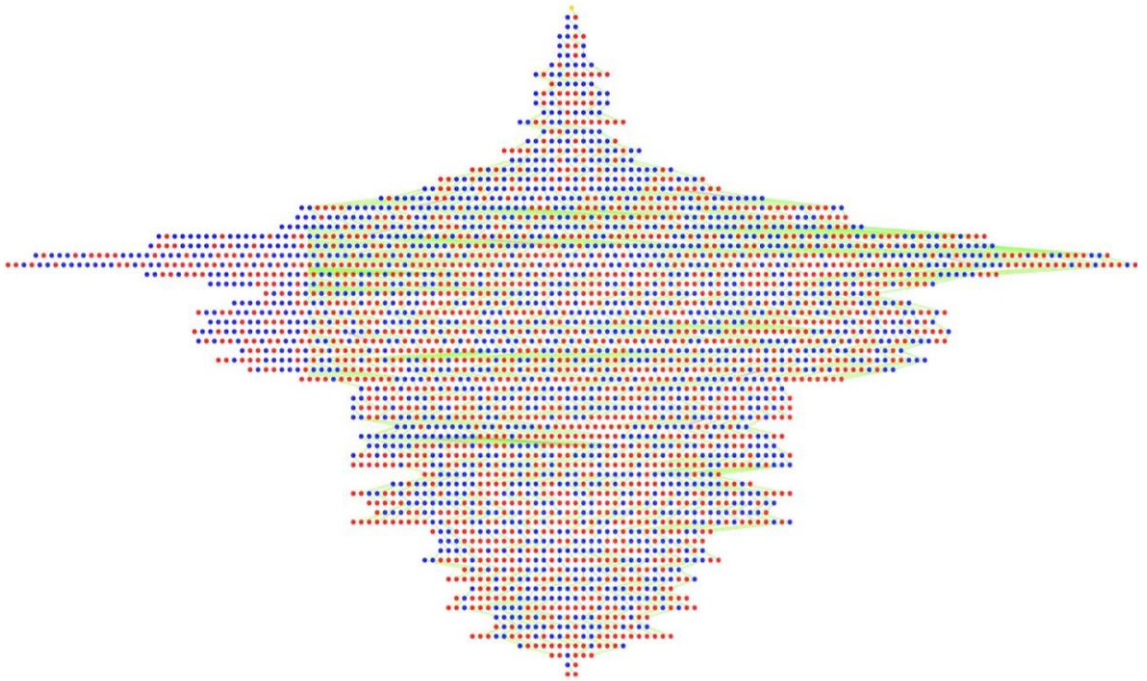
Figure 5.2: Normal arterial tree 2

Figure 5.3: Normal arterial tree 3

Figure 5.4: Normal arterial tree 4
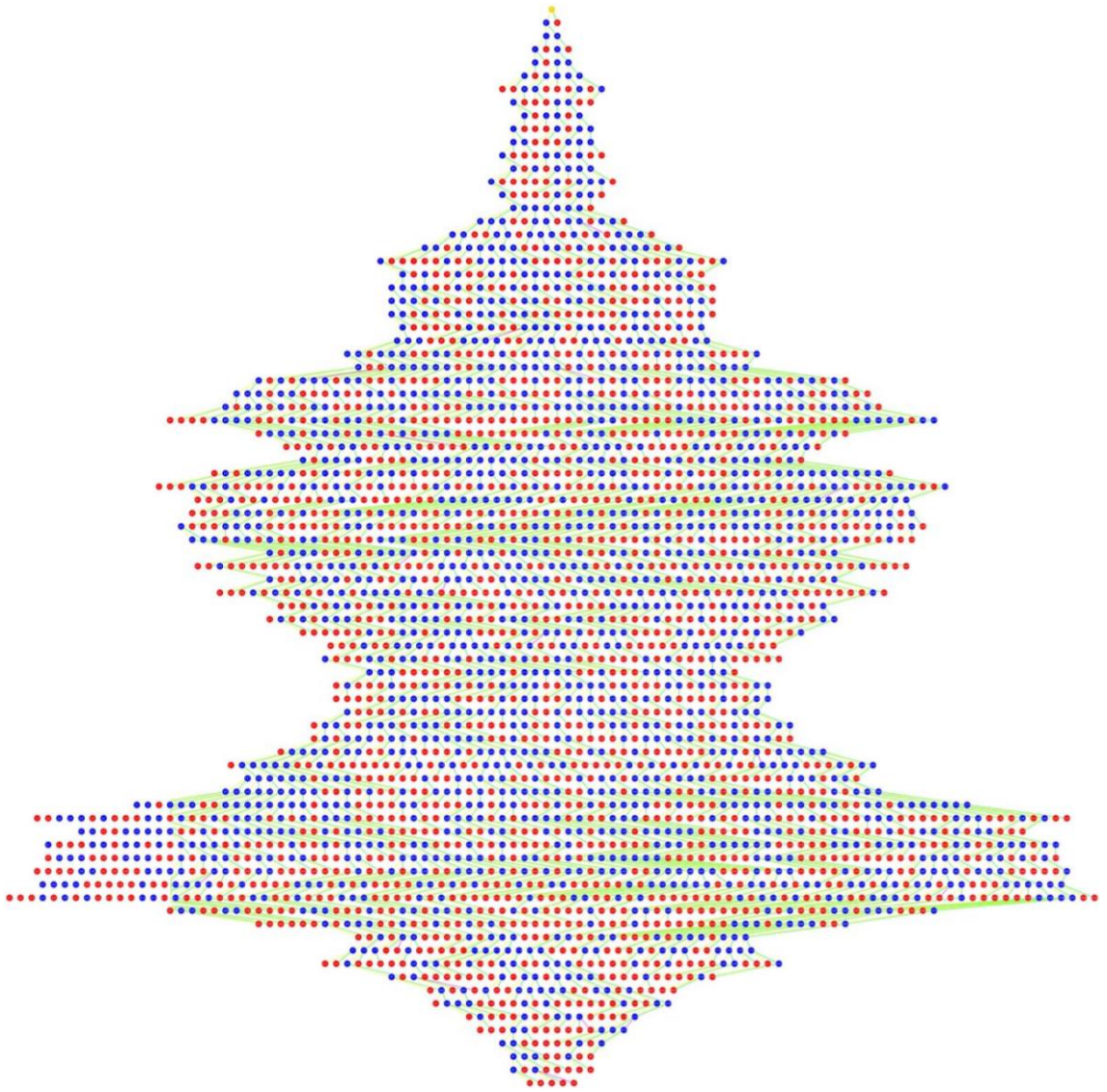
Figure 5.5: Normal arterial tree 5
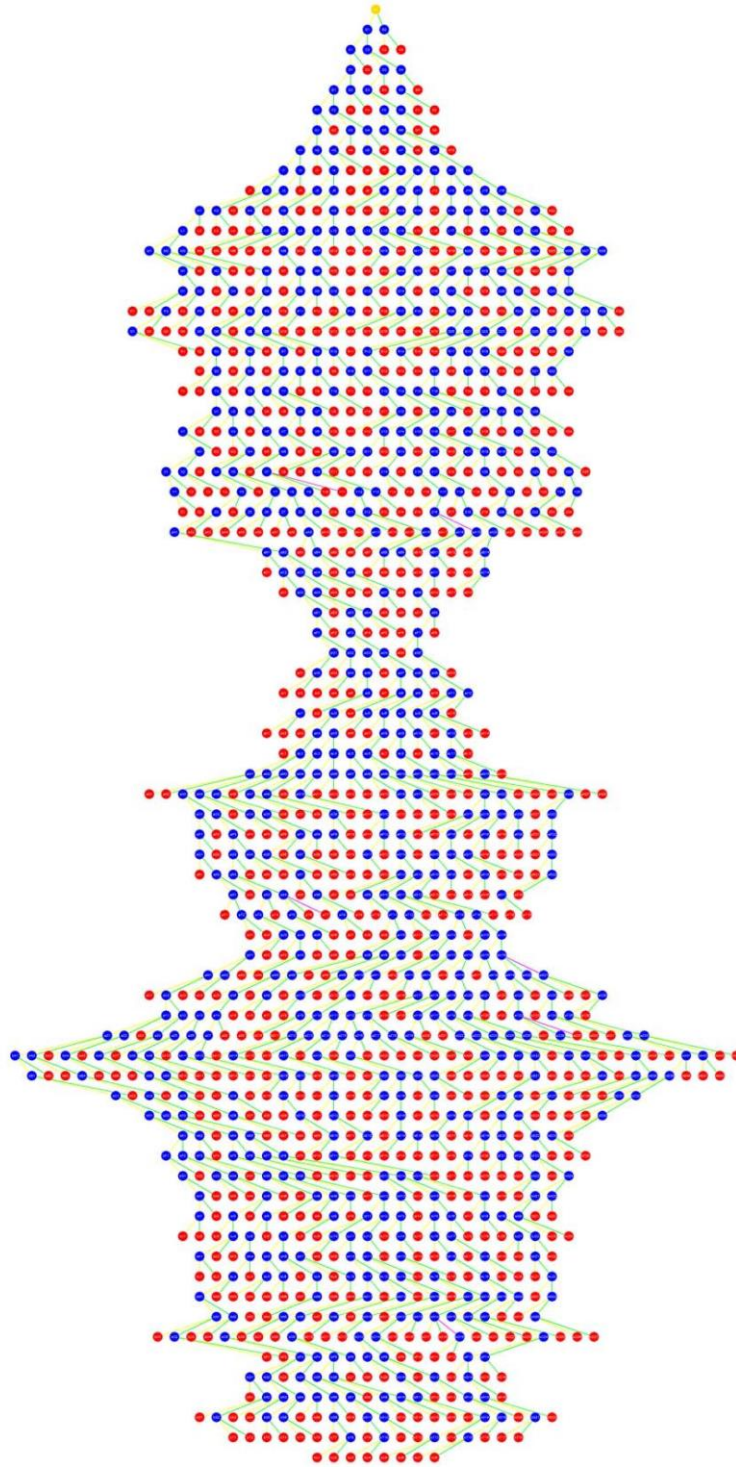
Figure 5.6: Normal arterial tree 6
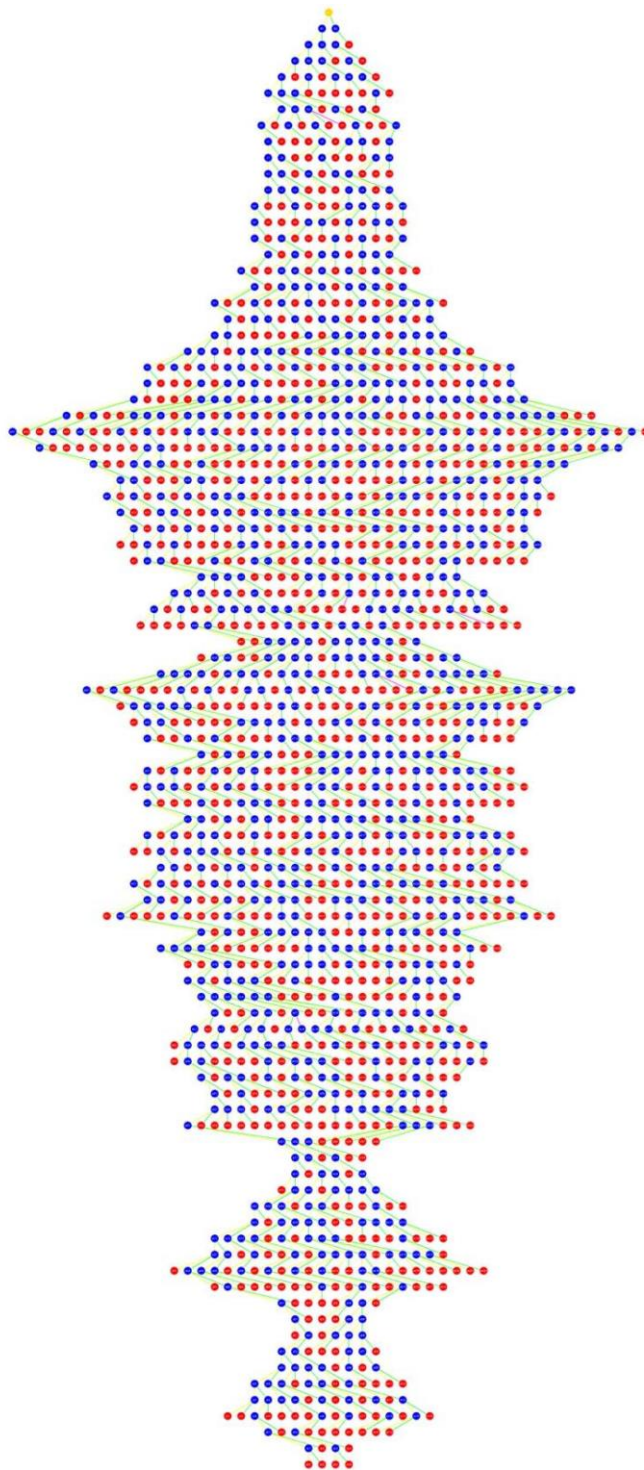
Figure 5.7: Normal venous tree 1

Figure 5.8: Normal venous tree 2
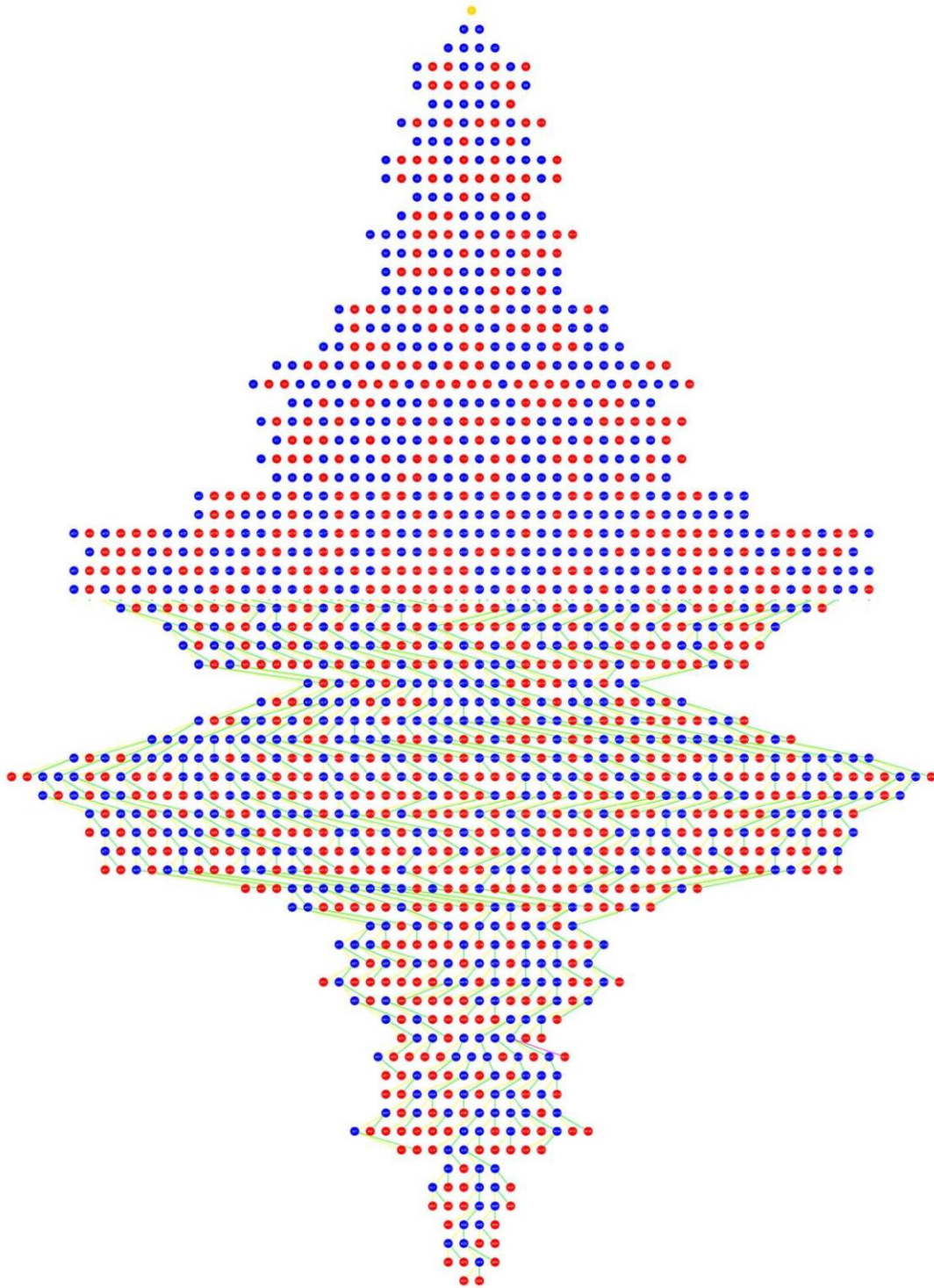
Figure 5.9: Normal venous tree 3

Figure 5.10: Normal venous tree 4

Figure 5.11: Normal venous tree 5

Figure 5.12: Normal venous tree 6

Figure 5.13: FGR arterial tree 1
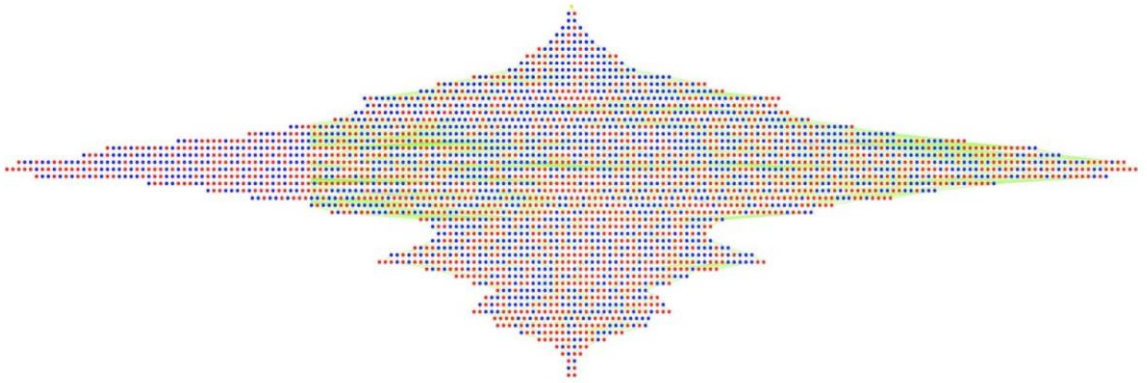
Figure 5.14: FGR arterial tree 2

Figure 5.15: FGR arterial tree 3
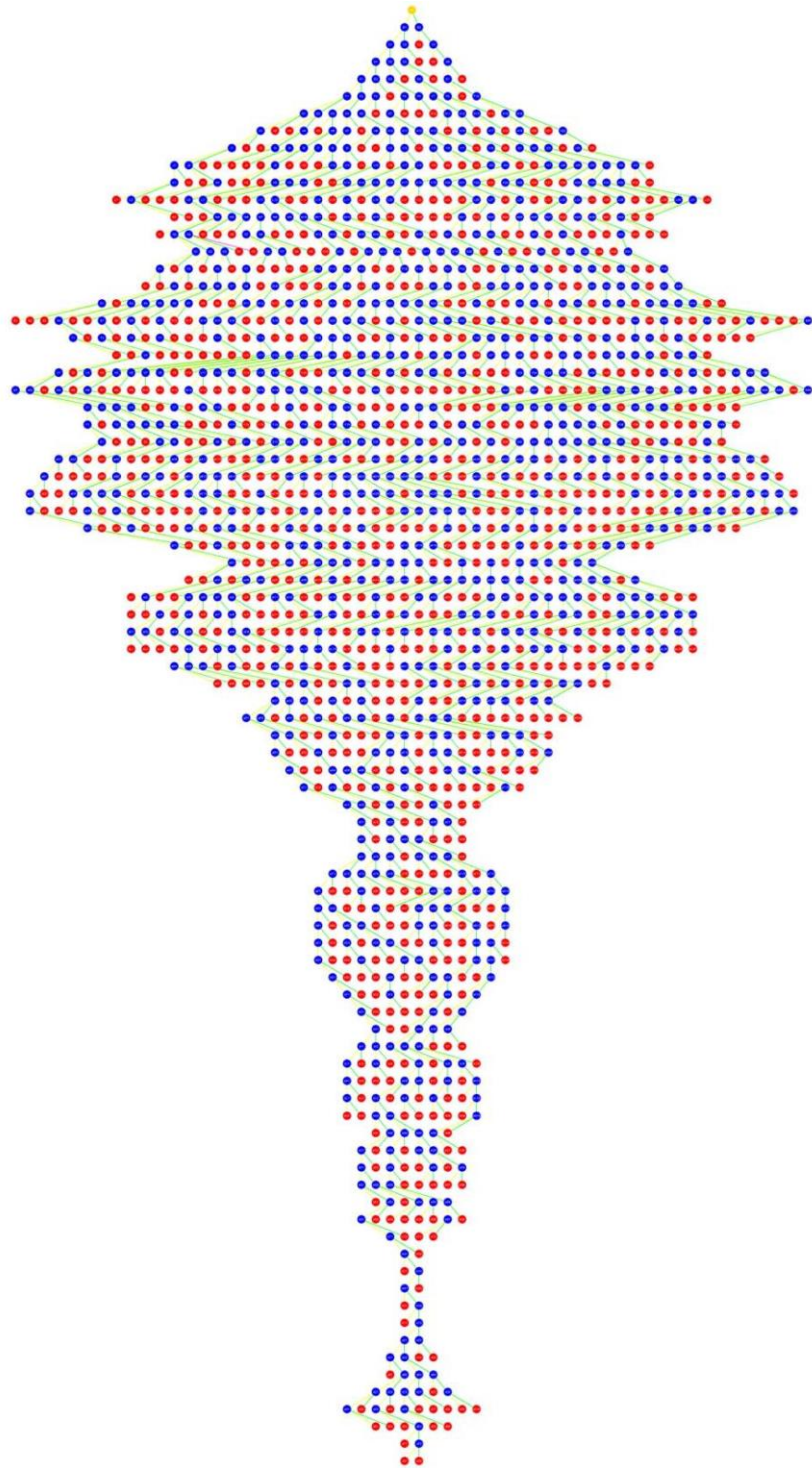
Figure 5.16: FGR arterial tree 4

Figure 5.17: FGR arterial tree 5
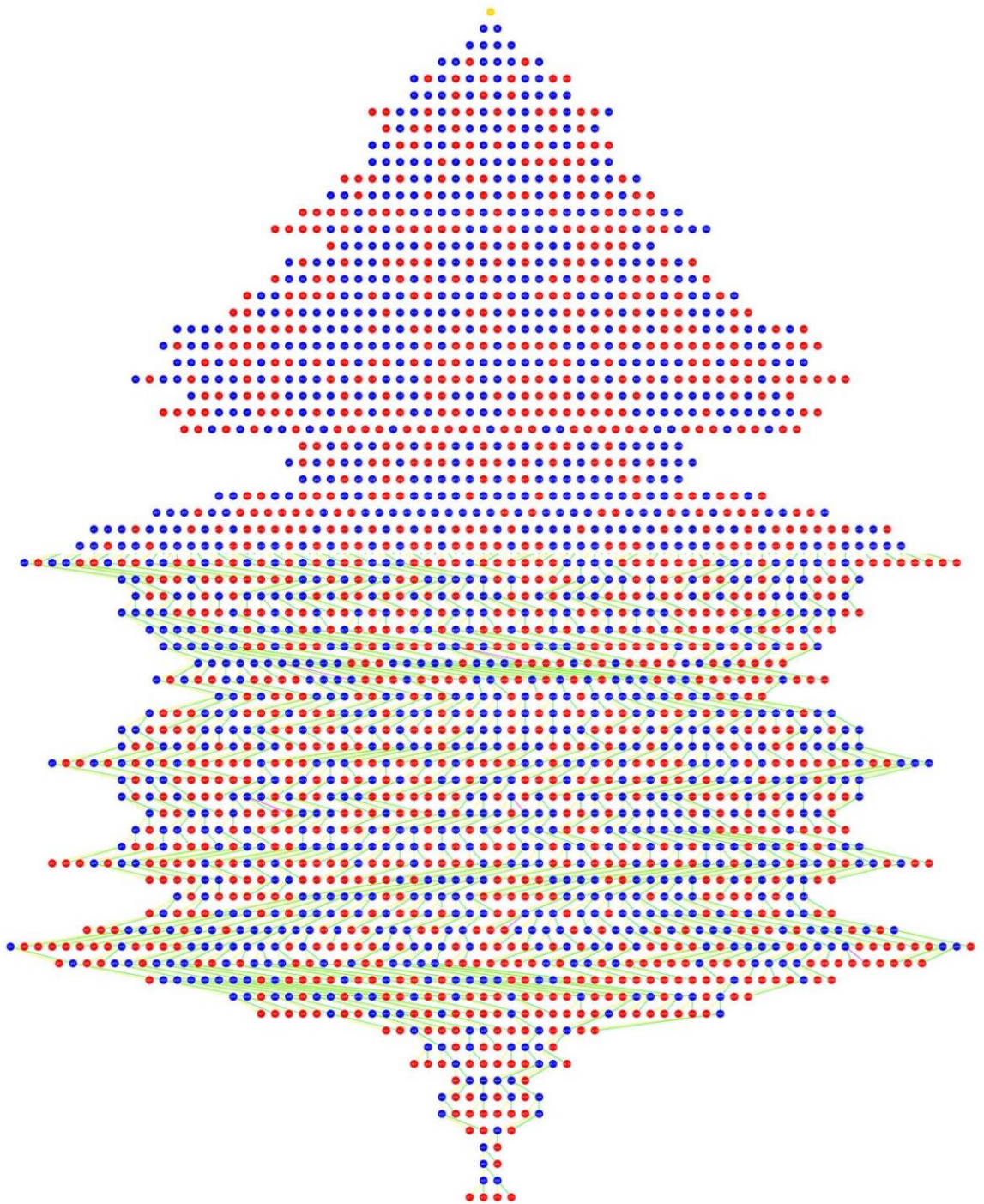
Figure 5.18: FGR arterial tree 6

Figure 5.19: FGR venous tree 1

Figure 5.20: FGR venous tree 2
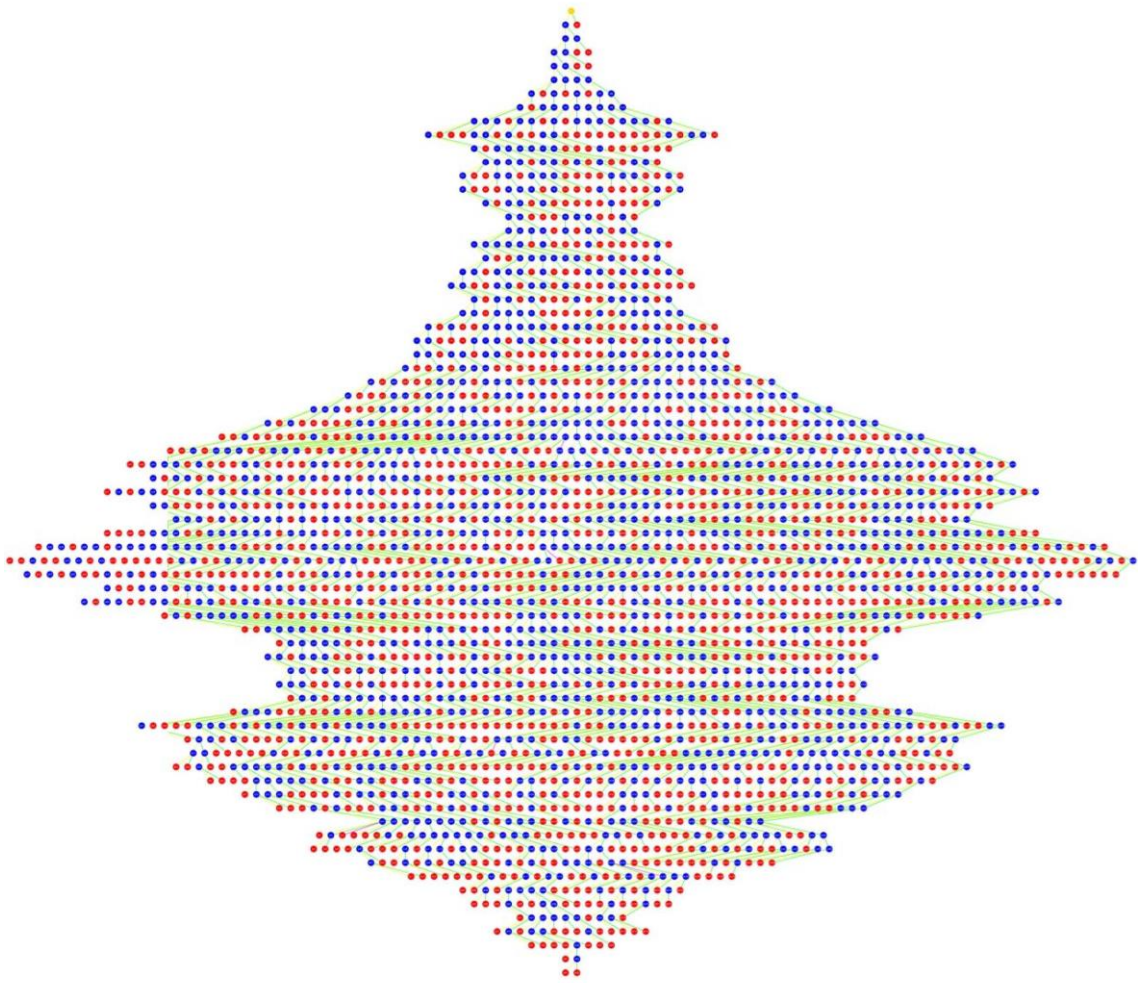
Figure 5.21: FGR venous tree 3
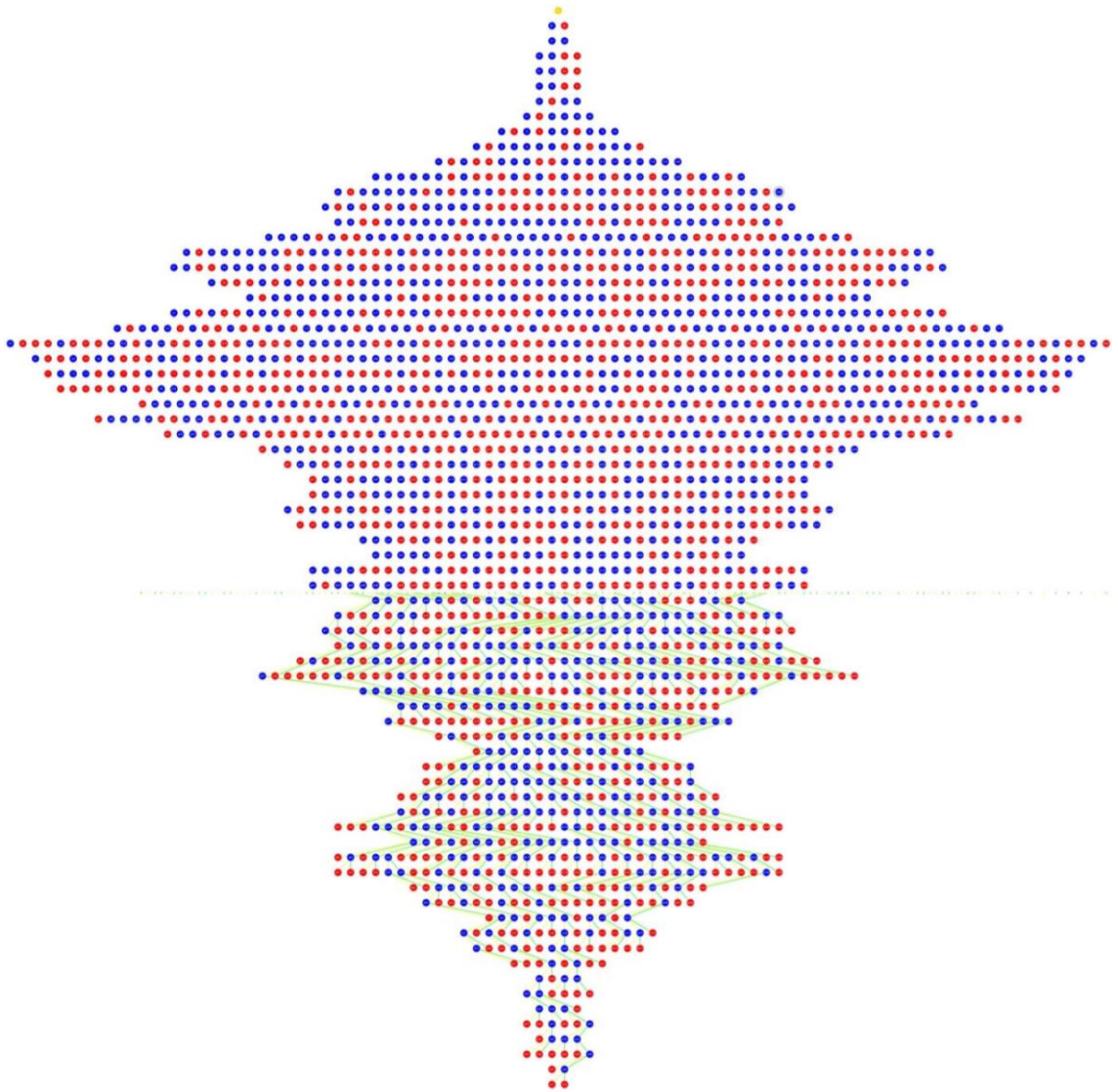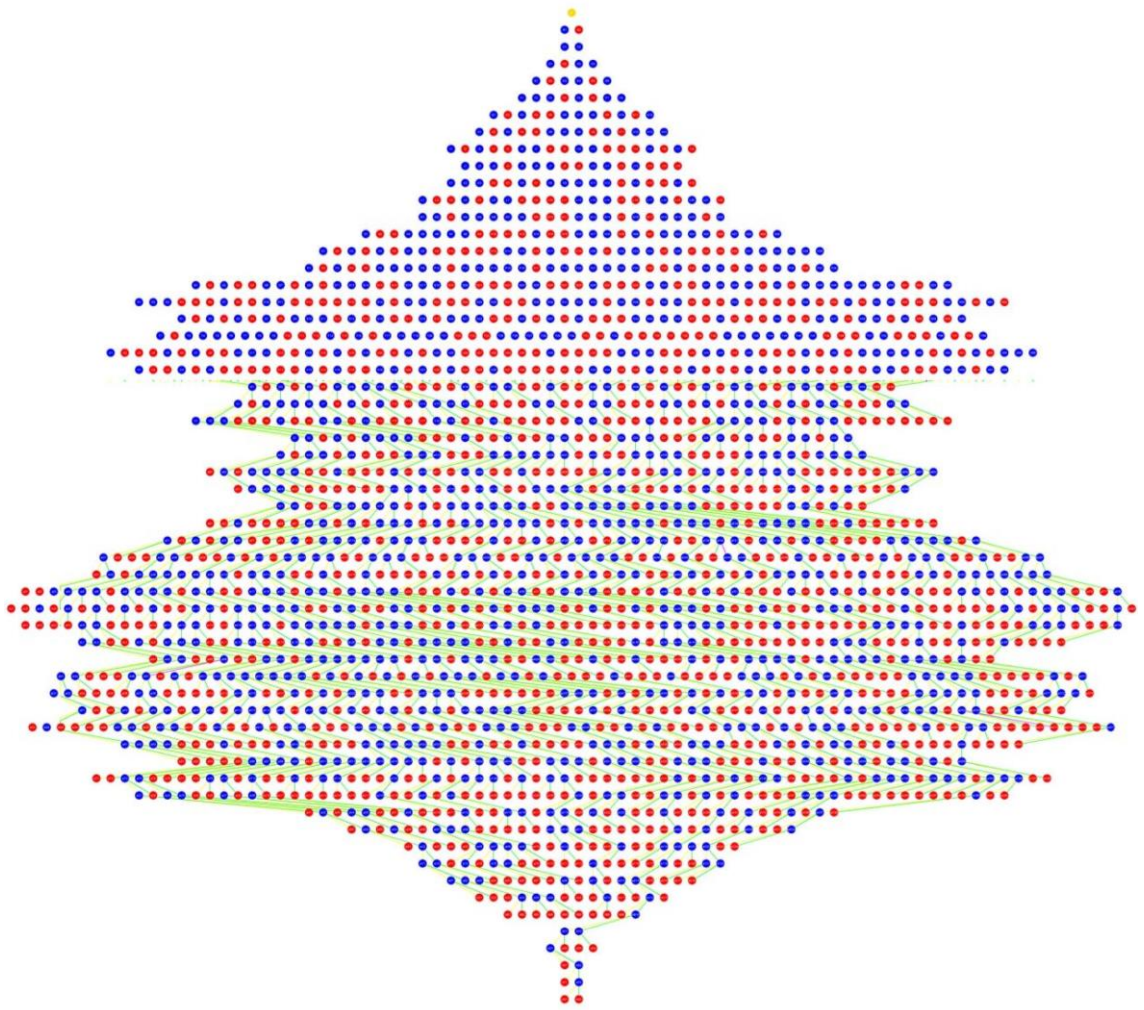
Figure 5.22: FGR venous tree 4

Figure 5.23: FGR venous tree 5

Figure 5.24: FGR venous tree 6

Appendix 4: <u>Attempts to distinguish arteriole and venule identity</u>

Arteries and veins are distinguishable based on diameter and muscle wall thickness (arteries are usually more muscular), but this applies majorly to large calibre vessels and perhaps some arterioles and venules. Smaller calibre arterioles, venules and capillaries are harder to distinguish, especially in histologic sections. Attempts, using whole mount preparations (figure 5.25), immunohistochemistry (figure 5.26) and immunofluorescence (figure 5.27), were made to identify placental villi venules by marking with EphB4 (a venous specific marker). The results were inconclusive (see images below).
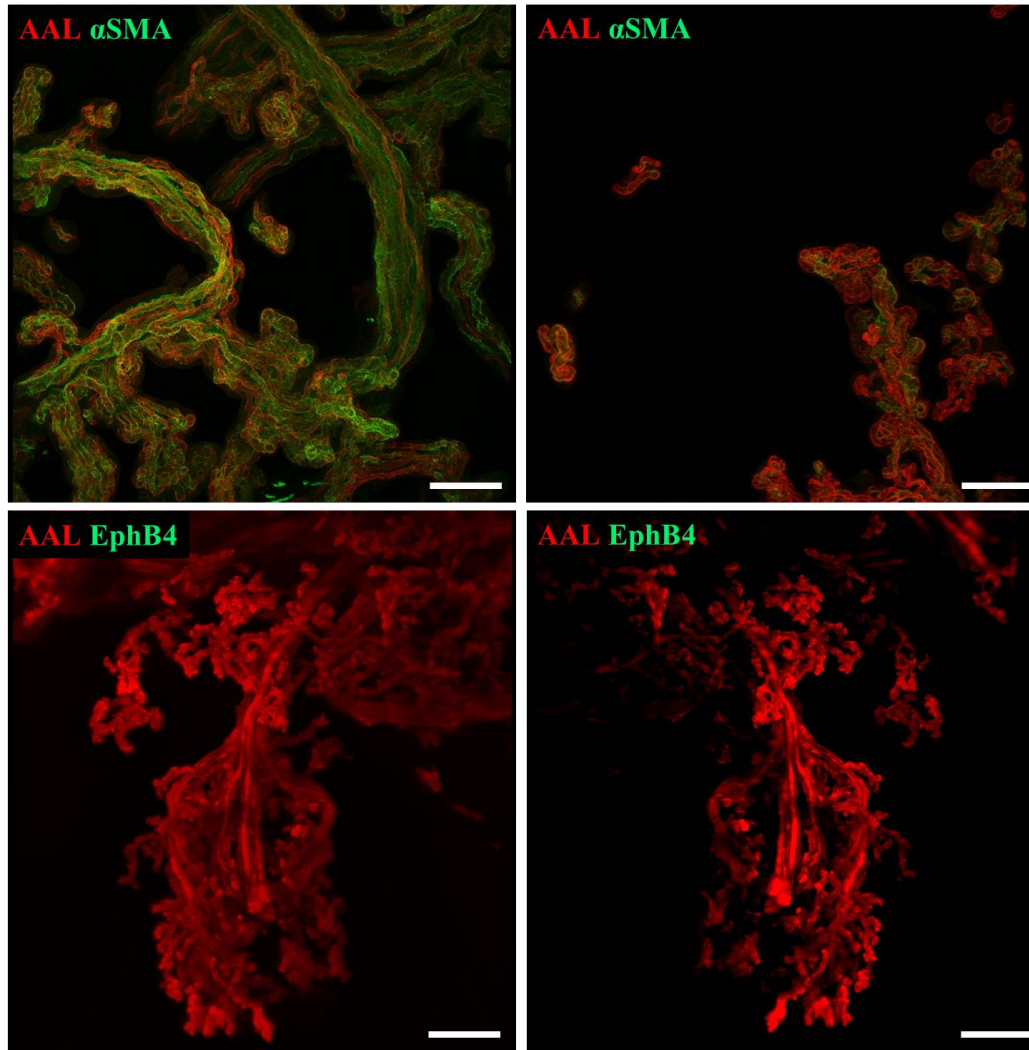
Figure 5.25: Whole mount sections of placental villi.

AAL (aleuria aurantia lectin) marks blood vessels; αSMA (alpha smooth muscle actin) marks smooth muscle; EphB4 marks venous structures. As shown in the top left and top right images, the villi were positive for AAL (red) as well as αSMA (green), confirming presence of blood vessels. However, while the bottom left and bottom right images demonstrated villi positivity for AAL (red), there was no EphB4 (green) positivity. Scale bars represent 1000μm.
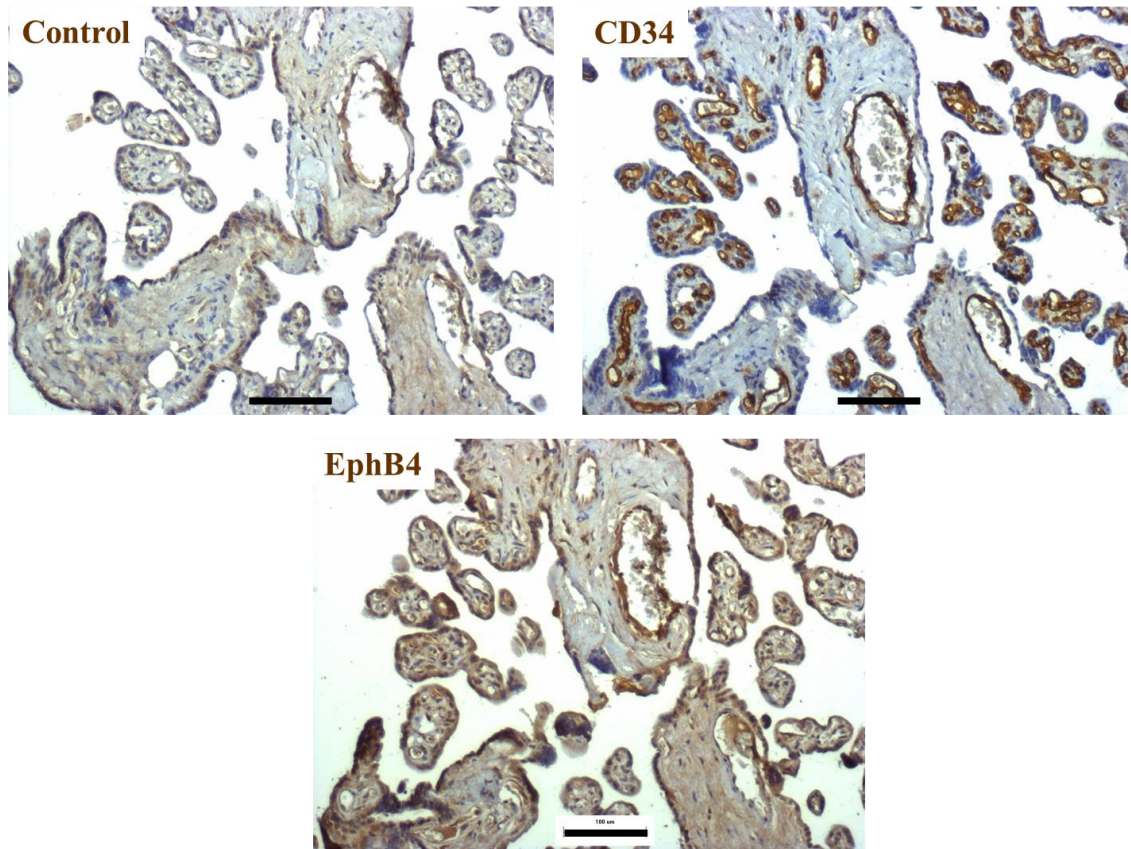
Figure 5.26: Histologic sections of placental villi stained with vascular probes.

Villi vessels were strongly positive (brown) for CD34, an endothelial cell marker (top right) but no specific EphB4 positivity was demonstrated (bottom). Scale bars represent 100μm.
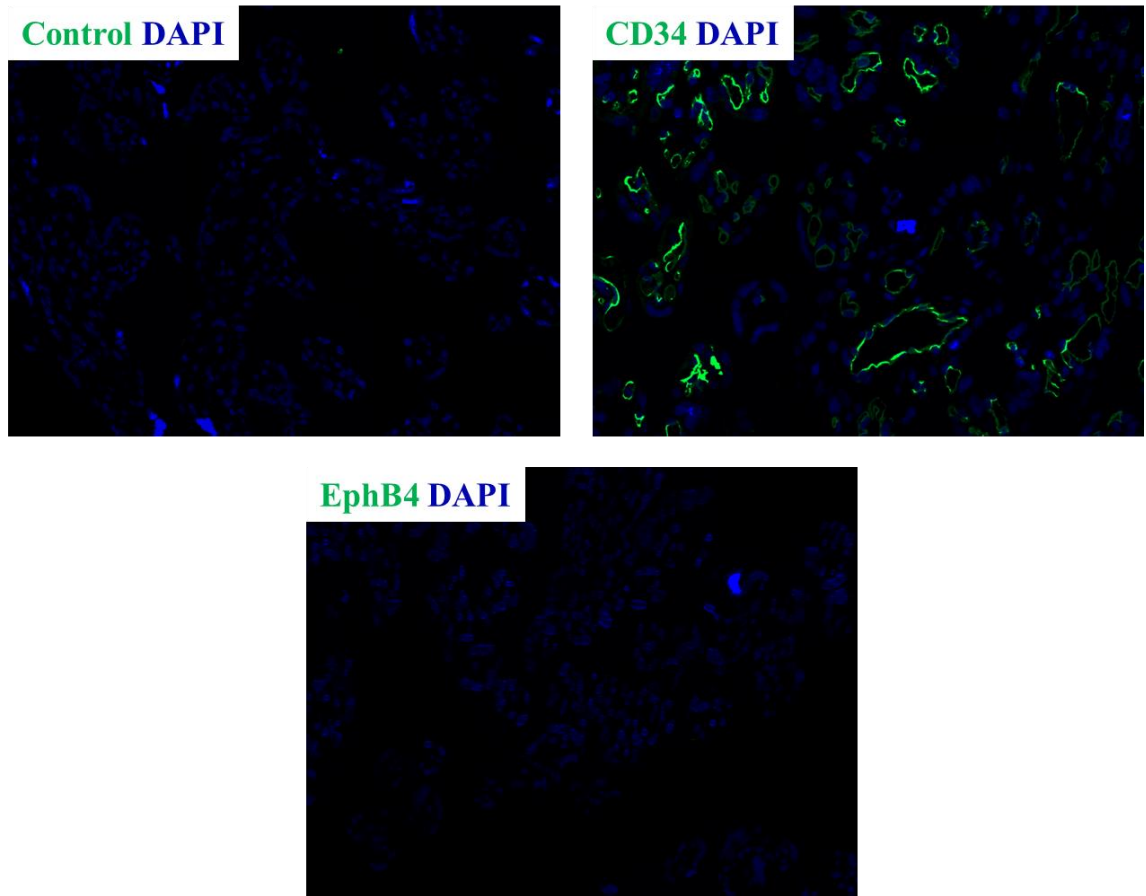
Figure 5.27: Histologic sections of placental villi stained with fluorescent vascular probes.

Villi vessels were positive (green) for CD34, an endothelial cell marker (top right) but no specific EphB4 (green) positivity was demonstrated (bottom). DAPI (blue) positive structures are nuclei. Magnification x10.